A NEW DYNAMICAL CLASSIFICATION OF NEAR EARTH ASTEROIDS BASED ON FUZZY LOGIC

Florian Freistetter
Astrophysikalisches Institut und Universitätssternwarte
Friedrich Schiller Universität Jena
Schillergässchen 2-3
D-07745 Jena, Germany
florian@astro.uni-jena.de

Abstract This work investigates the problem of NEA (Near Earth Asteroids) dynamics. Due to their many close encounters with the inner planets, their motion is highly chaotic - which leads to problems when one wants to calculate their orbits for long time scales. As of the restrictions of the existing classifications (which can be applied only on short or mid term scales), also a statistical treatment of NEAs leads to ambigious results. We introduce a new classification scheme, based on Fuzzy Logic. With this method, it is possible to derive quantitative and qualitativ results on the dynamics of NEAs even for very long time scales.

Keywords: asteroids – NEAs – classification – chaos – dynamics – fuzzy logic – collisions

1. Introduction

Our Solar System is populated with a large number of bodies orbiting the Sun in more or less eccentric orbits. Near circular orbits – like that of the planets – do not cross the orbits of other bodies while smaller bodies are known to suffer from close approaches and even collisions, as we know from many craters on the surfaces of the Solar System bodies. In this work we are investigating the the so called “Near Earth Asteroids (NEAs)” whose orbits bring them close to the Earth. We want to show the problems that arise when one wants to deal with the longterm evolution of this asteroids and how they can be solved by introducing a new classification scheme.

2. Why a new classification of NEAs?

Why is there a need to classify Near Earth Asteroids (NEAs)? And why are the existent classifications no longer suitable for some aspects of scientific research? In order to answer this questions, one has to understand why the existing classifications where created at all. Up tow, there are two different models of NEA classifications.

2.1 Shoemaker's Model

The members of G4, the **N**ear **E**arth **A**steroids (=NEAs), are usually divided into three subgroups[1]:

- the ATENS, with a semimajor axis smaller than the one of the Earth and an aphelion distance $Q = a(1 + e) > 0.983$ AU (mean perihelion distance of Earth)
- the APOLLOS, with a semimajor axis larger than or equal to the one of the Earth and a perihelion distance $q = a(1 - e) \leq 1.017$ AU (mean aphelion distance of Earth)
- the AMORS, with a semimajor axis larger than the one of the Earth and a perihelion distance $1.017 \text{ AU} < q < 1.3$ AU

Today (March 2006) the total number of discovered NEAs is 2787 (324 Atens, 1923 Apollos, 1672 Amors). NEAs larger than 1 km in diameter is about 2000 and that of the asteroids larger than 0.1 km in diameter is about 320 000 [8]. A new estimation with slightly different values can be found in Bottke et al. [1].

2.2 Milani's Model

Milanis Model of asteroid classification was derived by the data of the SPACEGUARD project. This project includes data from the integration of 410 asteroids for 200 000 years. The classification of the fore mentioned 89 asteroids was performed by observing their long term behavior. There are four main criteria :

- Values and changes of the orbital elements (a, e, i, q, Q)
- Number and changes of node crossings (NC)
- Number and depth of the close approaches (CA)
- Resonances[2]

According to this main criteria, one distinguishes between the following classes (for details see Milani et al. [7] or Sec. 4): Geographos Class, Toro Class, Kozai Class, Alinda Class, Oljato Class and Comet Class

2.3 Problems with the classification

The need for a new classification is easily explained if one considers the dynamical evolution of NEAs: a large amount of NEAs suffers under continuous close encounters with the inner planets of our solar system. Such a close encounter changes drastically the orbital elements of the asteroid, especially the semimajor axis. The strength of the change depends on the depth of the encounter and the masses involved. This can be seen in Fig. 1, where every close encounter of the asteroid (10563) Izhdubar is reflected in a jump of the semimajor axis. These close encounters and the resulting changes of orbital elements make the orbits of the NEAs highly chaotic (see also [4] and [3] for details on the chaotic behaviour of NEAs)

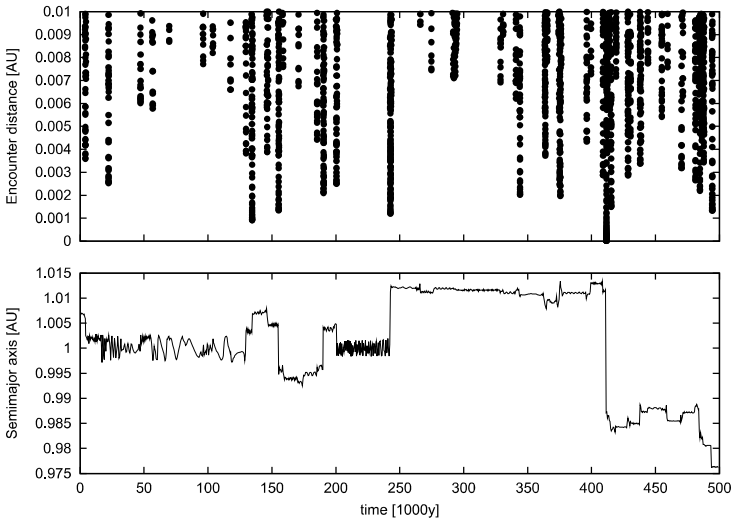

Figure 1. The semimajor axis of the NEA (10563) Izhdubar for 5×10^5 years (lower graph) and the encounters with the inner planets (upper graph); every jump in a reflects a close encounter.

How does this chaoticity affect the classifications? Fig. 2 shows the evolution of the eccentricity and semimajor axis of an Amor asteroid (1993 BX3) in the $a - e$ plane. One can see that the asteroid (which was initially inside the Amor group) has crossed all group borders and has become a member of the Apollo group, then changed to an Aten; in the end, the asteroid has become a Subaten (such changes of initial group have also been reported in [2]). Here one sees how the restrictions of the Aten/Apollo/Amor classification can cause problems. Initially meant to be only used for observational purposes, these groups are only valid for some 100 years. If one tries to apply the classes for longer time scales, one certainly has to fail – thus the Shoemaker classification can not be used when one deals with the longterm dynamics of asteroids. The SPACEGUARD classification is based on the dynamics of the real NEAs that were obtained from numerical integrations for 200 000 years – thus it can be

used to classify the dynamical properties of NEAs for some 100 000 years. What happens now, if one tries to use these existing classifications for other purposes? – the classifications will fail and one will encounter major difficulties when dealing with the dynamics of NEAs. Table 1 shows the *mean membership times* of the classification - that is the time a "mean" asteroids spends inside its initial group. One can see that both classifications are comparable concerning these percentages.

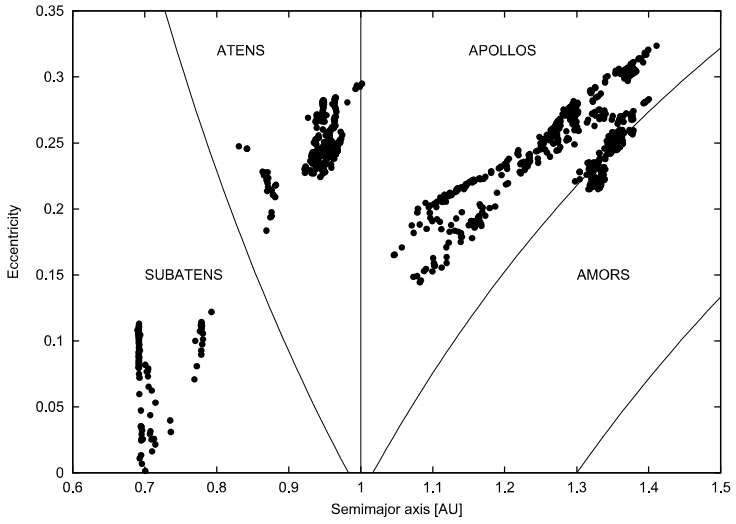

Figure 2. Motion of 1993 BX3 in the $a - e$ plane - the asteroid is a member of all three classes (according to the Shoemaker classification) during the integration time.

Table 1. Mean membership times (in percent of the integration time) for the Shoemaker and the Spaceguard classification (the numbers for the Spaceguard classification where taken from Milani et al. (1989)).

Shoemaker classification		
Atens	Apollos	Amors
76.81	80.98	51.87

Spaceguard classification					
Geographos	Toro	Kozai	Alinda	Eros	Oljato
75.86	22.90	91.70	55.05	83.72	65.13

2.4 Single objects versus groups

If the classifications can not be applied anymore when dealing with longer time scales, why not investigate only single objects? Single objects on chaotic

trajectories can not be investigated independently – one has to work with groups of asteroids. If the properties one wants to investigate are the ones the existing classifications were made for (observational properties, short/mid term dynamics), there are no difficulties. But as shown in the last subsection, there are certain problems were the chaoticity of NEAs makes things complicated. If, for example, one wants to calculate the collision probability of 1993 BX3, Fig. 2 shows the problems that arise: to derive the collision probability, one has to take into account the data of the whole time-series – that means the values of the orbital elements for all time steps to derive a single value. It was shown [4] that it makes no sense to use this number – the collision probability – as a property of 1993 BX3 itself: any other integration on another machine would result in a different number. Thus one has to use statistics and to interpret the collision probability of 1993 BX3 as one contribution to the common collision probability of a certain group, whereof 1993 BX3 is a member. But which group would be the right for 1993 BX3? Fig. 2 shows that there is no evident choice – the asteroid is a member of all three groups during the integration time.

2.5 Mixing

The behavior described above is called *mixing*[3]. Because of the *chaoticity* it is difficult to investigate single objects. Because of the *mixing* it is difficult to investigate groups of objects. Thus, for certain problems, a new way of grouping asteroids is needed! For this purpose it is useful to perform a detailed investigation on the mixing behaviour of NEAs. To obtain a new classification, two properties of NEAs were especially important: the collision probability with the inner planets Venus, Earth and Mars and the *BCN* (Border Crossing Number) - a quantity defined as the number of times an asteroid crosses any group border in the Aten/Apollo/Amor classification. These parameters were calculated for all known NEAs (in 2003) - for details see [4]. The next section will explain how they can be used to construct a new classification.

3. Fuzzy classification of NEAs

This section will give some general comments on fuzzy classification and then it will propose new fuzzy classes for NEAs. For an introduction on fuzzy sets see the appendix.

3.1 General remarks

In general, the process of fuzzy classification will proceed as described in the following:

- **Definition:** To obtain a fuzzy set, first of all, a valid definition has to be found. Although fuzzy sets are mathematically exact constructions, their *definition remains relative*. That means, it is possible to translate every "vague" linguistic definition into mathematical notation. Thus one has to be careful, *how* one defines a new class: e.g. although, in spoken language, the words "large" and "tall" can often be interchanged, there exists a difference in their meaning. So a fuzzy class of "large people" should not be identically with a fuzzy class of "tall people". When defining fuzzy classes, one has always to be aware of the meaning of the definition.

- **Membership Functions:** If the definition of the fuzzy class is set up, one will have to obtain the membership function. These functions should represent reality and describe the properties of objects in the basic set according to the definition. Thus one needs a certain parameter that is connected with the definition and according to the distribution of this parameter among the members of the basic set, construct a valid membership function.

- **Classification:** The objects of the basic set can now be classified according to the membership functions. That means, one calculates their grade of membership to all defined fuzzy classes.

- **Analysis:** After all objects were classified, they have to be analyzed. This can be done by using α-cuts (see Equ. (A.6)). As now, in contrary to classical sets, objects can simultaneously be members in different fuzzy sets, they are an adequate tool to obtain a deeper understanding of the new groups: if an α-cut is applied on a fuzzy class, one obtains a classical set, whose members have special properties. E.g. one could apply an α-cut with $\alpha = 0.95$ on the fuzzy set of "large people" (and obtains a set containing only people that belong to this group with a grade of membership larger than 0.95). The important advantage lies therefore in the cross relations of the members of an α-cut and the remaining other fuzzy classes. The α-cut represents an important feature of the objects in the basic set (e.g. "being large") – but every object has also a certain grade of membership to the other groups that were defined. Investigating the distribution of these grades of membership henceforth delivers information on the additional "tendencies" that the objects have besides their dominant features. This makes a fuzzy classification especially interesting for the investigation of the long term dynamics of asteroids!

3.2 Fuzzy NEA classes

The most interesting (and important) feature of NEAs is the possibility that they can collide with the planets of the inner Solar System. Thus, the proposed new classification will describe the collisional properties of NEAs. As of the chaoticity of NEAs an *exact* prediction of collisions (that is, forecasting the date, the time and the place of a collision) is only possible for very short time scales (some hundred years). In this work, the focus lies on the long term behavior and the collision *probabilities* of the asteroids. The fuzzy classification shall now be used to investigate the *tendency of a collision* (which is a slightly different feature). An asteroid, that e.g., due to its orbits has many close encounters with Venus will of course also have a high collision probability with Venus – the "Venus-crossing" orbit is the dominant feature in its dynamics. But deep close encounters with Venus can cause a and e to change drastically and bring the asteroid also close to Earth – so a Venus-crossing NEA can also have a certain tendency for a collision with Earth (and also Mars). These interactions and connections between the planet crossing NEAs can be investigated quantitatively and qualitatively by using fuzzy classes and α-cuts.

3.2.1 Definition. As said before, defining fuzzy classes needs to be done carefully. The purpose of the proposed new classification is to investigate the connections between planet crossing asteroids. So the definition of the new NEA classes will be the following:

- The class of NEAs that can collide with Venus.
- The class of NEAs that can collide with Earth.
- The class of NEAs that can collide with Mars.

Note that the classes are defined by using the words "can collide": an asteroid, that "can collide" with Earth not necessarily has to collide with Earth! As said before, the proposed new classification will be used to investigate the interactions between the planet crossing asteroids – thus a too strict definition would not give the desired results. To get also some information on the variations of the orbital elements, an additional class is introduced:

- The class of NEAs that show almost no mixing.

"Mixing" is defined as above (asteroids that cross group borders during integration time). The underlying classification will be the one according to Shoemaker. The mixing in the Aten/Apollo/Amor classification gives (for long time scales) information on the variations of a and e. If they are very large, the asteroid will cross many group borders and have a larger amount of mixing. As the group borders are "centered" on Earth and (more or less) marked-off by the

influence of Venus and Mars, the mixing also gives information, if the motion of the asteroid is "bounded" or not: as described in Sec. 2.3, if the asteroid moves in the right region, larger variations in a and e do not necessarily lead to the crossing of group borders – e.g. an asteroid with moderate variations in a and e can still be in the region between the orbits of Venus and Earth (and thus an Aten) for a very long time and is not related to the population of the group of Mars-crossing asteroids – but *if* it develops tendencies to encounter also Mars, this will be reflected by an increasing amount of mixing[4].

3.2.2 Membership Functions. After having defined the new fuzzy classes

- **G1:** The class of NEAs that show almost no mixing.
- **G2:** The class of NEAs that can collide with Venus.
- **G3:** The class of NEAs that can collide with Earth.
- **G4:** The class of NEAs that can collide with Mars.

now the membership functions have to be derived. One starts with an investigation of the distribution of the basic parameters that are most important for these groups: for G1 this is the BCN, for G2, G3 and G4 these are the close encounters with Venus, Earth and Mars. The distributions for these four quantities are shown in Fig. 3.

These distributions can now be used to obtain a fuzzy membership function:

- **1:** Fit a function through the data (this can be e.g. a linear interpolation).
- **2:** Normalize this function to have only values between 0 and 1.
- **3:** Adjust this function to make sure that it really describes the properties of the desired group.

Fig. 4 shows now the membership functions for the four classes (the necessary numerical integrations of the asteroids were done with initial orbital elements of the JPL Horizons system using the Lie-Series integration technique (see [6, 5])

It can be seen that the shape of the membership functions for G2-G4 are quite similar - which is not very surprising because of the definition of the groups: they were meant to describe classes of asteroids "that can collide" with a planet. Having in mind the chaotic motion of NEAs, it is very unlikely that an asteroid has no close encounters with any planet during its evolution for long times. Thus, also the grade of membership in these classes will be high for a large amount of asteroids. If one would construct a membership

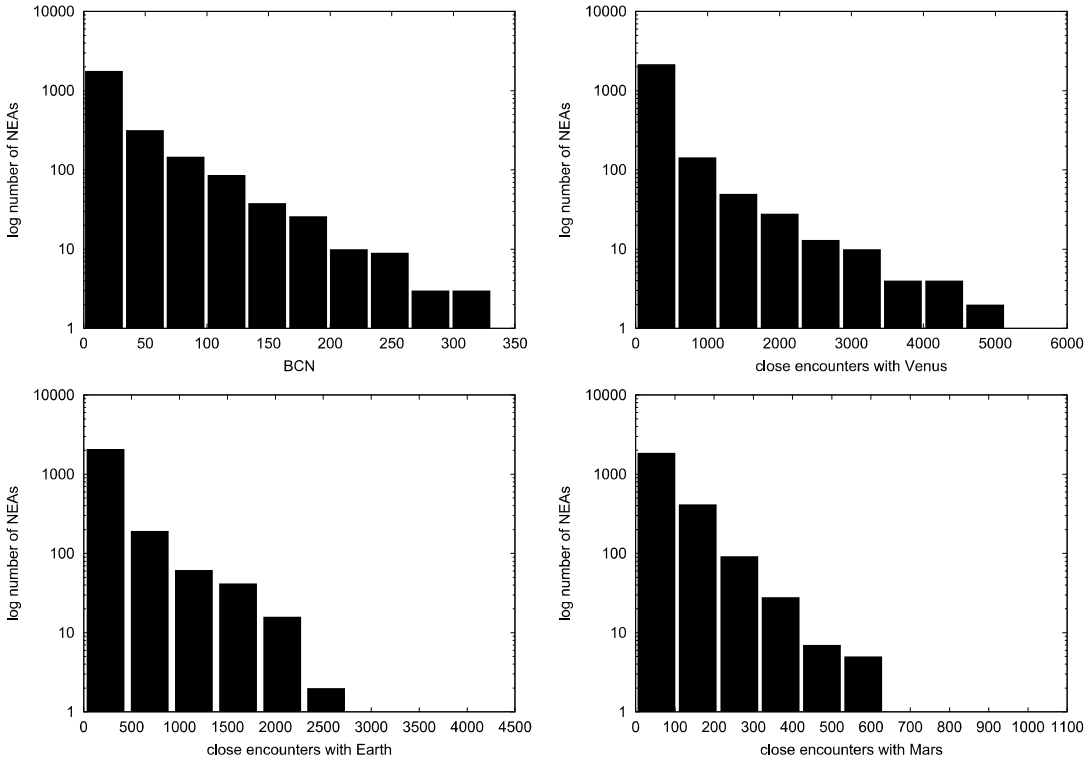

Figure 3. Distribution of BCN (top left) and close encounters with Venus (top right), Earth (bottom left), Mars (bottom right) for the real NEAs (y scale is logarithmic).

function for the group of *"asteroids that are very likely to collide with Earth"* or *"asteroids that could be really dangerous for Earth"*, one would obtain a membership function which is much less steep than the ones presented here. The largest increase shows the membership function for G4 - the class of NEAs that are probable to collide with Mars. As Mars has a very small mass, it is also not so likely for an asteroid to collide with it. Thus *almost any* asteroid that shows at least some encounters with Mars should belong to the group with a higher grade of membership – because due to the chaotic motion every close encounter gives rise to a probable collision in the following evolution.

3.2.3 Classification. With the membership functions derived in the last section, it is now possible to calculate the grade of membership of every real NEA to G1-G4.

Fig. 5 shows the distribution of all real NEAs according to their grade of membership to G1-G4. It can be seen, that for G1, most asteroids have a grade of membership of ~ 1 and thus seem to show only small or moderate changes in a and e. The local maximum of the distribution sets near 0; for the intermediate values, there is a slight increase of the number of asteroids from values for the grade of membership of 0.2 up to 0.9. For G2, G3 and G4, most asteroids have a grade of membership of ~ 0. This maximum is well defined for G2 and

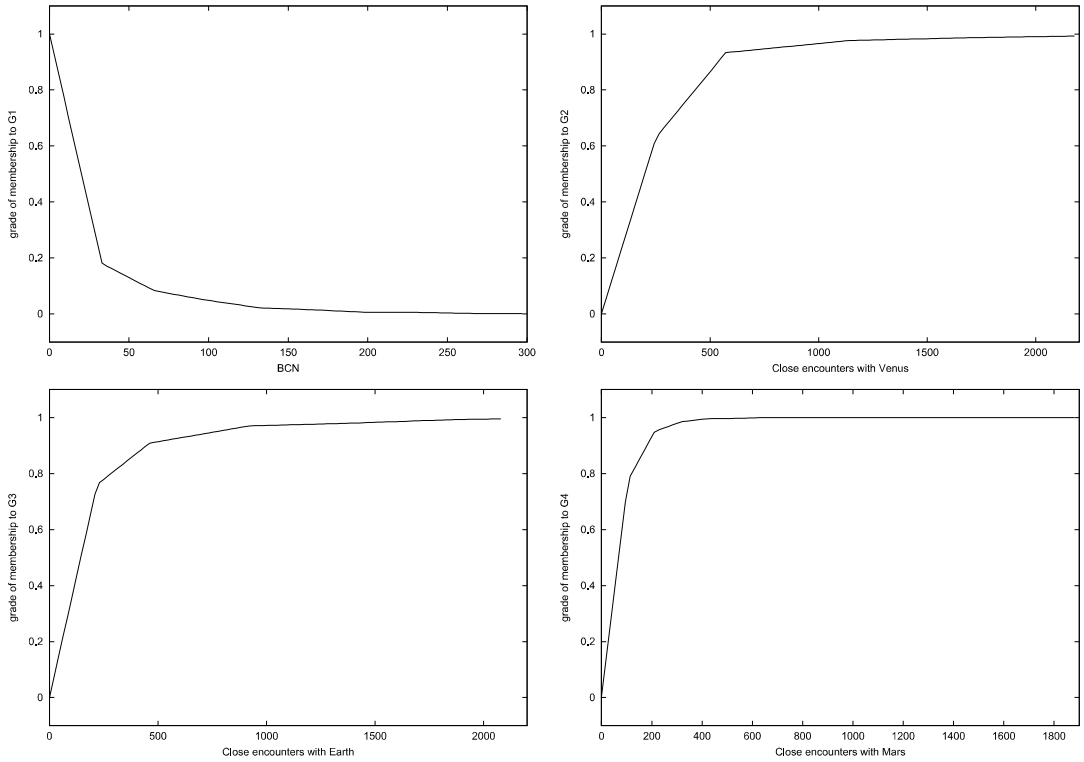

Figure 4. Membership function for the group G1 (top left), G2 (top right), G3 (bottom left), G4 (bottom right).

G3 but for G4, asteroids with a zero grade of membership have only a slight majority. Again, for G2 and G3 the second maximum sets near values of 1; for G4 at slightly smaller values. Also the intermediate values show the same characteristic: the number of asteroids decreases slightly up to grades of membership of ~ 0.6, then increases again. The grades of membership for all NEAs[5] can be found online under `http://www.astro.uni-jena.de/~florian`.

4. Results

Before starting with analyzing the new classes by means of α-cuts, the validity of the classification can also be checked by a comparison with the existing SPACEGUARD classification. As Milani et al. [7] have also classified the asteroids i.a. according to their collision probabilities and close encounters the results should be consistent – at least there, where the two classifications are comparable. The new fuzzy classification will now also include the long term behavior; additionally the basic set of asteroids was much bigger (Milani et al. could only use 410 asteroids – here 2442 NEAs were included). For comparison, we can look at the namesakes of the seven SPACEGUARD classes:

- **(1620) Geographos:** according to the SPACEGU‘Dynamical evolution and collisions of asteroids with EarthARD classification, an asteroid of

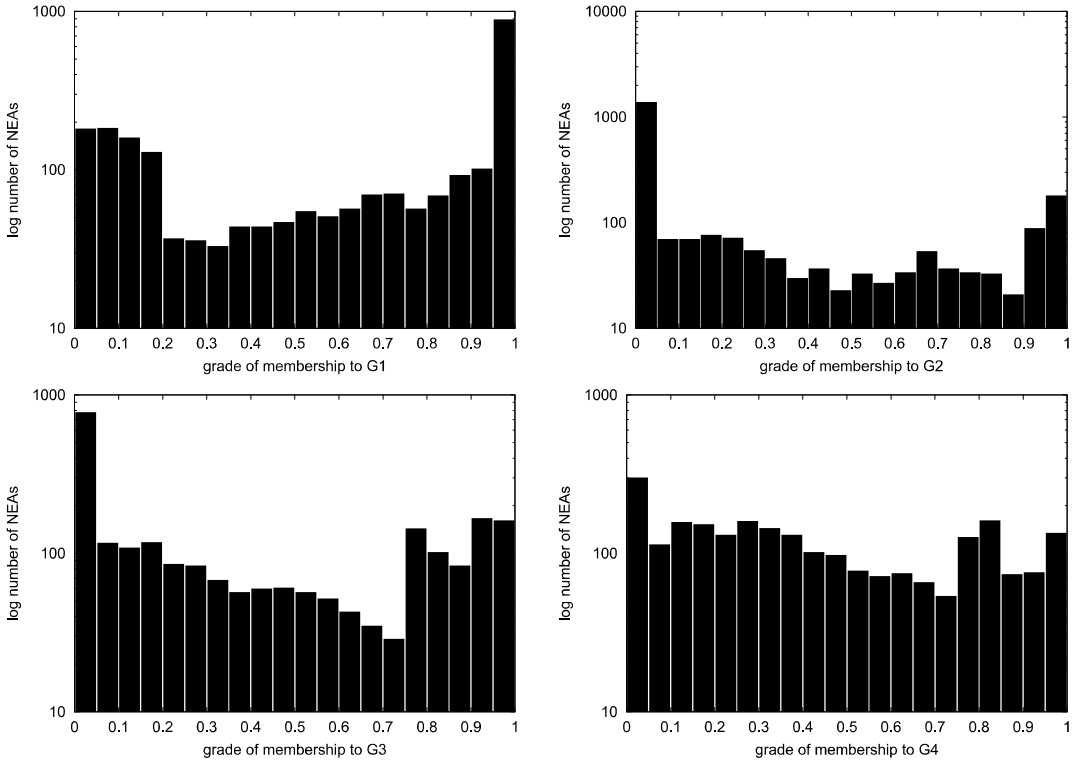

Figure 5. Distribution of real NEAs according to their grade of membership to G1 (top left), G2 (top right), G3 (bottom left) and G4 (bottom right) (y scale is logarithmic).

the Geographos group should show many close approaches to Earth and some to Venus. This means that physical collisions with Earth can occur, if the time scale is long enough. The semimajor axis of a Geographos is almost constant; the eccentricity shows secular trends on small scales – thus it is not expected to move very much in the $a - e$ plane. (1620) Geographos has a membership grade to G1 of 1 – so it is indeed a full member of the group of asteroids that show almost no mixing and its semimajor axis and eccentricity are not expected to change very much. Also the membership grade to G2 (0.03) and G3 (0.76) reflect the behavior described above. The membership grade to G4 (0.86) shows now the influence of the long time scales: during the integration time, some deep close encounters can change drastically the semimajor axis of an asteroid inside the Geographos class (see e.g. figure 5 in [7] for the asteroid (1862) Apollo) and thus force the asteroid to leave the group. Depending on the "direction" of the close encounter such an asteroid can now have also many close encounters with Mars (like for (1620) Geographos) or with Venus (like for (1862) Apollo, which has a grade of membership to G2=0.91). This is a good example how the problems of mixing are bypassed by the new fuzzy classification: in the SPACEGUARD classification, after the close encounter with Venus, (1862) Apollo was no longer

a member of the Geographos group – in the fuzzy classification, however, all the dynamical properties that belong both, to the Geographos group and the one, (1862) Apollo would enter afterwards, are known simultaneously.

- **(1685) Toro:** according to the SPACEGUARD classification an asteroid of the Toro group shows close approaches with Earth. Toros are the most unstable group of the SPACEGUARD classification – they tend to leave the group after very short times (In [7], the group of Toro asteroids has only 9 members – thus the statistics are very bad in that case)[6]. Although Toros have close encounters with Earth, they are very shallow; Toros are also protected against collision with Earth by mean motion resonances. *If* they are Venus crossers (which happens not very often), the close approaches with Venus could result in very large changes of the semimajor axis (and thus the resonance with Earth is disrupted). In general, the semimajor axis and eccentricity show only small variations. (1685) Toro indeed has a membership grade to G1 of 1 – so its semimajor axis and eccentricity are not expected to change very much. The membership grade to G2 (asteroids that can collide with Venus) is 0 – also in [7] (1685) Toro is in resonance with Venus and thus protected from close encounters. Membership grades to G3 (0.77) and G4 (0.73) show, that for longtime integration the fore mentioned resonant protection against close encounters with Earth ceases to exist – due to deep close approaches, also encounters with Mars are possible.

- **(1863) Antinous:** it was not possible to compare the results for (3040) Kozai (the most prominent member of the class of Kozai asteroids) because although it belongs to the Mars-crossing asteroids, its perihelion distance is larger than 1.3 and thus is not a NEA in strict sense (Milani et al. did not just use NEAs but all planet crossing asteroids for their classification). (1863) Antinous is, according to the SPACEGUARD classification an asteroid of the Kozai group. Kozai asteroids are, due to Kozai resonances of type I, protected against close encounters and collisions. The evolution of the semimajor axis is very regular and shows only small oscillations. The group of Kozai asteroids is the most stable class in the SPACEGUARD classification. (1863) Antinous indeed shows the described behavior: the grade of membership to G1 is 1, that to G2 (0.23), G3 (0.16) and G4 (0.14) is considerably smaller than that of the fore mentioned asteroids. Nevertheless, although Kozai asteroids should be protected from collisions, the time scales, that the fuzzy classification is based on, are longer than the protection time scale – thus the grades of membership to G2-G4 are not zero.

- **(887) Alinda:** according to SPACEGUARD classification, asteroids of the Alinda group are in (low order) mean motion resonances with Jupiter. The Alinda class is the one, for which the most difficult boundary problems existed – thus it was often difficult to decide, if an asteroid was an Alinda or not. Their eccentricities can undergo large changes, the semimajor axes oscillate around the resonant value. As of their probable large changes asteroids can encounter all inner planets but are often protected against collision by resonances.(887) Alinda has a smaller grade of membership to G1 (0.93) than the asteroids mentioned before; also the grades of membership to G2 (0.12), G3 (0.08) and G4 (0.04) are considerably smaller – showing the resonant protection.

- **(433) Eros:** according to SPACEGUARD classification, asteroids of the Eros group are those, which do not cross the orbit of Earth because their perihelion is always higher than 1 AU. All Eros asteroids are Mars crossers and have close approaches with Mars. The eccentricities of Eros asteroids can show very large changes. The grade of membership of (433) Eros to G2 and G3 is 0, it is only a member of G4 (0.72). Also the membership to G1 (0.9) is smaller than 1, indicating the larger changes of a and e. Another good example for the behavior of Eros asteroids is (719) Albert. Its membership to G1 (0.08) is very low (indicating very large changes in a and e), again the grade of membership to G2 and G3 is zero and that to G4 is 0.32.

- **(2201) Oljato:** according to the SPACEGUARD classification, asteroids of the Oljato group have orbits that show large-scale chaotic effects. They have very high eccentricities and can have close approaches to all inner planets. (2201) Oljato indeed has a grade of membership to G1 of 0.04, indicating the chaotic changes in a and e; it also shows a medium grade of membership to G2 (0.38), G3 (0.36) and G4 (0.28) – thus it encounters all inner planets.

- **Comet class:** a comparison with the class of Comet asteroids of the SPACEGUARD classification is not possible in this work. This class consists of all asteroids that spent a sufficient part of integration time in the outer Solar System. In this work, asteroids with that behavior were excluded from the fuzzy classification – first because of reasons of comparison: some of these asteroids escaped the inner Solar System that fast that not enough data would be left to calculate a valid membership grade. Second, to compare the data with the SPACEGUARD classification, it would have been also necessary to investigate the entry/exit path of the asteroid in the inner Solar System, which would have resulted in the calculation of hyperbolic/parabolic orbits which lies outside the framework of this study

The new fuzzy classification is indeed capabale to describe the dynamics of NEAs. In contrary to the SPACEGUARD classification, now the effects that take only place on long time scales are included; also the problem of mixing has been bypassed!

4.1 α-cut analysis

In contrary to classical sets, the asteroids can simultaneously be members in different fuzzy sets. Thus an adequate tool to investigate the fuzzy classes has to be used. As shown before, α-cuts are a proper way to investigate fuzzy classes. By applying an α-cut to a certain fuzzy group, one obtains classical sets and can now investigate the properties of its members. For this purpose, out of the fuzzy classes of *"asteroids that can collide"* with a planet, classical sets containing that bodies, that are *very likely to collide* are extracted by means of α-cuts. Then the members of the classical sets can be examined according to their grade of membership to the remaining groups. This type of investigation is the greatest advantage of the new fuzzy classification. In contrary to existing theories, where asteroids can inhabit only one class at time and transitions between the classes can only be investigated as time passes by, the fuzzy classes allow one to examine the membership to the different classes *simultaneously*. We will show the details of the α-cut analysis only in one case; additional studies can be found in [4].

4.1.1 $G3^{>0.9}$. The set $G3^{>0.9}$ contains all NEAs with μ_{G3} larger than 0.9 – these are "*asteroids that are likely to collide with Earth*". This group contains 329 bodies. Fig. 6 shows the distribution of these asteroids according to their grade of membershipe[7] to G1, G2 and G4.

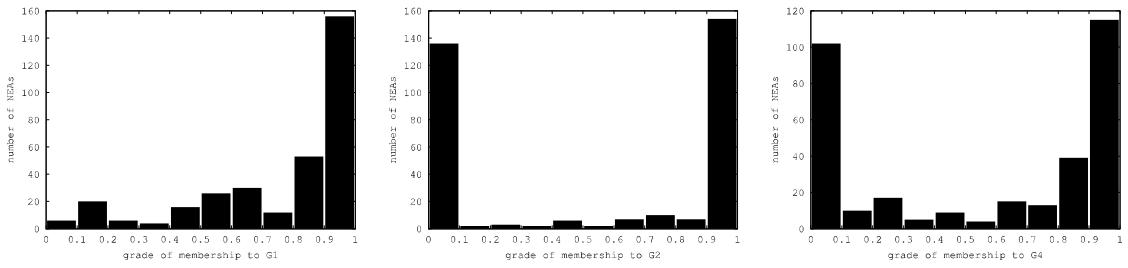

Figure 6. Distribution of asteroids in the group $G3^{>0.9}$ according to their grade of membership to G1, G2 and G4.

Unlike $G2^{>0.9}$, $G3^{>0.9}$ has more members with a medium grade of membership (50.76%), only 47.52% have high grades. The fact, that NEAs that are likely to collide with Earth show more mixing (and thus larger variations in a and e) is first due to the type of basic groups that is used to derive the mixing: the Shoemaker classification is "centered" on Earth – so asteroids that often

come close to Earth also have a higher probability to cross the border between Atens and Apollos. But Fig. 6 (middle and right) shows, that asteroids from $G3^{>0.9}$ also have larger variations of a and e in general and thus come (very) close to Venus and Mars too: 46.81% of them have high grades of membership to G2, 34.95% to G4. An important property of $G3^{>0.9}$ asteroids can be seen in the difference of low and intermediate values to G3 and G4: only 11.85% of them have medium grades to G2, whereas three times more of them (34.04%) have intermediates grades to G4. Thus, the "connection" between Earth and Mars-crossing asteroids is more fluent: NEAs that are likely to collide with Earth in the majority are also likely to collide with Mars – and, also in the majority, are likely to collide with Venus; but the lack of intermediate grades of membership to G2 shows that the interaction between Earth and Venus is much stronger. *If* deep close encounters bring an asteroid near Venus (which is the case for slightly more than half of asteroids), it is very probable that they have very much close encounters (and thus also a higher collision probability) with Venus. On the other hand, if they come close to Mars (which is also the case for slighlty more than half of asteroids) the probability that they have a high or intermediate number of close encounters is almost equal (34.04% of $G3^{>0.9}$ have medium grades of membership, 34.95% have high grades). Earth is able to "protect" its crossing asteroids much more easier from the influence of Mars than that of Venus.

5. Conclusions

Concerning the question of the danger of Earth by NEAs, Fig. 7 shows in detail, how the different groups consist of members of the other groups. One should stress again the fact, that due to the combination of fuzzy set theory and dynamical studies of NEAs, it was possible to obtain a *quantitatively* description of the planet-crossing behaviour on long time scales – that was not possible in the past because of the chaoticity of the NEAs and the problems that were due to the fixed, not flexible existing classifications! The group of NEAs that are likely to collide with Earth not only itself has the largest number of members, also the asteroids in the other groups are more often members in the group of NEAs that are likely to collide with Earth than vice versa. This leads to the following conclusion: NEAs move on orbits with semimajor axes from ~ 0.6 to ~ 3 AU (depending on their eccentricity). They can come close (and also collide) with all large inner planets. For long time scales, the NEA population is of course not constant: their number can be reduced due to collisions with the planets or the sun ("sun grazers"); it can be increased by asteroids that are thrown out of the main belt. But *as long* as they are NEAs, independent from their position in the $a - e$ plane, it was shown by introducing fuzzy classes, that they have the tendency to evolve Earth-crossing orbits. Thus, for very long

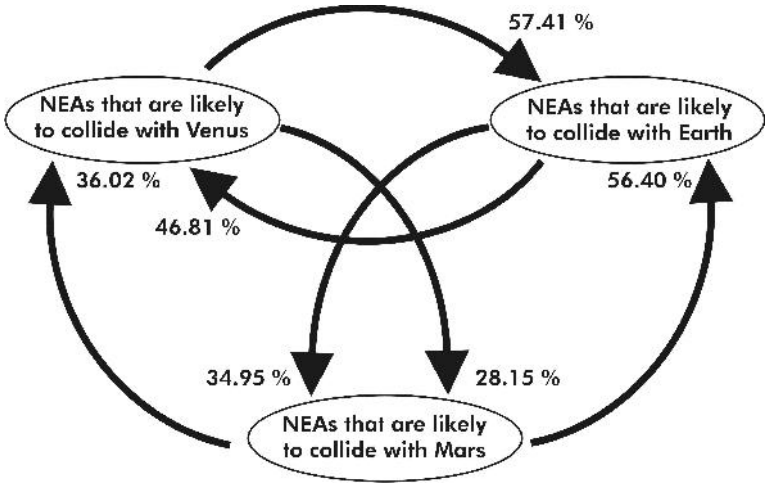

Figure 7. Groups of asteroids that are likely to collide with a planet. The arrows show, how many NEAs of one group, are also members of an other group.

time scales, the major reason for the decrease of NEA population will be due to collision with Earth! Encounter and collision frequencies of asteroids with Earth (and the other planets) will therefore differ from the current values when including the evolution of NEAs for very long times. Future studies, that have to include the flux from main belt asteroids to NEAs and also the effect of sun-grazing bodies, should confirm these statistical results numerically.

Appendix: Fuzzy sets

Fuzzy set theory or *Fuzzy Logic* was developed in 1965 by L.A. Zadeh [10]. Fuzzy sets are an extension of classical sets. A classical set is *two-valued*: for every set A there exists a function f_A that has either the value 1 or 0 with:

$$f_A(x) = 1 \Leftrightarrow x \in A \text{ and } f_A(x) = 0 \Leftrightarrow x \notin A. \tag{A.1}$$

This function is called *characteristic function* of A. Fuzzy sets, in contrary, have a characteristic function μ_A defined for *all values between (0,1)*, describing the degree to which an element x is included in the set A. Fig. A.1 shows an example of the membership functions describing the degree of membership to the groups of "short", "huge" and "average" sized people.

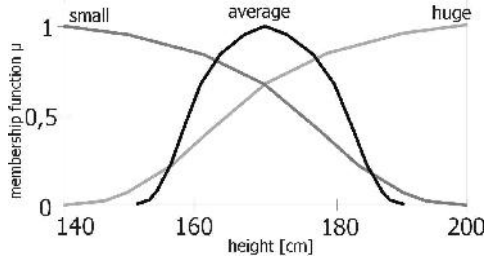

Figure A.1. Fuzzy membership functions for the classes "short", "huge" and "average".

Fuzzy sets have the following properties:

- Classical sets can be interpreted as fuzzy sets with membership grades of only 0 and 1
- Two fuzzy sets A and B are equal over a whole set X if

$$A = B \Leftrightarrow \mu_A(x) = \mu_B(x) \qquad \forall x \in X \tag{A.2}$$

- The union of fuzzy sets A and B is the fuzzy set defined by the following membership function:

$$\mu_{A\cup B}(x) = \mu_A(x) \vee \mu_B(x) \tag{A.3}$$

- The intersection of fuzzy sets A and B is the fuzzy set defined by the following membership function:

$$\mu_{A\cap B}(x) = \mu_A(x) \wedge \mu_B(x) \tag{A.4}$$

- The complement $\bar{A}$ of a fuzzy set A is defined by the following membership function:

$$\mu_{\bar{A}}(x) = 1 - \mu_A(x) \tag{A.5}$$

- For a fuzzy set A

$$A^{>\alpha} = \{x \in X \mid \mu_A(x) > \alpha\}, \qquad \alpha \in [0,1] \tag{A.6}$$

$$A^{\geq\alpha} = \{x \in X \mid \mu_A(x) \geq \alpha\}, \qquad \alpha \in [0,1] \tag{A.7}$$

  are called the **weak α-cut** and the **strong α-cut**, respectively.

- The α-cuts of fuzzy sets are classical sets.

Notes

1. This definition follows [9]

2. The typical periods of resonances are longer than 200 years, therefore the analysis of resonances is not affected by the filtering process.

3. In this work, the word *mixing* is only used to describe the fact that an asteroid changes from one class to another – it is not meant to be confused with other definitions of mixing (like in statistics or chaos theory).

4. Note that the mixing itself does not depend on the type of classification (see Sec. 2.3) – the Aten/Apollo/Amor classes were chosen because they are much simpler to handle than the SPACEGUARD classification.

5. Note that here some asteroids were excluded because they escaped the Solar System during integration time

6. In this context, the word "unstable" is not related to orbital stability! It only means, that asteroids do not fulfill the requirements to be a Toro for long time scales and change to other groups often.

7. Here and in the following, *high* grades of membership are defined by $\mu_{Gi} \geq 0.9$, *medium* grades by $0.1 \leq \mu_{Gi} < 0.9$ and *low* grades by $\mu_{Gi} < 0.1$.

References

[1] Bottke, W.F., Jedicke, R., Morbidelli, A., Petit, J., Gladman, B.: 2000,"Understanding the Distribution of Near-Earth Asteroids", *Science* **288**, 2190–2194

[2] Dvorak, R., pilat-Lohinger, E.: 1999, 'On the dynamical evolution of the Atens and Apollos", *P&SS* **47**, 665–677

[3] Dvorak, R., Freistetter, F.: 2000, "Dynamical evolution and collisions of asteroids with Earth", *P&SS* **49**, 803–809

[4] Freistetter, F.: 2004, "A new dynamical classification of asteroids", Dissertation, Universität Wien

[5] Hanslmeier, A., Dvorak, R.: 1984, "Numerical Integrations with Lie Series", *Astronomy & Astrophysics* **132**, 203-211

[6] Lichtenegger, H.: 1984, "The dynamics of bodies with variable masses", *Celestial Mechanics and Dynamical Astronomy* **34**, 357

[7] Milani, A., Carpino, M., Hahn, G. and Nobili, A.M.: 1989, "Dynamics of Planet-Crossing Asteroids: Classes of Orbital Behavior", *Icarus* **78**, pp. 212–269

[8] Morrison, D.: 1992, in *The Spaceguard Survey. Report of the NASA International Near-Earth-Object Detection Workshop* NASA, Pasadena

[9] Rabinowitz, D., Bowell, E., Shoemaker, E. and Muinonen, K., 1994. "The Population of Earth-Crossing Asteroids" in *Hazards due to comets and asteroids (ed. T. Gehrels)*. Univ. of Arizona Press, pp. 285–306

[10] Zadeh, L.A.: 1975, "The concept of a Linguistic Variable and Its Application to Approximation Reasoning – I", *Information Sciences* **8**, pp. 199-249

TRIGONOMETRIC CALCULATION OF THE ELEMENTS OF ORBIT OF CELESTIAL BODIES BY TWO TELESCOPES SITUATED IN THE LAGRANGIAN POINTS L_4 AND L_5

Josaphat Gromaczkiewicz
Institute for Astronomy
University of Vienna
Türkenschanzstrasse 17
A-1180 Vienna, Austria
j.gromaczkiewicz@kabsi.at

Abstract This paper describes a method to calculate the elements of orbit of a celestial body, detected by two telescopes situated in the Lagrangian points L_4 and L_5 by two satellites. Here the angles between the object and the points L_4 and L_5 are surveyed. Then it is possible to calculate by only these two measurements simultaneous in these points all elements of orbit of the detected object very fast and accurate.

Keywords: NEAs – observation – Lagrange points

1. Introduction

The problem to calculate the elements of the orbit of a detected object was solved in the beginning of the ninetenth century by the methods of J. P. Laplace and C. F. Gauss. We need in order to use these methods at least two observations from *one* point (Earth or satellite). Both methods have the disadvantage, that after the first measurement more measurements are necessary in order to approximate the elements of orbit better and better[1]. It is assumed, that one satellite is situated in the Lagrangian Point L_4 and a second one in L_5. The satellites are equipped with telescopes, in order to observe and to measure the angles of objects in the plane of the Ecliptic and also the perpendicular angles to this plane. With these angles it is possible, to calculate the distance of a detected object, to the Earth and the Sun by only one observation. Also it is possible to computer the other orbital elements of such an object by two observations.

2. Calculation of the distance AE by the angles α and β measured in L_4 and L_5

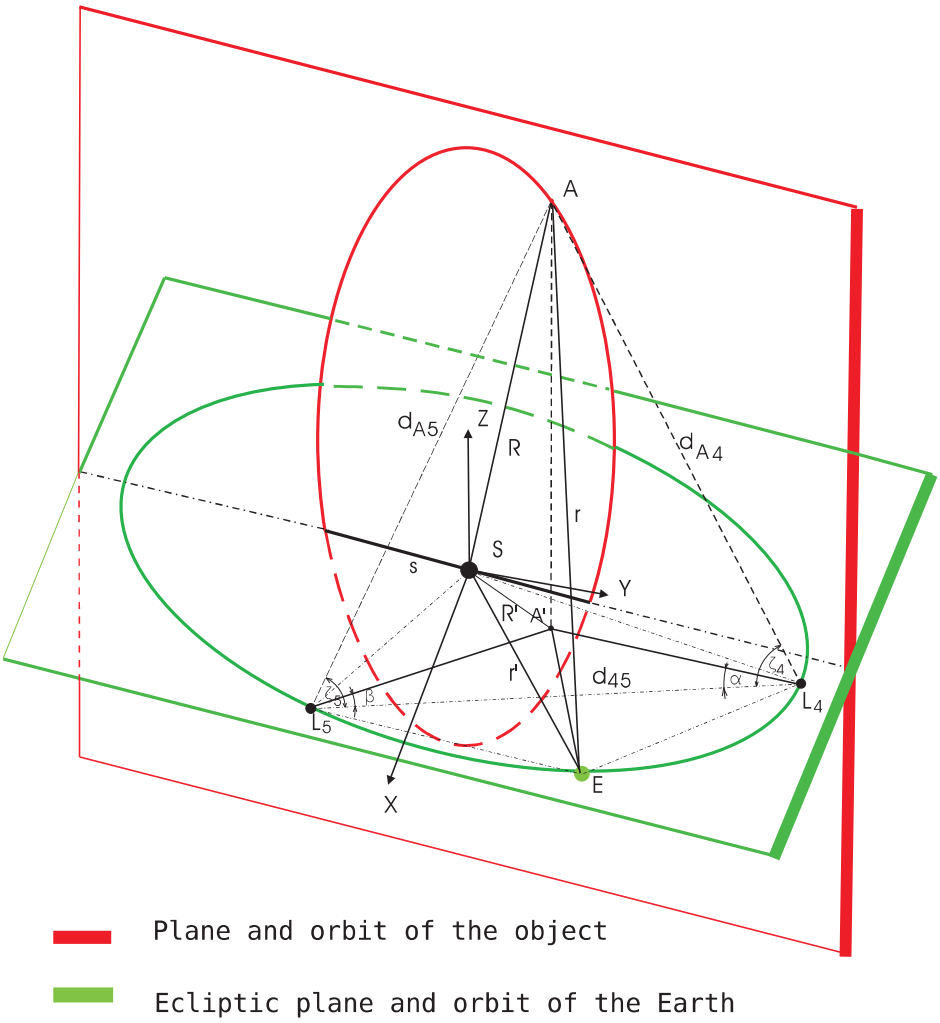

Figure 1. Oblique view

From the points L_4 and L_5 the angles are measured in the plane of the Ecliptic (α in L_4 and β in L_5) and the angles of elevation (ζ_4 at L_4 and ζ_5 at L_5). For the orientation see Fig. 2[2]

2.1 Calculation of the distances d_{A4} and d_{A5} in the triangle $\triangle : AL_4L_5$:

Here the telescope in L_4 (angle α) is orientated with $0°$ in the direction to L_5 and the angle counts clockwise. The telescope in L_5 (angle β) is orientated with $0°$ and counts conterclockwise. Therefore it is possible that α and β can accept values between $0°$ and $360°$ (see Fig. 2).

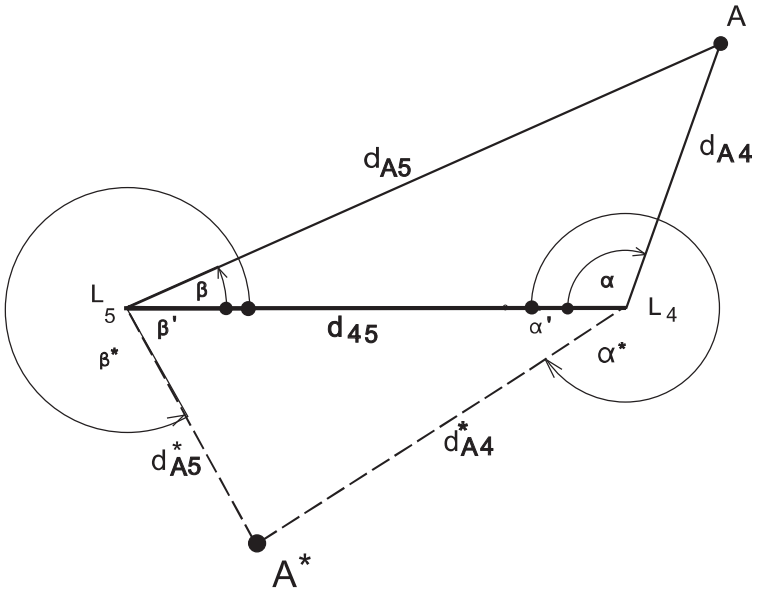

Figure 2. Orientation of the angles

For angles α^* and β^*, between 270° and 360° we calculate with the angles $\alpha' = 360° - \alpha^*$ respectively $\beta' = 360° - \beta^*$.

Known are the distances between the Lagrangian points L_4 and L_5 and also the distances L_4 and L_5 from the Earth ($L_4 - L_5 = d_{45} = \sqrt{3}$ AU). It is assumed that the necessery angles α and β are determined with very high precision simultaneous.

We observe the angles α and β with errors $\Delta\alpha$ and $\Delta\beta$. Also we can observe the angles between the the two Lagrangian points and the Earth. These observations are "surplus measures", because the condition $\alpha + \beta = (\alpha' + 30°) + (\beta' + 30°)$ exists (α' resp. β' are the angles object – Lagrangian point – Earth).

First we have to calculate the distances d_{A4} = distance L_4 – object and d_{A5} = distance L_5 – object. The calculation is done in the plane of the Ecliptic (see Equ. (1) and Equ. (2)).

$$d_{A4} = d_{45} \frac{\sin\,\beta}{\sin\,(\alpha + \beta)} \tag{1}$$

and:

$$d_{A5} = d_{45} \frac{\sin\,\alpha}{\sin\,(\alpha + \beta)} \tag{2}$$

2.2 Distance AE by mean of the angles α and β .

We calculate now the distance Earth – object r' in the plane of the Ecliptic by the calculated angles η and ζ in the triangle Earth – L_4 – object, resp. the trian-

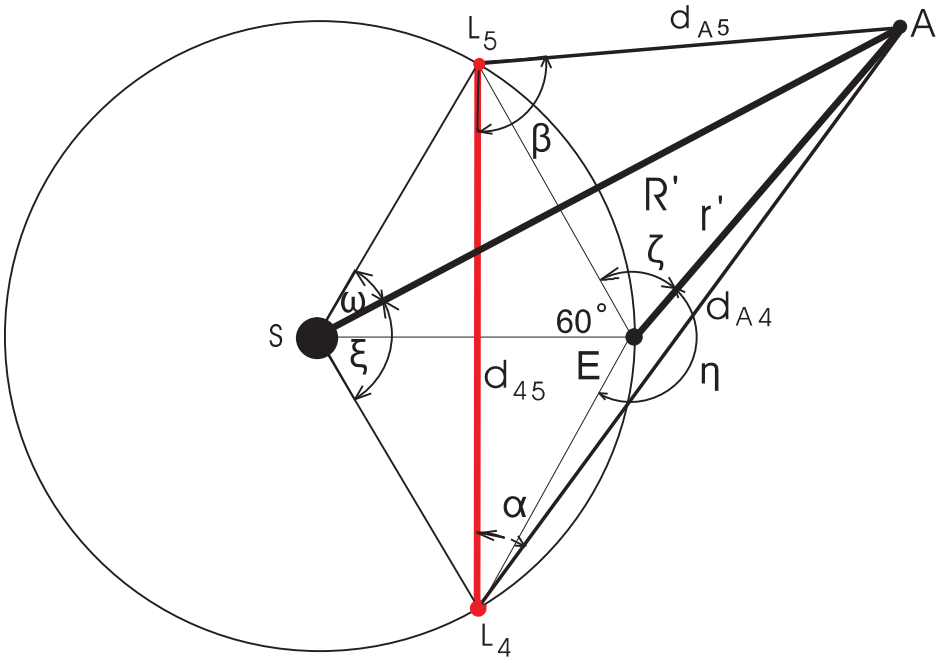

Figure 3. Calculation of the distances d_{A4} and d_{A5}

gle Earth – L_5- object (see Equs. (3) and (4) also see Fig. 3). The real distance Earth – object now we can calculate with the measured angles of elevation ζ_4 in L_4 resp. ζ_5 in L_5.

In the same manner we can calculate the distance R' (Sun – object) by the calculated angles ξ and ω in the Plane of the Ecliptic. (see Equs. (3) and (6) also Fig. 3) Also we can calculate the real distance R by the angles ζ_4 and ζ_5.

It is useful to make these calculations by the distance $L_4 - L_5 = d_{45} = \sqrt{3}$ AU, because this distance is the longest in this configuration and by this kind of calculation we achieve the best values (All values of angles are given in degrees, because the telescopes should show degrees). In order to calculate the angles η and ζ, which are necessary to determine the distance Earth – object resp. the angles ξ and ω for the distance Sun – object , there is a distinction necessary, because the angles α and β can be smaller or bigger than $30°$.

The values of r' in the plane of the ecliptic are:

$$r' = d_{A4} \frac{\sin(\alpha - 30°)}{\sin \eta} \tag{3}$$

and:

$$r' = d_{A5} \frac{\sin(\beta - 30°)}{\sin \zeta} \tag{4}$$

now we can set Equ. (3) = Equ. (4):

$$d_{A4} \frac{\sin(\alpha - 30°)}{\sin \eta} = d_{A5} \frac{\sin(\beta - 30°)}{\sin \zeta} \tag{5}$$

Also we can calculate:

$$R' = d_{A4}\,\frac{\sin\left(\alpha + 30^\circ\right)}{\sin\,\xi} \tag{6}$$

and

$$R' = d_{A5}\,\frac{\sin\left(\beta + 30^\circ\right)}{\sin\,\omega} \tag{7}$$

and in similiar manner: Equ. (6) = Equ. (7)

$$d_{A4}\,\frac{\sin\left(\alpha + 30^\circ\right)}{\sin\,\xi} = d_{A5}\,\frac{\sin\left(\beta + 30^\circ\right)}{\sin\,\omega} \tag{8}$$

Importing auxiliar values y, h_1,h_2 we get the following equations:

$$y = \frac{\sin\,\beta}{\sin\,\alpha} \tag{9}$$

$$h_1 = \frac{\sin\left(\alpha - 30^\circ\right)}{\sin\left(\beta - 30^\circ\right)} \tag{10}$$

$$h_2 = \frac{\sin\left(\alpha + 30^\circ\right)}{\sin\left(\beta + 30^\circ\right)} \tag{11}$$

Now we can calculate the following equations for the angles η and ζ by mean of Equ. (3) and Equ. (4)

$$\tan\,\eta = \frac{\sqrt{3}\,y\,h_1}{y\,h_1 - 2} \tag{12}$$

and

$$\tan\,\zeta = \frac{\sqrt{3}}{1 - 2\,y\,h_1} \tag{13}$$

and for the angles ξ and ω by mean of Equ. (6) and Equ. (7).

$$\tan\,\xi = \frac{\sqrt{3}\,y\,h_2}{y\,h_2 - 2} \tag{14}$$

and:

$$\tan\omega = \frac{\sqrt{3}}{1 - 2\,y\,h_2} \tag{15}$$

With these angles from the Equ. (12) or Equ. (13) and Equ. (3) or Equ. (4) now we can calculate r' and R' by the equations Equ. (6) or Equ. (7) by the equations: Equ. (14) or Equ. (15). The possibility to calculate r' and R' by two calculations should be used in every case in order to control the calculations[3].

2.3 Observation of the angles η and ζ from the Earth.

An additional possibility to determine the distance Earth – object directly from the Earth. This are the angles η' and ζ' (see Fig. 3). After reduction of these angles to the center of the Earth we can find the angles η and ζ. From this indirect determination and the values of the angles by measuring from L_4 and L_5now we can calculate an average value and so we have more accurate values.

2.3.1 Another possibility is the calculation with the Cosine theorem.

With the triangles: L_4 – Sun – object, or L_5 – Sun – object it is possible to calculate R' (distance Sun – object, see Fig. 3) Also it is possible to calculate r' (distance Earth - object) with the triangle L_4 – Earth – object, or the triangle L_5 – Earth – object . The distances d_{A4} and d_{A5} are known from the calculations from chapter 1.2. The distance Earth - L_4 and Earth $-L_5$ is known. See Equ. (1) and Equ. (2)

$$r' = \sqrt{d_{A4}^2 + 1 - 2\,d_{A4}\,\cos\left(\alpha - 30^\circ\right)} \tag{16}$$

$$R' = \sqrt{d_{A4}^2 + 1 - 2\,d_{A4}\,\cos\left(\alpha + 30^\circ\right)} \tag{17}$$

or:

$$r' = \sqrt{d_{A5}^2 + 1 - 2\,d_{A5}\,\cos\left(\beta - 30^\circ\right)} \tag{18}$$

$$R' = \sqrt{d_{A5}^2 + 1 - 2\,d_{A5}\,\cos\left(\beta + 30^\circ\right)} \tag{19}$$

We do not use this kind of calculation because of the minor precision o the square root.

2.4 Determination of the distance AE = r and R from r' and R' in the plane of the Ecliptic.

Now we can calculate by the measured elevation – angles ζ_4 in L_4 and ζ_5 in L_5 the distances r and R: (See Equ. (25) or Equ. (26) for the distance r and Equ. (28) or Equ. (29) for R)

$$h = d_{A4}\tan\,\zeta_4 \tag{20}$$

or

$$h = d_{A5}\tan\,\zeta_5 \tag{21}$$

By the calculation of d_{A4} rsp. d_{A5} from Equ. (1) and Equ. (2) we can find:

$$h = d_{45}\,\frac{\sin\,\alpha}{\sin\left(\alpha + \beta\right)}\,\tan\,\zeta_4 \tag{22}$$

or

$$h = d_{45} \frac{\sin \beta}{\sin (\alpha + \beta)} \tan \zeta_5 \tag{23}$$

and with:

$$r^2 = r'^2 + h^2 \tag{24}$$

$$r = \sqrt{r'^2 + d_{A4}^2 \tan^2 \zeta_4} \tag{25}$$

or

$$r = \sqrt{r'^2 + d_{A5}^2 \tan^2 \zeta_5} \tag{26}$$

and for the distance Sun – object:

$$R^2 = R'^2 + h^2 \tag{27}$$

$$R = \sqrt{R'^2 + d_{A4}^2 \tan^2 \zeta_4} \tag{28}$$

or

$$R = \sqrt{R'^2 + d_{A5}^2 \tan^2 \zeta_5} \tag{29}$$

The values for d_{A4} and d_{A5} ar known from Equ. (1) and Equ. (2).

For small values of the angles ζ_i we cannot find exact values for r and R , but that means only, that the position of the object lies nearly in the plane of the Ecliptic, therefore we can say that the distances at this moment are: $R \sim R'$ and $r \sim r'$. [4]

3. Calculation of the elements of orbit of the object

$$\varphi_A = v_E + (60^\circ - \omega) \tag{30}$$

$$\varphi_E = v_E - (60^\circ - \xi) \tag{31}$$

and

$$\varphi_A = v_E - \frac{1}{2}(\omega - \xi) \tag{32}$$

3.1 Calculation of the rectangular coordinates of the object.

Now it is possible to calculate the rectangular coordinates by the angles ξ and ω and the angle φ_A and (see Fig. 4 and Equ. (32)):

Therefore the rectangular coordinates X_A,Y_A, Z_A are now:

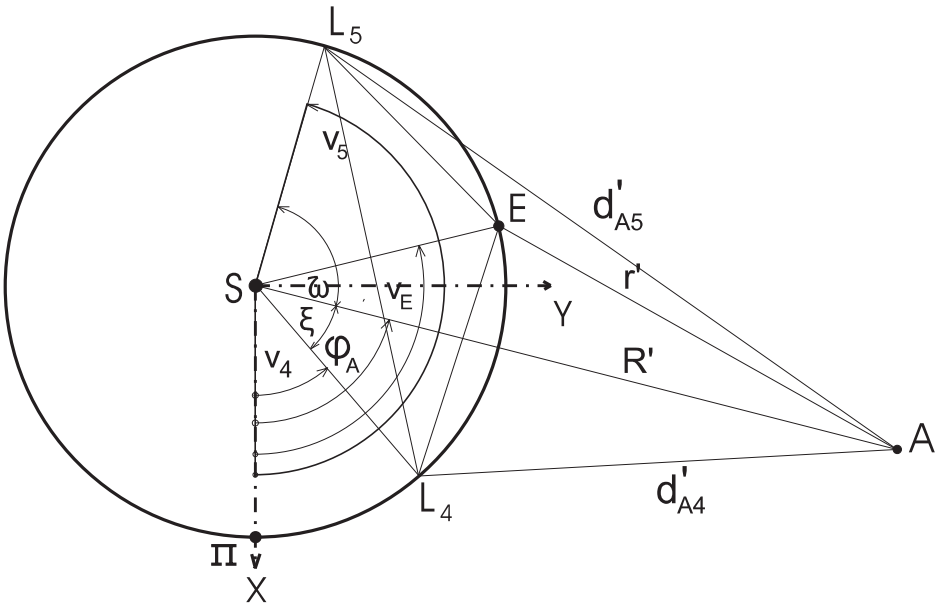

Figure 4. Calculation of the elements of orbit

$$X_A = R' \cos \varphi_A \tag{33}$$
$$Y_A = R' \sin \varphi_A \tag{34}$$
$$Z_A = h \tag{35}$$

The calculation of φ_A can be done by the Mean Anomaly M by Kepler's equation. t_0 is the time of passing the perihel. These values come from the U.S. Naval Observatory, Astronomical Applications Department 2001: Earth's seasons; Equinoxes, Solstices, Perihelon, and Aphelion 1–2-2005 . (e.g for 2005 January 2.at 1h UT).

v_E is the True Anomaly of the earth in the moment of observation.

3.2 Determination of the plane of orbit

From the observation of two or more locations of the asteroid we can calculate by the distances R' and the elevation h above the plane of Ecliptic the equation of the plane of orbit in rectangular and polar coordinates as follows:

Because the Sun as origin of the system lies in the plane of orbit, we have the equation:

$$a\,x + b\,y + z = 0 \tag{36}$$

With two values of the vector $R\ (X, Y, Z)$ (see Equ. (33) to Equ. (35)) the coefficients of the plane of orbit are:

$$a = \frac{Y_{A1}\, h_2 - Y_{A2}\, h_1}{X_{A1}\, Y_{A2} - X_{A2}\, Y_{A1}} \tag{37}$$

$$b = \frac{X_{A1}\, h_2 - X_{A2}\, h_1}{X_{A1}\, Y_{A2}\, Y_{A1}} \tag{38}$$

To calculate the trace of the plane of orbit with the Plane of the Ecliptic $z = 0$ so the equation of the plane is: $ax + by = 0$, or with the values for a and b:

$$(Y_{A1}\, h_2 - Y_{A2}\, h_1)\, x + (X_{A1}\, h_2 - X_{A2}\, h_1)\, y = 0 \tag{39}$$

After the first observation it is possible to make more measures of the angles. So we do a smoothing of the values with the method of Least Squares. We have $n - 2$ more values then we need. Therefore we can calculate the values of the parameters a and b more and more exactly.

For n measurements the parameters a and b are therefore:

$$a = \frac{\sum\limits_{i=1}^{n} x_i\, y_i \sum\limits_{i=1}^{n} y_i\, z_i - \sum\limits_{i=1}^{n} x_i\, z_i \sum\limits_{i=1}^{n} y_i\, y_i}{D} \tag{40}$$

$$b = \frac{\sum\limits_{i=1}^{n} x_i\, x_i \sum\limits_{i=1}^{n} y_i\, z_i - \sum\limits_{i=1}^{n} x_i\, y_i \sum\limits_{i=1}^{n} x_i\, z_i}{D} \tag{41}$$

$$D = \left(\sum_{i=1}^{n} x_i\, y_i\right)^2 - \sum_{i=1}^{n} x_i\, x_i \sum_{i=1}^{n} y_i\, y_i \tag{42}$$

The gradient of the plane of orbit can calculated from two observations as follows:

$$\vec{N} = \vec{R}_i \times \vec{R}_{i+1} \tag{43}$$

and so we get for the gradient:

$$i = \arccos\left(\frac{\vec{N}_3}{|\vec{N}|}\right) \tag{44}$$

3.3 Calculation of the other necessary parameters of the orbit

We assume: After the first measurement of the angles further observations follow. By two measures at times t_0 and t_1 with a relatively short difference of time, now it is possible to calculate the velocity of the asteroid as follows:

$$\vec{v}_{12} = \frac{\vec{R}_2 - \vec{R}_1}{t_2 - t_1} \tag{45}$$

and the vector of angular momentum $\vec{C}$:

$$\vec{C} = \vec{R}_{12} \times \vec{v}_{12} \tag{46}$$

Also we calculate the Runge – Lenz Vector $\overrightarrow{P}$:

$$\vec{P} = \vec{v}_{12} \times \vec{C} - k^2 \frac{\vec{r}_{12}}{|\vec{r}_{12}|} \tag{47}$$

The distance of Perihelion ω now is (see Equ. (48))

$$\omega = \text{arc cos} \left(\frac{\vec{P} \cdot \vec{N}}{|\vec{P}||\vec{N}|} \right) \tag{48}$$

for $N \neq 0$. If $N = 0$ ist, the slope of the orbit $i = 0$.

By substituting the Gauss – constant k and the value of the angular momentum $\overrightarrow{C}$ it is possible to calculate by the following equation the parameter p (see Equ. (49)) of the equation of orbit:

$$p = \left(\frac{|C|}{k} \right)^2 \tag{49}$$

From the initial values of $\overrightarrow{R}$ and $\overrightarrow{v_0}$ we can calculate the specific energy E_0 by

$$E_0 = \frac{1}{2} |v_{12}|^2 - \frac{k^2}{|\vec{r}_{12}|} \tag{50}$$

With this value E_0 from Equ. (50) we can calculate the excentricity of the orbit e.

$$e = 1 + 2 \frac{E_0 |\vec{C}|^2}{k^4} \tag{51}$$

and the major axis a by Equ. (52)

$$a = -\frac{1}{E} \tag{52}$$

The further values of the orbit: Ω (see Equ. (53)) and ω (see Equ. (54)) we also can calculate by the equations:

$$\Omega = \text{arc cos} \left(\frac{|\vec{N_3}|}{|\vec{N}|} \right) \tag{53}$$

$$\omega = \text{arc cos} \left(\frac{\vec{P} \cdot \vec{N}}{|\vec{P}\,\vec{N}|} \right) \tag{54}$$

and again (see Equ. (55))

$$i = \text{arc cos} \left(\frac{|\vec{C}_3|}{|\vec{C}|} \right) \tag{55}$$

So we have all elemtes of the orbit of the asteroid by two observations of the angles α and β.

This method was preferred, because the for this method necessary basis is with $\sqrt{3}$ AU the longest basis that could be easy realised. (The ocillation of the Lagrangian Points is very small and could be taken in mind by an error calculation.). Also all observations are free from influences of the earth's atmosphere.

4. Conclusion

By observation of objects by satellites positioned in the Lagrangian points and simultaneous determination of the angles α and β and it is possible to calculate the distances r (Earth – object) and R (Sun – object) only by one calculation. By two simultaneous observations we can calculate all other elements of orbit of the detected methods very exactly.

Notes

1. After a meeting between R. Dvorak and W. Grandl about the possibility to observe objects from the Lagranian points L_4 and L_5 by satellites.

2. Note: This method is not applicable for angles α and $\beta = 90°$, or $270°$. If α and $\beta = 0°$, $\alpha = 180°$, $\beta = 0°$ or $\alpha = 0°$, $\beta = 180°$, or α and $\beta = 180°$, the object is situated on the straight line $L_4 - L_5$ and it is not possible to calculate the position for any angle of elevation ζ_i. (The object lies in a plane, perpendicular to the plane of the Ecliptic, wich includes the straight line $L_4 - L_5$)

3. The possibility to use the triangles Earth – object – L_4 resp. Earth – object – L_5 in order to determine r' should not be used, because the distance Earth – L_4 resp. Earth – L_5 is only 1 AU and therefore smaller then the distance $L_4 - L_5 = \sqrt{3}$ AU.

4. In the case that the position of the object lies in a plane perpendicular to the plane of the Ecliptic through $L_4$and L_5, the angles α and β are $0°$ or $180°$ and therefore there exists no possibility to determine the distances r', and R' but we can measure the angles at an other time t_i

References

[1] W.Großmann: Vermessungskunde Bd. II: *12. Auflage 1975* Verlag: Walter de Gruyter Berlin - New York

[2] W. Torge: Geodäsie: Verlag: Walter de Gruyter Berlin - New York 1975

[3] W. Höpke: Fehlerlehre und Ausgleichsrechnung: Verlag Walter de Gruyter Berlin - New York 1980

[4] J. Bauschinger: *Die Bahnbestimmung der Himmelskörper: 2. Auflage 1928* Verlag von Wilhelm Engelmann Leipzig 1928

[5] K. Stumpff: Himmelsmechanik Bd. I: Deutscher Verlag der Wissenschaften Berlin 1959

[6] A. Guthmann: Einführung in die Himmelsmechanik und Ephemeridenrechnung: 2. Auflage 2000 Verlag: Spektrum Akademischer Verlag

[7] H. Bucerius: Vorlesungen über Himmelsmechanik Bd I: Verlag BI - Hochschultaschenbücher 1967

A NEW DETERMINATION OF THE FUNDAMENTAL FREQUENCIES IN OUR SOLAR SYSTEM

Christoph Lhotka and Rudolf Dvorak
Institute of Astronomy
University of Vienna
Türkenschanzstrasse 17
A-1180 Vienna, Austria
lhotka@astro.univie.ac.at

Abstract In this investigation we integrated the orbits of the planets of our Solar System over 1 billion years (-500 million back and 500 million into the future) based on the Newtonian model of the Solar System including the 8 major planets Mercury to Neptune. For the integration we used the very stable and highly precise Lie-Integration method. The output of the simulation were the osculating orbital elements, stored every 66,6 years. We transformed the data set to Laplace-Lagrange variables and analyzed it using windowed fourier transformation with a windowsize of 10 million years, overlapping with 1 million years. In this paper we present the maximum and minimum values of the orbital elements of the planets and give the time varying fundamental frequencies of all eight planets.

Keywords: Solar System - Fundamental Frequencies - Windowed Fourier Transform

1. Introduction

The numerical simulation of the dynamics of our Solar System on computer systems is a field not older than 50 years. Various people have been working on it: Eckert et al. (1951) integrated the system, using the 5 outer most planets over 3.5×10^2 years. Cohen & Hubbard (1973), Kinoshita & Nakai (1984), Applegate et al. (1986), Sussman & Wisdom (1988), Nobili et al. (1989), Nakai & Kinoshita & (1995) used the same model (5 planets) but varied the stepsize (between 0.5 and 40 days) and increased the integration time of the simulation. Newhall et al. (1983) integrated the whole system of major planets (9) using a very small stepsize (0.25 days), so did Richardson & Walker (1989) (0.5 days), Quinn et al. (1991) (0.75 days), or Sussman and Wisdom (1992) using a stepsize of 7.2 days but integrated the whole system for 10^9 years. Ito

et al. (1996) increased the simulation time up to 4.3×10^{10} years but only took the outer four planets into account. Duncan & Lissauer (1998) used Venus to Neptune in their model and integrated the system for 10^9 years.

The main question is still open: How long will our Solar System be stable inspite of its chaotical nature? Are there resonances, which will kick one of our planets from its nowadays known orbit, thus leading to a completely different configuration of our Solar System? Laskar (1990) used a semianalytical solution and showed, that there are no secular variations in the semi major axes. He integrated the Solar System in his paper for 200 Myr years and found secular resonances between the precession periods of Earth and Mars, $2(g_4 - g_3) - (s_4 - s_3)$ and between the main secular frequencies associated with the perihelia and nodes of the planets (Mercury and Jupiter, $(g_1 - g_5) - (s_1 - s_2)$). In this paper we extended the integration time for the full system up to 10^9 years to see the variation of the fundamental frequencies and the possible chaotic nature of our planetary system.

This paper is organized as follows: In the second section we give an overview of the methods used to produce the results outlined in this paper. We introduce the reader into the windowed fourier transform (WFT) - also known as Gabor transform, a special topic from wavelet analysis, and show the mechanism, how we separated the spectral lines in the corresponding power spectrum. In the third section we summarize the evolution of the elements of the planets during 1 billion years of integration time. We present the maximum and minimum values of the eccentricities and semi major axes of the main planets of our Solar System and take a look on the evolution of their characteristic orbital elements in short. The fourth section introduces the frame work of Laplace-Lagrange and defines the fundamental frequencies based on the Laplace-Lagrangian (h, k, p, q) coordinate system. The fifth section reflects the main results of the present work and compares them with those found by Laskar and other results found in literature.

2. Methods

To calculate the motions of the eight major planets we used a standard Newtonian model and integrated the full system of nonlinear equations of motions using the Lie - integration method (Hanslmeier & Dvorak, 1984) in the Cartesian reference frame. Starting from present time we simulated the system 500 million years into the back and 500 million years into the future and collected the positions and velocities referring to the classical orbital elements of all planets every 66,6 years. Thus the time span of 1 billion years resulted in 15 million "observations" of their orbital elements leading to a multivariate time series of 90 million data points, which leads to a set of 720 million real numbers, which is necessary to represent the evolution of our Solar Sys-

tem (eccentricity e_k, semi major axes a_k, inclination i_k, argument of pericenter ω_k, longitude of the ascending node Ω_k and mean anomaly M_k, where $k = 1$ (Mercury), $\ldots, 8$ (Neptune)).

The initial values for the simulation were taken from the JPL (1st August, 1965), the effective computation time just for the integration was about 1 year. To organize and analyze the resulting data set we wrote sophisticated algorithms in *Mathematica* and Fortran. The method used for the frequency analysis of the time series was the approximated windowed fourier transformation (WFT) also known as Gabor Transform and an exponential fitting and optimization algorithm in the power spectrum. For the analysis we split the data set into pieces of equal length – 10 million years per unit, overlapping with 1 million years. Thus we were able to get a time evolution of the frequency space of the system resulting in 1000 data points in time per element, frequency and planet.

To cope with the known problem in Celestial Mechanics, when doing frequency analysis of the orbital elements, namely the mixture between high and low frequencies – resulting from the chaotic structure of the system, we tried various filter methods to smooth the spectrum (Hanning, Hamming and Blackman - Tukey windows) and compared with the respective methods, when smoothing in the time domain, before starting the frequency analysis on the whole data set. In the end we decided to use a linear filter in the time domain, to get rid of high oscillation components. The second problem is, that there are actually no constant frequencies in the orbital elements (because of the nonlinear character of the system, they are time and amplitude dependent). Thus every method based on Fourier analysis will fail, as it was invented for signals of infinite length and a constant frequency domain. This problem can be solved using the WFT: When we split the data set into smaller pieces, we can regard the elements being constant within those lag windows: But using a lag window, which is to small will not cover the frequency range, we are interested in, using a lag window, which is to big, will result in a dispersion of the frequencies in the power spectrum of the signal. So it is a non trivial and difficult task to find the right tuning for the parameters (size of lag windows, overlapping & filtering) to cope with this kind of problems. Other approaches doing frequency analysis in Celestial Mechanics were done by e.g. Laskar (1993) and Chapront (1995).

Our approach used in this paper was to use the WFT on the one hand to cope with the time dependence of the frequencies and to refit the frequency lines in the power spectrum on the other hand using an exponential fitting model. Thus we considered a set of lines around a peak in the power spectrum as belonging to the same line and fitted an exponential curve through it to get a more accurate and not dispersed form of each spectral line. The resulting fitting model was

maximized and so we could easily improve the accuracy of the determination of the frequency.

The windowed fourier analysis is the simplest way to extract both the frequency and its respective time evolution of a time series, giving us insights of the evolution of the signal in the time and frequency domain. The background or theory can be found in Wavelet analysis, where the WFT is based on the implementation of Gabor functions. In our approach we approximated the method and used lag windows of equal length of 10 million years (150 000 data points per element and planet) and used a simple but fast FFT procedure to obtain the power spectrum within the window. The overlapping of the windows was 1 million years, thus leading to 1000 frequency spectra for each element and planet. In the next step we used a self written sorting algorithm, which extracted the spectra lines according to their amplitudes and fitted each spectral line within using an exponential model. We calculated the maxima in the models of the first dominant 100 frequencies in each element and planet and searched within for the set of fundamental frequencies according to a reference list given by Bretagnon (1984), Laskar (1992) and Gamsjäger (2002). To check our results, we visualized random samples and overlooked our results to proof the correctness of the automatized identification method of the spectral lines.

3. Evolution of the Orbital Elements

The evolution of the semi major axes of the eight major planets over the integration period is almost constant, which is due to the quasi conservation of energy of every single planet, because of the smallness of the inclinations and eccentricities. This is also a first indicator for the accuracy of the integration method. There are no slopes or gradients in the data set – regarding long time scales. The semi major axes just oscillate around their mean values with small amplitudes. Mercury, the inner most planet moves at 0.39 AU over the whole time span, Neptune – the outer most planet stays at approximately 30 AU. Fig. 1 takes a closer look onto the evolution of the semi major axes of Mercury - the most influenced body in our Solar System 500 million years ago (left graph) vs. 500 million years in the future (right graph). One can see, that the evolution of the semi major axes still lies in the range of present time (see Table 1) but that there are large and chaotic variations, which seem not to follow any periodic behaviour.

In contrast to the nearby constant semi major axis of our planets the eccentricities show large variations with large periods. This effect raises, when going from the outer Solar to the inner Solar System and becomes largest, when arriving at the inner most planet Mercury, where the eccentricity may lie between ~ 0.08 and ~ 0.3. In Fig. 2 one can see the coupling between the eccentric-

Table 1. The maximum and minimum values of the orbital elements of our planets. The semi major axes are given in AU, the eccentricities are numeric, the inclinations are given in degrees.

Planet	a_{max}	a_{min}	e_{max}	e_{min}	i_{max}	i_{min}
Mercury	0.3871	0.3870	0.30120	0.078730	11.40720	0.17599
Venus	0.7233	0.7234	0.07709	0.000020	4.91516	0.00246
Earth	1.00003	0.9998	0.06753	0.000083	4.49496	0.00075
Mars	1.5239	1.5235	0.13110	0.000080	8.60320	0.00291
Jupiter	5.2050	5.2012	0.06188	0.025140	2.06597	0.55867
Saturn	9.5927	9.5128	0.08959	0.007423	2.60186	0.56037
Uranus	19.3351	19.0989	0.07834	0.000095	2.73889	0.42615
Neptune	30.4325	29.9101	0.02316	0.000024	2.38176	0.77977

ities of Earth and Venus due to the 13:8 mean motion resonance and also the coupling between Jupiter and Saturn (due to the 5:2 mean motion resonance) as an example for the outer planetary system: one minima of the first leads to a maxima of the second and vice versa. These resonances stabilize the system over the whole integration time. The mean values and the minima and maxima of the eccentricities can be found in Table 1.

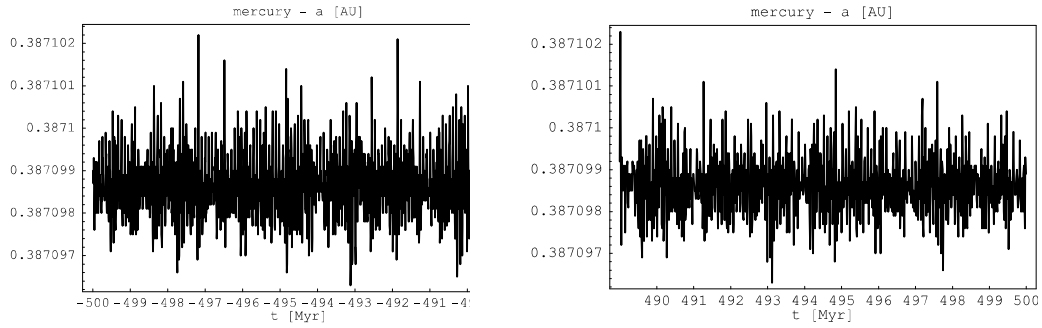

Figure 1. The evolution of the semi major axes of mercury (a_1) 500 million years ago and 500 million years in the future. Although there are chaotic variations around a constant mean value, there is no secular trend, which indicates the stability of the integration method (Lie - integrator).

The inclinations of the orbits of the planets show a similar resonant behaviour like those found in the eccentricities. The influence of the other planets in contrast seems to be more dominant, than e.g. in the eccentricities, the maximum and minimum values of the inclinations of the 8 major planets can also be found in Tab. 1, two representatives of the outer system (Uranus vs. Neptune) are given in Fig. 3 (left graph), another two representatives of the inner system (Mercury vs. Mars) are given in the right graph.

Resonances in our Solar System may stabilize or destabilize the system. Looking to the evolution of the inner and outer planets one can see the coupling of the orbital elements (e and i). Although we are not able to calculate

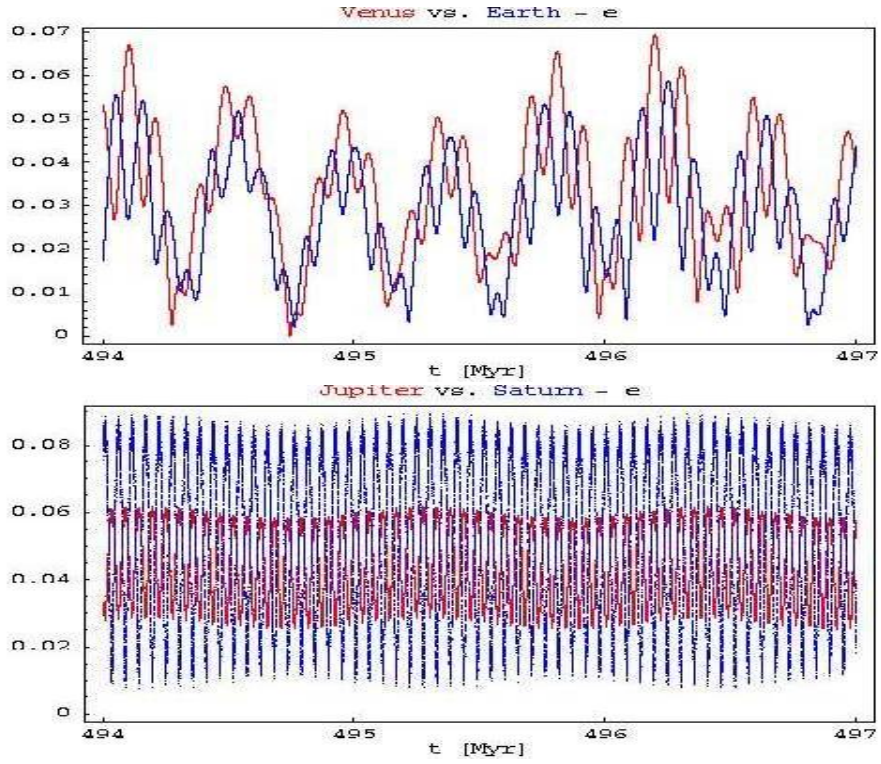

Figure 2. The evolution of the eccentricities of Venus and Earth (upper) and Jupiter and Saturn (lower) over the last 3 million years of the integration time. One can see the coupling between the planets also over the whole time span (upper:the curve with the higher amplitudes belongs to Venus, lower:the curve with the higher amplitudes belongs to Saturn).

the real positions and velocities of all planets for long time scales, it is important to see, that those resonances found last for long time scales. The answer to the question of stability in our Solar System thus needs a better understanding of the resonances in it – stabilizing, as one can see in the coupling effect of the planets or destabilizing, like those found by Laskar (1990).

4. Canonical Elements

The question, if our Solar System is stable or not needs new analytical results and of course a highly accurate and precise numerical investigation of the system. There have been several approaches to derive better and higher order approximations for the analytical part of the solutions. It was first studied by Laplace in the 18th century. He found out, that the semimajor-axes of the planets of our Solar System suffer only from periodic changes up to first order. Poincaré showed, that the formal series of small parameters, like the eccentricities, the inclinations or the masses of the planets are not convergent due to the problem of small divisors.

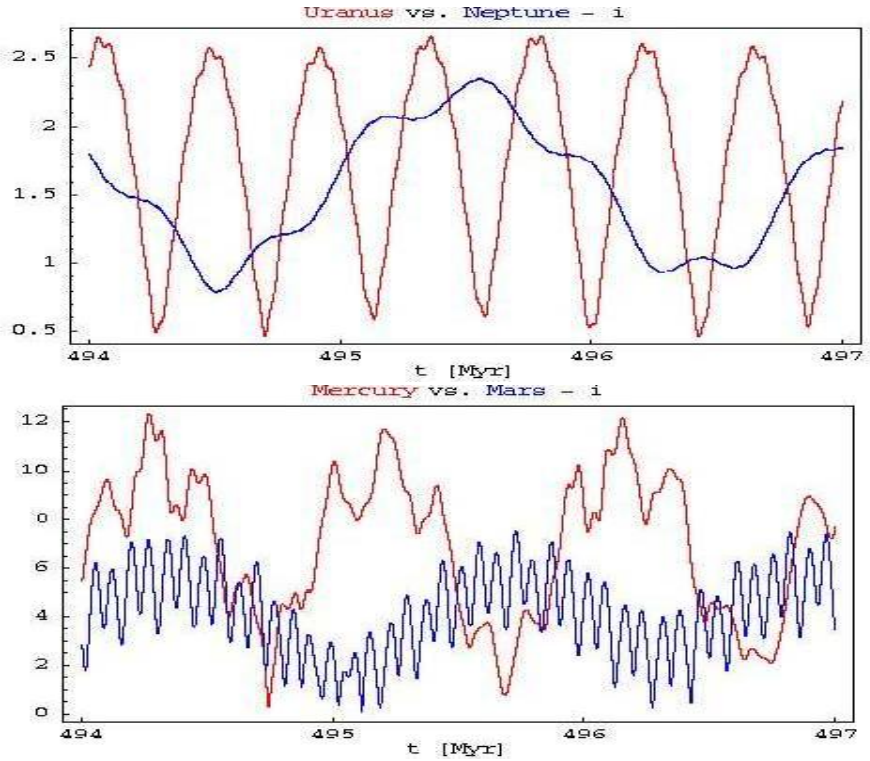

Figure 3. The evolution of the inclinations in time of Uranus and Neptune (upper) and Mercury and Mars (lower) over the last 3 million years of the whole integration time (lower:the curve showing a higher frequency represents Neptune, upper: the curve with the higher amplitudes belongs to Mercury).

Nowadays we are able to find good analytic approximations of the solutions, which allow us to reconstruct the shifting of the proper mode frequencies and the combinations of them, but it is still a problem to give long time predictions of the evolution of our Solar System. Analytical approaches may lead to results, which are good for millions of years and with numerical techniques one may integrate over billion of years, like in this paper. But without the knowing of the structure of the solution, the exact resonance conditions for the inner and outer planets, we will not be able to give a final answer to the question, if our Solar System can be regarded as stable or not. In this chapter we introduce the results of the theory of Laplace-Lagrange. We transform the orbital elements to better ones, canonical and not singular. The benefit is the better treatement when doing frequency analysis in the time depending orbital elements.

Using secular perturbation theory in the N-body system with one heavy mass in the center of gravitiy it is possible to derive the Laplace – Lagrange solution

of the system, given in Laplace-Lagrange coordinates (h, k, p, q) defined as:

$$h_j = \sum_{i=1}^{N} e_{j,i} \sin\left(g_i t + \beta_i\right), \quad (1)$$

$$k_j = \sum_{i=1}^{N} e_{j,i} \cos\left(g_i t + \beta_i\right), \quad (2)$$

$$p_j = \sum_{i=1}^{N} I_{j,i} \sin\left(s_i t + \gamma_i\right), \quad (3)$$

$$q_j = \sum_{i=1}^{N} I_{j,i} \cos\left(s_i t + \gamma_i\right), \quad (4)$$

which implies stability for the system for all times assuming small values for the eccentricities $e_{j,i}$ and for the inclinations $I_{j,i}$. The conjugated variables (h_j,k_j) and (p_j, q_j) respectively are the vertical and horizontal components of the eccentricities and the inclinations, so called Lagrange-Laplace coordinates are defined via the relations:

$$h_j = e_j \sin\left(\omega_j + \Omega_j\right), \; k_j = e_j \cos\left(\omega_j + \Omega_j\right), \quad (5)$$

and

$$p_j = \sin\left(I_j / 2\right) \sin\Omega_j, \; q_j = \sin\left(I_j\right) \cos\Omega_j. \quad (6)$$

Here ω_j are the arguments of pericenter and Ω_j are the longitudes of the ascending nodes. The quantities g_j and s_j refer to the fundamental frequencies, the quantities β_i and γ_i are the corresponding phases in the solution of the system. The indices (i, j) refer to the bodies in the system (Mercury = 1, ..., Neptune = 8). The advantage of using this variables is the fact, that they are canonical conjugated to each other and can not become singular. The orbital elements e_j and I_j can be easily derived via the equations:

$$e_j = \sqrt{h_j^2 + k_j^2}, \; I_j = 4\sqrt{p_j^2 + q_j^2}. \quad (7)$$

The solution of Laplace-Lagrange given here to introduce the idea of the fundamental frequencies used in the proceding sections, is based on a secular and second order perturbation theory (in e and I) and neglects nonlinear effects, which lead to chaotic phenomena in our Solar System. Looking to equations (1) - (4) one can see that the elements are bounded and somewhat called linearly stable. But this is not true, when going to higher orders of approximations in the analytical formulas.

5. Resulting Fundamental Frequencies

The frequency analysis in the variables (h, k, p, q) show more or less regular periodic behaviour in the evolution of the elements for the outer planets, complex and irregular evolution in the time series of the elements of the inner planets (see Fig. 4 and Fig. 5), overlapping of different frequencies and beats for example in Mars. The parameters h and k are identical but phase-delayed, which is the same for the canonical conjugates p and q. In principle we will find every fundamental frequency of the planets in the frequency spectrum of the other planets, limited due to the fact, that the basic frequencies of the planets of the outer Solar System are more dominant in the spectra of the planets of the inner Solar System, than vice versa and that frequencies, which can be found in (h, k) may be too small to be found in (p, q) and vice versa (note that this effect can not be described by the Lagrange-Laplace solution, given in (1)-(6)). In fact we did the frequency analysis in all four elements using the WFT method. We searched for the fundamental frequencies in the frequency space of all four elements and planets and averaged corresponding ones including their influence according to their amplitudes. To check consistency we compared the results given by the canonical conjugates and found minor neglectible differences between them.

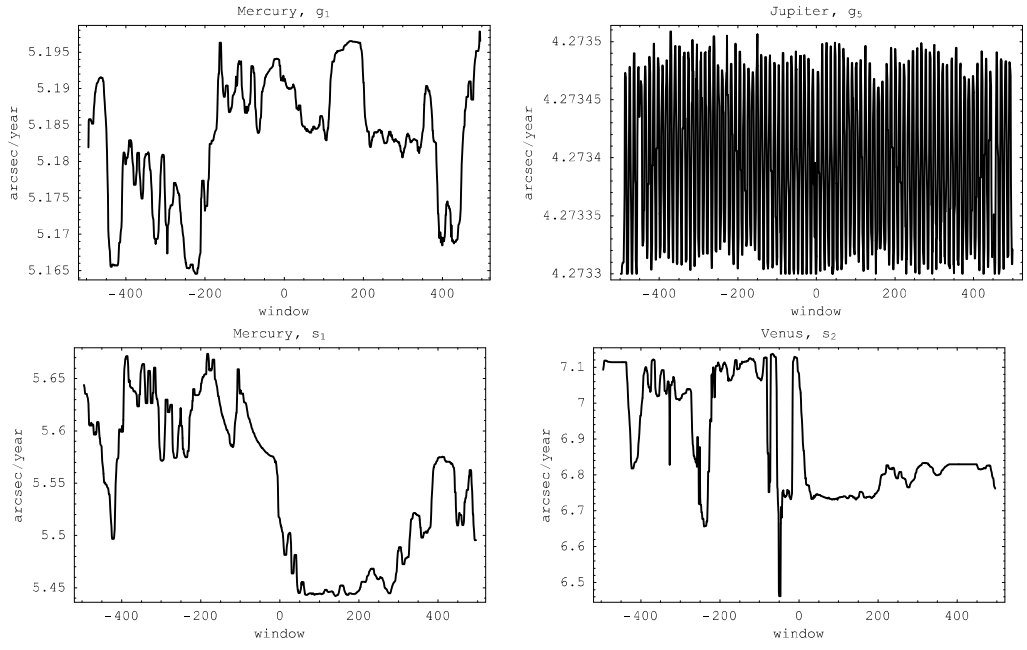

Figure 4. The evolution of the time varying fundamental frequencies g_1 of Mercury (upper left), g_5 of Jupiter (upper right), s_1 of Mercury (lower left) and s_2 of Venus (lower right) over 1 billion years. The samples shown correspond to the critical angle $(g_1 - g_5) - (s_1 - s_2)$.

In Laskar (1990) two angles related to the combinations of the secular frequencies associated with the perihelia and nodes of the planets are responsable

for the positive value of the Liapunov exponent in the order of 1/5 million years. Another numerical integration Laskar et al. (1992) confirmed the results found in the previous paper over the time span of 6 million years. The work of Dvorak et. al (2003) has increased the integration time up to 200 million years. Based on an extension of this work we will improve the accuracy of the determination of the critical angles and may find additional ones, when analyzing the fundamental frequency set.

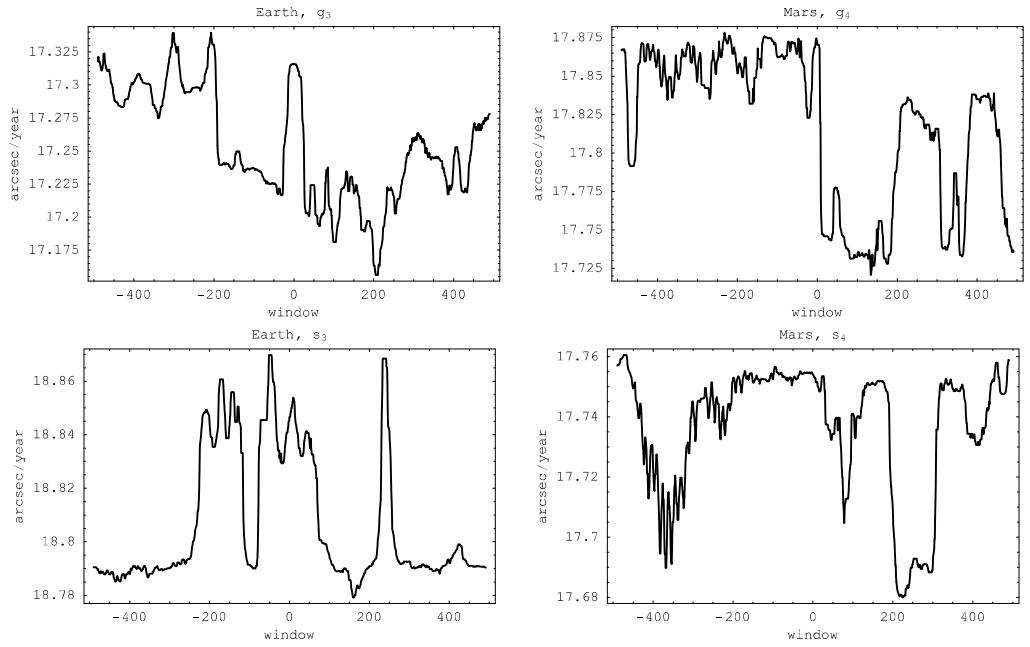

Figure 5. The evolution of the time varying fundamental frequencies g_3 of Earth (upper left), g_4 of Mars (upper right), s_3 of Earth (lower left) and s_4 of Venus (lower right) over 1 billion years in arcseconds per year. The samples shown correspond to the critical angle $2(g_3 - g_4) - (s_3 - s_4)$.

The evolution of the time varying fundamental frequencies g_i of the inner planets over the whole time span can be found in Fig. 6 (upper) and of s_i (lower). The time evolution of the respective frequencies for the outer planets g_i and s_i show no significant variations. The mean values of them over the whole integration time can be found in Tab. 2 (NEW). The standard deviation is small regarding the evolution of the frequencies of the outer planets, it is larger for the inner planetary system. The table compares the results of this work with an analytical work by Lagrange (LAG), a semianalytical approach by Laskar (NGT) and the values found by Gamsjäger (GAMS).

Due to the nonlinear structure of the system, the fundamental frequencies which are constant in the first order approximation of Laplace (see Eq.(1) - (3)) are in reality varying with time. Some of them look like, they are changing randomly (see Fig. 4 and Fig. 5), others look like they follow secular trends or seem to have periodic changes around their mean values. If some of them

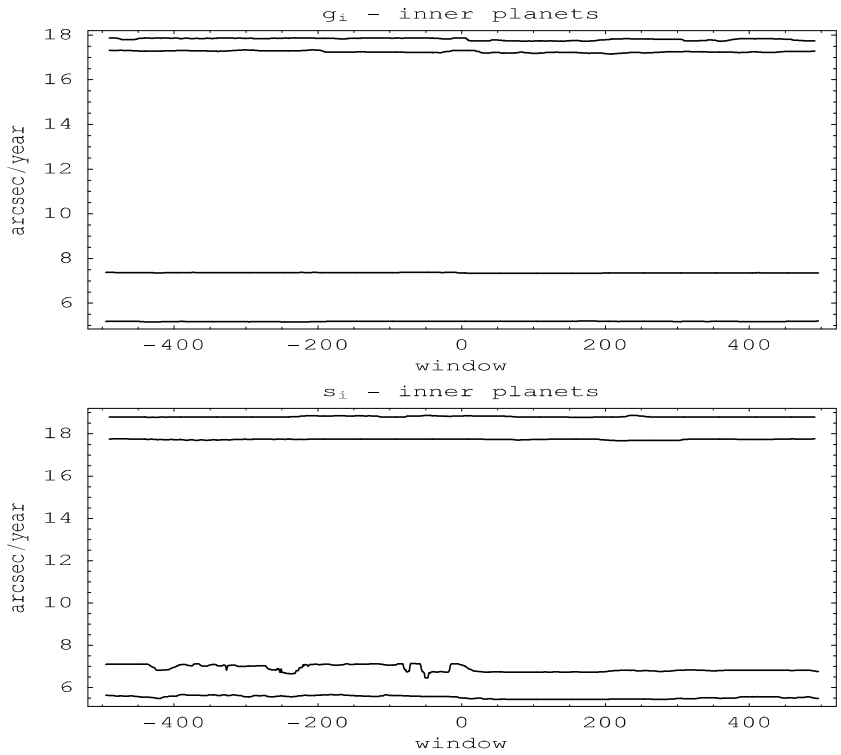

Figure 6. The evolution of the time varying fundamental frequencies g_i (upper panel) and s_i (lower) of the inner planets given in arcseconds per year.

in combination - called critical angles - lead to secular frequencies, their corresponding orbital elements may change from libration to circulation, so that they will cross the separatrix in the phase space - which will directly lead to chaos.

6. Conclusions

Although we were yet not able to confirm the resonant structure of our Solar System, we showed that the system is stable over 1 billion years. There is no planet showing any slightest sign of beeing unstable. The maximum values of the orbital elements also give no evidence, why one of the planets should escape in the next future. There exist a couple of resonances, which stabilize the whole system. The frequency spectrum, particularly the time evolution of the fundamental frequencies of the planets show a very irregular behaviour over the whole time span, if you take a closer look on it. The variances from the mean values are quite big – indicating the chaotical nature of the system. The outer bodies of the system show a more regular behaviour in their time-evolution of the orbital elements and fundamental frequencies (see Fig. 6, lower left and right panels), the inner bodies are highly chaotic but seem to be stabilized by the more massive outer bodies (see Fig. 6, upper left and

Table 2. Fundamental Frequencies of the planets in arcseconds per year. LAG is based on the analytical result of Lagrange (analytical), NGT is the work of Laskar (semianalytical), GAMS presents the results of Gamsjäger (numerical). Our new results are based on windowed frequency analysis with a lag size of 10 million years (1000 lag windows) and average over the elements (h, k, p, q).

Planet	**LAG**	**NGT**	**GAMS**	***NEW***
g_1	5.4615	5.5689	5.2130	5.1832 $\pm$ 0.0086
g_2	7.3459	7.4555	7.3343	7.3592 $\pm$ 0.0124
g_3	17.3307	17.3769	17.5022	17.2541 $\pm$ 0.0419
g_4	18.0042	17.9217	17.8921	17.8176 $\pm$ 0.0050
s_1	-5.2007	-5.6043	-5.5010	-5.5467 $\pm$ 0.0739
s_2	-6.5701	-7.0530	-6.2230	-6.8978 $\pm$ 0.1528
s_3	-18.7455	-18.8499	-18.8574	-18.8069 $\pm$ 0.02501
s_4	-17.6358	-17.7614	-17.7167	-17.7363 $\pm$ 0.0216
g_5	3.7109	4.2489	4.2567	4.2743 $\pm$ 0.00007
g_6	22.2868	27.9606	28.2445	28.2523 $\pm$ 0.00006
g_7	2.7014	3.0695	3.0468	3.1075 $\pm$ 0.0022
g_8	0.6333	0.6669	0.6727	0.6711 $\pm$ 0.00003
s_5	-0.0000	-0.0000	-0.0000	0.0000
s_6	-25.7411	-26.3300	-26.3473	-26.3256 $\pm$ 0.00007
s_7	-2.9038	-2.9854	-2.9944	-2.9818 $\pm$ 0.00008
s_8	-0.6777	-0.6927	0.7381	-0.6710 $\pm$ 0.0001

right panels). The windowed fourier transform is a good tool, when analyzing the time dependent and nonlinear time-evolution of the orbital elements, lag windows of 10 million years overlapping with one million year produced good results. We were not able to confirm the resonances proposed by Laskar (1990) yet, but look forward to find them and maybe additional ones, when using the larger integration time for the simulation of our Solar System.

Acknowledgments

We wish to thank the Hochschuljubiläumsstiftung der Stadt Wien (project H-1217/03) and the Austrian Science Foundation (FWF, P16024-N05).

References

[1] Applegate, J. H., Douglas, M. R., Gursel, Y., Sussman, G. J., Wisdom, J., 1986: "The outer solar system for 200 million years", *Astronomical Journal* **92**, pp.176-194.

[2] Bretagnon, P. 1982: "Theory of the motion of all planets - The VSOP82 solution", *Astronomy and Astrophysics* **114**, pp.278-288.

[3] Bretagnon, P. 1982: "Long periodic terms in the solar system", *Astronomy and Astrophysics* **30**, pp.141-154.

[4] Bretagnon, P. 1982: "Integration constants and mean elements for the planetary system", *Astronomy and Astrophysics* **108**, pp.69-75 (in french).

[5] Bretagnon, P. 1982: "Theory of the inner planets", *Celestial Mechanics and Dynaical Astronomy* **26**, pp.161-167.

[6] Brouwer, D., van Woerkom, A.J., 1950: "The secular variations of the orbital elements of the principal planets", *Astronomical Papers of the American Ephermeri and Nautic Almanac* **XIII**, part II.

[7] Brouwer, D., 1955: "The motions of the outer planets (George Darwin Lecture)", *Monthly Notices of the Royal Astronomical Society* **115**, p.221.

[8] Brouwer, D. VanWoerkom, A., Jasper, J., 1950: "The secular variations of the orbital elements of the principal planets", *Washington, U.S.Gov.Print.Off.1950*

[9] Carpino, M., Milani, A. Nobili, A.M., 1987: "Long-term numerical integrations and synthetic theories for the motion of the outer planets", *Astronomy and Astrophysics* **181**, pp.182-194.

[10] Chapront, J., 1995: "Representation of planetary ephemerides by frequency analysis. Application to the five outer planets", *Astronomy and Astrophysics* **109**, pp.181-192.

[11] Clemence, G.M., Brouwer, D., 1951: "The motions of the Five Outer Planets", *Sky and Telescope* **10**, p.83.

[12] Cohen & Hubbard, 1965, "Libration of the close approaches of Pluto to Neptune" *Astronomical Journal* **70**, pp.10ff.

[13] Cohen & Hubbard, 1973, "Elements of the outer planets for one million years" *Washington, Nautical Almanac Office* **92**

[14] Duncan, M.J., Lissauer, J., 1998: "The Effect of Post-Main-Sequence Solar Mass Loss on the sability of Our Planetary System", *Icarus* **134**, pp.303-310.

[15] Dvorak, R., 1992: "Unser Planetensystem - ein chaotisches Uhrwerk", *Sitzungsberichte der mathematisch-naturwissenschaftlichen Klasse der österreichischen Akademie der Wissenschaften, Abt.II* **Band 201**, pp.131-159.

[16] Dvorak, R., Freistetter, F., 2001: "Ist Merkur auf einer chaotischen, instabilen Bahn", *Algorismus* **37**, pp.25-37.

[17] Dvorak, R., Gamsjäger, C., 2003: "A New Determination of the Basic Frequencies in Planetary Motion", *Proceedings of the 3rd Austrian-Hungarian Workshop on Trojans and related Topics (Eds. F. Freistetter, R. Dvorak and B. Érdi* **3**, pp.49-58.

[18] Eckert et al., 1951:, *Astronomical Papers of the American Ephermeris and Nautical Almanaca,* **XII**

[19] Hanslmeier, A., Dvorak, R., 1984: "Numerical Integration with Lie-series", *Astronomy and Astrophysics* **132**, pp.203-211.

[20] Ito, T., Tanikawa K., 2000: "Long-term stability of our solar system", *Proceddings of the 32nd Symposium on Celestial Mechanicsm Hayama, Kanagawa*, Graduate University of Advanced Studies, pp.47-96.

[21] Ito, T., Kinoshita, H., Nakai, H., Fukushima, T. 1996, "Numerical Experiments to Inspect the Long-Term Stability of the Planetary Motion" *Proceedings of the 28th Symposium on Celestial Mechanics, held 29-30 January, 1996 in Tokyo, Japan. Edited by Hiroshi Kinoshita and Hiroshi Nakai. Tokyo, Japan, 1996.*, p.123.

[22] Kinoshita, H., Nakai, H., 1984, "Motions of the perihelions of Neptune and Pluto" *Celestial Mechanics and Dynamical Astronomy* **34**, pp.203ff.

[23] Laskar, J., 1984: "Progress in General Planetary Theory", *Celestial Mechanics and Dynamical Astronomy* **34**, pp.219ff.

[24] Laskar, J., 1988: "Secular evolution of the solar system over 10 million years", *Astronomy and Astrophysics* **198**, pp.341-362.

[25] Laskar, J., 1990: "The chaotic Motion of the Solar System. A numerical estimate of the size of the chaotic zones", *Icarus* **88**, pp.266-291.

[26] Laskar, J., Quinn, T., Tremaine, S., 1992: "Confirmation of the Resonant Structure in the Solar System", *Icarus* **95**, pp.148-152.

[27] Laskar, J., 1993: "Frequency Analysis of a Dynamical System", *Celestial Mechanics and Dynamical Astronomy* **56**, pp.291-196.

[28] Milani, A., Nobili, A.M., Carpino, M.:, 1987: "Secular Variations of the semimajor axes - Theory and experiments", *Astronomy and Astrophysics* **172**, pp.265-279.

[29] Murray, C.D., Dermott, S.F., 1999: "Solar System Dynamics", *Cambridge University Press*

[30] Nakai, H., Kinoshita, H., 1995: "Simulation of the Outer Planets System", *Proceedings of the 27th Symposium on Celestial Mechanics, held 10-11 January, 1995 in Tokyo, Japan. Edited by Hiroshi Kinoshita and Hiroshi Nakai. Tokyo, Japan, 1995.* **27**, p1.

[31] Newhall et al., 1983: "Solar System Dynamics", *Cambridge University Press*

[32] Nobili, A.M., Milani, A., Carpino, M., 1989: "The fundamental frequencies and small divisors in the orbits of the outer planets", *Astronomy and Astrophysics* **210**, pp.313-336.

[33] Quinn, T.R., Tremaine S., Duncan M., 1991: AJ, 101, 2287

[34] Richardson, D.L., Walker, C.F., 1989: "Numerical Simulation of the Nine-body Planetary System Spanning Two Million Years", *The Journal of Astronautical Sciences* **37**, pp.159-182.

[35] Sussman, G.J., Wisdom, J., 1988: *Science* **241, 5066**, pp.433.

[36] Sussman, G.J., Wisdom, J., 1992: "Chaotic Evolution of the solar system", *Science* **257, 5066**, pp.56-62.

[37] Süli, A., Dvorak, R. 1991: "The fundamental frequencies of N-body systems", *2nd Workshop of Young Researchers in Astronomy & Astrophysics, Publications of the Astronomy Department of the Eötvös University (PADEU)* **12**, p.38-44

[38] Wisdom, J., Sussman, G.J., 1991: "Chaotic Evolution of the Solar System", *Bulletin of the American Astronomical Society* **23**, pp.1231.

THE ROTATION OF IRREGULARLY SHAPED NATURAL SATELLITES IN THE SOLAR SYSTEM

Thomas Löeger and Maria G. Firneis
Institute of Astronomy
University of Vienna
Türkenschanzstrasse 17
A-1180 Vienna, Austria
T.Loeger@gmx.at

Abstract The temporal evolution of the rotational motion along with the attitude of a set of irregularly shaped small planetary satellites is studied. For this problem a computer application was developed featuring an FFT implementation scalable in terms of the available computer hardware optimized for fast execution, performed by reducing the amount of mass-storage operations with the aid of an adaptive multi-buffer cache strategy. Every satellite is modelled as a homogenous triaxial ellipsoid precessing under the torque of the main body. For a set of eight satellites the evolution of their spin-angular velocity vectors is numerically tracked using non-singular matrix differential equations. Calculations were carried out with a 4^{th} order Runge-Kutta algorithm using a grid of 1620 different initial conditions for the attitudes of the satellites. An FFT was applied to the results to observe, whether the spin axis tumbles chaotically in conjunction with chaotic rotation, or if the obliquity and the spin angular velocity remains constant or changes periodically for certain initial conditions. It is shown that for each satellite investigated a regular rotation is possible for spin axes with an obliquity near zero degrees. Other stable regions exist for each satellite as well. For Proteus, a satellite of Neptune, the stable region is maximally extended of all objects investigated.

Keywords: Satellites – Rotation – Stability

1. Introduction

The investigation of the temporal evolution of the spin-axes of natural satellites has a long history in celestial mechanics (see [11], [10], [14], [13], [6], [3], [7], [8]). The stability of the attitude of the rotation axes and the existence of resonant spin states is of special interest. All the above mentioned investigations have in common that a spin axis perpendicular to the orbital plane was

assumed. Thus only a small region in the phase space was investigated or the calculations were only carried out for one satellite.

Due to tidal forces rotational evolution tends to erect the spin axis until it is perpendicular to the orbital plane of the satellite. For some satellites these spin states however are not stable, e.g. for Hyperion. This behavior can only be found if a satellite is non-spherical, hence small in size. A numerical analysis of the stability of the attitude and the spin period of small, irregularly shaped natural satellites with an obliquity between 0 and 45 degrees with an unknown rotation state is presented in this work.

This analysis was performed with the aid of computer programs written in C# and Mathematica. This extensive program package can be used for further research tasks.

2. Theory

Many satellites' highly aspherical shapes can roughly by described as ellipsoidals. For the orientation of a satellite with respect to the main body two sets of coordinates are necessary; a reference frame and a body frame. The origins of both sets are situated in the satellites' center of mass. Every vector in the reference frame can be expressed in terms of the body frame with the aid of 3 right-hand rotations (through 3 Eulerian angles) around a sequence of (principal) body axes [4], [12]. Every rotation can be described by a 3x3 matrix with time-dependent elements. Consequently differential equations with the Eulerian angles as variables, describing the time development of the spin axis, are developed.

A body fixed coordinate system is given as follows. Let three vectors, $\overrightarrow{a}$, $\overrightarrow{b}$ and $\overrightarrow{c}$ define a right-hand set of axes fixed to the satellite which correspond to the principal moments of inertia $A \leq B \leq C$.

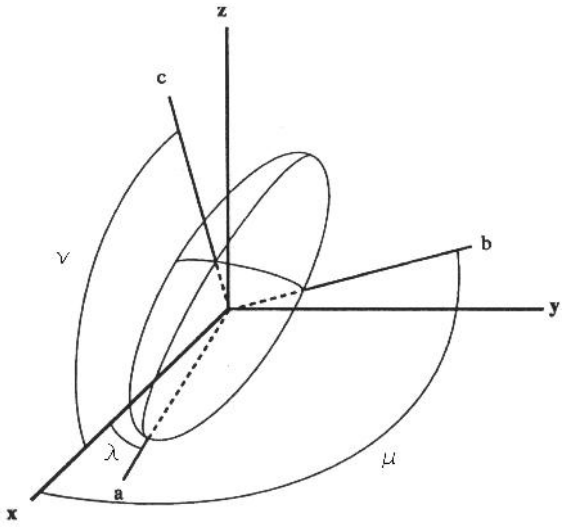

The reference coordinate system is given as follows. The trihedral $(\overrightarrow{x},\ \overrightarrow{y},\ \overrightarrow{z})$ is defined as:

$\overrightarrow{x}$ axis parallel to the planet-to-satellite vector,

$\overrightarrow{y}$ axis parallel to the orbital velocity,

$\overrightarrow{z}$ axis normal to the orbit of the satellite.

Starting with this reference system the trihedral system $\left(\overrightarrow{a},\ \overrightarrow{b},\ \overrightarrow{c}\right)$ is obtained through the rotation along the Eulerian angles $(\psi,\ \theta,\ \varphi)$:

At first the body axes are rotated around the $\overrightarrow{z}$ axis along an angle ψ, then around the new $\overrightarrow{x}$ axis (denoted by $\overrightarrow{x'}$) along an angle θ and finally around the new $\overrightarrow{z}$ axis (denoted by $\overrightarrow{c}$) along an angle φ.

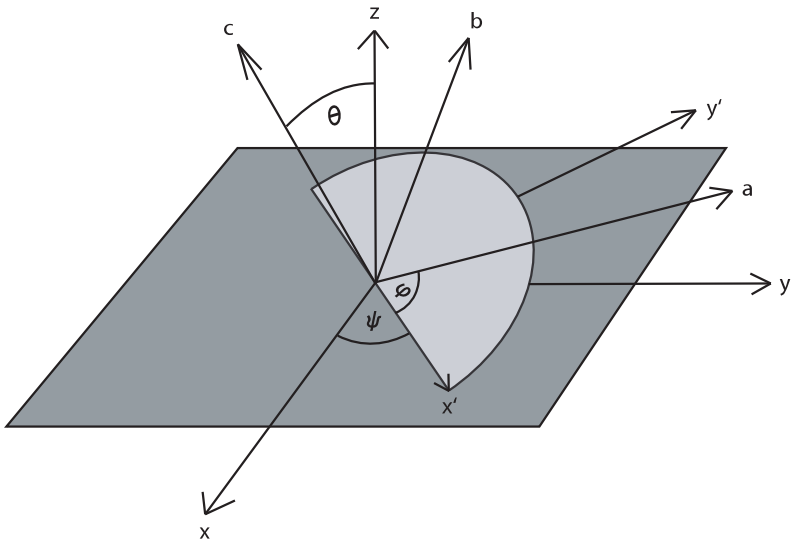

The axes $\overrightarrow{x},\ \overrightarrow{y}$ are rotated along the Eulerian angle ψ to give $\overrightarrow{x'},\ \overrightarrow{y'}$.

For the direction cosines $(\lambda,\ \mu,\ \nu)$ [6] one obtains:

$$\begin{aligned} \lambda &= \cos(\varphi)\cos(\psi) - \sin(\varphi)\cos(\theta)\sin(\psi), \\ \mu &= -\cos(\varphi)\sin(\psi) - \sin(\varphi)\cos(\theta)\cos(\psi), \\ \nu &= \sin(\theta)\sin(\varphi). \end{aligned} \tag{1}$$

With the components $(\omega_a,\ \omega_b,\ \omega_c)$ of the angular velocity vector referenced to the axes $\left(\overrightarrow{a},\ \overrightarrow{b},\ \overrightarrow{c}\right)$ the Eulerian equations can be written as [2]:

$$\begin{aligned} A\cdot\frac{\mathrm{d}\omega_a}{\mathrm{d}t} - (B-C)\cdot\omega_b\cdot\omega_c &= -\frac{3\cdot M\cdot G}{r^3}\cdot(B-C)\cdot\mu\cdot\nu, \\ B\cdot\frac{\mathrm{d}\omega_b}{\mathrm{d}t} - (C-A)\cdot\omega_c\cdot\omega_a &= -\frac{3\cdot M\cdot G}{r^3}\cdot(C-A)\cdot\nu\cdot\lambda, \\ C\cdot\frac{\mathrm{d}\omega_c}{\mathrm{d}t} - (A-B)\cdot\omega_a\cdot\omega_b &= -\frac{3\cdot M\cdot G}{r^3}\cdot(A-B)\cdot\lambda\cdot\mu. \end{aligned} \tag{2}$$

The equations in terms of the Eulerian angles experience a singularity however, when the spin axis is perpendicular to the orbital plane [5].

To circumvene this problem the attitude of the satellite with respect to its main body can be described as follows.

An initial coordinate system $(\overrightarrow{x},\ \overrightarrow{y},\ \overrightarrow{z})$ is given in such a way that the x axis is pointing from the main body to the perihelion of the satellites' orbit. The z axis is perpendicular to the $(x,\ y)$ plane originating in the center of the main body.

Let the principal moments of inertia be $(A,\ B,\ C)$. Three axis $\left(\overrightarrow{a},\ \overrightarrow{b},\ \overrightarrow{c}\right)$ parallel to these principal moments can be used to describe a coordinate system fixed to the satellite (body fixed coordinate system).

E_{ij} are the cosines of the angle between the i^{th} body fixed axis (a, b, or c) and the j^{th} initial axis (x, y, or z). The nine E_{ij}s represent a 3x3 rotation matrix E. With the aid of this matrix, every vector in the initial frame can be transformed to the corresponding vector in the body fixed (rotating) frame. Because of the orthogonality of E, the transposed matrix E^t describes the inverse transformation.

Let $\overrightarrow{l}$ be the torque and let $\overrightarrow{\omega}$ be the angular velocity vector of the satellite in the inertial frame.

Furthermore let $\overrightarrow{\sigma} \equiv \overrightarrow{\omega}\frac{\mathrm{d}t}{\mathrm{d}f}$ with f denoting the true anomaly. One can define $\overrightarrow{L} = E\overrightarrow{l}$ as torque and $\overrightarrow{\Omega} = E\overrightarrow{\omega}$ as the spin angular velocity vector in the body fixed frame, thus $\overrightarrow{\Sigma} \equiv \overrightarrow{\Omega}\frac{\mathrm{d}t}{\mathrm{d}f} = E\overrightarrow{\sigma}$.

The components of the torque in the body fixed coordinate system are:

$$L_A = A\,\Omega_A, \tag{3}$$

$$L_B = B\,\Omega_B, \tag{4}$$

$$L_C = C\,\Omega_C. \tag{5}$$

This leads to the following form of the Eulerian equations [5]:

$$\begin{aligned}
\frac{\mathrm{d}}{\mathrm{d}f}\Sigma_A &= \frac{\Sigma_A 2e\sin(f)}{1+e\cos(f)} - \alpha\Sigma_B\Sigma_C + \\
&\quad \frac{3\alpha\left(E_{21}\cos(f)+E_{22}\sin(f)\right)\left(E_{31}\cos(f)+E_{32}\sin(f)\right)}{1+e\cos(f)}, \\
\frac{\mathrm{d}}{\mathrm{d}f}\Sigma_B &= \frac{\Sigma_B 2e\sin(f)}{1+e\cos(f)} + \beta\Sigma_A\Sigma_C - \\
&\quad \frac{3\beta\left(E_{11}\cos(f)+E_{12}\sin(f)\right)\left(E_{31}\cos(f)+E_{32}\sin(f)\right)}{1+e\cos(f)}, \\
\frac{\mathrm{d}}{\mathrm{d}f}\Sigma_C &= \frac{\Sigma_C 2e\sin(f)}{1+e\cos(f)} - \gamma\Sigma_A\Sigma_B + \\
&\quad \frac{3\gamma\left(E_{11}\cos(f)+E_{12}\sin(f)\right)\left(E_{21}\cos(f)+E_{22}\sin(f)\right)}{1+e\cos(f)}.
\end{aligned} \tag{6}$$

With the following equations, one can describe the temporal evolution of the spin axis of a satellite with the aid of direction cosines:

$$\begin{aligned}
\frac{\mathrm{d}}{\mathrm{d}f}E_{11} &= \Sigma_C E_{21} - \Sigma_B E_{31}, \\
\frac{\mathrm{d}}{\mathrm{d}f}E_{21} &= \Sigma_A E_{31} - \Sigma_C E_{11}, \\
\frac{\mathrm{d}}{\mathrm{d}f}E_{31} &= \Sigma_B E_{11} - \Sigma_A E_{21}, \\
\frac{\mathrm{d}}{\mathrm{d}f}E_{12} &= \Sigma_C E_{22} - \Sigma_B E_{32}, \\
\frac{\mathrm{d}}{\mathrm{d}f}E_{22} &= \Sigma_A E_{32} - \Sigma_C E_{12}, \\
\frac{\mathrm{d}}{\mathrm{d}f}E_{32} &= \Sigma_B E_{12} - \Sigma_A E_{22}, \\
\frac{\mathrm{d}}{\mathrm{d}f}E_{13} &= \Sigma_C E_{23} - \Sigma_B E_{33}, \\
\frac{\mathrm{d}}{\mathrm{d}f}E_{23} &= \Sigma_A E_{33} - \Sigma_C E_{13}, \\
\frac{\mathrm{d}}{\mathrm{d}f}E_{33} &= \Sigma_B E_{13} - \Sigma_A E_{23}.
\end{aligned} \tag{7}$$

3. Numerical investigation

A computer program in C# was developed to numerically integrate the equations of motion. For this purpose a 4^{th} order Runge-Kutta [9] with variable

step-size was used. The results were analyzed by calculating a frequency spectrum using an optimized Fast Fourier (FFT) algorithm implemented by one of the authors of this treatise (T. Loeger). This implementation contains an intelligent multi-buffer cache strategy to reduce Hard-Disk operations.

To visualize the results, the program was designed to create Mathematica notebooks with dynamically structured plot-expressions. A specially designed notebook is used to read all these notebooks and execute them. After the paths to the output-files of the C# program are properly set, this notebook reads all the files and creates the plots showing the results of the integration. The formulae used by the application were set up by Mathematica.

It is sufficient to describe the initial attitude of a satellite in terms of two angles as initial conditions rather than using the elements of the rotation matrix E.

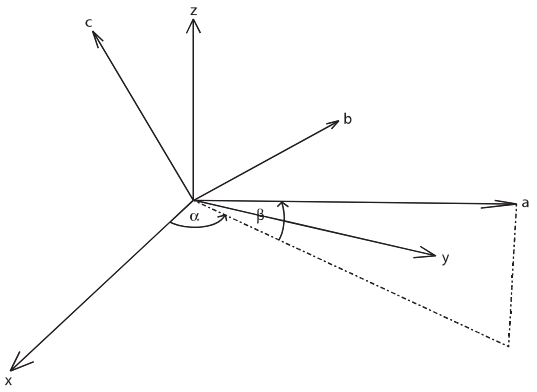

The angle α is varied between 0 and 180 degrees in steps of 5 degrees, β is varied between 0 and 45 degrees in steps of 1 degrees. The mean rotation period expressed in terms of the true anomaly (corresponding to normalization) was selected as the z-element of the spin angular velocity vector.

The variation of the spin axis attitude and the evolution of the spin angular velocity vector were calculated for 1620 initial conditions with a 4^{th} order Rung-Kutta algorithm.

An FFT was applied to the results obtained above. For each satellite and initial condition, a histogram over all the frequencies obtained in the Fourier-spectra was calculated. Histograms were used to distinguish the frequencies indicating resonant spin states and "noise"-frequencies.

For each satellite a plot for all initial conditions was created showing the values of the remaining frequency-peaks found for each initial condition (see Fig. 1 – Fig. 8).

4. Results

The frequency-values in terms of the orbital period were gray-coded as shown in Fig. 1 – Fig. 8. Left to each figure values markers of the correspond-

ing frequencies are displayed. Due to the fact, that the frequency corresponding to a certain gray-code differs for each satellite, these code plots cannot be directly compared, with the exception that black regions always indicate initial conditions for which the satellite's rotation state becomes chaotic. Each point in the plot corresponds to the result of one initial condition for α and β, where alpha is the azimuthal and beta the polar angle describing the initial attitude of the satellite (the initial conditions for the subsequent integration).

4.1 Satellites of Jupiter

4.1.1 Adrastea.

Physical and orbital characteristics	
Period of revolution [days]	0.29826
Eccentricity	0.0018
Mass of main body (Jupiter) [kg]	$1.899 \cdot 10^{27}$
Mass of satellite [kg]	$1.91 \cdot 10^{16}$
Diameter [km]	$25 \times 20 \times 15$

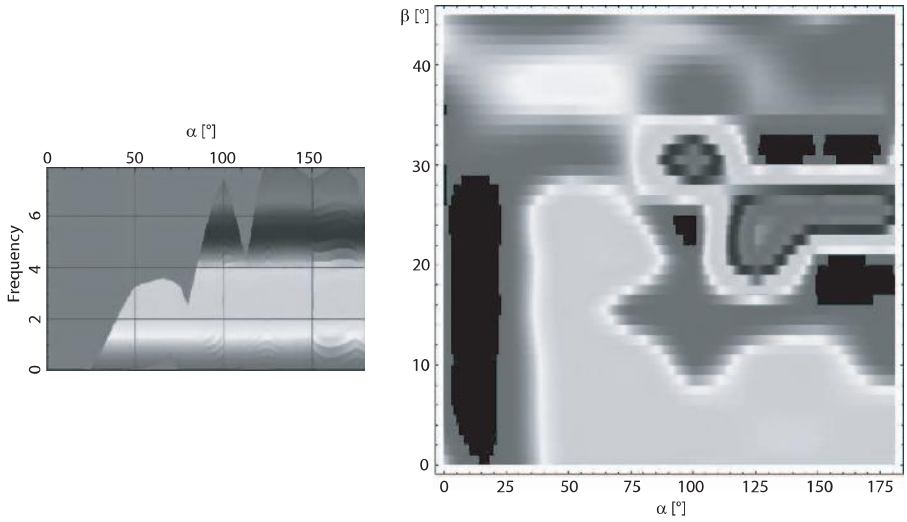

Figure 1. A plot showing the gray-coded values of the frequency-peaks found for all initial conditions (α,β) for Adrastea.

As one can see in Fig. 1 the eccentricity e is relatively large, leading to a large chaotic region for values of the azimuthal angle α between 10 and 20 degrees and the polar angle β between 0 and 30 degrees (black regions in the right plot of Fig. 1). Small regions of initial conditions leading to chaotic rotation can be found for alpha between 150 and 180 degrees and beta between 18 and 20 degrees and beta between 35 and 40 degrees. In the region of initial conditions leading to regular rotation states, one observes resonances between 2:1 and 3:1 for alpha between 50 and 180 degrees and beta between 0 and 20 degrees and

an approximate 1:1 resonance for alpha between 0 and 180 degrees and beta between 32 and 45 degrees.

4.2 Satellites of Saturn

4.2.1 Atlas.

Physical and orbital characteristics	
Period of revolution [days]	0.6019
Eccentricity	0
Mass of main body (Saturn) [kg]	$5.6846 \cdot 10^{26}$
Mass of satellite [kg]	$1.91 \cdot 10^{16}$
Diameter [km]	$18.5 \times 17.2 \times 13.5$

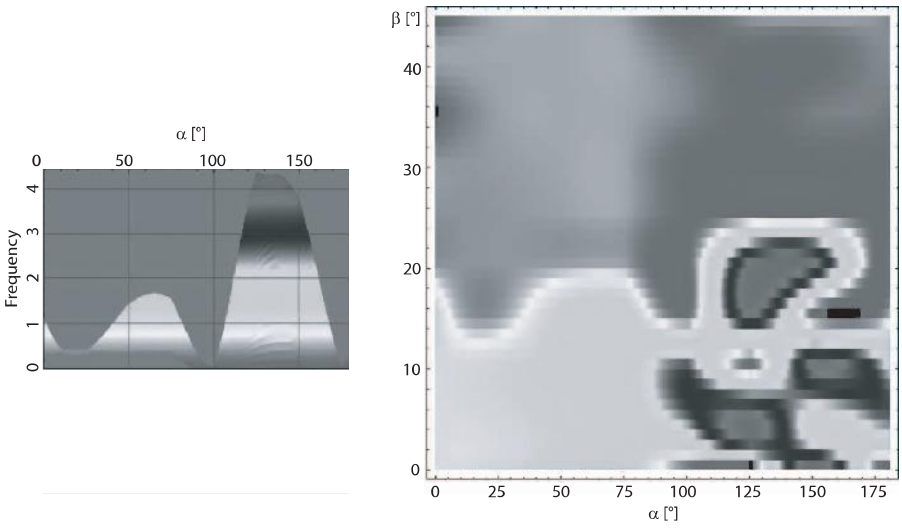

Figure 2. A plot showing the gray-coded values of the frequency-peaks found for all initial conditions (α,β) for Atlas.

The eccentricity e is zero, leading only to non-chaotic regions as one can observe in Fig. 2. One can find initial conditions leading to resonances between 1:1 and 2:1 for values of alpha between 0 and 80 degrees and beta between 0 and 15 degrees and 1:2 resonances for alpha between 0 and 80 degrees and beta between 20 and 45 degrees.

4.2.2 Prometheus.

Physical and orbital characteristics	
Period of revolution [days]	0.61299
Eccentricity	0.0024
Mass of main body (Saturn) [kg]	$5.6846 \cdot 10^{26}$
Mass of satellite [kg]	$3.3 \cdot 10^{17}$
Diameter [km]	$145 \times 85 \times 65$

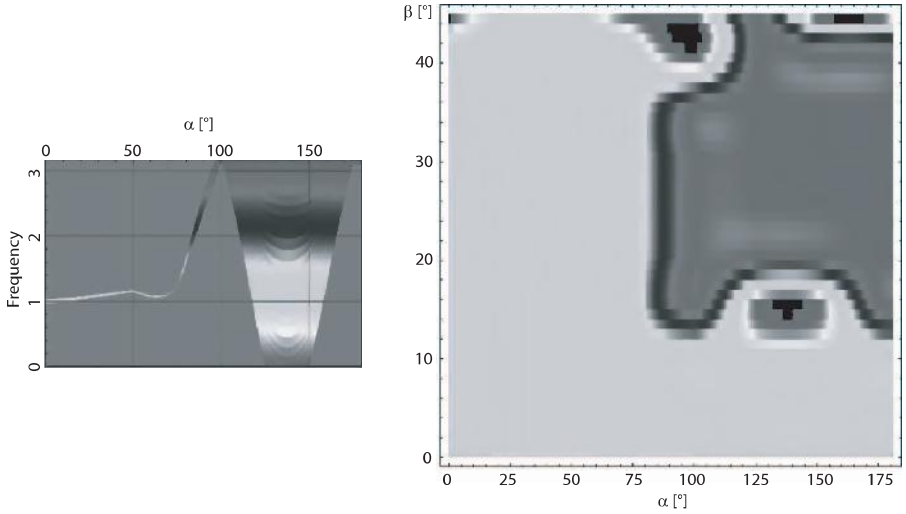

Figure 3. A plot showing the gray-coded values of the frequency-peaks found for all initial conditions (α,β) for Prometheus.

The eccentricity e is relatively small, leading to small chaotic regions for values of alpha between 110 and 120 degrees and for values of beta around 10 degrees, around values of alpha 70 degrees and 150 degrees, and values of beta between 35 and 45 degrees (shown black in Fig. 3). One can find large regions of initial conditions leading to 1:1 and 1:3 resonances for initial conditions for alpha between 0 and 180 degrees and for beta between 0 and 20 degrees, and further for alpha between 0 and 50 degrees and beta between 0 and 45 degrees.

4.2.3 Pandora.

Physical and orbital characteristics	
Period of revolution [days]	0.628
Eccentricity	0.0042
Mass of main body (Saturn) [kg]	$5.6846 \cdot 10^{26}$
Mass of satellite [kg]	$1.94 \cdot 10^{17}$
Diameter [km]	$114 \times 84 \times 62$

The eccentricity e is relatively large, leading to a large chaotic region for initial conditions for alpha between 0 and 10 degrees and beta between 20 and 30 degrees, and a small region for initial conditions for alpha of 100 and 130 degrees and values of beta for 25 and 40 degrees (black regions in Fig. 4). One can find initial conditions leading to resonances between 1:1 and 2:1 for initial conditions of alpha between 50 and 180 degrees and beta between 0 and 15 degrees.

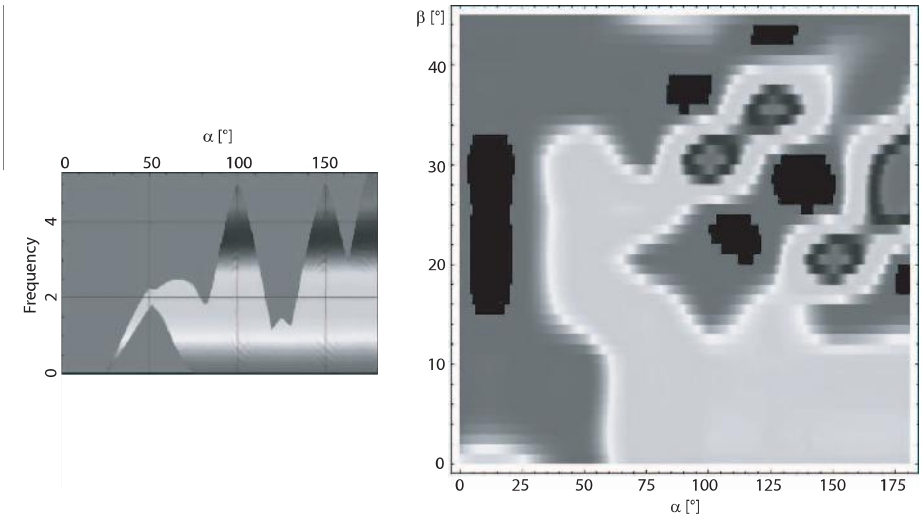

Figure 4. A plot showing the gray-coded values of the frequency-peaks found for all initial conditions (α,β) for Pandora.

4.2.4 Telesto.

Physical and orbital characteristics	
Period of revolution [days]	1.8878
Eccentricity	0
Mass of main body (Saturn) [kg]	$5.6846 \cdot 10^{26}$
Diameter [km]	$34 \times 28 \times 26$

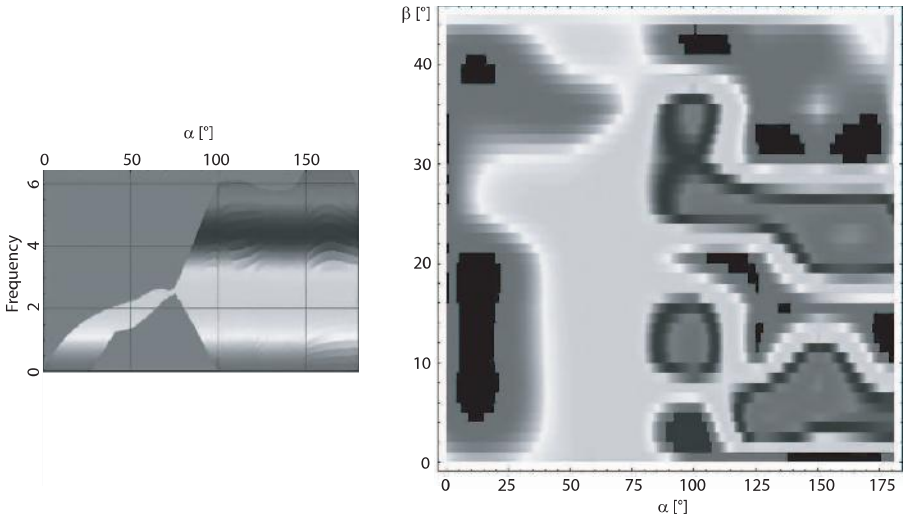

Figure 5. A plot showing the gray-coded values of the frequency-peaks found for all initial conditions (α,β) for Telesto.

Even if Telesto's eccentricity is zero, one can recognize many initial conditions leading to chaotic rotation, because Telesto is highly aspherical. These

regions can be found for alpha around 10, 100 and 180 degrees and for initial conditions for beta between 10 and 30 degrees, at 0 degrees and at 30 degrees (black regions in Fig. 5). A distinct region leading to a 1:2 resonance can be observed in the diagrams of Fig. 5 for values of alpha between 30 and 40 degrees and beta between 0 and 40 degrees.

4.2.5 Calypso.

Physical and orbital characteristics	
Period of revolution [days]	1.8878
Eccentricity	0
Mass of main body (Saturn) [kg]	$5.6846 \cdot 10^{26}$
Diameter [km]	$34 \times 22 \times 22$

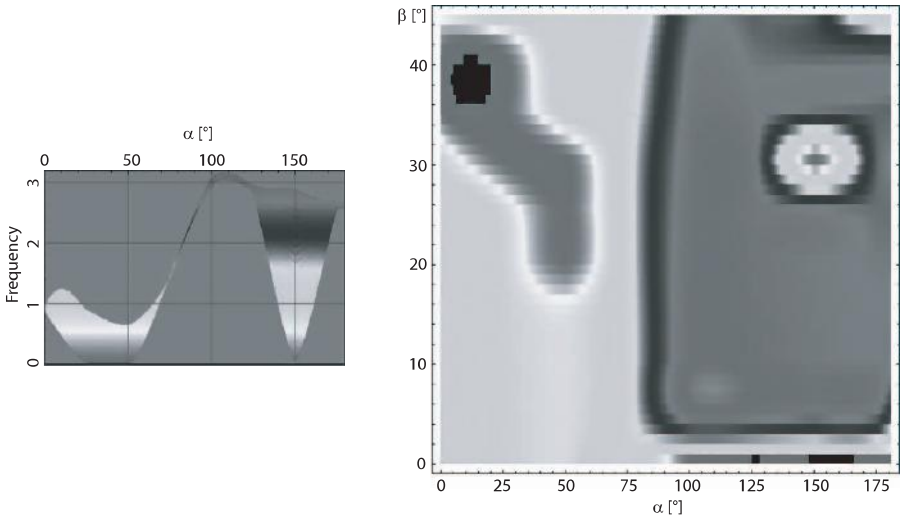

Figure 6. A plot showing the gray-coded values of the frequency-peaks found for all initial conditions (α,β) for Calypso.

Considering the very small eccentricity of Calypso, only a small chaotic region can be observed. This region can be found for initial conditions of alpha around 10 degrees and for beta around 35 degrees (black regions in Fig. 6). There is a large region of initial conditions leading to a 3:1 resonance for alpha between 70 and 180 degrees and beta between 5 and 45 degrees and a region of initial conditions leading to 1:1 resonances for alpha between 0 and 70 degrees and beta between 0 and 40 degrees.

4.2.6 Helene.

Physical and orbital characteristics	
Period of revolution [days]	2.7369
Eccentricity	0.0022
Mass of main body (Saturn) [kg]	$5.6846 \cdot 10^{26}$
Diameter [km]	$34 \times 22 \times 22$

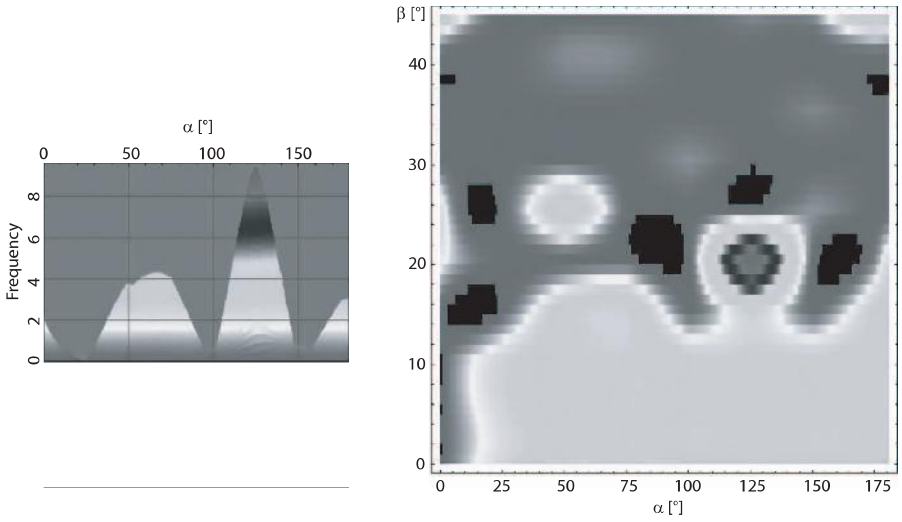

Figure 7. A plot showing the gray-coded values of the frequency-peaks found for all initial conditions (α,β) for Helene.

Even though the eccentricity of this satellite is small, some chaotic regions are visible, more precisely at alpha around 10 degrees, 80 degrees, 170 degrees and 180 degrees and beta around 20, 30 and 40 degrees (black regions in Fig. 7). There is a large region of initial conditions leading to resonances between 1:2 and 1:4 at alpha between 20 and 180 degrees and beta between 0 and 20 degrees, and a region leading to a 1:1 resonance for alpha between 0 and 180 degrees and beta greater than 25 degrees.

4.3 Satellites of Neptune

4.3.1 Proteus.

Physical and orbital characteristics	
Period of revolution [days]	1.122
Eccentricity	0.0022
Mass of main body (Neptune) [kg]	$1.0243 \cdot 10^{26}$
Mass of satellite [kg]	$5 \cdot 10^{19}$
Diameter [km]	$440 \times 416 \times 404$

Proteus is nearly spherical, but its orbit shows a small eccentricity, so there are some regions leading to chaotic rotation for initial conditions for alpha of 10 and 140 degrees and for beta at 15 and 40 degrees (black regions in the right plot above). A large region leading to a synchronous rotation state (1:1 resonance) can be observed for alpha between 0 and 180 degrees and beta between 0 and 15, respectively 45 degrees, as well as a region leading to a 3:1 resonance for alpha between 100 and 180 degrees and beta between 10 and 40 degrees.

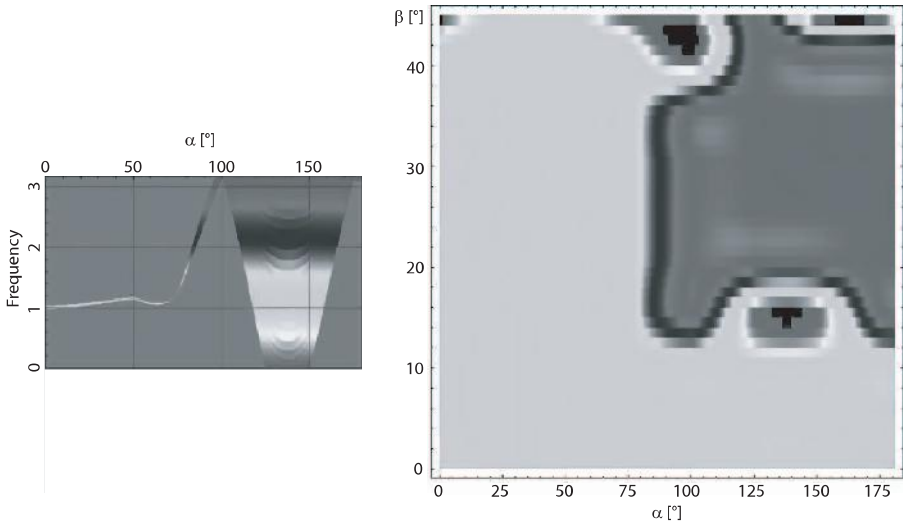

Figure 8. A plot showing the gray coded values of the frequency-peaks found for all initial conditions (α,β) for Proteus.

References

[1] Boehme, G. 1991, Algebra 7. Auflage,
Springer-Verlag, Berlin, Heidelberg, New York

[2] Danby, J. M. A. 1992, Fundamentals of Celestial Mechanics, Second Edition (Willmann-Bell)

[3] Dobrovolskis, R., Anthony 1995, Chaotic Rotation of Nereid?,
Icarus, **118**, 181-198

[4] Goldstein, H. 1950, Classical Mechanics,
Addison-Wesley, Reading, Mass.

[5] Julian, W. H. 1990, The Comet Halley nucleus: Random jets,
Icarus, **88**, 355-371

[6] Klavetter, James, Jay 1989, Rotation of Hyperion II Dynamics,
The Astronomical Journal, **98**, 5, 1855-1874

[7] Kouprianov, V. V., Shevchenko, I. I. 2002, On the chaotic rotation of planetary satellites: The Lyapunov spectra and the maximum Lyapunov exponents,
Astron. and Astrophysics, **394**, 663-674

[8] Kouprianov, V. V., Shevchenko, I. I. 2003, On the chaotic rotation of planetary satellites: The Lyapunov exponents and the energy,
Astron. and Astrophysics, **410**, 749-757

[9] Pang, Tao 1997, An Introduction to Computational Physics,
Cambridge University Press

[10] Peale, S. J., Rotation Histories of the natural Satellites
in Planetary Satellites, ed. Burns, J., A. 1977, 87-112

[11] Peale, S. J.: 1973, Rotation of Solid Bodies in the Solar System,
Reviews of Geophysics and Space Physics, **Vol 11**, No 4, 767-793

[12] Plummer, H. C. 1960, An Introductory Treatise on Dynamical Astronomy, Dover, NY

[13] Wisdom, J. 1987, Chaotic Dynamics in the Solar System, Icarus, **72**, 241-275

[14] Wisdom, J., Peale, S. J., Mignard, F. 1984, The chaotic rotation of Hyperion, Icarus, **58**, 137-152

EXCHANGE ORBITS IN PLANETARY SYSTEMS

Rudolf Dvorak
Institute for Astronomy
University of Vienna
Türkenschanzstrasse 17
A-1180, Vienna, Austria
dvorak@astro.univie.ac.at

Abstract In this study we show the results of a numerical determination of the stability of planets in exchange orbits. These kinds of orbits are defined such that two small but massive bodies with almost the same semimajor axes on nearly circular orbits are moving around a much more massive host. Because the planet on the inner orbit is faster it approaches the outer body from behind. Before they meet, the inner body is shifted to the orbit of the outer and vice-versa the former outer body moves to an orbit with a smaller semimajor axis. We did our numerical experiments for different masses of the two planets involved and different initial separation of the semimajor axis. It turned out that for stable exchange orbits the sum of the mass of the two planets can only slightly exceed the one of Saturn.

Keywords: Extrasolar planetary systems, terrestrial planets, exchange orbits

1. Introduction

The search for extrasolar planets led up to now to the knowledge of 185 planets in 149 extrasolar planetary systems (EPS)[1]. Almost all these planets are giants with a few exceptions; the planet with the lowest mass found has 5.5 masses of the Earth. One primary goal of searching for EPS is to find terrestrial planets in so-called habitable zones (HZ) ([10]). There are different possibilities for terrestrial planets (TP) to move on stable orbits even when a large planet is present: when the giant is outside the HZ a TP may move inside (like in our Solar System), when a hot Jupiter is moving close to the host star a TP may move on a stable orbit in the HZ. A lot of effort has been undertaken to define such stability zones in existing EPS (e.g. [1], [4], [5], [6], [12], [11], [13], [14], [16], [18], [19], [20], [21]). Additionally we can imagine TPs as satellites of giant planets and also in 1:1 mean motion resonances (MMR) with a Jupiter like planet.

These 1:1 resonant orbits are of special interest for asteroids in our Solar System. It is due to the fact that in a region 60° before Jupiter and 60° behind the largest planet a large number of asteroids are populating this region. Many analytical and numerical work has been devoted to the stability of these two 'clouds' of asteroids, which are named after the warriors of the Trojan war. The Trojans librate about these two stable equilibrium points[2] in the so-called tadpole orbits having orbits with two well distinct periods (almost 12 years and 149.6 years) which are visible in Fig. 1 (upper graph).

When the libration around the one Lagangian point grows and reaches a point which is opposite to the location of Jupiter with respect to the Sun the orbits merge with the orbits around the other equilibrium point. These kind of orbits – because of their appearance in a rotating frame in which Jupiter and the Lagrangian points have fixed positions – are called horseshoe orbits (see Fig. 1, lower panel)

In the case of an asteroid and Jupiter in the 1:1 resonance there is not any 'measurable' effect on Jupiters orbit, because of the smallness of the mass of the asteroid compared to the one of Jupiter. The situation is quite different when the two celestial bodies involved have comparable masses and are both small compared to the central mass. Surprisingly enough some years ago two satellites in the Saturn system were discovered which have exactly these kind of orbits which we call now *exchange orbits*. The exchange orbits (e-orbits) of the general three body problem can be described as follows:

Two small but massive bodies are moving on nearly circular orbits with almost the same semimajor axes around a much more massive host. Because of the 3^{rd} *Keplerian law the one with the inner orbit is faster and approaches the outer body from behind. Before they meet, the inner body is shifted to the orbit of the outer and vice-versa the former outer body moves to an orbit with a smaller semimajor axis: they have changed their orbits and their semimajor axis!*

This interesting interplay may be stable for millions of encounters as we will see in the next chapters. In the satellite system of Saturn the two moons Janus and Epimetheus (the orbits of these two moons differ only by 50 km[3] and have themselves diameters of more than 100 km) have exactly these kinds of orbits; so we postulate that this may apply to extrasolar planets too. Early work concerning exchange orbits was accomplished by [22] who described the u-shaped orbits during the close encounter (in a rotating frame!) and also [2] who established stability regions depending on the masses involved. Recent numerical integrations and analytical estimations show that e-orbits are stable up to a mass ratio where a TP is in exchange with a Saturn like planet (e.g. [14]).

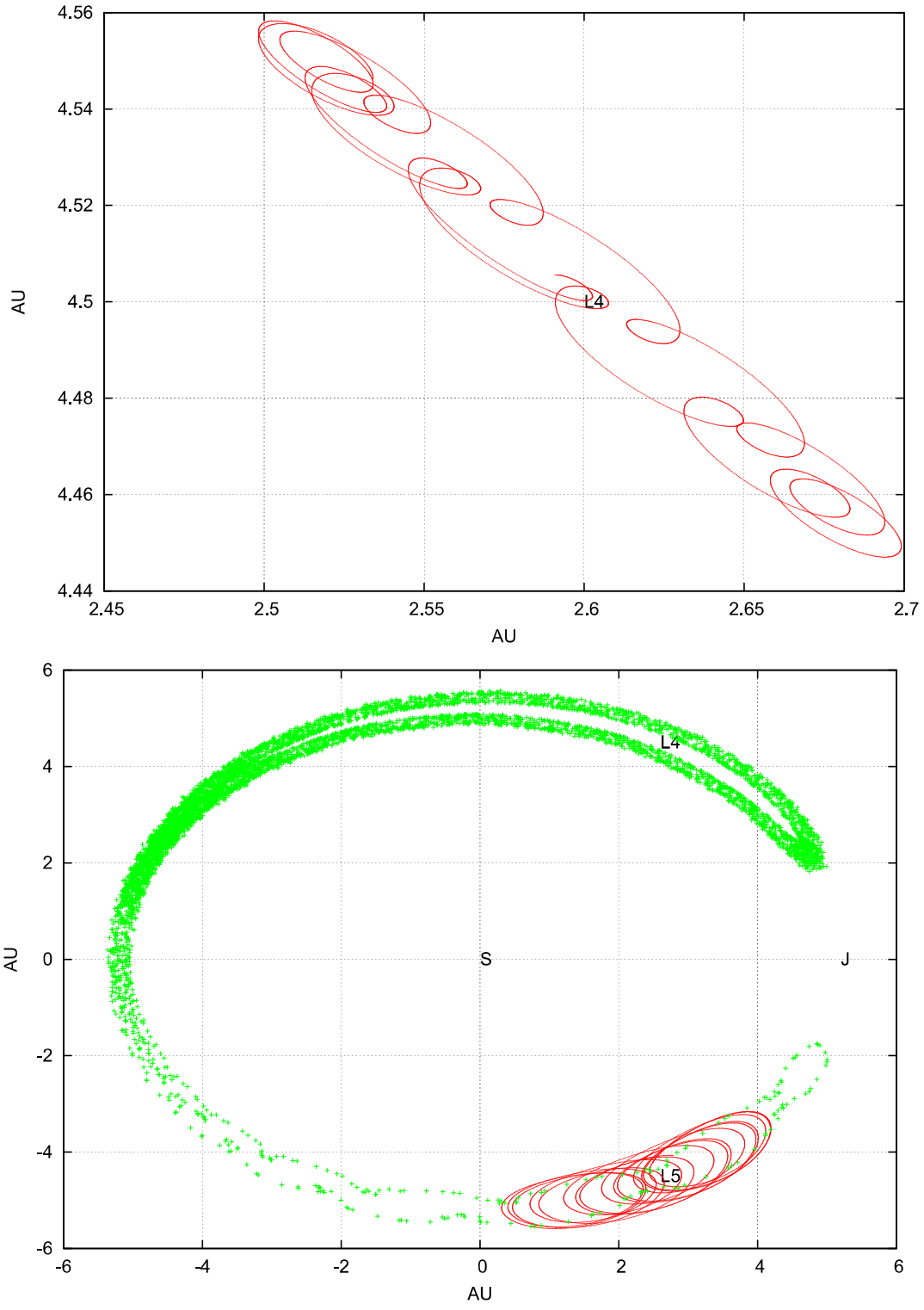

Figure 1. Orbit in the restricted three-body problem around the Lagrangian points in the rotating frame: around L_4 (upper graph), around L_5 and around both equilibrium points (lower graph). Note that the last orbit is in an exchange orbit in the full three body problem; for detailed explanation see in the text.

Another study by [7] was devoted to the problem of the dynamics of systems of two close planets which is in a certain sense similar to the problem we are dealing with. But in contrary to exchange orbits there he studied stability against close encounters which may led to escapes when they come as close as the Hill's radius[4]. [13], [14] studied the different possibilities for two planets in 1:1 resonance and how they would be detectable with the aid of their radial velocity curves. [17] have shown that two planets in 1:1 MMR can be stable for quite different orbital parameters. In a recent paper [8] showed that two ESP with planets in a possible 2:1 MMR could also be in the 1:1 MMR with more or less the same Radial Velocity Curve.

2. The stability limits

To establish stability regions depending on the parameters which determine the exchange orbits (mass ratio of the planets and total mass of the planets compared to the central body and difference in semimajor axis Δa) we did numerical integrations of the equations of motion of the full 3-body problem. We used the Lie-integration (e.g. [9], [15]) with an adaptive step-size to be able to model in a proper way the encounters of the two planets. We always started the two planets on circular orbits on both sides of the central star in 1 AU with an increasing value of the difference in semimajor axes Δa for every single experiment. We checked the maximum eccentricity during the integration time of 10000 years; we emphasize that the number of encounters depend on Δa.

In Fig. 2 we can see the limits of stability for e-orbits where two equally massive TPs are involved. We plotted these differences Δa versus the maximum of the eccentricity . There it is visible (upper graph, shaded region in Fig. 2) that up to the distance $\Delta a = 0.02$ AU ($a = 1.01$ AU for the outer and $a = 0.99$ AU for the inner planet) the eccentricity stays very small; it means that the orbits were stable even after thousands of encounters. Then we see large maximum eccentricities between 0.96 AU and 0.99 AU (1.01 AU and 10.4 AU) which are the sign that after an encounter the planets had quite different orbits and left the exchange orbits. Then they are again stable because they are too far from each other and may pass without major perturbations (the eccentricities are again small). The small 'hills' on both sides are due to high order resonances which cause slightly larger perturbations, but the two orbits are well separated and almost circular. We have undertaken these numerical experiments for four different pairs of planets with equal masses are the following ones: Earth – Earth, S-Earth – S-Earth[5], Uranus – Uranus and Saturn – Saturn.

In Fig. 3 we depicted a zoom of the results shown in Fig. 2: here it can be seen that for large masses involved the differences in semimajor axis can be

larger and the e-orbits are still stable: the respective results for two equally massive planets in exchange orbits with a mean semimajor axis $a = 1$ AU are shown in Table 1.

Table 1. The extension of the stable regions for exchange orbits for two equally massive planets around a Sun-like star with a small difference Δa in semimajor axes

2 planets	**lower limit**	**upper limit**	Δa
Earth – Earth	0.994 AU	1.006 AU	0.012 AU
S-Earth – S-Earth	0.990 AU	1.010 AU	0.020 AU
Uranus – Uranus	0.988 AU	1.012 AU	0.024 AU
Saturn – Saturn	0.982 AU	1.018 AU	0.036 AU

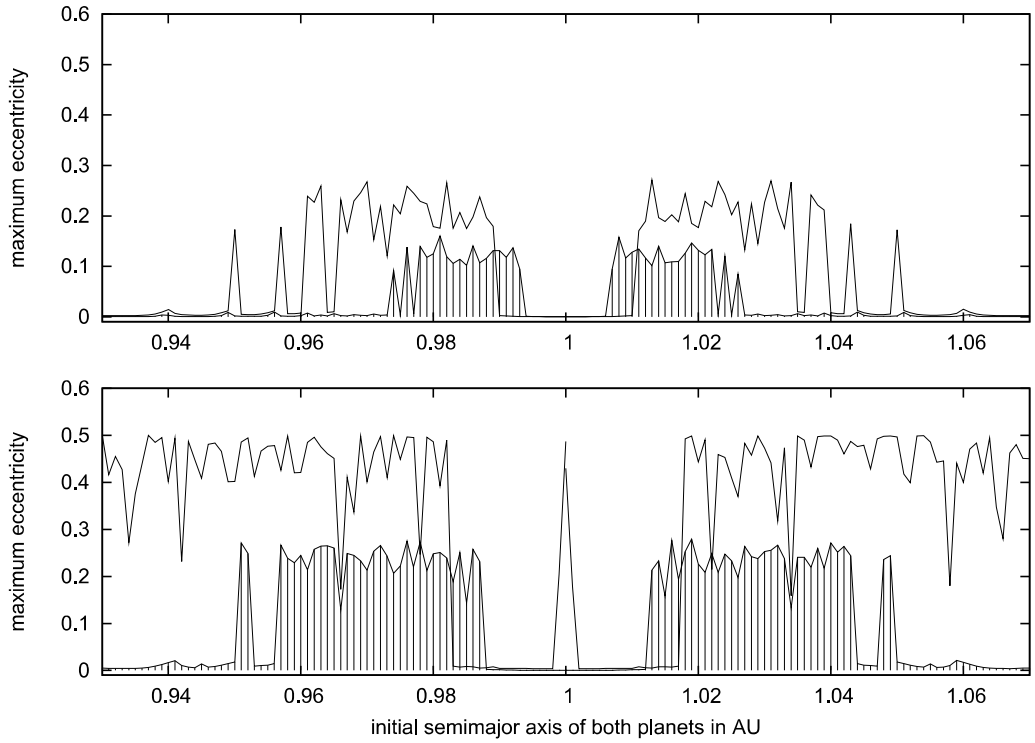

Figure 2. Stable regions for exchange orbits for 4 examples of two equally massive TPs: Earth, Super-Earth, Uranus, Saturn; the initial semimajor axis of the two planets is plotted versus the maximum eccentricity.

In Fig. 4 we plotted the stability regions for three different pairs of planets in e-orbits: upper graph the Earth (as inner planet for the beginning of the integration) with S-Earth (as outer planet for the beginning of the integration); middle graph the Earth with Uranus and lower graph the Earth with Saturn. The large $e_{\max}$ values (y-axis on left part of the plot) are the ones of the Earth, the smaller ones (y-axis on right part of the plot) are the $e_{\max}$ values for the more massive planet. The region in the middle, with $e_{\max}$ close to zero, is the

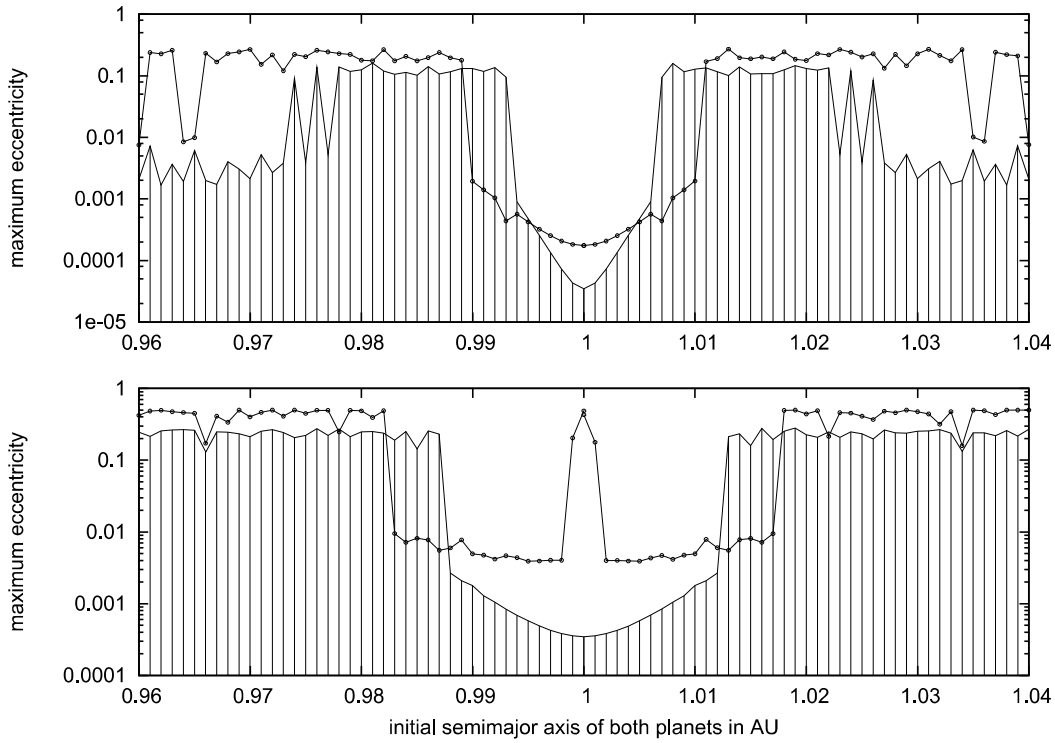

Figure 3. Zoom of Fig. 2 but for logscale in y.

domain of stable e-orbits. One can also see that the larger the total mass, the larger is the stable region, a fact which is also visible from Tab. 1.

In Fig. 5 we show the results of numerical integrations of different pairs of planets in e-orbits: S-Earth with Uranus (upper graph); S-Earth with Saturn (middle graph) and as Uranus with Saturn. The trend is the same as already shown in the last figures: the stable region increases with the masses involved. Nevertheless there is a limit for the total mass of the planets: the numerical experiments for e-orbits have shown that approximately 2 Saturnmasses are this limit (which also agrees with the analytical model by [3]).

In Fig. 6 we show for three examples of equally massive planets how the semimjaor axes evolves during 2000 years. We can see a butterfly - like diagramm: the 2 planets start on opposite sides of the planet($\Delta\lambda = 180°$) with a small difference in semimajor axes (Δa). During the integration the two planets approach, Δa increases and just before their encounter Δa has its largest value. Now the two planets change their orbits: the inner one, which is moving faster, is shifted outwards and the outer one is shifted innwards and therefore it is on a 'faster track'. Consequently now this planet approaches the other planet from the inside; when they are on the opposite sides of the host star the Δa is again as small as at the beginning of the integration and the procedure repeats. The upper graph is for an Earth-Earth pair, the middle graph for S-Earth –

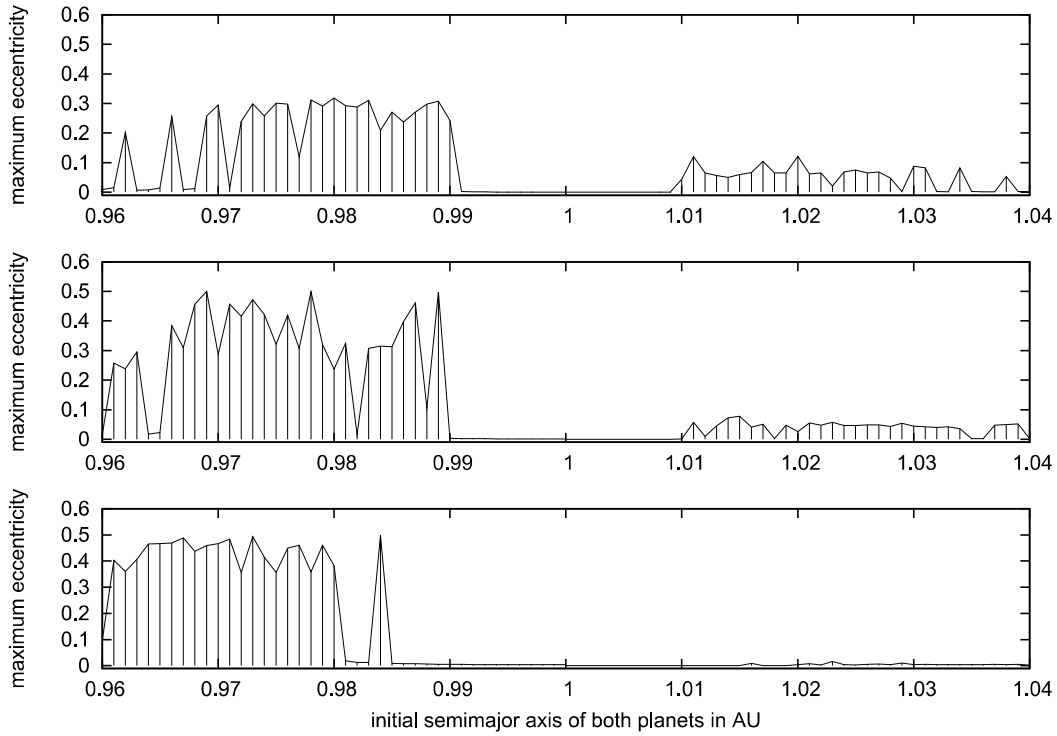

Figure 4. Stable regions for exchange orbits for 3 examples of pairs of planets: in all three examples the inner planet is the Earth; the outer planet is a S-Earth (upper graph), Uranus (middle graph) and Saturn (lower graph). The initial semimajor axis of the planets is plotted versus the maximum eccentricity of their orbits.

S-Earth and the lower graph for Uranus – Uranus. The encounter frequency depends on the separation of the semimajor axes Δa.

In Fig. 7 we depicted the change of the semimajor axes after every close encounter of a pair of Earth and Saturn. It is clearly visible that the Earth suffers from bigger jumps in semimajor axis during the encounter than Saturn, a consequence of the smaller mass of the Earth.

An important point is the long-term stability of such orbits. Is this a transit configuration, or, can these kind of orbits survive for millions of encounters? To answer this question severeal tests were undertaken and we could show that these kind of orbits are very stable. In the respective Fig. 8 we depicted the semimajor axes for the first million years and for the time interval from 9 to 10 million years; in Fig. 9 we show the development of the eccentricity for the same periods of time. The results of two Earth-like planets with an initial $\Delta a = 0.08$ show the regularity of the orbits even after almost ten thousands of encounters (exchanges).

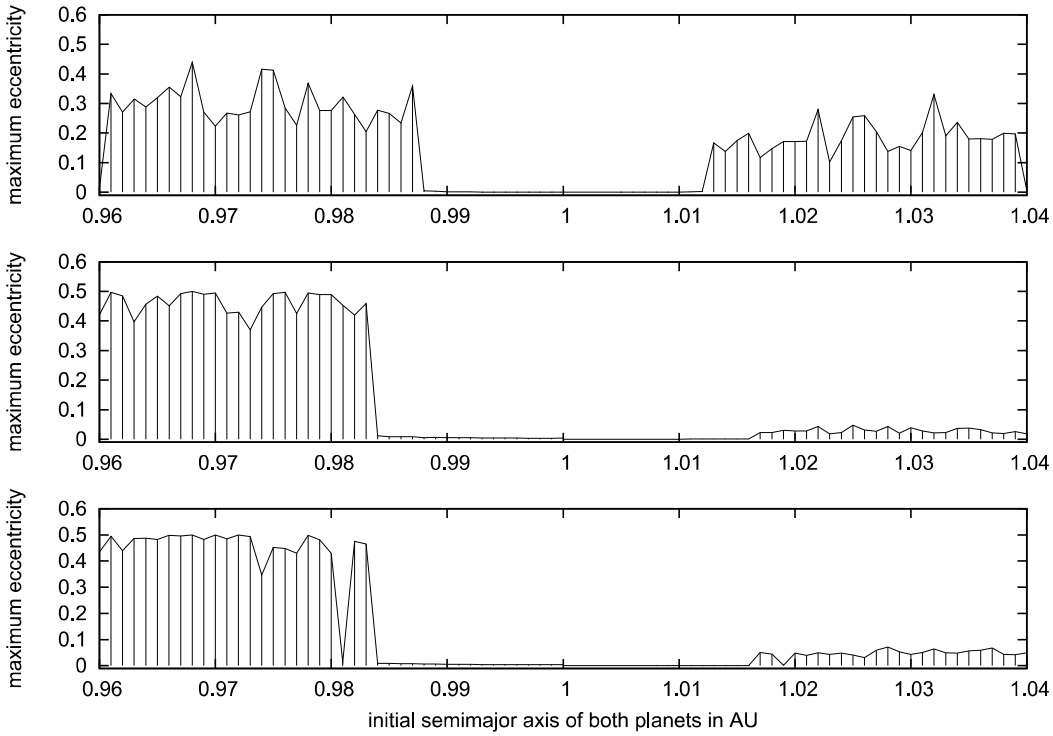

Figure 5. Stable regions for exchange orbits for 3 examples of pairs of planets: S-Earth and Uranus (upper graph), S-Earth and Saturn (middle graph) and Uranus and Saturn (lower graph). The initial semimajor axis of the planets is plotted versus the maximum eccentricity of their orbits.

3. Conclusions

The search for terrestrial planets in EPSs is a hot topic for observing astronomers nowadays. To establish regions where stable orbits of TPs in extrasolar planetary systems may survive is a challenge for astronomners working in Astrodynamics. Besides inside or outside the orbit of a giant planety one possibility for TPs is to move in 1:1 MMR like Trojans and satellites of Jupiter-like planets. Numerical estimations led to the conclusion that for a Solar type host star the mass limit for exchange orbits in the distance of 1 AU (thought as the habitable zone) is just below two Saturns ($0.0003 M_{\rm sun}$). These means that even a Saturn like giant may exchange orbits with an Earth-like planet; unfortunately most of the gasplanets discovered up to now are in the size of Jupiter or even larger. Nevertheless we expect for planetary systems to host also Neptune and Uranus like planets – and also smaller planets, namely the terrestrial ones – and consequently we cannot exclude the realisation for planets in this type of orbit. Although it seems to be a very unlikely configuration the fact, that Janus and Epimetheus in the Saturn satellite system have such orbits, teaches us that the probability of a realisation of planets in e-orbits is not zero. To summarize we can see that e-orbits are possible only for almost

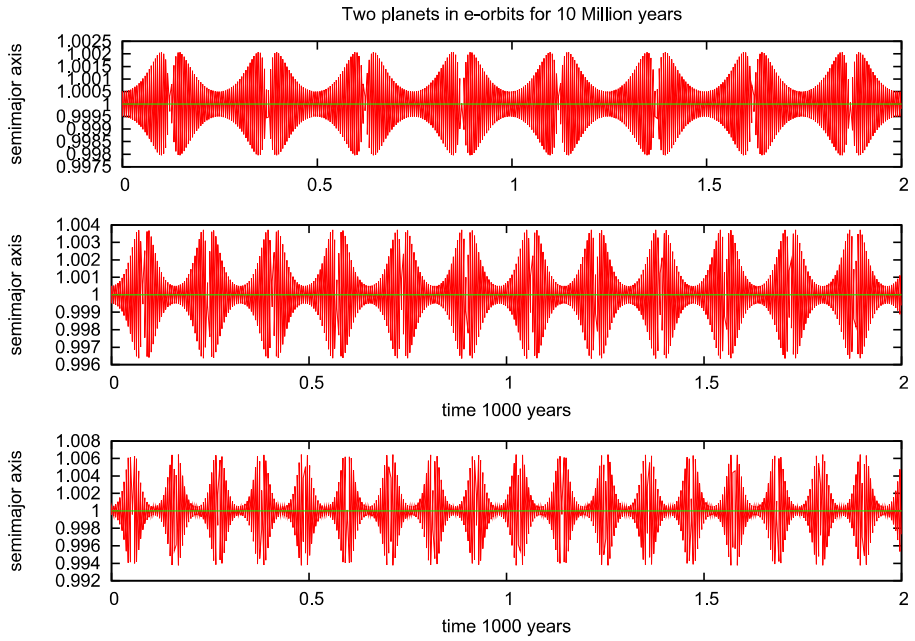

Figure 6. Time development of semimajor axis for 200 years of 3 different pairs of planets: Erath – Earth (upper graph), S-Earth – S-Earth (middle graph) and Uranus – Uranus (lower graph).

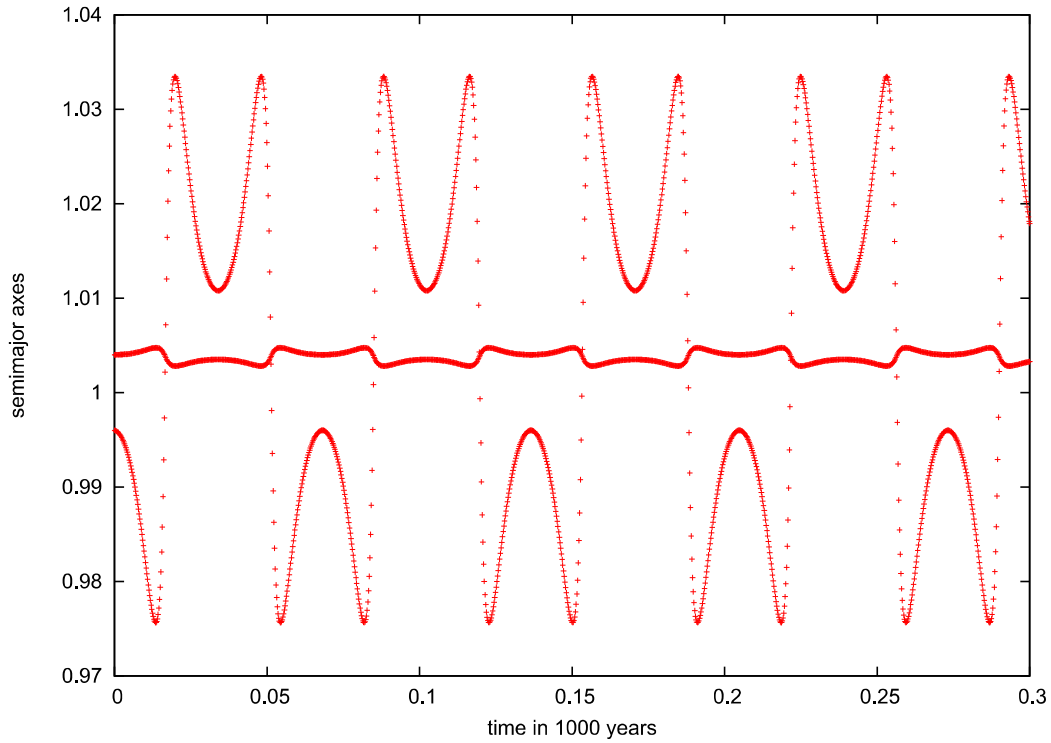

Figure 7. Exchange orbits for Earth and Saturn for 300 years in a distance of 1 AU; every 40 years the close encounter leads to an exchange of the orbits. The semimajor axes (y-axis) are plotted with respect to the time; the thick line close to $a = 1$ AU is a_{Saturn}.

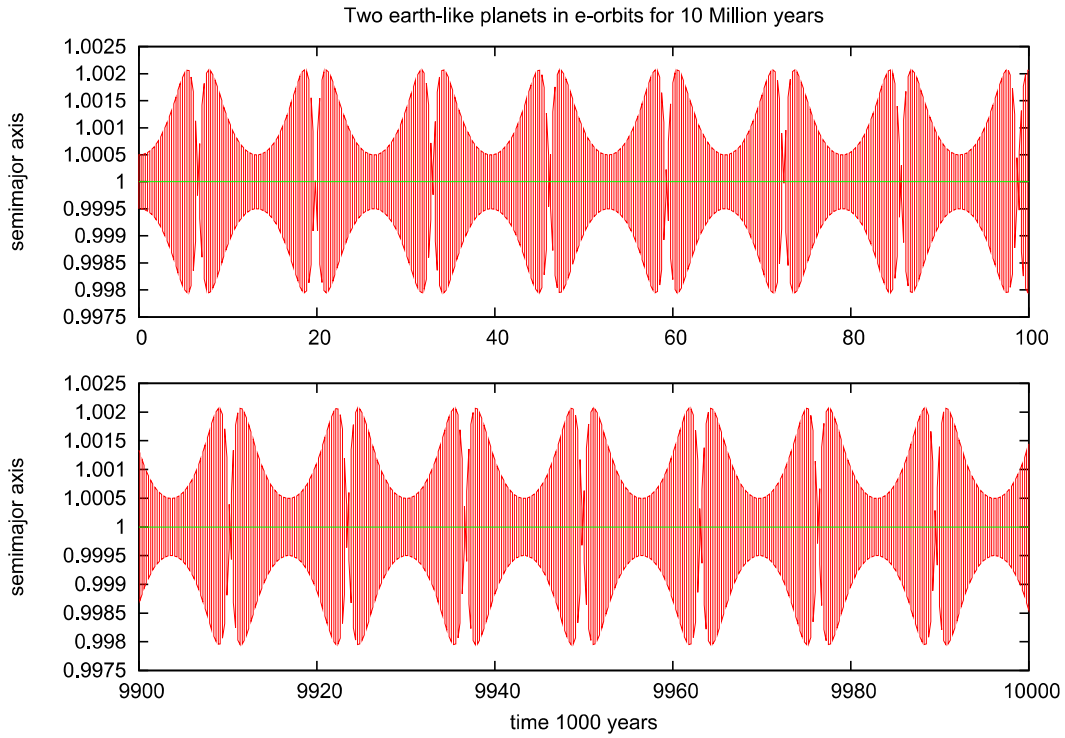

Figure 8. Semimajor axes of the exchange orbits for 10 million years; upper graph: first million years, lower graph last 1 million years.

circular orbits ($e < 0.001$) and almost coplanar orbits. These limits for eccentricity and inclination depend on the mass and also on the seperation of the two planets involved: a numerical results (which fit well to analytical estimations) give for the values of the separation in semimajor axis Δa in a distance of 1 AU to a sunlike planet: 0.012 AU (Earth), 0.020 AU (S-Earth), 0.024 AU (Uranus) and 0.034 AU (just below Saturn). In a next step we will investigate how perturbations of an inner or outer perturbing gas giant may destroy these limits.

Acknowledgments

For the realisation of this study I need to thank the Austrian Science Foundation (FWF, project P16024-N05) and the ISSI Institute in Bern which supported us in the framework of the ISSI team “Evolution of habitable planets”. Additionally I have to thank the ’Wissenschaftlich-technische Zusammenarbeit Österreich-Ungarn’ project A-12/04: ’Dynamics of extrasolar planetary Systems’.

Notes

1. The homepage for the catalogue of extrasolar planets is maintained by J. Schneider: http://vo.obspm.fr/exoplanetes/encyclo/catalog.php

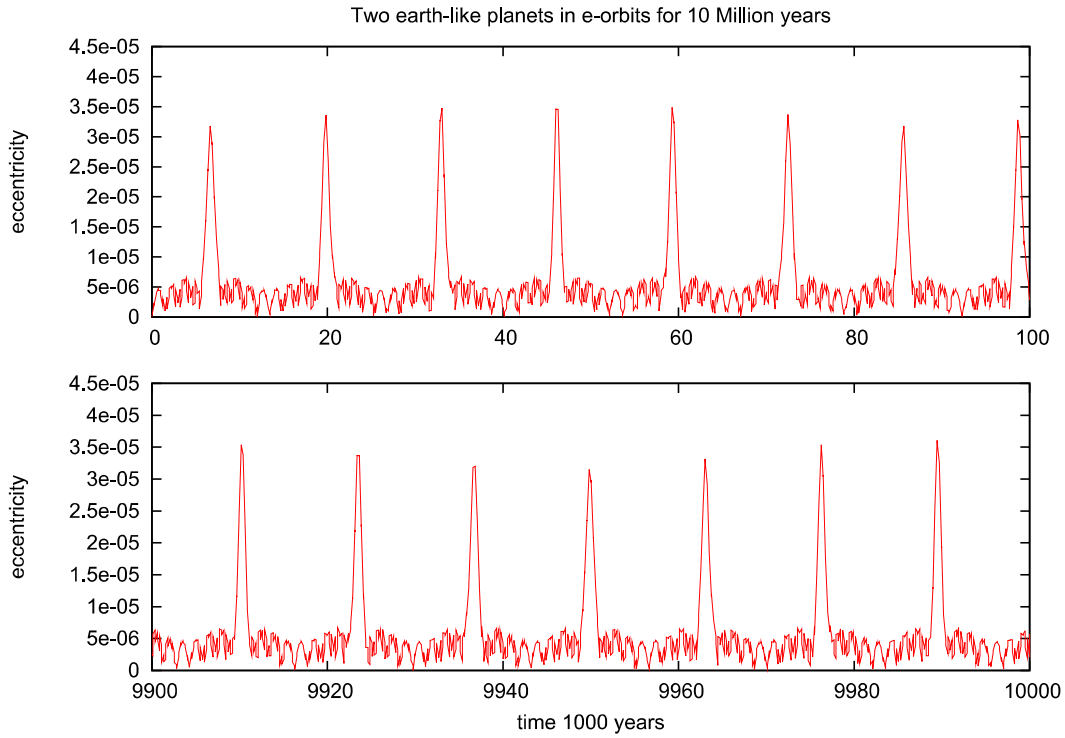

Figure 9. Eccentricities of the exchange orbits for 10 million years; upper graph: first million years, lower graph last 1 million years.

2. named after Joseph Louis, comte de Lagrange (Giuseppe Lodovico Lagrangia, 1736, Turin - 1813, Paris)
3. 151472 km and 151422 km
4. $r = a_{\text{planet}}(m/3M)^{1/3}$; M the larger mass and m the smaller one
5. With S-Earth we mean a TP with the mass $m_{\text{S-Earth}} = 5m_{\text{Earth}}$

References

[1] Asghari et al.: 2004, "Stability of terrestrial planets in the habitable zone of Gl 777 A, HD 72659, Gl 614, 47 Uma and HD 4208", *Astronomy and Astrophysics* **426**, p. 353–365

[2] Auner, G.: 2001, "Exchange orbits", in F.Freistetter, R. Dvorak and B. Erdi (eds.): 2nd Austrian Hungarian Workshop on Trojans and related Topics, *Eötvs̈ University Press* p. 49

[3] Cors, J. M., Hall, G. R.: 2003, "Coorbital Periodic Orbits in the Three Body Problem", *SIAM, J. Applied Dynamical Systems* **2**, No. 2 p. 219

[4] Dvorak et al.: 2003, "Planets in habitable zones:. A study of the binary Gamma Cephei", *Astronomy and Astrophysics* **398**, p. L1–L4

[5] Dvorak et al.: 2003, "A study of the stability regions in the planetary system HD 74156: Can it host earthlike planets in habitable zones?" submitted to *Astronomy and Astrophysics*

[6] Dvorak et al.: 2004, "Extrasolar Trojan planets close to habitable zones", *Astronomy and Astrophysics* **426**, p. L37–L40

[7] Gladman, B.: 1993, Dynamics of systems of two close planets",*Icarus* **106** p.247

[8] Gozdziewski, K., Konacki, M.: 2005, "Trojan pairs in the HD128311 and HD 82943 Planetary Systems", *astro-ph/0510109*

[9] Hanslmeier, A., Dvorak, R.: 1984, "Numerical Integrations with Lie-series", *Astronomy & Astrophysics* **132**, p. 203–211

[10] Kasting et al.: 1993, "Habitable Zones around Main Sequence Stars", *Icarus* **101**, p. 108–128

[11] Kiseleva-Eggleton et al.: 2002, "Global Dynamics and Stability Limits for Planetary Systems around HD 12661, HD 38529, HD 37124, and HD 160691", *Astrophysical Journal* **578**, p. L145–L148 *Monthly Notice of the Royal Astronomical Society* **341**, p. 760–770

[12] Lammer et al.: 2003, "Atmosphere and orbital stability of exosolar planets orbiting gamma Cephei" in *Proceedings EGS-AGU-EUG Joint Assembly, Nice* (in press)

[13] Laughlin, G., Chambers, J.E.: 2001, "Short-Term Dynamical Interactions among Extrasolar Planets", *Astrophysical Journal* **551**, L109

[14] Laughlin, G., Chambers, J.E.: 2002, "Extrasolar Trojans: The Viability and Detectability of Planets in the 1:1 Resonance", *Astronomical Journal* **124** p. 592

[15] Lichtenegger, H.: 1984, "The dynamics of bodies with variable masses", *Celestial Mechanics and Dynamical Astronomy* **34**, p. 357–368

[16] Menou, K., Tabachnik, S.: 2003, "Dynamical Habitability of Known Extrasolar Planetary Systems´´, *Astrophysical Journal* **583**, p. 473

[17] Nauenberg, M.: 2002, "Stability and Eccentricity for Two Planets in a 1:1 Resonance, and Their Possible Occurrence in Extrasolar Planetary Systems" *Astrophysical Journal* **568**, p. 369

[18] Noble et al.: 2002, "Orbital Stability of Terrestrial Planets inside the Habitable Zones of Extrasolar Planetary Systems", *The Astrophysical Journal* **572**, p. 1024–1030

[19] Pilat-Lohinger, E., Dvorak, R.: 2002, "Stability of S-type Orbits in Binaries", *Celestial Mechanics and Dynamical Astronomy* **82**, p. 143–153

[20] Pilat-Lohinger et al.: 2002, "Stability of planetary orbits in double stars", in *Proceedings of the First European Workshop on Exo-Astrobiology (ed. Huguette Lacoste)*, ISBN 92-9092-828-X, p. 547–548

[21] Pilat-Lohinger et al.: 2003, "Stability limits in double stars. A study of inclined planetary orbits", *Astronomy and Astrophysics* **400**, p. 1085–1094

[22] Spirig, F., Waldvogel, J.: 1985, "The three-body problem with two small masses", in V.G. Szebehely (ed.) 'Stability of the Solar System and its minor natural and artificial bodies', D. Reidel, p. 53

DYNAMICAL STABILITY INSIDE THE HABITABLE ZONE OF 55 CNC AND υ AND

Barbara Funk
Institute for Astronomy
University of Vienna
Türkenschanzstrasse 17
A-1180 Vienna, Austria
funk@astro.univie.ac.at

Abstract The main goal of this study is to investigate the long term stability of orbits of terrestrial like planets in the habitable zone (HZ) of the extrasolar systems 55 Cnc and υ And. The habitable zone is defined as the region, where liquid water can exist on the surface of a terrestrial planet. From the dynamical point of view the most interesting planetary systems are multiple planetary systems, to which the two planetary systems belong, since they have at least three known exoplanets. To determine the orbital behavior in the different systems we used (a) direct numerical computations (Lie-Integration method), where we determined the escape-times and the maximum eccentricity (MEM) and (b) for the long term stability the FLI, which is an effective chaos indicator. Because of the uncertainties in the observational data for the initial conditions we varied the eccentricity of the known planets as well as the inclination of the test-planets. For the system 55 Cnc we found a very stable HZ more or less independent of the eccentricity of 55 Cnc d and up to an eccentricity of 0.38 of 55 Cnc c. For higher eccentricities of 55 Cnc c the whole system becomes unstable. The system υ And has a nearly completely unstable HZ for all initial conditions.

Keywords: dynamical Astronomy, multiple exoplanetary systems, habitable zone

1. Introduction

In 1995 the first extrasolar planet was discovered [21] and until now (May 2006) we know 188 planets in 152 extrasolar systems. The investigation of the dynamical stability of extrasolar planetary systems is more interesting in multiple planetary systems. Beside some general studies for such systems (e.g. [3]) many exosolar planetary systems, like γ Cephei [5], HD 12661, HD 38529, HD 37124 and HD 160691 [8], HD 74156 [6] and Gl 777 A, HD 72659, Gl 614, 47 Uma and HD 4208 [1] were investigated. Furthermore an extensive study

including 97 exosolar systems and their resonances was done by [24]. These investigations determined on the one hand the stability limits, and checked on the other hand the orbital parameters obtained by observations ([13], [14]). In our study we investigate two multiple exoplanetary systems with three planets: 55 Cnc and υ And, which are both located in wide binary systems.
Since υ And was the first system with three known planets there exist a lot of studies, which checked the observational data as well as the stability of this system (e.g. [22], [15], [11], [2], [17]). For example [25] and [26] calculated additional some fictive planets to find out, if there are some stable regions for other lower-mass planets. Other works showed, that the planets c and d inhabit a secular resonance. [18] found, that the system υ And has a stellar companion, approximately 750 AU away ([18]).
55 Cancri is part of a wide binary system and the planets were discovered by the California & Carnegie Planet Search Team [19]. The inner two planets were found to move in a 3:1 mean motion resonance, which was studied in detail e.g. by [27], [10], [4] and [20]. Recently (August, 2004) a fourth planet was detected, which moves very close to the primary (0.038 AU) and has just 14.21 $\pm$2 2.91 Earth-masses ([23]), which was not included in our computations (The planet has no influence on the HZ, since it moves very close to the star). In our study we concentrate on the HZ (see [12]) in these two systems and try to find out if there could exist any additional planets within. In the following we introduce the dynamical model and the methods with which dynamical stability was established: (a) long-term numerical integrations and (b) chaos-indicators. Finally we discuss the results for both systems.

2. The dynamical model and the methods

The orbital parameters for both investigated systems are given in Table 1. These systems were investigated numerically using two different models. In

Table 1. Orbital parameters for the 55 Cnc and the υ And extrasolar planetary systems.

Name	M	**Spectraltype**	a [AU]	e	ω [$\circ$]
55 Cnc	0.95 $M_{\odot}$	G8 V	-	-	-
Star 2	3.2 $M_{\odot}$	A0	1150	?	-
55 Cnc b	0.84 M_{Jup}	-	0.115	0.02	99
55 Cnc c	0.21 M_{Jup}	-	0.24	0.34	61
55 Cnc d	4.05 M_{Jup}	-	5.9	0.16	201
υ Andromedae	1.3 $M_{\odot}$	F8 V	-	-	-
Star 2	0.2 $M_{\odot}$	M4,5 V	750	?	-
υ Andromedae b	0.69 M_{Jup}	-	0.059	0.012	73
υ Andromedae c	1.89 M_{Jup}	-	0.829	0.28	250
υ Andromedae d	3.75 M_{Jup}	-	2.53	0.27	260

both cases we use the restricted 6-body problem (for this study we ignore the recently new discovered planet in the 55 Cnc system, because test-calculations showed, that it has no influence on the HZ) consisting of the binary, the three planets and massless test-planets, that move either in the same plane or on inclined orbits. Because of the observational uncertainties in the eccentricities of the planets we varied the eccentricities of those planets, which are next to the HZ. Since the eccentricity of the binary is not known and because of the large distance of the stellar companions (see table 1) we investigated only an extreme case: e_{Bin} = 0.9 to see, if there is any dependence at all. The integration of the Newtonian equations of motion was undertaken with the Lie integration method [9], [16], which uses an automatic step-size and is, because of the recurrence of the Lie-terms, a precise integration method. The integration time was 10^5 years and our stability criterion was such that no close encounters within the Hill's sphere of one of the massive planets were allowed. As a second independent tool to investigate the region between the two known planets we used the Fast Lyapunov Indicators (FLI) [7]. This program uses the Bulirsch Stoer integration method and is especially adapted for distinguishing between chaotic and regular orbits. The criterion for the FLIs is given by their time evolution, which defines clearly the orbital behaviour. In our study we define orbits with FLI $< 10^9$ as stable; the integration time was 50000 years for the FLI's. Both methods were used complementary and showed a quite good agreement.

3. 55 Cnc

For a primary-mass of 0.95 $M_\odot$ the HZ lies approximately between 0.5 and 1.4 AU [12]. In Fig. 1 the orbits of all three known planets are shown as black circles and the HZ is marked as a grey circle. As one can see 55 Cnc d moves far away from the HZ, but 55 Cnc c moves very close to the inner edge of the HZ as well as very close to 55 Cnc b; thus the mean motion resonances with 55 Cnc c could play an important role. Additionally we found out, that 55 Cnc c itself become unstable for higher eccentricities, because then it has close encounters with 55 Cnc b. The HZ lies between 55 Cnc c and 55 Cnc d, thus we change the eccentricities for these two planets as follows: The eccentricity given from the observations (e_{Obs}) for 55 Cnc c is 0.34 and for 55 Cnc d 0.16, so we changed the eccentricity of 55 Cnc c between 0.14 and 0.54 with a step of 0.1 and the eccentricity of 55 Cnc d between 0.06 and 0.36 again with a step of 0.1. All these calculations were additional done for inclined test-planets (for inclinations from 0° to 50° with a step of 5°). The results for e_{Obs} are shown in Fig. 2. As one can see, the region of the HZ is nearly completely stable with very low eccentricities, just for high inclinations an unstable region near the outer edge of the HZ occurs. The inner edge of the

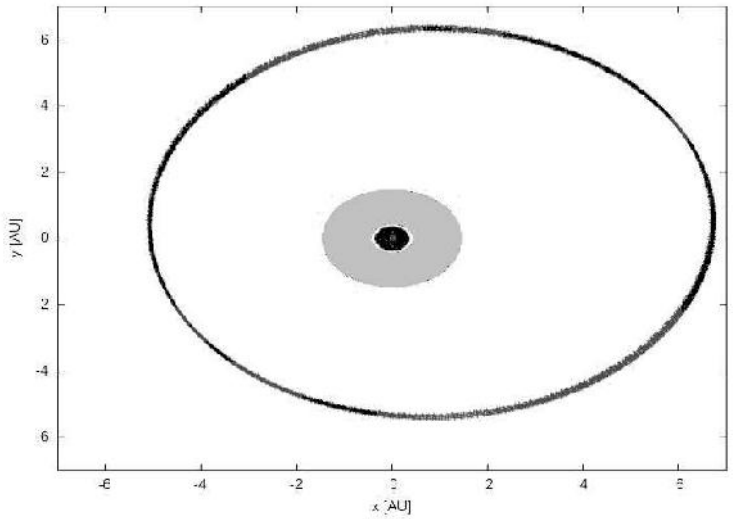

Figure 1. Heliocentric orbit for the planets in the system 55 Cnc (black circles); the grey region mark the HZ in this system.

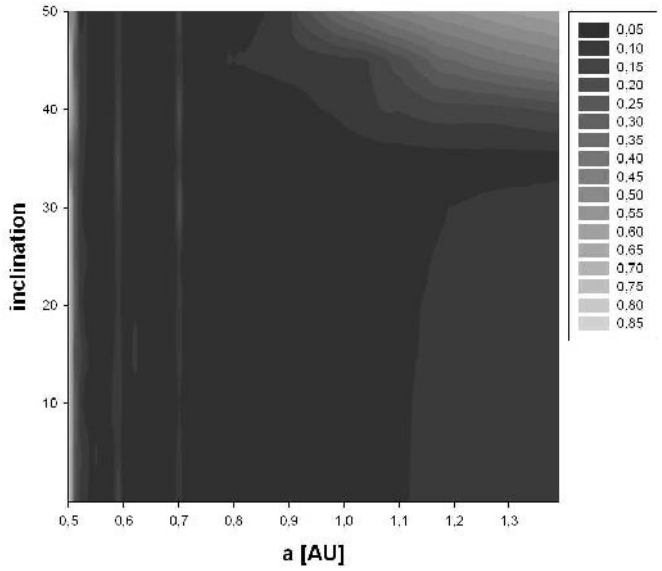

Figure 2. Maximum eccentricity plot for the system 55 Cnc with $e_{55\,\mathrm{Cnc\,c}} = 0.34$ and $e_{55\,\mathrm{Cnc\,d}} = 0.16$. Dark regions show low eccentricities (stable motion) and the grey scales go to higher eccentricities (unstable motion, see color code). Additionally one can see the $19:5 = 0.5844$ and the $5:1 = 0.7018$ mean motion resonances with 55 Cnc c.

HZ shows also a small unstable strip, which indicates the influence of the inner planet (55 Cnc c), as well as some mean motion resonances with 55 Cnc c. For lower eccentricities than the observed one, the HZ remains very stable and also a higher eccentricity of 55 Cnc d has no considerably influence on the HZ (see Fig. 3). For higher eccentricities of 55 Cnc c the whole system becomes

unstable. Fig. 4 (upper) shows the orbits of 55 Cnc b and 55 Cnc c in the case of

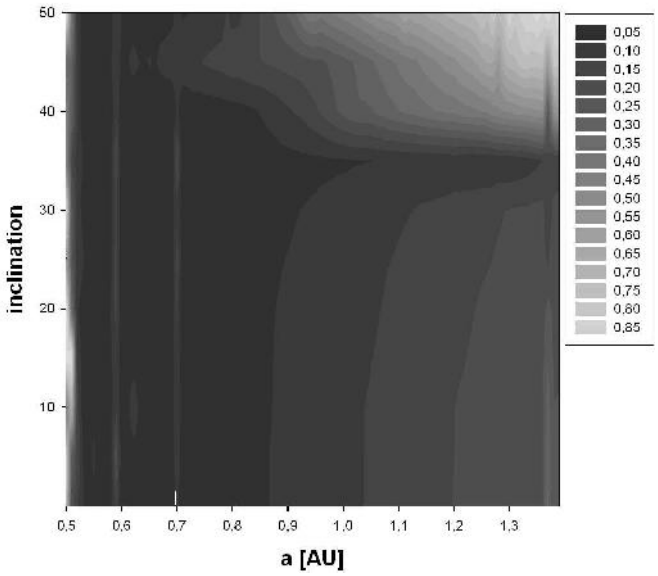

Figure 3. Maximum eccentricity plot for the system 55 Cnc with $e_{55\,\mathrm{Cnc\,c}} = 0.34$ and $e_{55\,\mathrm{Cnc\,d}} = 0.36$. Dark regions show low eccentricities (stable motion) and the grey scales go to higher eccentricities (unstable motion).

$e_{55\,\mathrm{Cnc\,b}} = 0.02$ and $e_{55\,\mathrm{Cnc\,c}} = 0.42$. As one can see, the high eccentric orbit of 55 Cnc c comes already very close to the orbit of 55 Cnc b, which leads to close encounters with this planet (see Fig. 4, lower), so that after approximately 6000 years 55 Cnc c becomes completely unstable as it can be seen from the time evolution of the semi-major axis of 55 Cnc b and 55 Cnc c (Fig. 4, lower). These results were also confirmed with the FLI's.

4. υ And

For a primary-mass of 1.3 $M_\odot$ the HZ lies approximately between 1.2 and 2.6 AU [12]. In Fig. 5 the orbits of all three known planets are shown as black circles and the HZ is marked as a grey circle. As one can see υ And d moves partly inside the HZ and also υ And c moves very close to the inner edge of the HZ; so we can assume a very unstable HZ, where the mean motion resonances with the two nearby planets play an important role. Additionally the known planets themselves become unstable for higher eccentricities. For υ And c we choose eccentricities between 0.08 and 0.48 with a step of 0.1 and for υ And d we choose eccentricities between 0.07 and 0.47 again with a step of 0.1. All calculations were done for inclinations of the test-planets from $0°$ to $50°$ with a step of $5°$. Fig. 6 shows the results for this calculations in the case of $e_{\upsilon\ \mathrm{And\,c}} = 0.08$ and $e_{\upsilon\ \mathrm{And\,d}} = 0.07$, here one can see a stable region between 1.38 and 1.6 AU (black region) up to an inclination of about $40°$. Already for

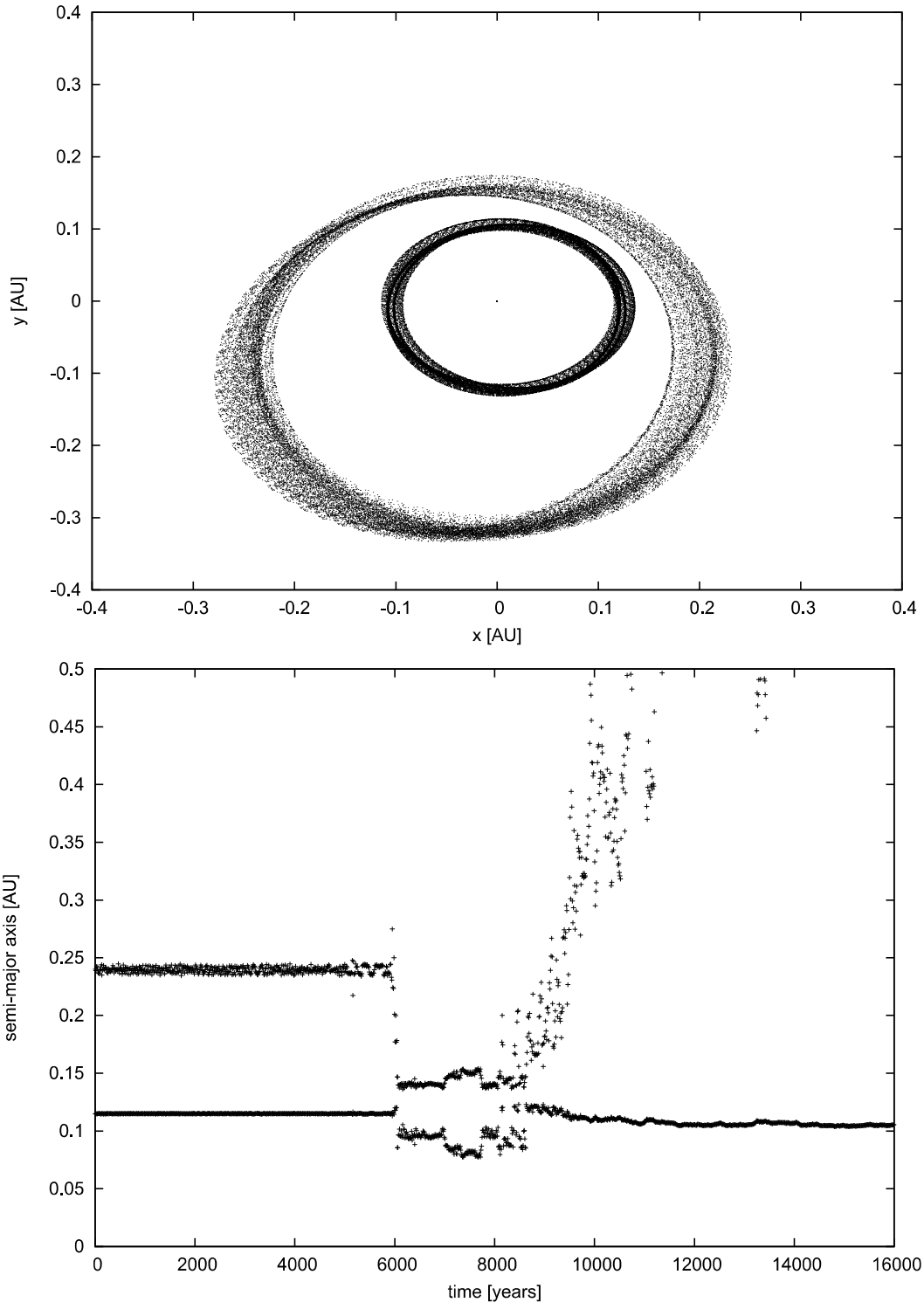

Figure 4. upper: shows the orbits of 55 Cnc b and 55 Cnc c; lower: shows the time evolution of the semi-major axis of 55 Cnc b and 55 Cnc c (the lower line shows 55 Cnc b; the upper line shows 55 Cnc c) for $e_{55\ \mathrm{Cnc\ b}} = 0.02$, $e_{55\ \mathrm{Cnc\ c}} = 0.44$ and $e_{55\ \mathrm{Cnc\ d}} = 0.06$.

an eccentricity of υ And c of 0.18 the stable region shrinks drastically and for an eccentricity of υ And d of 0.17 the stable region disappears completely.

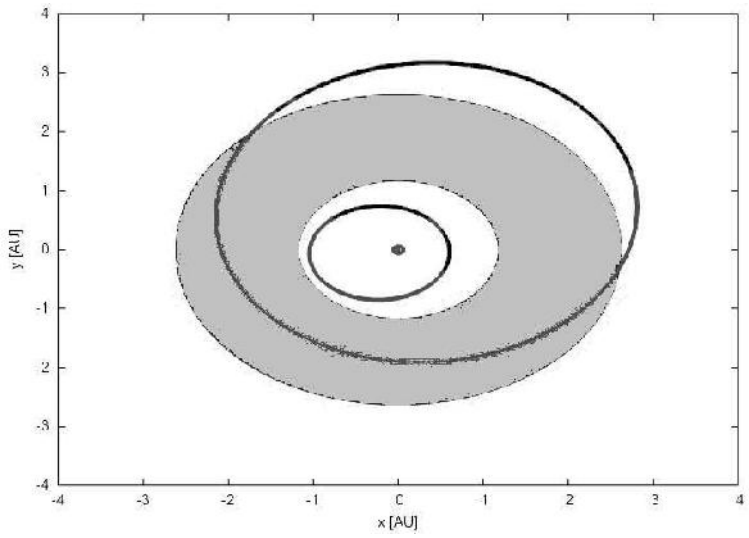

Figure 5. Heliocentric orbit for the planets in the system υ And (black circles); the grey region mark the HZ in this system.

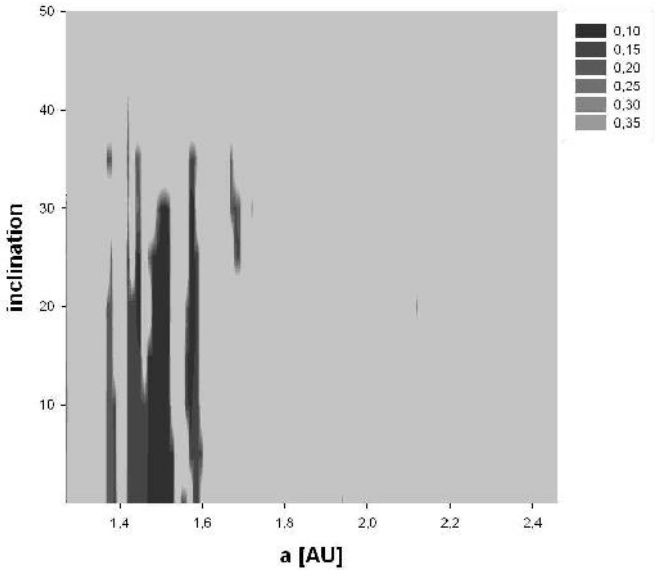

Figure 6. Maximum eccentricity plot for the system υ And with $e_{\upsilon \text{ And c}} = 0.08$ and $e_{\upsilon \text{ And d}} = 0.07$. Black regions show low eccentricities (stable motion) and the grey scales show higher eccentricities (unstable motion).

5. Conclusions

In this study we investigated the dynamical stability inside the HZ of the two systems 55 Cnc and υ And, which are both multiple planetary systems and parts of binaries. Our investigation showed, that the HZ of the system υ And is, because of the two very close planets on high eccentric orbits, very chaotic. In the HZ of this system stable motion is just possible in a small region (be-

tween 1.37 AU and 1.6 AU) and only for very low eccentricities of both known planets. Thus this system is not a good candidate for additional, habitable planets. The results for the system 55 Cnc are completely different. Here the HZ is very stable for a lot of initial conditions, just for high inclinations ($i > 40°$) and for high eccentricities of 55 Cnc c ($e_{55\,\mathrm{Cnc\,c}} > 0.34$) the orbits within the HZ are unstable, where 55 Cnc c itself would have close encounters with 55 Cnc b and becomes unstable. If the eccentricity of 55 Cnc c is not higher than 0.42, stable motion in the HZ is possible and therefore this system may be, from the dynamical point of view, a good candidate for additional planets inside the HZ.

Acknowledgments

The support of the Austrian-Hungarian Scientific and Technology Cooperation, grant number A-12/04 is acknowledged.

References

[1] Asghari, N., Broeg, C., Carone, L., Casas-Miranda, R., Castro Palacio, J.C., Csillik, I., Dvorak, R., Freistetter, F., Hadjivantsides, G., Hussmann, H., Khramova, A., Khristoforova, M., Khromova, I., Kitiashivilli, I., Kozlowski, S., Laakso, T., Laczkowski, T., Lytvinenko, D., Miloni, O., Morishima, R., Moro-Martin, A., Paksyutov, V., Pal, A., Patidar, V., Pecnik, B., Peles, O., Pyo, J., Quinn, T., Rodriguez, A., Romano, C., Saikia, E., Stadel, J., Thiel, M., Todorovic, N., Veras, D., Vieira Neto, E., Vilagi, J., von Bloh, W., Zechner, R., Zhuchkova, E.: 2004, "Stability of terrestrial planets in the habitable zone of Gl 777 A, HD 72659, Gl 614, 47 Uma and HD 4208", *Astronomy and Astrophysics* **426**, pp.353

[2] Barnes, R., Quinn, T.: 2001, "A Statistical Examination of the Short-Term Stability of the υ Andromedae Planetary System", *The Astrophysical Journal* **550**, pp.884

[3] Beaugé, C., Michtchenko, T.A.: 2003, "Modelling the high-eccentricity planetary three-body problem. Application to the GJ876 planetary system", *Monthly Notices of the Royal Astronomical Society* **341**, pp.760

[4] Beaugé, C., Ferraz-Mello, S., Michtchenko, T.A.: 2003, "Extrasolar Planets in Mean-Motion Resonance: Apses Alignment and Asymmetric Stationary Solutions", *The Astrophysical Journal* **593**, pp.1124

[5] Dvorak, R., Pilat-Lohinger, E., Funk, B., Freistetter, F.: 2003, "Planets in habitable zones: A study of the binary Gamma Cephei", *Astronomy and Astrophysics* **398**, pp.L1

[6] Dvorak, R., Pilat-Lohinger, E., Funk, B., Freistetter, F.: 2003, "A study of the stability regions in the planetary system HD 74156: Can it host earthlike planets in habitable zones?", *Astronomy and Astrophysics* **410**, pp.L13

[7] Froeschlé, C., Lega, E., Gonzi, R.: 1997, "Fast Lyapunov Indicators. Application to Asteroidal Motion", *Celestial Mechanics and Dynamical Astronomy* **67**, pp.41

[8] Gozdziewski, K., Bois, E., Maciejewski, A.J., Kiseleva-Eggleton, L.: 2001, "Global dynamics of planetary systems with the MEGNO criterion", *Astronomy and Astrophysics* **378**, pp.569

[9] Hanslmeier, A., Dvorak, R.: 1984, "Numerical Integrations with Lie-series", *Astronomy and Astrophysics* **132**, pp.203

[10] Ji, J., Kinoshita, H. Liu, L. and Li, G.: 2003, "Could the 55 Cancri Planetary System Really Be in the 3:1 Mean Motion Resonance?" *The Astrophysical Journal* **585**, pp.L139

[11] Jiang, I., Ip, W.: 2001, "The planetary system of upsilon Andromedae", *Astronomy and Astrophysics* **367**, pp.943

[12] Kasting, J.F., Whitmire, D.P., Reynolds, R.T.: 1993, "Habitable Zones around Main Sequence Stars", *Icarus* **101**, pp.108

[13] Kiseleva-Eggleton, L., Bois, E., Rambaux, N., Dvorak, R.: 2002, "Global Dynamics and Stability Limits for Planetary Systems around HD 12661, HD 38529, HD 37124 and HD 160691", *The Astrophysical Journal* **578**, pp.L145

[14] Kiseleva-Eggleton, L., Bois, E., Rambaux, N., Dvorak, R., Rivera, E.J.: 2002, "On the Dynamical State of New Multi-Planet Systems", *American Astronomical Society Meeting* **201.24.04**

[15] Laughlin, G., Adams, F.C.: 1999, "Stability and Chaos in the υ Andromedae Planetary System", *The Astrophysical Journal* **526**, pp.881

[16] Lichtenegger, H.: 1984, "The dynamics of bodies with variable masses", *Celestial Mechanics and Dynamical Astronomy* **34**, pp.357

[17] Lissauer, J.J., Rivera, E.J.: 2001, "Stability Analysis of the Planetary System Orbiting υ Andromedae. II. Simulations Using New Lick Observatory Fits", *The Astrophysical Journal* **554**, pp.1141

[18] Lowrence, P.J., Kirkpatrick, J.D., Beichman, C.A.: 2002, "A Distant stellar companion in the ups Andromedae System", *The Astrophysikal Journal* **572**, pp.L79

[19] Marcy, G.W., Butler, R.P., Fischer, D.A., Laughlin, G., Vogt, S.S., Henry, G.W. and Pourbaix, D.: 2002, "A Planet at 5 AU around 55 Cancri", *The Astrophysical Journal* **581**, pp.1375

[20] Marzari, F., Scholl, H., Tricarico, P.: 2005, "Frequency map analysis of the 3/1 resonance between planets b and c in the 55 Cancri system", *Astronomy and Astrophysics* **442**, pp.359

[21] Mayor, M., Queloz, D.: 1995, "A Jupiter-Mass Companion to a Solar-Type Star", *Nature* **378**, pp.355

[22] Mazeh, T., Zucker, S., dalla Torre, A., van Leeuwen, F.: 1999, "Analysis of the HIPPARCOS Measurements of upsilon Andromedae: A Mass Estimate of Its Outermost Known Planetary Companion", *The Astrophysical Journal* **522**, pp.L149

[23] McArthur, B., Endl, M., Cochran, W., Benedict, F., Fischer, D., Marcy, G., Butler, P., Naef, D., Mayor, M., Queloz, D., Udry, S., Harrison, T.: 2004, "Detection of a Neptune-Mass Planet in the rho1 Cancri System using the Hobby-Eberly Telescope." *ApJ. Letters*, accepted

[24] Menou, K., Tabachnik, S.: 2003, "Dynamical Habitability of Known Extrasolar Planetary Systems", *The Astrophysical Journal* **583**, pp.473

[25] Rivera, E.J., Lissauer, J.J.: 2000, "Stability Analysis of the Planetary System Orbiting υ Andromedae", *The Astrophysical Journal* **530**, pp.454

[26] Stepinski, T.F., Malhotra, R., Black, D.C.: 2000, "The υ Andromedae System: Models and Stability", *The Astrophysical Journal* **545**, pp.1044

[27] Zhou, L., Lehto, H.J., Sun, Y. and Zheng, J.: 2004, "Apsidal corotation in mean motion resonance: the 55 Cancri system as an example" *Monthly Notices of the Royal Astronomical Society* **350**, pp.1495

STABILITY OF HYPOTHETICAL TROJAN PLANETS IN EXOPLANETARY SYSTEMS

Bálint Érdi, Georgina Fröhlich, Imre Nagy and Zsolt Sándor
Department of Astronomy
Loránd Eötvös University
Pázmány Péter sétány 1/A
H-1117 Budapest, Hungary
B.Erdi@astro.elte.hu

Abstract The stability of hypothetical Trojan planets in exoplanetary systems is investigated. In the model of the planar three-body problem, corresponding to a gravitational system of a star, a giant planet and a Trojan planet, the stability regions for the Trojan planet around the Lagrangian point L_4 are determined depending on the mass of the two planets and the initial eccentricity of the orbit of the giant planet. The results indicate that in exoplanetary systems with one giant planet of several Jupiter-masses, a Trojan planet up to one Jupiter-mass can exist in stable motion around L_4.

Keywords: Trojan exoplanets – Stability

1. Introduction

The possible existence and stability of Trojan planets in exoplanetary systems have been the subject of several recent discussions. It is well known that Trojan asteroids exist in the Solar System in great number. It can be expected that Trojan-type objects exist also in exoplanetary systems. Laughlin and Chambers [3] outlined a possible formation mechanism of Trojan planets in protoplanetary accretion discs. They also discussed the question of detectability of extrasolar Trojan planets. According to their results two planets with masses comparable to the mass of Jupiter or Saturn around a solar-mass star can perform stable tadpole-type librations about the Lagrangian points L_4 or L_5 of the system. Pairs of Saturn-mass planets can also execute horseshoe orbits around a solar-mass star, but this is not possible for Jupiter-mass pairs. A pair of planets both in tadpole and horseshoe-type orbits induce a characteristic pattern in the radial velocity component of the central star that could be detected. Nauenberg [5] determined numerically the nonlinear stability do-

main of the triangular Lagrangian solutions in the general three-body problem as a function of the eccentricity of the orbits and the Routh's mass parameter. This study indicates that there is a wide range of Jupiter-size planetary masses (including brown dwarfs) and eccentricities for which such solutions could exist in exoplanetary systems.

Most of the known exoplanets are gaseos giant planets having large masses of the order of or several Jupiter-masses. The search for small terrestrial-like planets with solid surface is an outstanding aim of several ongoing and future research projects. It is an important question, whether Earth-like planets can exist in the habitable zone (HZ) of exoplanetary systems. If there is a giant planet in the HZ of a system, the existence of another planet there is unlikely. However, as Menou and Tabachnik [6] noted, terrestrial planets could exist at the stable Lagrangian points L_4 or L_5 of the giant planet moving in the HZ.

Érdi and Sándor [2] studied this possibility in detail, investigating five exoplanetary systems (HD 17051, HD 28185, HD 108874, HD 27442, and HD 114783) in which the only known giant planet moves in the HZ. By using the model of the elliptic restricted three-body problem they determined numerically the region around L_4 of each system where stable tadpole-type motion is possible. In [2] four other systems (HD 150706, HD 177830, HD 20367, and HD 23079) were also studied in which the orbit of the giant planet is partly outside the HZ due to its large eccentricity. It has been shown that in all studied systems there is an extended stability region around L_4, whose extent depend on the mass and the orbital eccentricity of the giant planet. It is possible that Trojan exoplanets of negligible mass exist in these systems.

Dvorak et al. [1] also studied three exoplanetary systems in which a giant planet moves close to the HZ in low eccentricity orbit. They determined the size and the structure of the stability region around L_4 and L_5 and pointed out that the stability region shrinks significantly with the increase of the orbital eccentricity of the giant planet. It is possible that in all three systems a small Trojan planet could exist in stable orbits with moderate eccentricities.

In our previous study [2] we assumed that the fictitious Trojan exoplanet had negligible mass. In this paper we study the problem more generally, giving mass to the Trojan planet up to 1 Jupiter-mass and determine the regions of stability around L_4 in the model of the planar three-body problem.

2. Dynamical model and method of investigation

For the investigation of the nonlinear stability of orbits around L_4 we used the model of the planar three-body problem, corresponding to a gravitational system of a star, a giant planet and a Trojan planet, by assuming, as a first step of a more general stability study, that the orbits of the two planets are in the same plane.

To determine the dynamical character of the orbits we used the method of the relative Lyapunov indicators (RLI) developed by Sándor et al. [7], [8]. The RLI measures the difference in the convergence of the finite-time Lyapunov indicators to the maximal Lyapunov characteristic exponents of two initially very close orbits. The values of the RLI are characteristically several orders of magnitude larger for orbits in a chaotic region than in a regular domain. The method is extremely fast in establishing the ordered or chaotic nature of individual orbits, and therefore is very well applicable to explore the dynamical structure of the phase space. According to our experiments, gained in different dynamical problems, it is enough to integrate the two very close orbits for a few hundred times of the longest orbital period of the studied system. In the present investigation we integrated the orbits for 10^3 periods of the giant planet.

In our computations we used the following parameters and initial orbital elements.

- Mass of the central star: $m_0 = 1\ m_\odot$ (solar mass)
- Mass of the giant planet: $m' = 1, 2, 3, 4, 5, 6, 7\ m_J$ (Jupiter-mass)
- Initial orbital elements of the giant planet:
  - semi-major axis: $a' = 1$ AU
  - eccentricity: $e' = 0 - 0.30$, stepsize: $\Delta e' = 0.05$
  - argument of the pericentre: $\omega = 0$
  - mean anomaly: $M' = 0$
- Mass of the Trojan planet: $m = 0, 1, 2, 3, 10, 100\ m_E$ (Earth-mass) and $1\ m_J$
- Initial orbital elements of the Trojan planet:
  - semi-major axis: $a = 0.8 - 1.2$ AU, stepsize: $\Delta a = 0.001$ AU
  - eccentricity: $e = 0$
  - synodic longitude: $\lambda - \lambda' = 20^\circ - 180^\circ$, stepsize: $\Delta\lambda = 2^\circ$,

where λ and λ' are the mean orbital longitudes of the Trojan and the giant planet, respectively. (Initially $\lambda' = 0$, since $\lambda' = M' + \omega'$.)

We computed maps of dynamical stability around L_4 in the following way. Selecting a value of m', e' and m from the given sets, we changed the semi-major axis and the synodic longitude of the Trojan planet in the given intervals with the given stepsize and computed the values of the RLI for all resulting orbits. Then we represented the logarithm of the values of the RLI corresponding to each initial point on the $(a, \lambda - \lambda')$ plane on a black and white scale. In

what follows we discuss the main characteristics of these maps. Some representatives of them are shown in Figures 1-8. Low RLI values (light regions) correspond to stable orbits, high RLI values (dark shades) indicate chaotic behaviour. The black background corresponds to escape or collision orbits with the giant planet. Considering that 7 values for the mass of both planets, and also 7 values for the initial orbital eccentricity of the giant planet were taken, altogether 343 maps were computed. These dynamical stability maps can be used to establish the stability region around L_4 in known exoplanetary systems with one giant planet.

3. Maps of dynamical stability

Fig. 1 shows the stability region around L_4 for $m = 0$, $m' = 1m_J$, $e' = 0$ (circular restricted three-body problem, with mass parameter $\mu = m'/(m_0 + m') \approx 0.001$). It can be seen that there is a central more stable region and going outwards a ring structure appears corresponding to higher order resonances between the short and long period components of the librational motion around L_4.

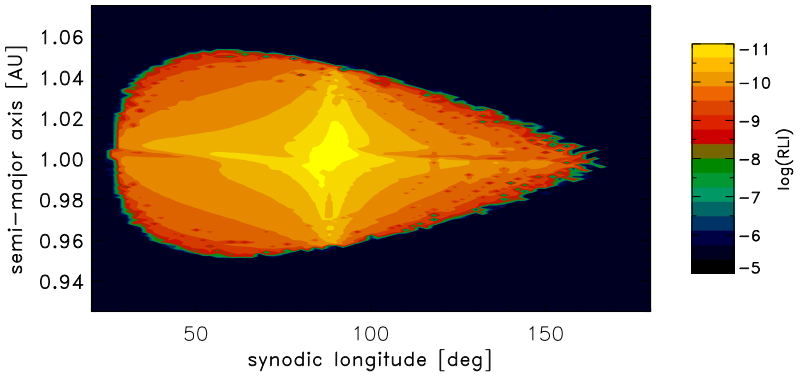

Figure 1. Structure of the stability region around L_4 in the circular restricted three-body problem ($m = 0$, $e' = 0$) for the mass parameter $\mu \approx 0.001$ ($m' = 1m_J$).

The computations show that increasing the mass of the giant planet, the stability region becomes shorter in the synodic longitude and wider in the semi-major axis. Near its edge the ring structure disrupts into a chain of islands. In Fig. 2, obtained for $m' = 2m_J$, both a ring and a chain of small islands can be seen. These islands are remnants of a former ring. The shrinking of the stability region with the increase of the mass of the giant planet is not monotonic, it reaches a minimum extension at $m' = 6m_J$ (Fig. 3), then it is larger again for $m' = 7m_J$ (not shown in the figures).

In the elliptic restricted three-body problem, when $m = 0$ and $e' \neq 0$, the structure of the stability regions is similar to that of the circular problem. Figs. 4 and 5 show two examples which are somewhat different from the general

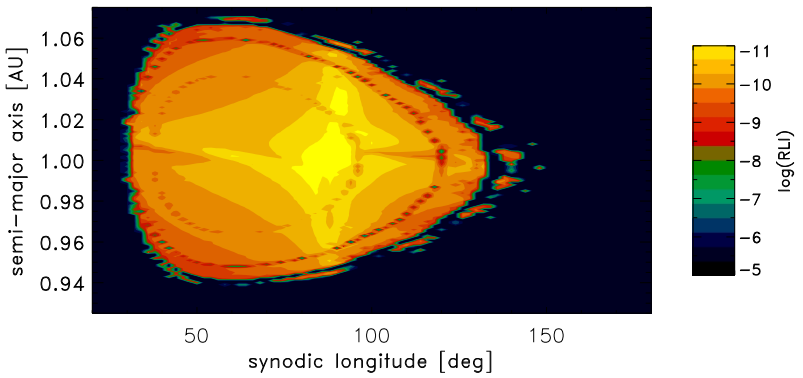

Figure 2. Structure of the stability region around L_4 in the circular restricted three-body problem ($m = 0$, $e' = 0$) for $\mu \approx 0.002$ ($m' = 2m_J$).

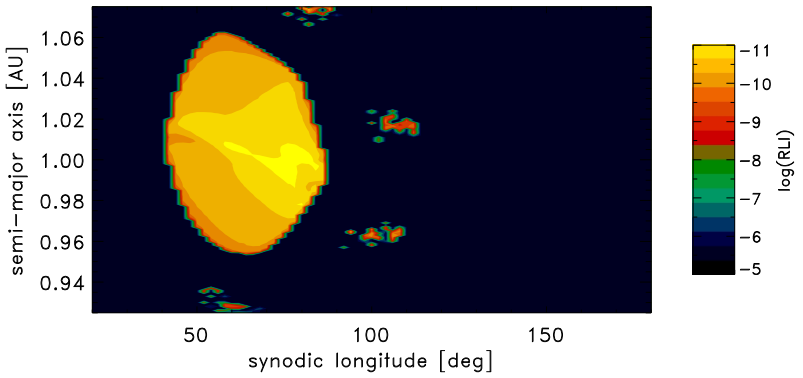

Figure 3. Structure of the stability region around L_4 in the circular restricted three-body problem ($m = 0$, $e' = 0$) for $\mu \approx 0.006$ ($m' = 6m_J$).

picture. Fig. 4, obtained for $e' = 0.1$, $m' = 4m_J$, exhibits a well structured stability region around L_4. In Fig. 5, obtained for $e' = 0.2$, $m' = 3m_J$, a compact stability region is present.

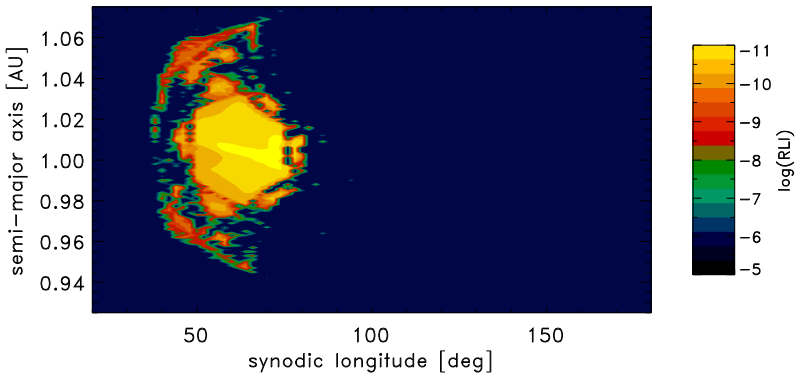

Figure 4. Structure of the stability region around L_4 in the elliptic restricted three-body problem for $e' = 0.1$, $\mu \approx 0.004$ ($m = 0$, $m' = 4m_J$).

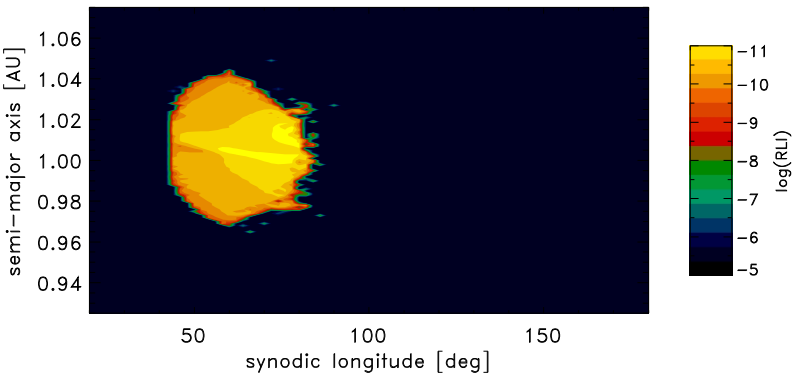

Figure 5. Structure of the stability region around L_4 in the elliptic restricted three-body problem for $e' = 0.2$, $\mu \approx 0.003$ ($m = 0$, $m' = 3m_J$).

When the Trojan planet has non-zero mass, the stability region is still quite extended. Figs. 6 and 7 show the cases when $m = 1m_E$ and $10m_E$ (in both cases $e' = 0$, $m' = 1m_J$). A comparison with Fig. 1 ($m = 0$, $e' = 0$) reveals that the size of the stability region is about the same for Trojan planets of several Earth-masses as for negligible mass.

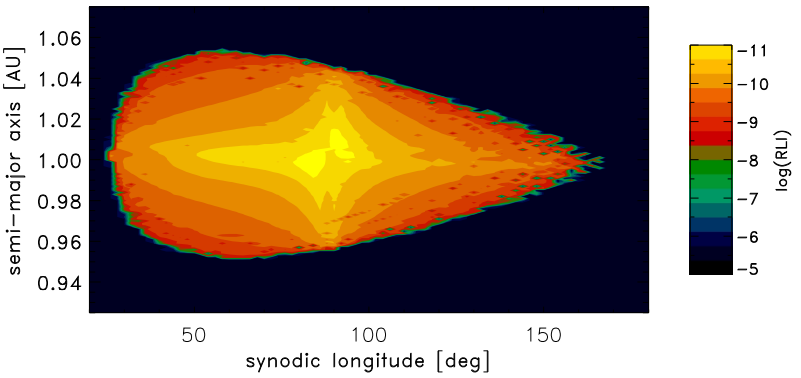

Figure 6. Structure of the stability region around L_4 in the three-body problem for $m = 1m_E$, $e' = 0$, $m' = 1m_J$.

We determined the stability regions around L_4 in the planar three-body problem for the combinations of the masses: $m = 1, 2, 3, 10, 100m_E$, and $1M_J$, $m' = 1, 2, 3, 4, 5, 6, 7m_J$, and initial eccenticity of the giant planet $e' = 0.05, 0.10, 0.15, 0.20, 0.25, 0.30$. For a given pair of m' and e' the size of the stability region does not change much with the increase of m. The changes are larger when m is fixed, and either m' or e' is changed while the other is kept constant. The computations confirm the existence of a stability region around L_4 even for $m = m_J$, when the mass of the giant planet is several Jupiter-masses and its orbit is very eccentric. Fig. 8 shows the stability region for $m = 1m_J$, $e' = 0.3$, and $m' = 1m_J$. Increasing m' at this value of m and e',

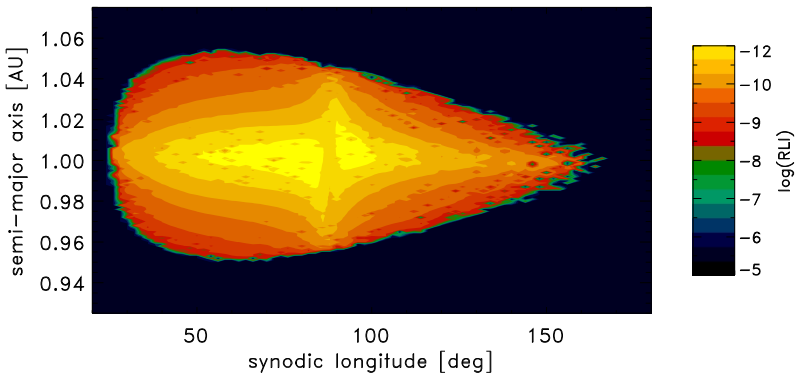

Figure 7. Structure of the stability region around L_4 in the three-body problem for $m = 10m_E$, $e' = 0$, $m' = 1m_J$.

the size of the stability region decreases reaching its minimum at $m' = 5m_J$, after which it grows again, as the computations show.

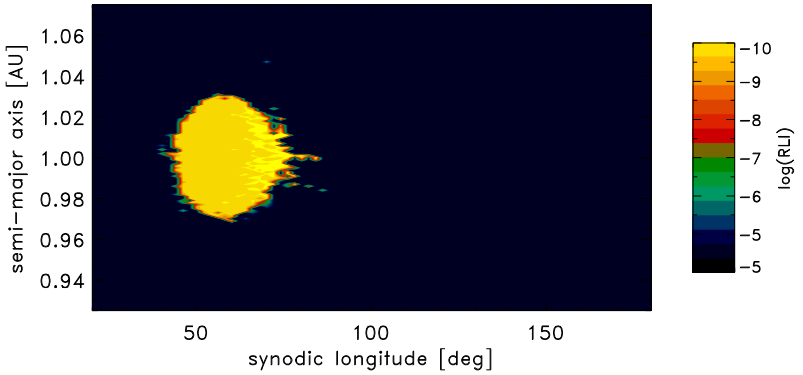

Figure 8. Structure of the stability region around L_4 in the three-body problem for $m = 1m_J$, $e' = 0.3$, $m' = 1m_J$.

4. Size of the stability region

The size of the stability region depends on the masses m, m' and the eccentricity e'. In [2] we determined this dependence for $m = 0$. Continuing that work we studied how the size of the stability region depends also on m. Fig. 9 shows the dependence of the size of the stability region around L_4 on m' and e' for $m = 1m_J$ for 500 periods of the primaries. The figure was obtained as follows.

For a given pair of e' and $\mu = m'/(m_0 + m')$ we put the Trojan planet in the point L_4 with zero relative initial velocity and checked if it stays there or performs librational motion around L_4 for 500 periods of the primaries. (Certainly, the time interval in this kind of investigations is crucial, we took this value as a compromise. The general features of the stability structure

appear during this time.) Then we moved the Trojan planet a little away from L_4 along a line going throgh L_4 perpendicular to the line of the primaries. We checked again the librational motion of the Trojan planet. Proceeding in this way we determined the largest distance ε from L_4 (perpendicular to the line of the primaries) at which the Trojan planet starting with zero relative initial velocity still performs librational motion around L_4 and does not cross the line of the primaries. We defined the stability region as the largest possible libration region. Changing e' and μ on a fine grid, we determined for each pair of (e', μ) the largest ε (in the unit of the distance of the primaries) corresponding to the largest libration region. For the sake of better visualization Fig. 9 shows the values of $1/\log(\varepsilon)$ instead of ϵ on a black and white scale. The light region above the V-shaped curve corresponds to instability, libration is possible below this curve. Darker regions correspond to larger librational regions. It can be seen that the size distribution of the stability regions shows a complex structure. The size is the largest when both e' and μ are small ($e' < 0.1$, $\mu < 0.01$). This means that in an exoplanetary system with one giant planet of several Jupiter-masses there can be a Trojan planet of one Jupiter-mass. The fine structure of the figure confirms our previous finding that the size of the stability region changes much either fixing e' and varying μ, or vice versa. There is also an extended stability region for small values of e' ($e' < 0.1$) between $\mu = 0.014 - 0.02$. This was also found by Lohinger and Dvorak [4]. The unstable regions below $\mu = 0.014$ and at $\mu = 0.023$ correspond to the resonances 3:1 and 2:1 between the frequencies of libration around L_4. The finger-like structure on the left side of the figure may be related to higher order resonances.

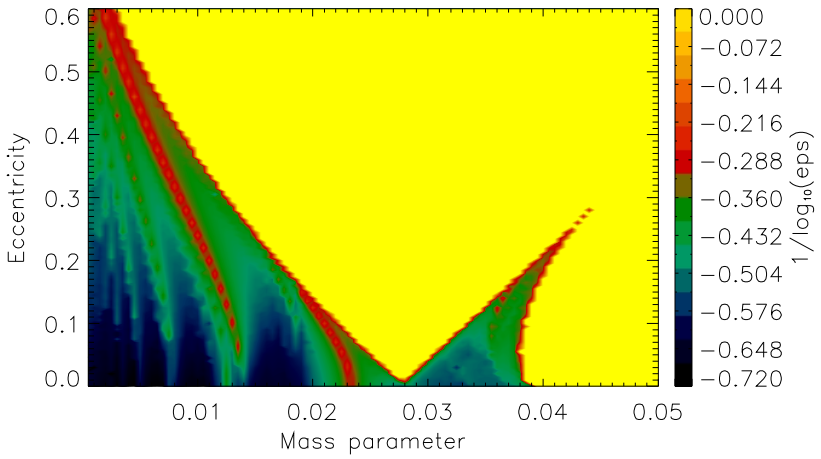

Figure 9. Size of the stability region around L_4 in the planar three-body problem for a Trojan planet of mass $m = 1m_J$ depending on the ecccentricity e' and mass parameter $\mu = m'/(m_0 + m')$ of the giant planet.

Acknowledgments

The support of the Hungarian Scientific Research Fund under the grants OTKA T043739 and D048424 is acknowledged. This research has also been supported by the Austrian-Hungarian Scientific and Technology Cooperation under the grant A-12/04.

References

[1] Dvorak, R., Pilat-Lohinger, E., Schwarz, R., Freistetter, F.: 2004, *Astron. & Astrophys.* **426**, L37

[2] Érdi, B., Sándor, Zs.: 2005, *Celest. Mech. & Dyn. Astron.* **92**, 113

[3] Laughlin, G., Chambers, J. E.: 2002, *Astron. J.* **124**, 592

[4] Lohinger, E., Dvorak, R.: 1993, *Astron.& Astrophys.* **280**, 683

[5] Nauenberg, M.: 2002, *Astron J.* **124**, 2332

[6] Menou, K., Tabachnik, S.: 2003, *Astrophys. J.* **583**, 473

[7] Sándor, Zs., Érdi, B., Efthymiopoulos, C.: 2000, *Celest. Mech. & Dyn. Astron.* **78**, 113

[8] Sándor, Zs., Érdi, B., Széll, A., Funk, B.: 2004, *Celest. Mech. & Dyn. Astron.* **90**, 127

STABILITY INVESTIGATIONS OF HIGHLY INCLINED PLANETARY ORBITS IN BINARY SYSTEMS

Imre Nagy, Áron Süli and Bálint Érdi
Department of Astronomy
Loránd Eötvös University
i.nagy@astro.elte.hu

Abstract The stability of P–type orbits in a binary system (mass–ratio equal to 0.5) was studied on the semi–major axis vs. inclination plane, similar to [10]. In the present work we investigate a larger part of the phase space, by calculating the relative Lyapunov Indicators and maximal eccentricities.

Keywords: exoplanets, binaries, stability of planetary systems

1. Introduction

Observations show that 60% of the main sequence stars are in binary or multiple systems (see [3]). Moreover, pre-main sequence stars may indicate that almost all of the stars are born in multiple systems (see [4], [5]). On the other hand, until now more than 160 exoplanets have been discovered, and some of them belong to binary systems. These facts show, that the investigation of the stability of planetary orbits in binaries is very important.

The discovered planets in binaries move on satellite orbits i.e. the planet revolves around one stellar component (S–type orbit; see Fig. 1). Theoretically there is another possible type of motion, the so called planetary orbit (P–type; see Fig. 1), whereas the planet moves around both stars. The S–type orbits were studied for some known systems by [6], [7], [8] and [9].

The stability of P–type orbits was also studied by [10] on the semi–major axis vs. inclination plane for a binary's mass–ratio ($\mu = m_2/(m_1 + m_2)$) equal to 0.5 by calculating the Fast Lyapunov Indicators (FLI) and escape times. They concluded that the stability limit varies between 2.1 and 3.85 binary separation (bs) depending on the eccentricity of the binary, and found a finger-like unstable island at inclinations $i = 15°$ to $i = 45°$.

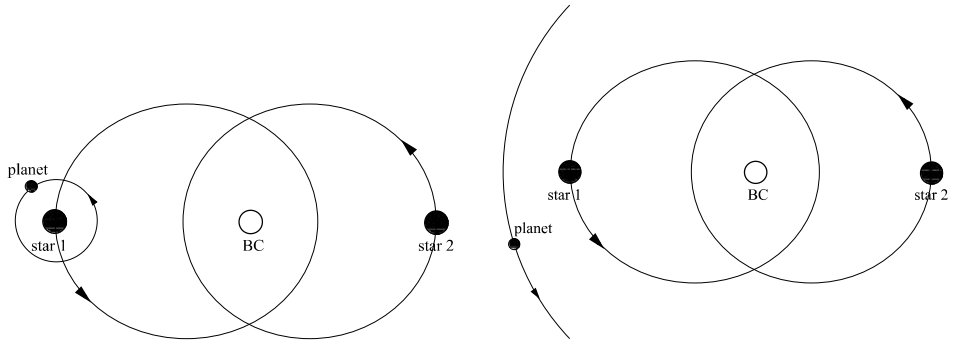

Figure 1. In the left panel: satellite–type or S–type motion: the planet revolves around one of the stars; right panel: planetary-type or P–type motion: the planet revolves around both star, i.e. it moves around the barycenter (BC).

In this paper we also study the stability of P–type orbits in a larger part of the phase space by using the methods of the Relative Lyapunov Indicators (RLI) and the maximum eccentricity. In the next section we give a description of the investigated system, the initial conditions and the applied numerical methods. After that we delineate and summarize our results.

2. Numerical setup

2.1 Initial conditions

For the integration of the equations of motion of the 3D restricted three-body problem we used the Bulirsch-Stoer integrator with adaptive stepsize control in the case of the RLI, and the Runge-Kutta-Neystrom-Felhberg RKN7(8) integrator with adaptive stepsize control for calculating the maximum eccentrity. The orbit of the primaries, and initially the massless planet's orbit is also circular, i.e. the eccentricity of the planet $e = 0$. The semi–major axis of the planet a is measured in the unit of the distance between the primaries and the initial value a_0 varies from 0.55 to 4 with stepsize $\Delta a = 0.005$. We use four starting mean anomaly (M_0) values for the planet: 0°, 45°, 90° and 135°. These angles are measured from the connecting line of the primaries (see Fig. 2). (The resulting maps are the average of the four M_0. See later.) The inclination i is the angle between the orbital plane of the planet and the reference plane (xy–plane), which is the orbital plane of the binaries; initial value i_0 varies from 0° to 180° with stepsize $\Delta i = 1.25^\circ$. The x–axis is the line connecting the primaries at $t = 0$. We note, that this line coincides with the line of node if $i \neq 0$, $t = 0$, i.e. the node of the planet is $\Omega_0 = 0^\circ$. Initially the argument of the pericenter of the planet is $\omega_0 = 0^\circ$.

The above defined orbital elements are referred to a barycentric reference frame, where the mass of the barycenter is $M = M_1 + M_2$. Using the usual procedure, the barycentric co-ordinates and velocities were calculated. After

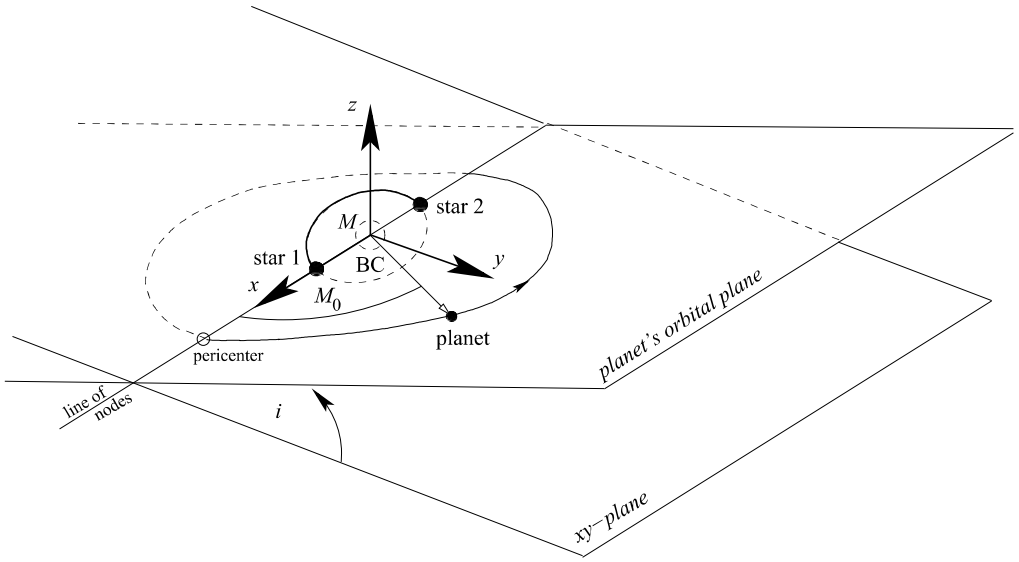

Figure 2. Configuration of the system: BC is the barycenter, the separation of the stars is the unit of distance, i is the planet's inclination with respect to the reference plane and M_0 is the initial mean anomaly of the planet.

that we transformed our co-ordinate and velocity vectors to a frame of reference with S_2 in the origin.

2.2 The maximum eccentricity method (MEM)

For an indication of stability a straightforward check based on the eccentricity was used. This osculating orbital element shows the probability of orbital crossing and close encounter of two planets, and therefore its value provides information on the stability of the orbit. We examined the behaviour of the eccentricity of the planet along the integration, and used the largest value as a stability indicator; in the following we call it the maximum eccentricity method (hereafter MEM). This is a reliable indicator of chaos, because the overlap of two or more resonances induce chaos and large excursions in the eccentricity. We know from experience, that instability comes from a chaotic growth of the eccentricity. This simple check has already been used in other stability studies, and was found to be a powerful indicator of the stability character of an orbit (see [2], [1]).

Calculating the maximum eccentricity an upper threshold was used. Whenever the eccentricity reached 0.8, the orbit was considered unstable, and the integration was stopped.

2.3 The relative Lyapunov indicator (RLI)

The method of the relative Lyapunov indicator (RLI) has been introduced by [11] for a particular problem, but its efficiency was demonstrated in a later paper [12] for 2D and 4D symplectic mappings and for Hamiltonian systems.

This method based on the idea that two initially nearby orbits are integrated simultaneously and also the evolution of their tangent vectors are followed. For both orbits the Lyapunov characteristic indicator (LCI) is calculated and the absolute value of their difference averaged over time is defined as RLI:

$$RLI(t) = \frac{1}{t}|LCI(x_0) - LCI(x_0 + \Delta x)|, \tag{1}$$

where Δx is the distance in phase space between the two orbits. The definition of RLI contains an arbitrary parameter Δx, which may affect the result. The authors have tested the sensitivity of RLI versus the norm of this parameter and found that the RLI depends almost linearly on Δx in the regular domain, while it is practically independent of it in the chaotic domain. Nevertheless, the value of the RLI is characteristically always several order of magnitudes smaller in a regular domain than in a chaotic region.

3. Results

The resulting figures were obtained as follows: we started the integration at mean anomaly $M_0 = 0°, 45°, 90°, 135°$ so we got $RLI^{(0)}$, $RLI^{(45)}$, $RLI^{(90)}$, $RLI^{(135)}$ and maximum eccentricity $ME^{(0)}$, $ME^{(45)}$, $ME^{(90)}$, $ME^{(135)}$ also. The plotted value is an average:

$$\frac{\overline{RLI}(a,i)}{\overline{ME}(a,i)} = \frac{1}{4} \sum_{M_0=0,45,90,135} \frac{RLI^{(M_0)}(a,i)}{ME^{(M_0)}(a,i)}. \tag{2}$$

We note, that this averaging in the case of the RLI stress the chaotic behaviour of an orbit, whereas in the case of the maximum eccentricity it is not so drastic.

At first we calculated the same part of the phase space as in [10], which is $a_0 = 1.8-2.5$ and $i_0 = 0-50°$. We performed the calculations on a finer grid: $\Delta a_0 = 0.005$ *bs* and $\Delta i_0 = 1.25°$ (see Fig. 3). Our maps are very similar to [10], except that our figures are more detailed, especially the second RLI map, where the system was integrated up to 1000 binary periods (*bp*). In Fig. 3 one can see some resonant formations, which appear at lower inclinations and are deviated at higher inclinations.

In Fig. 4 we show two maps for a larger domain of the phase space, which corresponds to $a_0 = 0.55-4$ *bs* and $i_0 = 0-180°$, with stepsizes $\Delta a_0 = 0.005$ *bs* $\Delta i_0 = 1.25°$. Both maps contain 691×145 points, resulting more than 10^5 orbits, if we take into account the averaging detailed above this number rises to

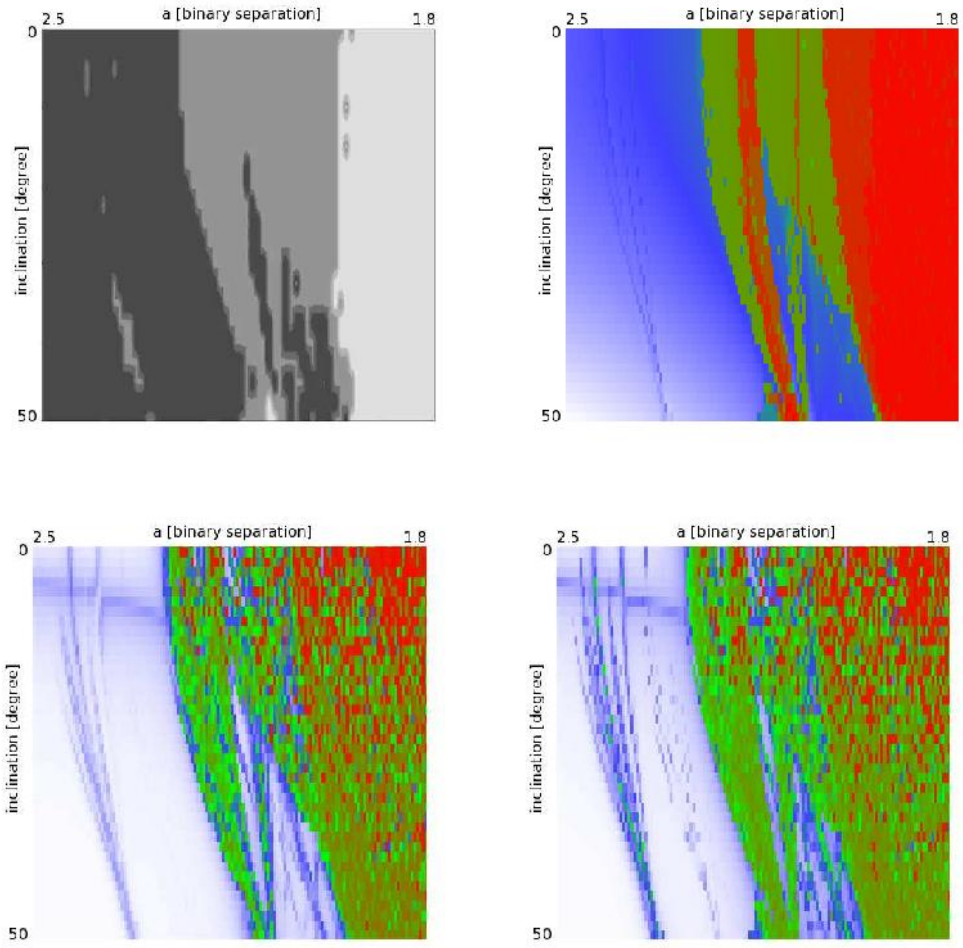

Figure 3. *Upper right*: FLI for 10000 *bp* in [10] Black indicates the stable zone, white the unstable. *Upper left:* Maximum eccentricity for 1000 *bp*. White shows the stable zone, black the unstable. *Lower left:* RLI for 200 *bp*. Colors like in max. ecc. *Lower right:* RLI for 1000 *bp*. Colors like in max. ecc.

4×10^5 orbits. Each orbit was integrated for 1000 *bp* in the case of the MEM and for 500 *bp* in the case of the RLI.

It is interesting, that the stable regions are wider in the case of retrograde orbits ($i_0 > 90°$) than for direct ones ($i_0 < 90°$). In the RLI map we can see several resonant formations. A resonant curve splits into three stronger and some fainter branches which makes it similar to a fork. The shape is generated by the applied averaging. For example in the case of the 3:1 resonance: when $M_0 = 0°$, we can see a sharp vertical line at $a = 2.085$ *bs*, at $M_0 = 45°$, the centre of the line is shifted to $a = 2.175$ *bs* and at $M_0 = 90°$ the centre is at $a = 2.23$ *bs*. The case of $M_0 = 135°$ is similar to $M_0 = 45°$. The width of the line grows with the distance from the 3:1 resonance ($a = 2.08$ *bs*). The averaging shows simultaneously the three cases, producing the fork shape. The

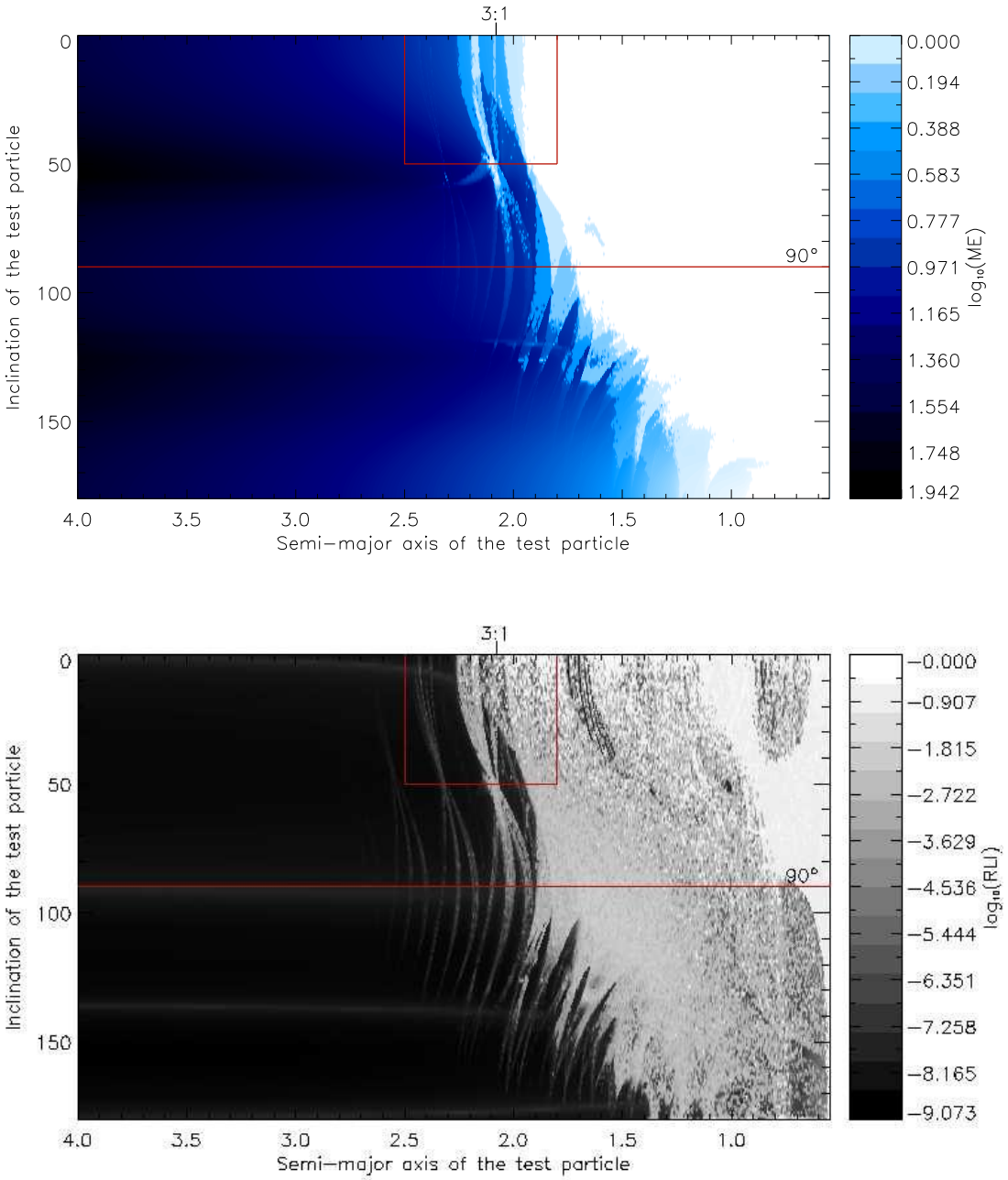

Figure 4. *Upper:* MEM for 1000 *bp Lower:* RLI for 500 *bp* White shows the unstable zone, black the stable.

fork belonging to the 3:1 resonance iduces Pilat-Lohinger's finger-like unstable island (see Fig. 4).

4. Summary

We investigated the stability region around a binary on the $a - i$ plane by calculating the RLI and the ME. Our results are in very good agreement with the results of [10], on the other hand they give information about a more extended part of the phase space. The maps obtained by the RLI show very fine resonant structures. The stable regions are wider when $i_0 > 90^\circ$ (retrograde orbits). The resonant curves have a fork-like shape which is caused by the averaging. We demonstrated that Pilat-Lohinger's unstable island is created by a triple fork-like resonant shape.

Acknowledgments

The support of the Austrian-Hungarian Scientific and Technology Cooperation, grant number A-12/04 is acknowledged.

References

[1] Asghari N. et al., 2004, A&A, 426, 353

[2] Dvorak R., Pilat-Lohinger E., Funk B., Freistetter F., 2003, A&A, 398, L1

[3] Duquennoy & Mayor 1991, A&A 248, 485

[4] Mathieu et al., 2000, Protostars and Planets IV, 703

[5] Zinnecker & Mathieu, 2001, The Formation of Binary Stars, IAU Symp., 2001

[6] Pilat-Lohinger, E. et al., 2002, Proceedings of the Second European Workshop on Exo/Astrobiology, 547

[7] Pilat-Lohinger, E. et al., 2003, Proc. "Towards Other Earths: DARWIN/TPF and the Search for Extrasolar Terrestrial Planets", 543

[8] Dvorak, R. et al., 2002, A&A, 398, L1

[9] Pilat-Lohinger, E., 2005, Dynamics of Populations of Planetary Systems Proceedings

[10] Pilat-Lohinger, E. et al., 2003, A&A, 400, 1085

[11] Sándor, Zsolt; Érdi, Bálint; Efthymiopoulos, Christos:The Phase Space Structure Around L4 in the Restricted Three-Body Problem Celestial Mechanics and Dynamical Astronomy, v. 78, Issue 1/4, p. 113-123 (2000).

[12] Sándor, Zsolt; Érdi, Bálint; Széll, András; Funk, Barbara: The Relative Lyapunov Indicator: An Efficient Method of Chaos Detection Celestial Mechanics and Dynamical Astronomy, v. 90, Issue 1, p. 127-138 (2004).

THE STABILITY OF EXOPLANETS IN THE BINARY GLIESE 86 AB

Elke Pilat-Lohinger and Barbara Funk
Institute for Astronomy
University of Vienna
Türkenschanzstrasse 17
A-1180 Vienna, Austria
lohinger@astro.univie.ac.at

Abstract Gliese 86 is one of 3 binary systems with a close stellar component, where an extra-solar planet was discovered. The host-star is classified as a K1 main-sequence star and its stellar companion was first identified as a brown dwarf (Els et al., 2001) and later as a white dwarf (Mugrauer & Neuhäuser, 2005). In our numerical investigation we determine the stable zone around the K1V star for different eccentricities of the binary system in both stellar configurations and compare the results of the systems. The planetary motion is analyzed by means of (a) the Fast Lyapunov Indicator (FLI) and (b) the maximum eccentricity (max-e). A study of mean motion resonances in the Gliese 86 system showed that the perturbative effects due to the discovered planet are restricted to very close orbits. Therefore, we distinguish 3 regions: (i) the *inner zone* (**IZ**), which is the region between the detected planet and the so-called habitable zone; (ii) the *habitable zone* (**HZ**) is defined as the region around a star where liquid water can exist on the surface of a terrestrial-like planet; and (iii) the *outer zone* (**OZ**) which is the region outside the HZ, which is not influenced by the detected giant planet. For the computations different dynamical models were applied – i.e. the restricted four body problem for the (**IZ**) and the **HZ**, the elliptic restricted three body problem for the (**OZ**). In general, the motion of fictitious planets in the Gliese 86 system is very stable. Only for high eccentricities of the binary (≥ 0.75) chaotic motion occurs even in the HZ. In this case the stable zone shrinks to a small region around Gliese 86, where the eccentricity of an additional fictitious planet should be < 0.5 due to perturbations of the detected giant planet.

Keywords: binary system: Gliese 86 – S-type orbits – stable regions – habitable zone – Fast Lyapunov Indicators – maximum eccentricity

1. Introduction

The discovery of extra-solar planets in binaries led to a growing interest of stability studies of such systems, where we distinguish between 2 types of motion[1]: the *planet (or P-) type motion* when the planet moves around both stars and the *satellite (or S-) type motion*, when the planet orbits one star. Up to now we know 14 double star systems, where planetary companions were found in S-type motion.

Dynamical studies of planetary motion in binaries were carried out during the last 25 years. There are general studies using either the three body problem (see e.g. Harrington (1977), Szebehely (1980), Szebehely & McKenzie (1981)) or the elliptic restricted three body problem[2] like the ones by Dvorak (1984 and 1986), Rabl & Dvorak (1988), Dvorak et al. (1989) and more recently by Holman & Wiegert (1999), Pilat-Lohinger & Dvorak (2002), Pilat-Lohinger et al. (2003) and Musielak et al. (2005). The last cited paper showed also an application to binary systems with observed giant planets, where they have chosen three systems with a close moving planet among which they selected as well Gliese 86 – which is studied in detail in the present investigation. Furthermore we have to mention that Benest studied in a series of papers several binaries numerically (see Benest 1988, 1989, 1996, 1998 and 2003).

The binary Gliese 86 is about 11 pc away from the Sun in the constellation Eridanus. The double star system consists of a K1 main sequence star ($m_1 = 0.7 M_S$) and in all probability a white dwarf (with a minimum mass of $0.55 M_S$) at about 21 AU as proposed by Mugrauer & Neuhäuser (2005) using NAOS-CONICA (NACO) and its new Simultaneous Differential Imager (SDI). The former detection by coronographic images using the ESO adaptive optic system ADONIS (Els et al., 2001) identified a late L or late T brown dwarf (BD) of about 50 Jupiter-masses moving at a distance of at least 18.75 AU. But Els et al. could not explain the linear trend in the observation, as it can be done by the new detection by Mugrauer & Neuhäuser (2005). However, the first who suggested a white dwarf (WD) companion for Gliese 86 was Jahreiß in 2001.

The planet is found to be very close to the K1 V star, at 0.11 AU with an orbital period of less than 16 days (Queloz et al., 2000). Due to the CORALIE measurements a minimum mass of $4 M_{\text{Jupiter}}$ was determined.

In our study we first examine numerically the dynamical behavior of fictitious low mass planets in the binary Gliese 86, where we neglect the detected planet in order to define the stable region for different eccentricities of the binary (e_{binary}). The results for both binary configurations (i.e. BD or WD as secondary) gave rise to carry out further investigation of this double star using $e_{\text{binary}} = 0.2$ and 0.7.

Then we determine the mean motion resonances (MMRs) of the system Gliese 86 and we divide the region between the detected planet at 0.11 AU and the secondary (at 21 AU and 18.75 AU, respectively) into 3 parts: (i) the *inner zone* (**IZ**) between the detected planet and the habitable zone, where we can expect a gravitational influence of Gliese 86 b; (ii) the *habitable zone* (**HZ**), where only the inner part might be perturbed by Gliese 86 b; and (iii) the *outer zone* (**OZ**) outside the habitable zone, which is not influenced by the giant planet. The results for the different regions are discussed in sections 4 – 6.

For the computations two dynamical models are used: (i) the restricted 4 body problem[3] (R4BP) for the **IZ** and the **HZ**, (ii) the elliptic restricted 3 body problem (ER3BP) for the **OZ**.

Contrary to most other studies, we determine the dynamical state of the orbits not only through straightforward orbital computations but we applied a chaos indicator, with which it is easier to define the regions of long-term stability. As chaos indicator we use the Fast Lyapunov Indicator (FLI) (Froeschlé et al. 1997) and combine the results with the evolution of the orbit's eccentricity. In the next section we describe the numerical methods and the initial conditions for the computations.

2. Numerical setup

For the different numerical studies of the binary Gliese 86 we determine the stable zones in the orbital element space mainly by means of the fast Lyapunov Indicator (FLI). This chaos indicator measures the length of the largest tangent vector

$$\psi(t) = \sup_i \|v_i(t)\| \tag{1}$$

(where $i = 1, \ldots n$ and n denotes the dimension of the phase space) and is therefore, a fast method to distinguish between regular and chaotic behavior. It was introduced by Froeschlé et al. in 1997. To carry out the necessary computations, we modified the n-body program[4] of R. Gonczi, (from the Observatory of Nice, France).

Moreover, we check the stability of the orbital motion by calculating the maximum eccentricity (max-e) (a) over the whole integration time and (b) for successive subintervals (of either 50 or 500 years[5]) to verify the variation of the max-e. This is an easy criterion to distinguish between regular and chaotic motion which was used e.g. by Laskar in 1994 to show the long-term evolution of the planets in the Solar System. In general it is called either *maximum action method* (see Morbidelli, 2002, p. 106) or *sup-map method* (according to Froeschlé & Lega, 1996). The computations for this study are carried out using the Lie-series method, which has also an adaptive step size control for

the correct handling of possible close encounters of celestial bodies (for details see e.g. Lichtenegger (1984) and Hanslmeier & Dvorak, (1984)).

The initial conditions of the massive bodies are taken from the papers by Els et al. (2001) – when the secondary m_2 is a brown dwarf (BD) – and by Mugrauer & Neuhäuser (2005) – when the secondary m_2 is a white dwarf (WD) – only the eccentricity of the binary (e_{binary}) was varied (see table 1) and all angles – inclination (i), node (Ω), perihelion distance (ω) and mean anomaly (M) – are set to zero.

Table 1. Orbital parameters of the binary Gliese 86

	m_1 (K1 V star)	m_2 (BD)	m_2 (WD)	m_3 (planet)
mass:	0.79 M_S	50 M_J	0.55 M_S	$4M_J$
semi-major axis [AU]:	0.	18.75	21	0.11
eccentricity:	0.0 – 0.7	0.0 – 0.7	0.0 – 0.7	0.046

The initial conditions of the fictitious planets are given in table 2

Table 2. Initial conditions of the massless bodies

	orbits in the R4BP	**orbits in the ER3BP**
semi-major axis [AU]:	0.14 – 1. (with step: 0.01)	0.3 – 10.5 (with step: 0.01)
eccentricity:	0., 0.1,0.2,. . . , 0.5	0., 0.1,0.2,. . . , 0.5
inclination [deg]:	0	0 – 45 (with a step of 5)
Ω, ω, M:	0	0

and the integration time for the FLI computations is between 1000 and 100000 periods of the binary, which seems to be not very much. But we have to point out that the dynamical state of an orbit can be determined with the FLIs about 200 times faster than by calculating the Lyapunov characteristic exponent (LCE)[6]. In addition we combine the FLI results with those of the maximum eccentricity.

3. General stability studies

3.1 Stability of S-type motion around Gliese 86 A (without the detected planet)

Since we do not have any knowledge about the binary's eccentricity – neither from the detection by Els et al., 2001 nor from the new observations by Mugrauer & Neuhäuser, 2005 – we study the region between the K1 V star and the secondary (BD and WD, respectively) – where we neglect the discovered giant planet – in order to define the stable zones of S-type motion around

Gliese 86 for different eccentricities of the binary ($e_{\text{binary}} = 0$ to 0.9 with a step of 0.05). As dynamical model we use the ER3BP, where the orbital behavior is determined by (a) the application of the FLIs and (b) the max-e. The initial conditions of the Gliese 86 system are given in table 1 of section 2 (i.e. m_1 and both m_2). The massless bodies are started in circular motion at semi-major axes between 0.3 and 12 AU with a step of 0.01 AU. And the computations time is 100000 years (i.e. more than 1000 periods of the binary).

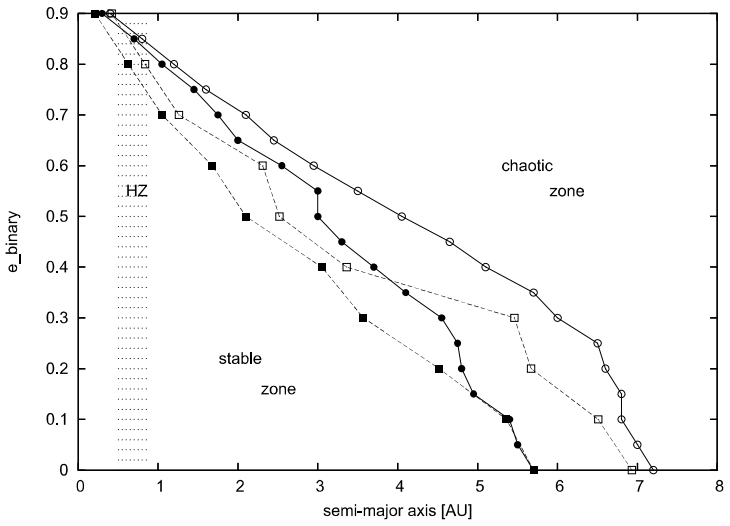

Figure 1. The stability of a fictitious mass-less body in the gravitational field of the binary Gliese86 AB, where the detected planet at 0.11 AU was neglected. One can see three zones (stable,mixed and chaotic) for both configurations: dashed lines with open and full squares for a WD and full lines with open and full circles for a BD as secondary.

The results of the FLI computations are shown in fig. 1 which splits the (semi-major axis,e_{binary}) parameter space into 3 zones: (i) a *stable zone* whose border (dashed lines with black squares (for $m_2 =$ WD)/solid line with black circles (for $m_2 =$ BD) is defined by the largest distance from Gliese 86 ($= m_1$) up to which we have found only regular motion; (ii) a *chaotic zone*, where no regular motion can be found – which is outside the dashed line with open circles; and in-between the two border-lines one can see (iii) a *mixed zone* where both regular and chaotic motion can be found (see e.g. fig. 5.a, where these 3 zones can be clearly seen). For the old system ($m_2 =$ BD) one can see that the border of the chaotic zone is nearly constant up to $e_{\text{binary}} = 0.2$ with values around 7.2 AU. An increase of the binary's eccentricity leads to an almost linear shift of this border towards the host-star Gliese 86. Moreover, one can recognize a quit similar development of both border-lines for high eccentricities ($e_{\text{binary}} \geq 0.65$), where the mixed zone is quite small. In contrast thereto, we have a large mixed zone for eccentricities up to 0.5.

For the new system ($m_2 =$ WD) the two border-lines show always a decrease of the stable zone and an enlargement of the chaotic zone when the binary's

eccentricity is increased. *Remark: As a comparison we did some computations using the general three body problem with a planet's mass of about 5 Jupiter-masses. For such a system the stable zone shrinks significantly only for high eccentricity motion of the fictitious planet ($e_{planet} \geq 0.3$) .*

According to the results illustrated in fig. 1, we have chosen two eccentricities of the binary: (i) $e_{\text{binary}} = 0.2$ and (ii) $e_{\text{binary}} = 0.7$ for which we carry out further numerical studies.

3.2 Mean motion resonances

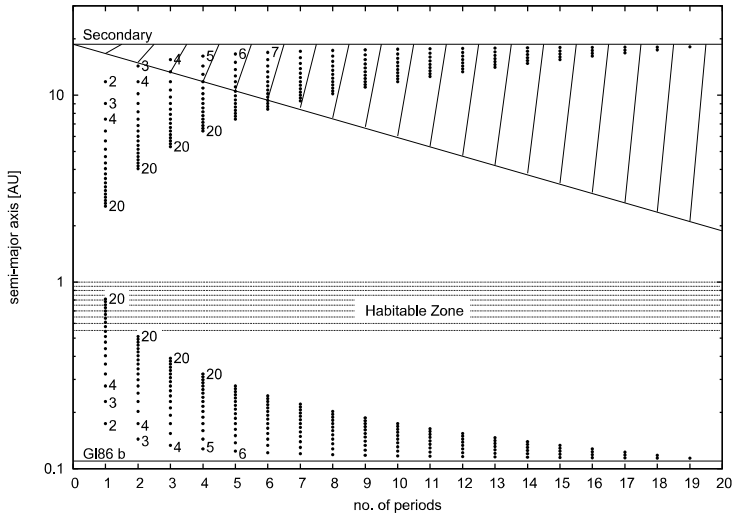

Figure 2. The mean motion resonances (MMRs) up to the order 20 of an additional fictitious planet with respect to Gliese 86b (lower part) and with respect to the secondary (upper part). The x-axis denotes the number of periods either for a fictitious planet (lower part) or for the secondary – BD – (upper part), and the y-axis shows the position of the resonances (on a log-scale). For a better understanding of the graphical presentation we give the following examples: e.g. "2" at $x = 1$ and $y = 11.14$ (upper part of the figure) means 2:1 resonance of a fictitious planet with the secondary at a=11.14 AU; and "2" at $x = 1$ and $y = 0.174$ (lower part) means 1:2 resonance of a fictitious planet with Gliese 86b at $a = 0.174$ AU. The hatching denotes the region which is occupied by the secondary, and since we do not have any knowledge about its eccentricity we marked this region for $e_{\text{secondary}}$ from 0 (left border) to 0.9 (right border). The dotted region labels the habitable zone of Gliese 86. Here it is clearly seen, that the MMRs do not influence the HZ of Gliese 86 except the high order MMRs with respect to the detected planet, which are not that important. We have to note that the MMR-plot for the new system ($m_2 =$ WD) is quite similar to fig. 2 – so it is useless to show both.

To get a first picture about the gravitational influence of the secondary (i.e. the brown dwarf) and of the discovered planet on a fictitious planet moving in the region between these two bodies, we computed the mean motion resonances (=MMR) up to the order 20. Its representation is given in fig. 2, where the lower part is with respect to the detected planet, the upper part is with respect to the secondary and the dotted region labels the habitable zone. It is

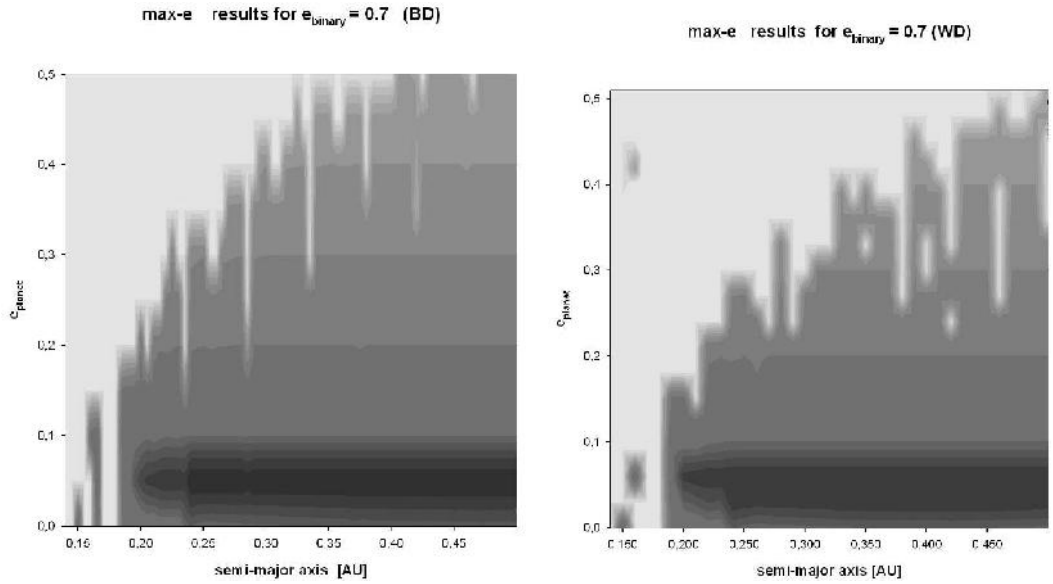

Figure 3. Stability maps of a fictitious massless planet in the **IZ**, where the eccentricity of this planet is varied between 0 and 0.5 and the binary's eccentricity was fixed to 0.7 (since we expect perturbations of the secondary in the **IZ** only for high values of e_{binary}). (a) The left panel summerizes the e-max results for the old system (BD as secondary) where the different gray shades in the stable zone indicates regions of various maximum eccentricities which increases permanently from 0.2 (black zone) around $e_{\text{planet}} = 0.05$ to 0.6 at $e_{\text{planet}} = 0.5$. Additionally, one can see that initial circular motion belongs to a higher max-e level. The faintest region represents the unstable motion where the maximum eccentricity was 1. (b) The right panel is the result for the new system (WD as secondary), which shows the same overall structure. For more details see section 4.

clearly seen that most of the resonances with respect to the detected planet are concentrated to distances < 0.3 AU from the K1V star and only a few, very high order resonances are in the habitable zone. Furthermore, fig. 2 explains quite well the application of different dynamical models: (i) the R4BP for the regions where we can expect an influence of the detected planet, i.e. the **IZ** and as well the **HZ**; (ii) the ER3BP for the **OZ**.

The slanted line defines the peri-center distance of the secondary for different eccentricities – from 0 (upper left position) to 0.9 (lower right position) – which indicates already an influence on the HZ for high eccentricity motion.

4. The orbital behavior of fictitious planets in the inner zone

For the study of the region, where we have to expect an influence of the detected giant planet according to the MMR result, we use the R4BP and the initial conditions given in section 2 for the massive bodies. The parameter space of Gliese 86 is explored in two planes: the (a_0, e_{binary})– and in the (a_0, e_{planet})–plane[7]. We determine the orbital behavior by means of the FLI, which are

computed for at least 1000 periods of the binary. Low values of the chaos indicator label regular motion which is given by the dark region in fig. 3.a.

The study in the (a_0, e_{binary})–plane for circular planetary motion is not mapped since it can be described easily as the border between regular and chaotic motion is at $a_0 = 0.19$ AU for all eccentricities of the binary. Within the chaotic region a stripe of stable motion (at $a_0 = 0.15$ AU) for all e_{binary} was found, which is connected to the 8:5 MMR with Gliese 86b. And in the stable zone two small chaotic islands appear: one at $a_0 \sim 0.23$ AU for $0.2 \leq e_{\text{binary}} \leq 0.4$ (next to the 1:3 MMR) and one at $a_0 \sim 0.206$ AU for $e_{\text{binary}} = 0$ (close to the 2:5 MMR).

The results of a similar study for various eccentricities of fictitious planets (e_{planet}) and a fixed eccentricity of the binary (i.e. 0.7) are given for both systems (BD and WD as secondary) in figs. 3.a and b. Comparing the two plots one can see the same overall structure: (1) An increase of the planet's eccentricity invokes as expected an increase of the chaotic region (white regions) (2) The border between regular and chaotic motion is dominated by the appearance of mean motion resonances. Which can either stabilize the motion – like at 0.15 AU for $e_{\text{planet}} = 0$ (8:5 MMR) or at 0.16 AU for $0.05 \leq e_{\text{planet}} \leq 0.1$ (7:4 MMR) – or destabilize the motion (faint stripes in the dark region – like the 3:1 MMR at about 0.23 AU); Both max-e plots show quite constant level-curves for the maximum eccentricity in the stable region so that we do not expect a significant influence of the detected giant planet especially on the outer part of the **IZ** for the BD secondary and at least for low-eccentricity motion of the fictitious planets in the case of a WD secondary.

5. The habitable zone around Gliese86 A

The HZ is roughly speaking the region around a star, where conditions similar to that of the earth can be found for a terrestrial-like planet, so that a biosphere can be built. One of the most famous work thereto was published by Kasting et al. in 1993, which is still a reference work for many studies nowadays. However, the discovery of numerous extra-solar planets[8] motivated scientists of different fields of research to improve the definition of the HZ based on the actual knowledge of research (Lammer et al. – ISSI project, 2005)[9].

Stability studies are important contributions thereto, since long-term stability of planetary motion in the HZ is a necessary requirement for the development of a biosphere. The wideness of the HZ is limited to a small region, depending on the spectral type and the age of the host-star, therefore the planet's eccentricity has to be small enough if we require that the planet is always in the HZ.

In the case of Gliese86 A the HZ is – according to Kasting et al. (1993) – between 0.48 and 0.95 AU. As the detected gas giant moves at 0.11 AU,

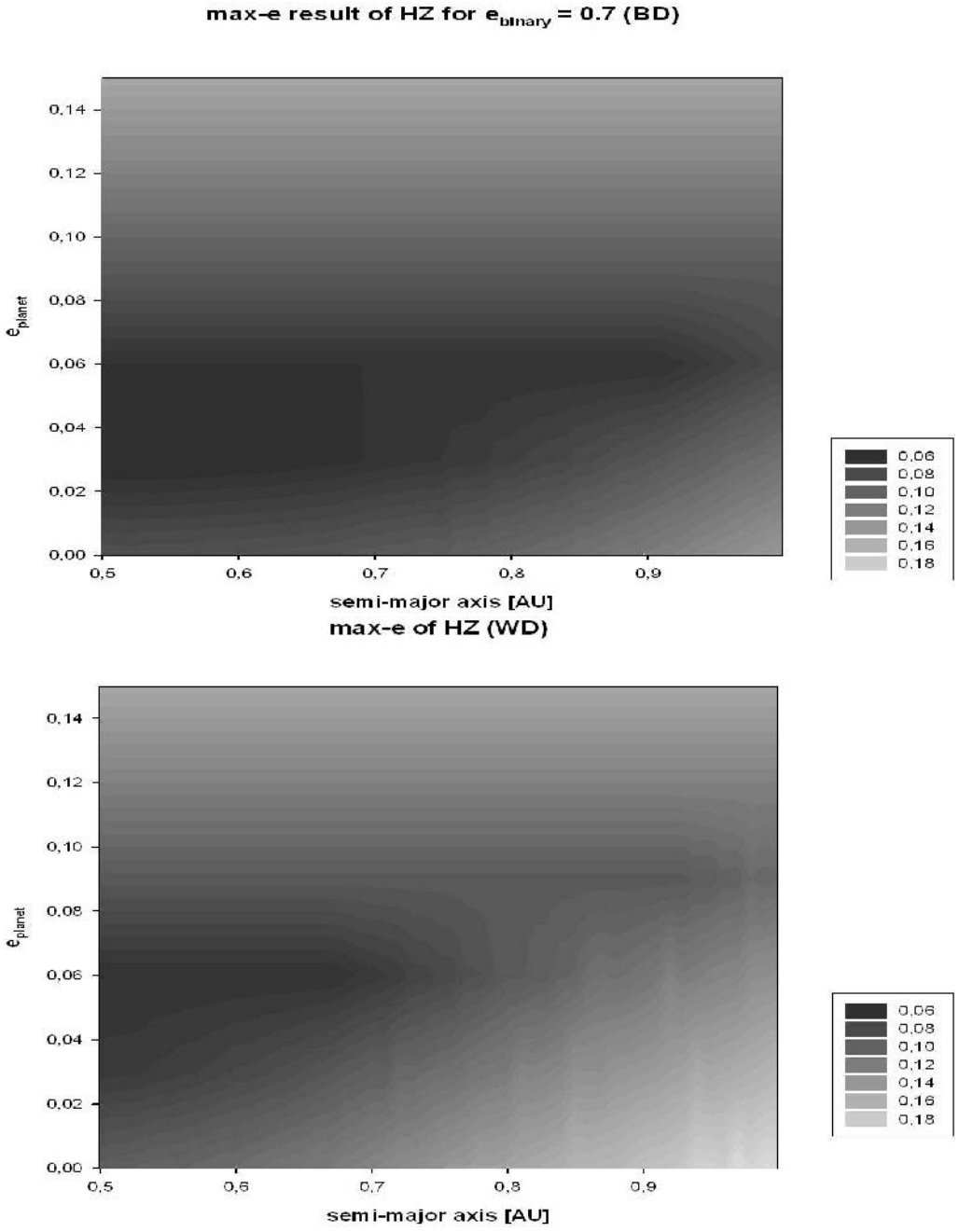

Figure 4. Maximum eccentricity plots of the HZ of Gliese86 A (x-axis) for fictitious planets with different initial eccentricities (y-axis) upper panel for a BD secondary and lower panel for a WD secondary. The gray shades indicate the different values of max-e, where the darkest area shows in each plot the region of highest maximum eccentricity. For more details see the text.

its gravitational influence on the HZ is not very strong, as it can be seen in fig. 2, where only high order resonances can be found in this zone. The most important question for the binary Gliese86 AB is, where was the planet built. If it was formed at a distance between 4 and 5 AU[10] and migrated towards the star through the HZ, an already existing terrestrial-like planet would have been

ejected from the system. But if the gas giant was built closer to the star – maybe quite near to the region, where it was found (see Wuchterl et al., 2000), then we can expect terrestrial-like planets in the HZ (which cannot be detected up to now). However, there are only a few studies that deal with the difficult problem of planetary formation in binaries (see e.g. Kley, 2001; Kley & Burkert, 2000; Nelson, 2001 or Nelson & Papaloizou, 2003), which needs still a lot of work.

Our stability study shows the HZ of Gliese 86 in a very stable state up to an eccentricity of the binary of 0.75 (for a BD secondary) an 0.7 (for a WD secondary). While for higher e_{binary} the HZ will be chaotic (see fig. 1).

In a dynamical study of the HZ it is important to control the evolution of the orbit's eccentricity, which should be small enough so that the planet moves always in the HZ. Therfore, we show the results of the max-e study for both systems (BD and WD as secondary). As dynamical model we used the R4BP, where we studied the influence of the giant planet on a massless body in the HZ. Figs. 4.a and b summarize the results of the two systems, which show constant level lines of the max-e for initial eccentricities of the planet ≥ 0.09 in both plots. More precisely, the value of the max-e level curve corresponds to the initial value of e_{planet}. For lower values of the planet's eccentricity differences can be clearly seen. However, the darkest region shows always the zone with the highest max-e value, and the "finger-like" shape – which is different for the two systems – indicates the region of lowest e-max.

The border of the so-called "continuously habitable zone (CHZ)" (i.e. the region, where the whole planetary orbit is in the HZ) depends – from the dynamical point of view – on the initial eccentricity of the planet in the HZ. In table 3 the boundaries for the CHZ are given for different eccentricities of the fictitious planets – up to 0.33, which is the largest eccentricity for the HZ of Gliese A to find a whole planetary orbit in this zone (for higher eccentricities the CHZ would not exist anymore).

The inner boundary for circular motion is in both panels around 0.52 and the outer boundary is around 0.88 AU for the old system and about 0.83 AU in the new system. For low eccentricities of the planet it is clearly seen that the two border-lines disperse up to $e_{\text{planet}} = 0.06$, due to lower values of max-e, while a further increase of the planet's eccentricity leads to an increase of the max-e value, where the two border-lines will converge. In both cases one can see the inner border at 0.565 AU and the outer border at 0.852 AU for $e_{\text{planet}} = 0.15$.

For a better understanding of the max-e level curves in the dynamical maps of figs. 4.a and b, we show as an example the evolution of the maximum eccentricity for an initial e_{planet} of 0.06, where the max-e value is constant (i.e. 0.06) up to a semi-major axis of 0.66 AU and increases linearly afterwards to 0.116 at 0.98 AU. In fig. 5 one can see different time evolutions of the maximum eccentricities for various initial semi-major axes of the planet (0.5 AU, 0.6 AU, 0.7 AU and 0.99 AU) where we computed the maximum eccentricity

Table 3. Boundaries for planetary motion in the HZ of Gliese 86

e_{planet}	**inner boundary** [AU]	**outer boundary** [AU]
0.06	0.5106	0.9245
0.07	0.5161	0.9159
0.08	0.5217	0.9074
0.09	0.5275	0.8991
0.1	0.5333	0.8909
0.11	0.5393	0.8829
0.12	0.5455	0.8750
0.13	0.5517	0.8673
0.14	0.5581	0.8596
0.15	0.5647	0.8522
0.20	0.6000	0.8167
0.25	0.6400	0.7840
0.30	0.6857	0.7538
0.33	0.7164	0.7368

for intervals of 500 years. All curves show a very regular behavior, certainly with different amplitudes and periods depending on the semi-major axis: (a) the variation of the semi-major axis from 0.5 to 0.66 AU causes a reduction of the amplitude and the period of the max-e curve (see lower 2 lines of fig. 5) and (b) on the contrary the variation of the semi-major axis from 0.67 to 0.98 AU blows up the amplitude and reduces the period of the curve (see upper 2 lines of fig. 5). This plot explains very good the difference between constant level-curves (lower 2 lines) – where the max-e value corresponds to the initial e_{planet} – and an increase of the maximum eccentricity depending on the semi-major axis (upper 2 curves).

6. Planetary motion in the outer zone

In figs. 6a-d we summarize the numerical results of the region outside the HZ in the two systems. As expected the more massive WD reduces the stable zone: for $e_{\text{binary}} = 0.2$ from more than 7 AU to less than 6 AU (compare the left panels) and for a high eccentricity motion of the binary ($e_{\text{binary}} = 0.7$) the border of stable motion is shifted from 2 AU to less than 1.5 AU. The most significant features of the max-e result (lower panels) are the non-dependency of the stable zone on the inclination of the planet up to about $38\,\text{deg}$, while higher inclinations show a decrease of the stable zone due to the Kozai resonance – which influences the whole zone at these high inclinations since we recognize an increase of the eccentricity according to the gray shades. The same behaviour was found for the new system, but the constant border

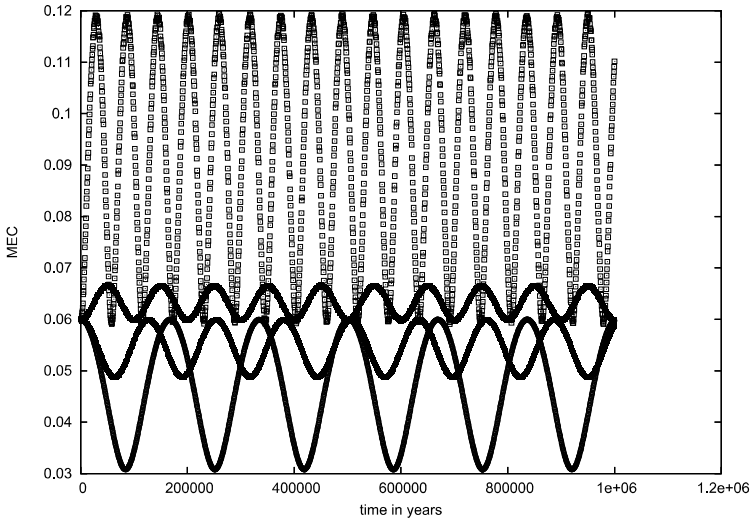

Figure 5. Time evolution of the maximum eccentricity for 4 different start positions of the planet: 0.5 AU, 0.6 AU, 0.7 AU and 0.99 AU, the initial eccentricity of the planet is in all cases 0.06; e_{binary} is set to 0.7 and the computation time is 1Myrs. The different behavior of the curves is described in the text (section 5).

between regular and chaotic motion is shifted to nearly 5 AU for $e_{\text{binary}} = 0.2$ and nearly 1.3 AU for $e_{\text{binary}} = 0.7$.

In the upper two panels of fig. 6 one can see that an increase of the planet's eccentricity leads to a slight decrease of the stable zone as it was already found in the old system with the BD secondary (see Pilat-Lohinger et al., 2003).

7. Conclusion

In our numerical stability study of the binary Gliese 86 we divide the investigated region between the detected giant planet at 0.11 AU and the secondary (a white dwarf at about 21 AU or a brown dwarf at about 18.75 AU) into 3 zones:

(i) IZ – inner zone – is the region from 0.14 to 0.48 AU which is influenced gravitationally by the giant planet, mainly by mean motion resonances, which can stabilize or destabilize the region.

(ii) HZ is the habitable zone, which is from the dynamical point of view very stable for this system, especially for weakly eccentric motion of the binary. From the 3 cases of HZ:

1 the HZ is between the host-star and the detected giant planet,

2 the giant planet moves in the HZ,

3 the HZ is outside the discovered giant planet,

that we can distinguish from the observations for dynamical studies, Gliese 86 A is an example for the third case. As a consequence we can

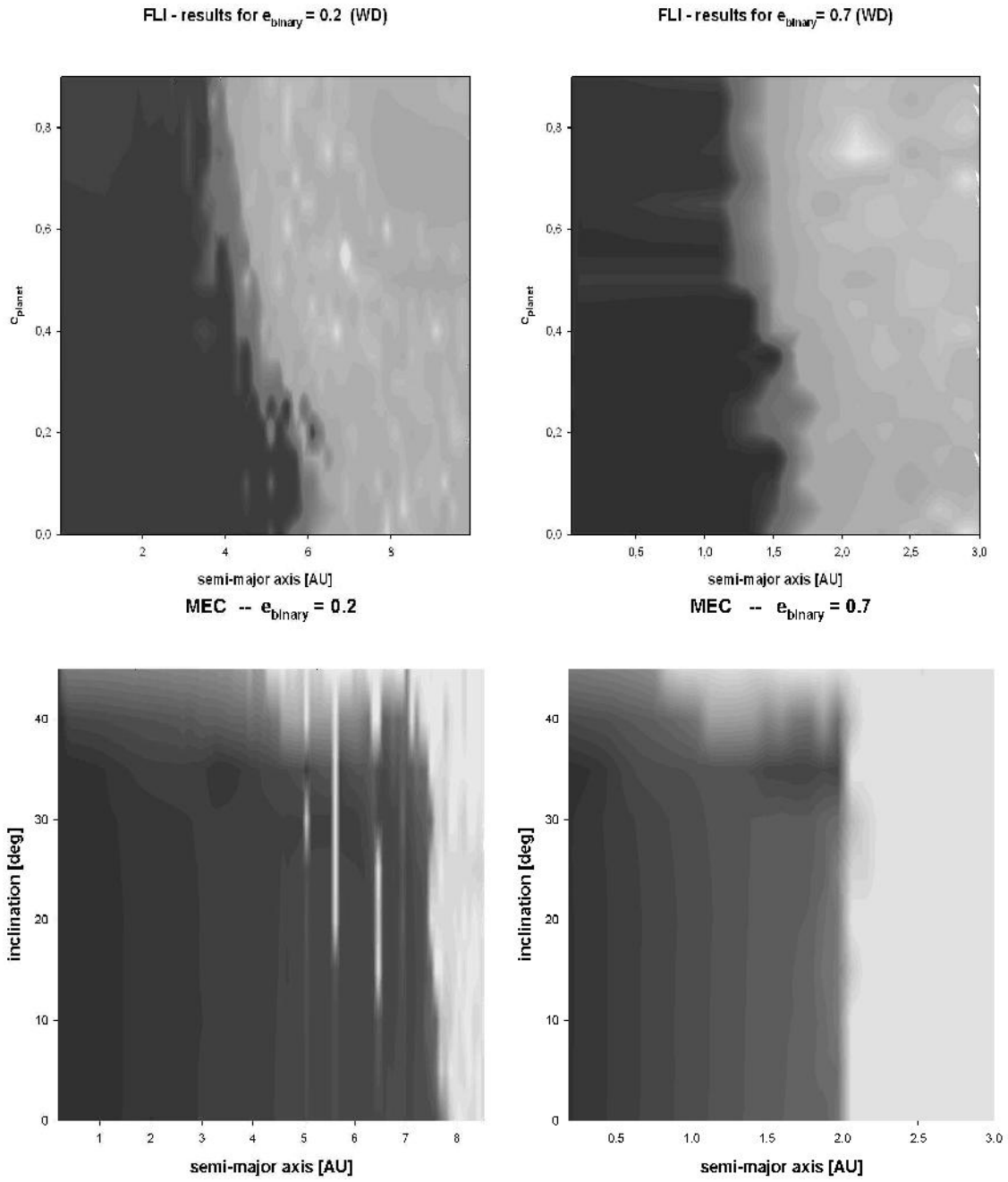

Figure 6. Stable zone for planetary motion in the binary Gliese 86 AB: the upper two panels show the results of FLI computations in the new system (the WD secondary) and the lower two panels show the e-max results of the old system (the BD secondary). The eccentricity of the binary is 0.2 for the left panels and 0.7 for the right panels. The stable motion in the (a,i)- or (a,e_planet)-plane is given by the dark region in all plots. Please note the different scaling for the figures.

say, it has from the dynamical point of view a high probability of hosting an Earth-like planet in the habitable zone, as it was also found in the study by Menou and Tabachnik (2003).

But for such systems the most important question is, where the giant planet was built – at or beyond 5 AU or closer to the position, where it was found – but this cannot be answered by pure dynamical studies. Although if the FLI result shows the HZ fully stable, an additional max-e study is necessary to define the dynamical continuously habitable zone (CHZ), within which the fictitious planets remain all the time.

However, we have found that even for an eccentricity of 0.7 of the binary the whole HZ of Gliese 86 is stable.

(iii) OZ – outer zone – is the outermost region, where the detected planet has no influence, so that the stable zone depends only on the mass-ratio and the eccentricity of the binary. A comparison of the old (the BD secondary) and the new system (the WD secondary) shows the expected decrease of the stable zone in the new system due to the higher mass of the secondary.

In a future work we will use this binary to study the influence of a hot-Jupiter on the HZ in detail.

Acknowledgments

The authors want to thank especially Dr. M. Endl from the McDonald Observatory for many fruitful discussions about Gliese 86. EP-L wishes to acknowledge the support by the Austrian FWF (Hertha Firnberg Project T122). BF wishes to acknowledge the support by the FWF project P16024. This study was also supported by the International Space Science Institute (ISSI) and benefits from the team ‘Evolution of Habitable Planets’. The support of the Austrian-Hungarian Scientific and Technology Cooperation, grant number A-12/04 is also acknowledged.

Notes

1. According to Dvorak (1986) there are 3 types of motion in binary systems but since the libration- (or L-)type motion is limited to certain mass-ratios of the two massive bodies ($\sim 1/25$), studies of binary systems can be restricted to the S-type and P-type motion.

2. The elliptic restricted three body problem studies the motion of a massless body moving in the gravitational field of two massive bodies, which move in Keplerian orbits around their center of mass.

3. In the restricted four body problem we study the motion of a massless body in the gravitational field of the primary ($= m_1$), the secondary ($= m_2$) and the giant planet ($= m_3$)

4. The program of R. Gonczi applies the Bulirsch-Stoer method for the orbital computations and determines also the Lyapunov Exponent in its original version.

5. The time interval for the maximum eccentricity depends on the chosen integration time.

6. private communication with C. Froeschlé and E. Lega

7. a_0 is the initial semi-major axis of a fictitious planet; e_{binary} is the initial eccentricity of the binary and e_{planet} is the initial eccentricity of a fictitious planet.

8. Due to the observational techniques all detected planets are gas giants - but hopefully the planned space missions (like COROT, Darwin, TPF, ...) will find terrestrial-like planets in the HZ of other sun-like stars

9. An ongoing project supported by the International Space Science Institute in Bern, Switzerland

10. Before the discovery of extra-solar planets it was claimed by A. Boss that the formation of gas planets is at or outside 5 AU (which is called snow-line).

References

[1] Benest, D. 1988, *A&A* **206**, 143

[2] Benest, D. 1989, *A&A* **223**, 361

[3] Benest, D. 1996, *A&A* **314**, 983

[4] Benest, D. 1998, *A&A* **332**, 1147

[5] Benest, D. 2003, *A&A* **400**, 1103

[6] Dvorak, R. 1984, *CMDA* **34**, 369

[7] Dvorak, R. 1986, *A&A* **167**, 379

[8] Dvorak, R., Froeschlé, Ch. Froeschlé, C. 1989, *A&A* **226**, 335

[9] Els, S.G., Sterzik M.F., Marchis F., Pantin E., Endl M., Kürster M. 2001, *A&A* **370**, L1–L4

[10] Froeschlé, C., Lega, E., Gonczi, R. 1997, *CMDA* **67**, 41

[11] Froeschlé, C., Lega, E. 1996, *CMDA* **64**, 21

[12] Hanslmeier, A., Dvorak, R. 1984, *A&A* **132**, 203

[13] Harrington, R.S. 1977, *AJ* **82**, 753

[14] Holman, M.J., Wiegert P.A. 1999, *AJ* **117**, 621

[15] Jahreiß, H. 2001, *Astronomische Gesellschaft Abstract Series* **18**,#P110

[16] Kasting, J.F. 1993, *Icarus* **101**, 108

[17] Kley, W. 2001, *IAUS in Potsdam 2000, eds. H. Zinnecker and R.D.Mathieu*,511

[18] Kley, W., Burkert, A. 2000, *ASP Conference Proceedings* **219** eds. F. Garzoń, C.Eiroa, D.de Winter and T.J.Mahoney Astron.Society of the Pacific, 189

[19] Laskar, J. 1994, *A&A* **287**, 9

[20] Lichtenegger, H. 1984, *CMDA* **34**, 357

[21] Menou, K., Tabachnik, S. 2003, *ApJ* **583**,473

[22] Morbidelli, A. 2002, *Modern Celestial Mechanics, Aspects of Solar System Dynamics* Taylor & Francis, London, 106

[23] Musielak, Z.E., Cuntz, M., Marshall, E.A., Stuit, T.D. 2005, *A&A* **434**, 355

[24] Nelson, R. 2001, *Astronomische Gesellschaft Abstract Series* **18**

[25] Nelson, R., Papaloizou J.C.B. 2003, *Proceedings of the DARWIN/TPF conference in Heidelberg 2003* ESA Publications Division, ISBN 92-9092-849-2, 175

[26] Pilat-Lohinger, E., Dvorak, R. 2002, *CMDA* **82**, 143

[27] Pilat-Lohinger, E., Funk, B., Dvorak, R. 2003, *A&A* **400**, 1085

[28] Pilat-Lohinger, E., Dvorak, R., Funk, B., Bois, E., Freistetter, F.: 2003, *Proceedings of the DARWIN/TPF conference in Heidelberg 2003* ESA Publications Division, ISBN 92-9092-849-2, 543

[29] Queloz, D.,Mayor, M., Weber, L.,Blicha, A., Burnet, M., Confino, B., Naef, D., Pepe, F., Santos, N., Udry, S. 2000, *A&A* **354**, 99

[30] Rabl, G., Dvorak, R. 1988, *A&A* **191**, 385

[31] Szebehely, V. 1980, *CMDA* **22**, 7

[32] Szebehely, V.,McKenzie, R. 1981, *CMDA* **23**, 131

[33] Wuchterl, G., Guillot, T., Lissauer, J.J. 2000, *in Protostars and Planets IV* eds. V. Mannings, A.P. Boss and S.S. Russel Univ. of Arizona Press, 1081

STELLAR INTRUDER IN AN EXOPLANETARY SYSTEM

Kálmán Posztobányi
Department of Astronomy
Loránd Eötvös University
Pázmány Péter sétány 1/A
H-1117 Budapest, Hungary
K.Posztobanyi@astro.elte.hu

Abstract To investigate the effect of a star approaching a planet-star system I made calculations for the orbital elements of the planet and initial conditions of the intruder star.

As a result of these calculations I got 2D and 3D graphicons about the changes of parameters at close encounters between stars.

Keywords: Stellar – Close Encounters – Exoplanets

1. Introduction

Examination is made of the effect of a star approaching a planet-star system. When a passing star encounters a planetary motion, it causes the changing of the semimajor axis a, the eccentricity e, and the inclination i of the planet's orbit. Calculations were made for penetrating encounters, when the approach of the intruder was less than a, and for close encounters, when the closest approach of the intruder was 1-10 a.

First let's consider the examined parameters and some of the results. Lyttleton and Yabushita [1] calculated the variation of the orbital elements. A Gaussian distribution of star velocities was assumed in order to estimate the cumulative effects of series of encounters. They used the central-limit theorem of probability and supposed that the velocity of the passing perturbing star was $v = 20\ \mathrm{km/s}$, the star density $0.1\ \mathrm{star/pc^3}$, and the examined time was $T = 4 \cdot 10^9$ years.

If stars are passing at a distance of some ten times greater than a, the cumulative effects are found to be of the order of 10^{-4} for Δe and Δi, and 10^{-6} for $\frac{\Delta}{a}$. For close stellar encounters direct numerical integrations show that both capture and disruption (expulsion of the planet) can occur.

Yabushita [2] examined the stellar perturbations of orbits of comets with long-periods and extremely eccentric orbits when the shortest distance between the passing star and the Sun is greater, than the aphelion distance of the comet. It was found that although the energy perturbation is only a few percent of the bounding energy of the comet, changes in r_p (perihelion distance) of a few AU can occur. Close encounters were investigated by numerical integration using random initial conditions. The probability of the expulsion of comets depends on the closest approach p and is 0.031 for $p = 10^2$ AU, 0.006 for $p = 10^3$ AU, and 0.001 for $p = 10^4$ AU.

Hills [3] reported the results of computer simulations of close encounters between a planet-star system and a stellar intruder. Using a Shampine-Gordon (variable order, variable stepsize) integrator the inputs were the closest approach p and the velocity v of the intruder. When p was $2 - 3a$, the result was orbit-increasing or dissociating of the planetary system. For $p > 3a$ mild shrinking occured. Close encounters are disruptive, in many cases disruption can occur. Another case is the planet capturing, when the stellar intruder captures the planet.

The effect of the mass and the impact velocity of the intruder was studied by Hills and Dissly [4]. In their simulations the mass of the intruder was 0.1 - 100 times the mass of the star of the star-planet system. They examined the cross sections for dissociation, the changing of the orbital energy and the eccentricity of the planet. According to their results if the impact velocity is less, than the orbital velocity, the planet's orbit shrinks, otherwise it expands. The star-planet system is soft if the bounding energy of the system is less than the kinetic energy of the intruder. Contrary to a myth that hard binaries shrink, soft binaries expand in encounters with stellar intruders, one should speak of fast or slow intruder limit (between the expanding and the shrinking) rather than soft or hard binary limit. This behaviour was first noticed by Aarseth and Hills [5], but they simulated star-star systems, not star-planet systems. Their study was based on computations relative to binary stars in which the binary and the intruder had nearly the same masses that is all three masses were equal. They examined the influence of encounters of the major planets with random massive objects.

Distant encounters and their importance on the dynamical evolution of planetary systems was studied by Brunini [6]. He considered the two-body problem with a massive primary and with smaller secondary in circular orbit. The system was perturbed by a third massive body. Closest approaches and high velocity encounters were examined too. In the case of penetrating encounters the closest approach is less, than the separation of the system. The change of the internal energy can be described accurately by an impulse approximation. In this case the time of relevant interaction is shorter than the orbital period of the system. Distant encounters take place in a time span longer than the

orbital period. The relative position of the binary members changes considerably. The interaction cannot be described by impulse approximation. The interaction can be studied by means of the Fokker-Planck equations or direct numerical integration. Brunini [6] made an application to the outer planets of the Solar System. Distant encounters may excite the orbital velocity of the planets. The secular transfer of impulse increases the orbital eccentricity, if e is negligible before the encounter. If the orbit is eccentric, the above eccentricity increaments adds to e quadratically, as in a random walk. It was made some approximations: the eccentricity of the planets was constant, perturbations from other planets were considered negligible. The regions of chaotic motion were very small. Brunini [6] obtained surprisingly high Δe values, which was 0.003 for Neptune, with the closest star-star approach $p = 230$ AU. The observed eccentricity for Neptune is 0.0085.

An application to the Kuiper belt was made too by Brunini [6]. In this case an algorithm was used to determine the effect of successive perturbations on binary systems by distant passing intruders. The algorithm is valid for eccentric orbits. Random passing stars almost completely thermalise the belt beyond some thousands AU from the Sun. The flattened structure of the Kuipert belt cannot extend much farther than this distance.

The frequencies of stellar encounters in an enviroment depend on the number-density of stars and the relative velocities. Table 1 shows the frequencies of encounters in some enviroments.

Table 1. Encounter frequencies. The large encounter-frequency at the Galactic Centre is due to the large velocities of stars.

enviroment	**stellar density**	**encounter frequency**
Solar environment	$0.1\ \mathrm{star/pc^3}$	$1\ \frac{\mathrm{encounter}}{\mathrm{star\cdot Gyr}}$
Stellar cluster	$1.5\ \mathrm{star/pc^3}$	$20\ \frac{\mathrm{encounter}}{\mathrm{star\cdot Gyr}}$
Galactic Centre	$100\ \mathrm{star/pc^3}$	$100\ \frac{\mathrm{encounter}}{\mathrm{star\cdot Gyr}}$

2. Application of the model to intruders

The Lie integration is a fast integration method for the differential equations of motion of celestial bodies, applying Lie-series. The basic idea to use the implicit Lie transformation to integrate the n-body problem is due to Gröbner [8], Hanslmeier and Dvorak [6] simplified the calculation of the Lie-terms and derived a recurrence formula. They solved in an optimal way the 2-body problem, then they derived a similar method for the solution of the n-body problem.

This integration method has two major advantages. First, it is a relatively fast method, about 3 - 10 times faster than the n-body problem of high accuracy by

Schubart and Stumpff [9]. Second, because larger step lengths can be used (e.g. a step length of 135 days for Jupiter), roundoff errors are smaller.

The Solar System is not isolated in space. Random passing stars, molecular clouds, and our galaxy, the Milky Way can play a role in the dynamical evolution of the planetary system and the cometary cloud. The dynamical effect of random passing stars is not negligible for the major planets. The effect of the passing stars could had been stronger, when the Solar System was young, especially if the Sun and the planets had come into existence in a stellar cluster. If it happened so, we do not know how much time the Solar System had spent in its parent cluster, how many closeup stellar approaches had formed its dynamics. I investigate the effect of close encounters taking place between a passing star and Sun or a star in an exoplanetary system.

I examined a special three-body problem, in which a stellar intruder is acting on a star-planet system. I was interested in whether the orbit of the planet shrinks or increases. My goal was to calculate the changing of the orbital elements (semimajor axis, eccentricity, inclination) of the planet and the changing of the bounding energy during the approach of the intruder to the system.

For the calculations I selected a special star-planet system, in which the mass of the star is 1 Sun-mass, and the mass of the planet is 1 Earth-mass. The initial orbit of the planet is circular, the semimajor axis a of the orbit is 1 AU, so the circular velocity v of the planet is $30km/s$. The basic plane of reference for the calculations is the planet's orbital plane.

The mass of the stellar intruder is 1 Sun-mass too, the relative velocity u between the two stars is $30km/s$. In the initial position the passing star is at $R_{init} = 1720$ AU from the star of the star-planet system. In a spherical coordinate system two angle are necessary for the position, λ and β. The angle λ is measured along the orbit of the planet, its value is between 0 and $360\circ$. The direction of $\lambda = 0\circ$ is opposite sense to the direction of the initial velocity of the planet. The angle β is between the intruder star and the plane of the planetary orbit, with values between -90 and $90°$. The initial velocity vector of the passing star is parallel to the star-star section, and its initial distance from this section is p. If gravity did not work and the intruder star conserved the direction of the initial velocity, then the minimal distance between the two stars would be p. The value of p is between 5 and 20 AU in the computations.

With these initial conditions I obtained the following results.

2.1 Bounding energy

The bounding energy of a celestial body is its mechanical energy, which is the sum of the kinetic and potential energy. Fig. 1 shows the change of the bounding energy in time.

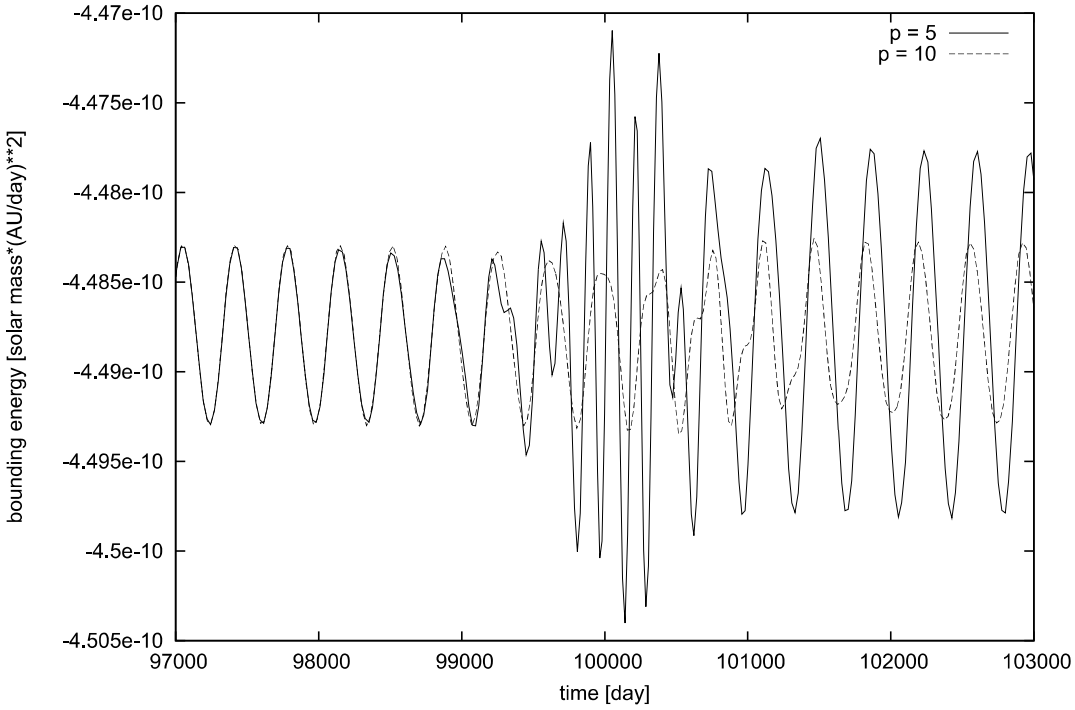

Figure 1. changing of bounding energy in time

The approach occurs about the 100 000th day. The value of the bounding energy oscillates before and after the approaching. The bounding energy of the planet is not proportional to the semimajor axis of its orbit because the potential energy of the intruder star is significant during the approach. The period of the change of the semimajor axis period of the planet before and after the approaching is the period of the planet-circulation, 360 days, but at the approaching it is 180 days.

2.2 Orbital elements

I investigated, how do the size, form and tilt of the orbital plane of the planet change, so the examined orbital elements are the semimajor axis a, the eccentricity e and the inclination i of the planet.

2.3 Changing of a in time

The changing of the semimajor axis becomes significant when the approaching intruder star is at 100 AU from the star-planet system. To show the effect of the distance on the changing of the semimajor axis I made calculations for $p = 5$ and 10 AU. In case of these values of p the effect of the gravitation of the intruder star is strong enough, but the star-planet system does not perish. In Fig. 2 we can see the result, the rising and then the declining of the amplitude

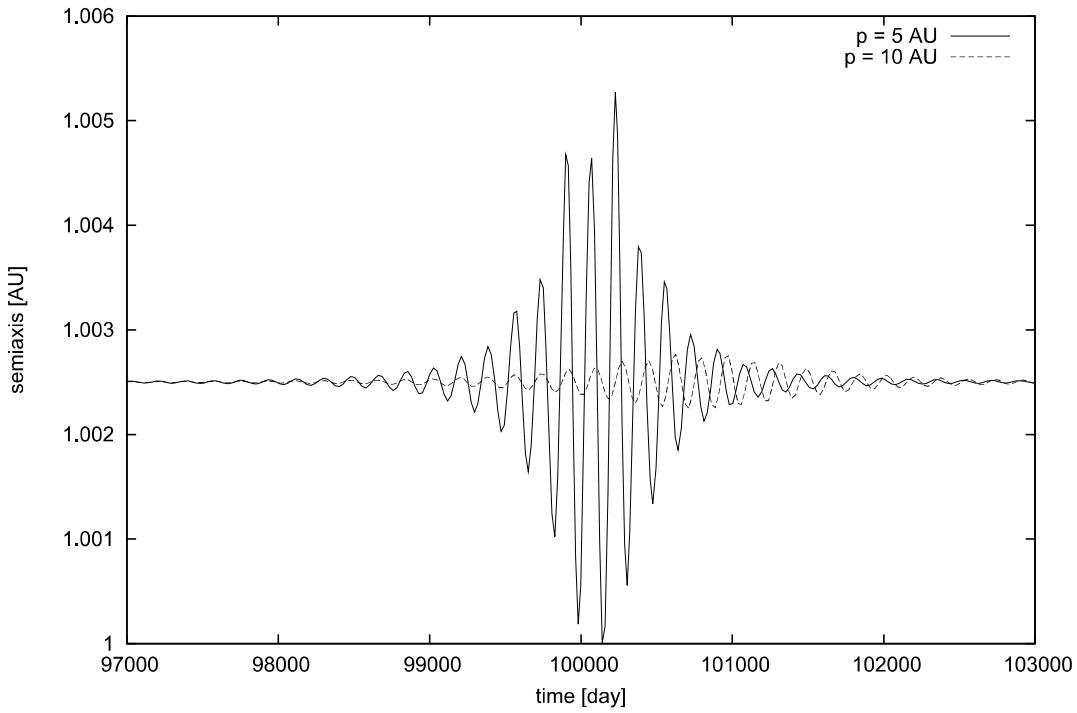

Figure 2. changing of a in time

of the semimajor axis-undulation; after relatively grand oscillations the new value of the semimajor axis is almost the initial; the difference between the initial and the final semimajor axis is low. The maximal amplitude of the oscillations of the semimajor axis is a hundred times greater, than the initial-final difference. When the value of p was 10 AU, the maximum of the undulation of the semimajor axis occured later than at $p = 5$ AU. The cause of this is the later pericentrum passage on the $p = 10$ AU orbit. The curves show that the period of the change of the semimajor axis is close to the half-period of the planet-circulation.

2.4 Changing of e in time

The value of the eccentricity of the orbit undulates and usually becomes greater during the passing, particularly at low initial values of p (see Fig. 3). The period of the change of the eccentricity is close to the half-period of the planet. The amplitude of the undulation is greater, than the difference between the initial and the final value of the eccentricity. When $p = 10$ AU, the maximal amplitude of the oscillations of the eccentricity is thirty times greater, when $p = 5$ AU, two times greater, than the initial-final difference. When the amplitude of the undulation is the biggest, the distance between the maxima following each other is about the half-period of the planet.

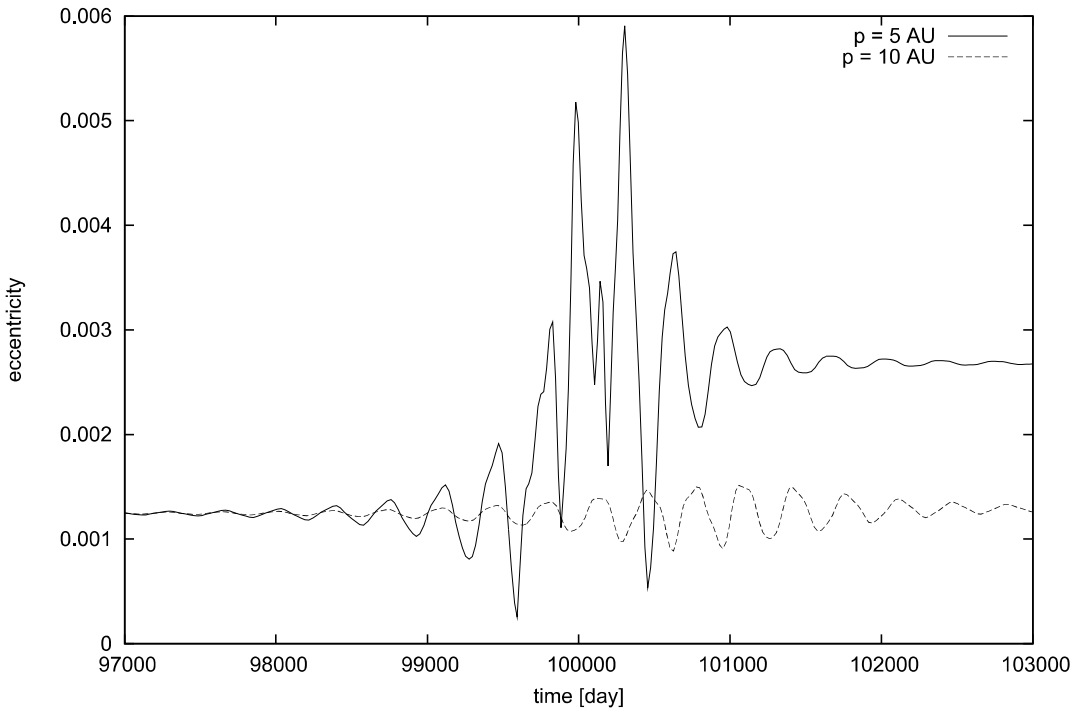

Figure 3. changing of e in time

2.5 Changing of i in time

For the computation of the changing of a and e I used the planar three-body problem, but for Fig. 4 the motion of the three bodies is not planar, the angle between the initial velocity of the intruder star and the orbital plane of the planet is $2.8°$. When $p = 10$ AU, the maximal amplitude of the oscillations of the inclination is forty times greater, when $p = 5$ AU, three times greater, than the difference between the initial and the final inclination (see Fig. 4). The approaching in both cases reduced the inclination of the orbital plane. The period of the change of the inclination is close to the half-period of the planet-circulation.

2.6 Changing of a, e, i in λ

In Fig. 5, Fig. 6 and Fig. 7 the differences between the initial and final values of the orbital elements a, e and i are shown for different values of λ, where λ is the initial longitude of the planet along its orbit. The initial inclination of the orbital plane is $2.8°$. When $p = 4$ AU, the semi-major axis vs. λ function has two maxima at $\lambda = 105°$ and at $\lambda = 295°$, the maxima of the eccentricity vs. λ function are at at $\lambda = 110°$ and at $\lambda = 300°$, and the maxima of the inclination vs. λ function are at at $\lambda = 55°$ and at $\lambda = 275°$. For bigger values

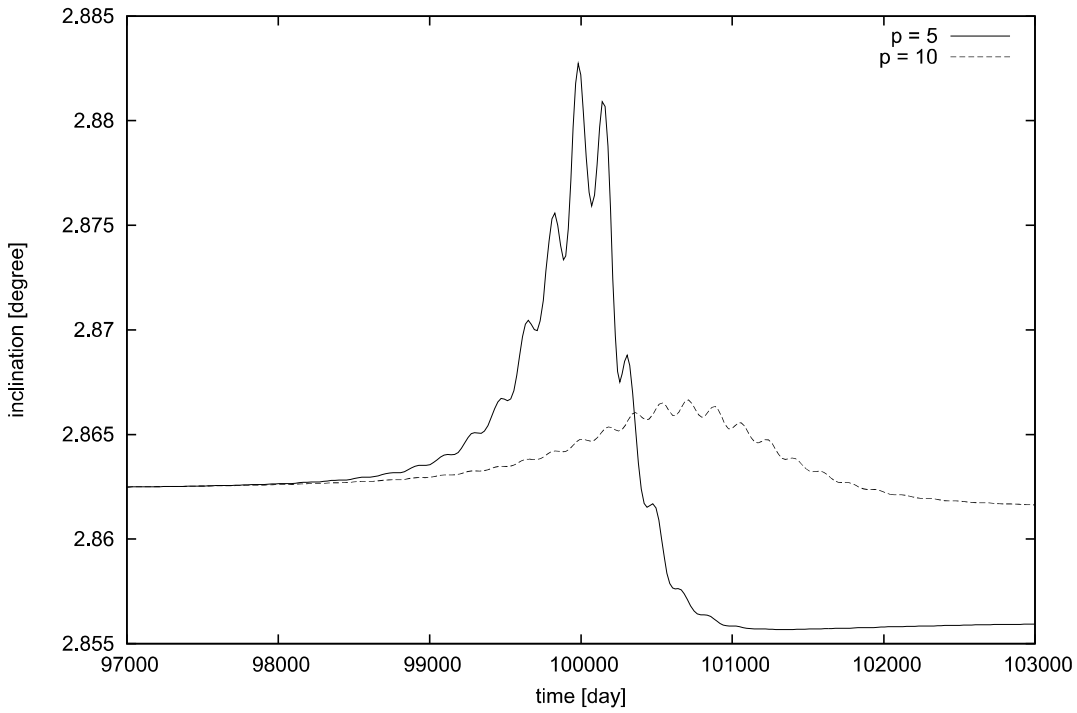

Figure 4. changing of i in time

of p the maxima of a, e, i are shifted to the right. When a grows, e and i grow as well.

2.7 Changing of a, e, i in β

β is the angle of arrival of the intruder star with respect to the orbital plane of the planet. The initial inclination of the orbital plane is $0.0°$. The difference between the initial and final value of the semimajor axis of the planet is biggest, when $\beta = 0$ (see Fig. 8). The orbit in all cases decreases. The final eccentricity is biggest, when $\beta = 0$ too. The change of the inclination is 0, when $\beta = 0°$, and maximal, when $\beta = 35°$ (see Fig. 9 and Fig. 10). The curves are symmetrical with respect to the initial conditions.

2.8 Changing of a, e, i as the function of $p = z_0$

Let the parameter p equal to the z_0-component of the initial position of the intruder star. In Fig. 11, Fig. 12 and Fig. 13 we can see the difference between the initial and the final values of the orbital elements in the case of different values of z_0 and y_0. When z_0 is smaller than 2.5, a decreases, the orbit shrinks, its eccentricity significantly grows. When $y_0 = 3$, the difference between the initial and the final inclinations can be $4.5°$. The cause of the asymmetry of the curve in Fig. 13 is the non-zero initial inclination of the orbit of planet.

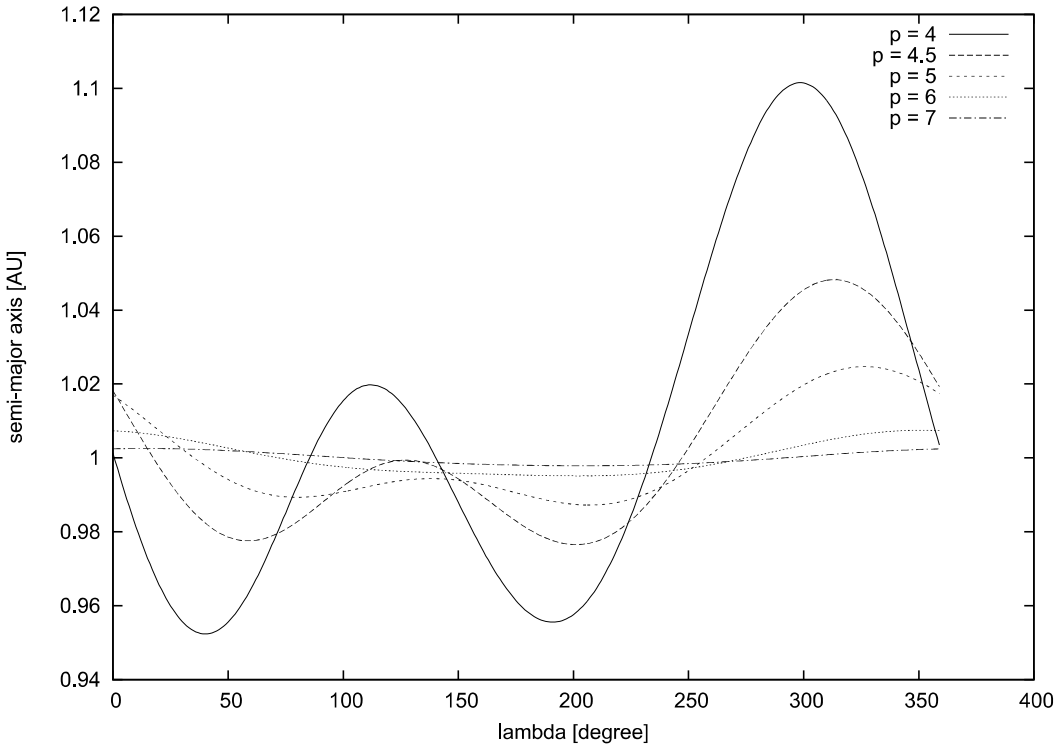

Figure 5. changing of a in λ

2.9 Changing of the orbital elements at close encounters

Fig. 14, Fig. 15 and Fig. 16 show the changing of a, e and i at close encounters, when the intruder star arrives perpendicular to the orbital plane of the planet. The parameters x and y mean the shift of the initial velocity vector of the intruder star. Their unit is AU. If both x and y are zero, the initial velocity vector points to the parent star. For other x, y values the initial velocity vector is parallel to the parent star-intruder star line and the coordinates of the intruder star is x and y on the plane which is perpendicular to the line. The change of a, e, i is indicated as the function of x and y. Fig. 14 shows, that the difference between the initial and the final semimajor axis is great, when the approach between the intruder star and the planet is close. Negative semimajor axis means, that the final value of the semimajor axis is also negative, and the planet is not bound. The initial value of the eccentricity is 0. According to Fig. 15 the new value of the eccentricity can be very big - especially if the planet is free. Fig. 16 shows, that the inclination can have any value.

2.10 Stellar intruder at star-two planets system

What is the effect of another planet? I tried to show it. I calculated the change of the orbital elements of the planet in the presence of an additional

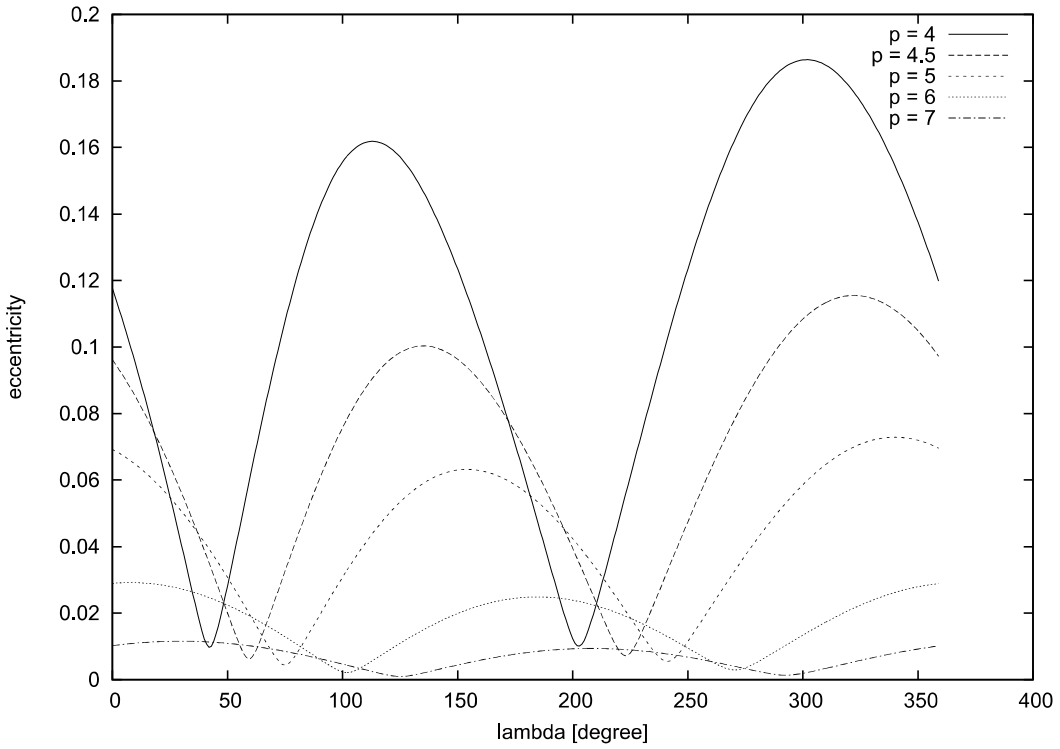

Figure 6. changing of e in λ

planet which has one Jupiter-mass and the semimajor axis of its orbit is 5 AU. Let us sign it with J, the planet of Earth-mass with E, and the home star with S. In Table 2 the number 45.3 in the column of $S-E$ means, that the final bounding energy is 45.3 per cent of the initial one, so the orbit expanded. In Table 2 we can see, that the expansion of the orbit is greater in $S-E$ system than in $S-E-J$ system. It should to investigate if this is true establishment in the case of different masses end semi-majos axes of the second planet J.

Table 2 shows the probability of shrinking of the orbit of the inner planet in a star-planet ($S-E$) and in a star-two planets ($S-E-J$) system. We can see that in the presence of a new, Jupiter-mass planet in the model, the probability of the shrinking of the orbit of the inner planet is bigger.

3. Conclusions

I considered encounters between star-planet systems and an intruder star and determined the effect of the distance- and angle parameters of the passing star. The examined encounters were close. The change of the semi-major axis and the inclination of the orbit of planet is significant, when the stellar approach is close - 4-5 a -, but they quickly fade, when the minimal distance between the two stars is greater.

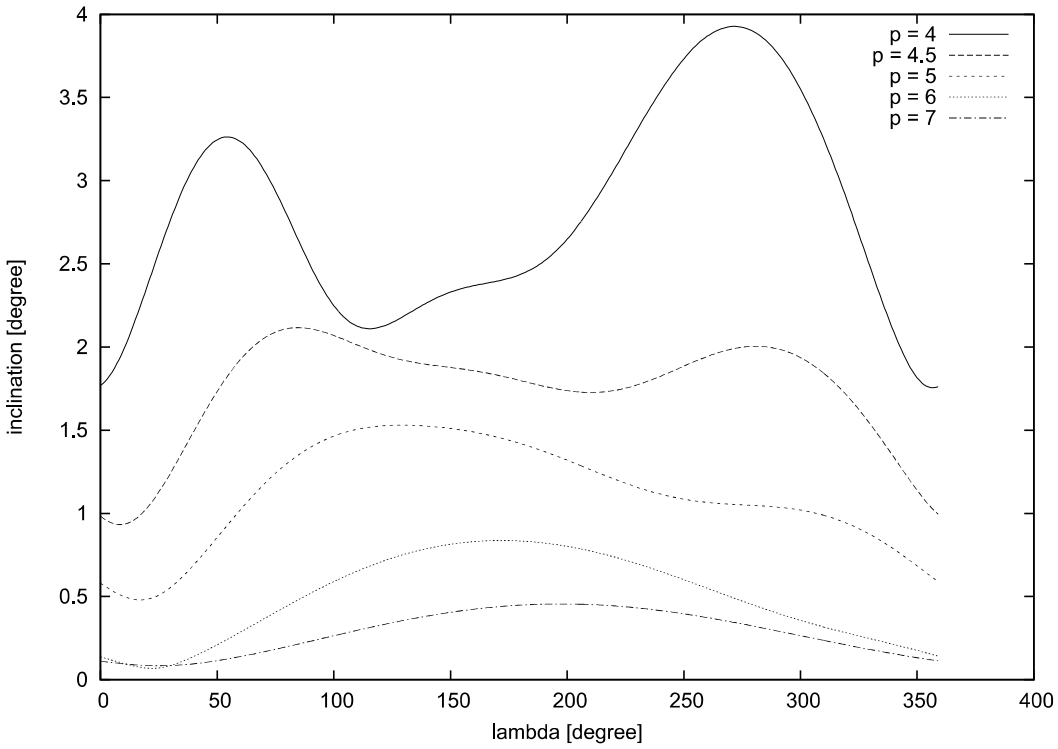

Figure 7. changing of i in λ

Table 2. The relative changing of the bounding energy in the presence and absence of a second planet. $S-E$ means a Sun-Earth, $S-E-J$ means a Sun-Earth-Jupiter system. The Earth-mass first planet has 1 AU semimajor axis orbit, the orbit of the Jupiter-mass second planet 5 AU semimajor axis. The probability of the shrinking of the orbit of the inner planet is expressed by per cent for different values of λ and β.

λ	β	$S-E$	$S-E-J$
0.0	0.0	45.3	99.1
45.0	0.0	43.8	100.0
90.0	0.0	32.2	99.3
180.0	0.0	43.3	100.0
270.0	0.0	33.9	99.2
0.0	45.0	41.3	97.5
0.0	90.0	9.1	98.3

Is there any pragmatic significance of the investigation of such close approaches? Neither in our Solar System, nor in any exoplanetary system there was any observation of close stellar encounter yet. Are they frequent events at all? We know that when two galaxies merge in one another, impacts of stars do not occur. Close encounters between stars are still extraordinary. In the environment of the Sun only one closer than 100 AU encounter is to be expected within 10^{12} years. However, close approaches are more frequent in dense core

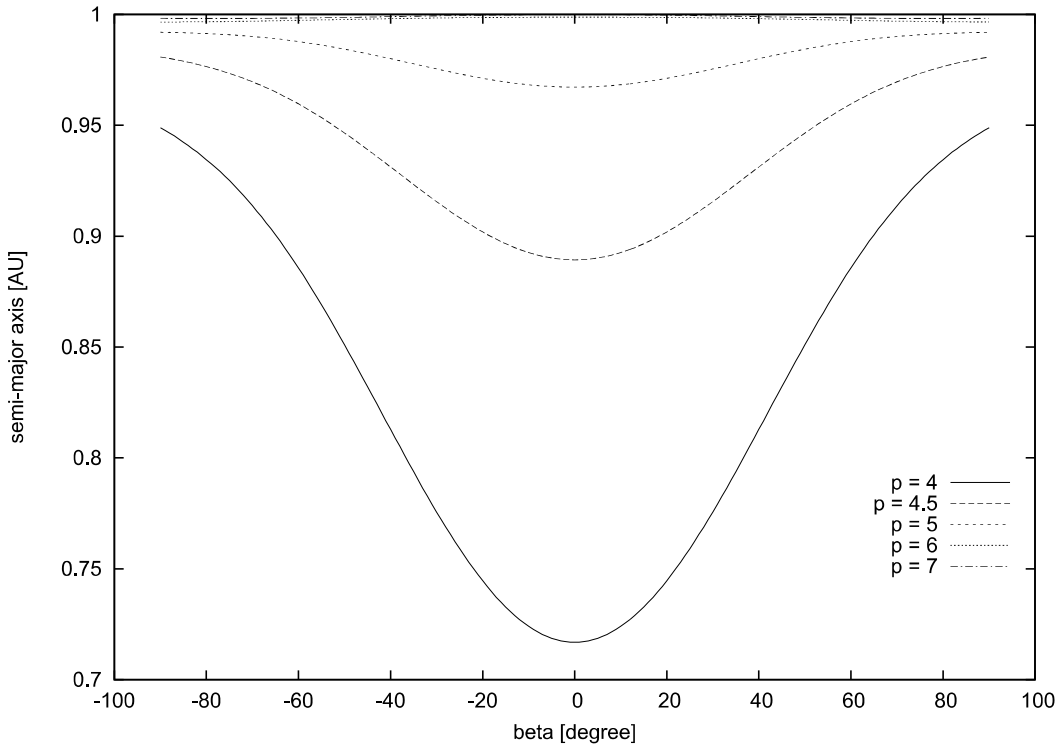

Figure 8. changing of a in β

star-clusters. If the Solar System were born in a stellar cluster, it could have several close approaches, these encounters could affect the dynamics of the planetary system. Tracks of such stellar encounters, their effects on the dynamical evolution may be observable in the Solar System and exoplanetary systems, if they could be separated from the effect of the planets.

Acknowledgments

The support of the Austrian-Hungarian Scientific and Technology Cooperation, grant number A-12/04 is acknowledged.

References

[1] Lyttleton, R. A., Yabushita, S.: 1965, "The Effect of Stellar Encounters on Planetary Motions", *Monthly Notices of the Royal Astronomy Society* **129**, pp.105-125

[2] Yabushita, S.: 1972, "Stellar Perturbations of Orbits of Long-Period Comets", *Astronomy and Astrophysics* **16**, pp. 395-340

[3] Hills, J. G.: 1984, "Close Encounters between a Star-planet System and a Stellar Intruder", *The Astronomical Journal* **89**, pp.1559-1564

[4] Hills, J. G., Dissly, R. W.: 1989, "Close Encounters between Star-planet Systems and a Stellar Intruders. II. Effect of the Mass and Impact Velocity of the Intruder", *The Astronomical Journal* **98**, pp.1069-1082

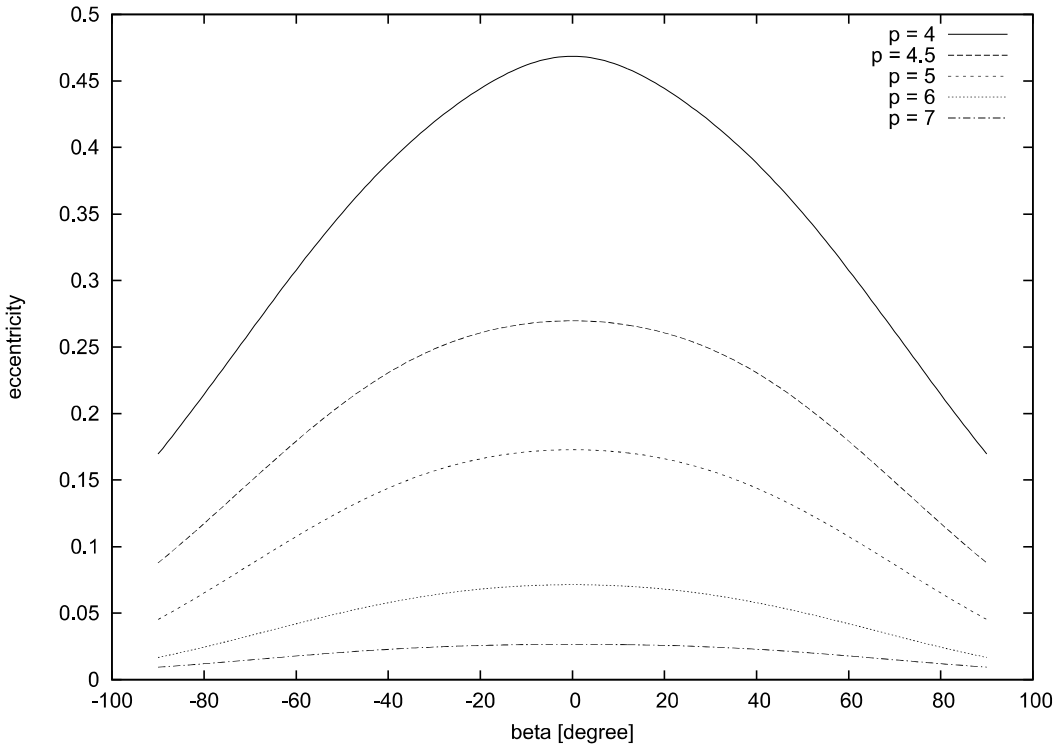

Figure 9. changing of e in β

[5] Aarseth, S. J.; Hills, J. G.: 1972, "Close Encounters between Star-planet Systems and a Stellar Intruders.", *Astronomy and Astrophysics* **21**, pp. 255

[6] Brunini, A.: 1995, "The Effect of distant Stellar Encounters on Planetary Systems. II", *Astronomy and Astrophysics* **293**, pp.935-940

[7] Hanslmeier, A.; Dvorak, R.: 1984, "Numerical Integration with Lie Series", *Astronomy and Astrophysics* **293**, pp.935-940

[8] Gröbner, W.: 1967, "Die Lie-Reihen und ihre Anwendungen" *VEB Deutscher Verlag der Wissenschaften, Berlin*

[9] Schubart, J.; Stumpff, P.: 1966, "On an N-Body Program of High Accuracy for the Computation of Ephemerides of Minor Planets and Comets" *Veröffentlichungen des Astronomischen Rechen-Instituts Heidelberg* **18**, pp.31

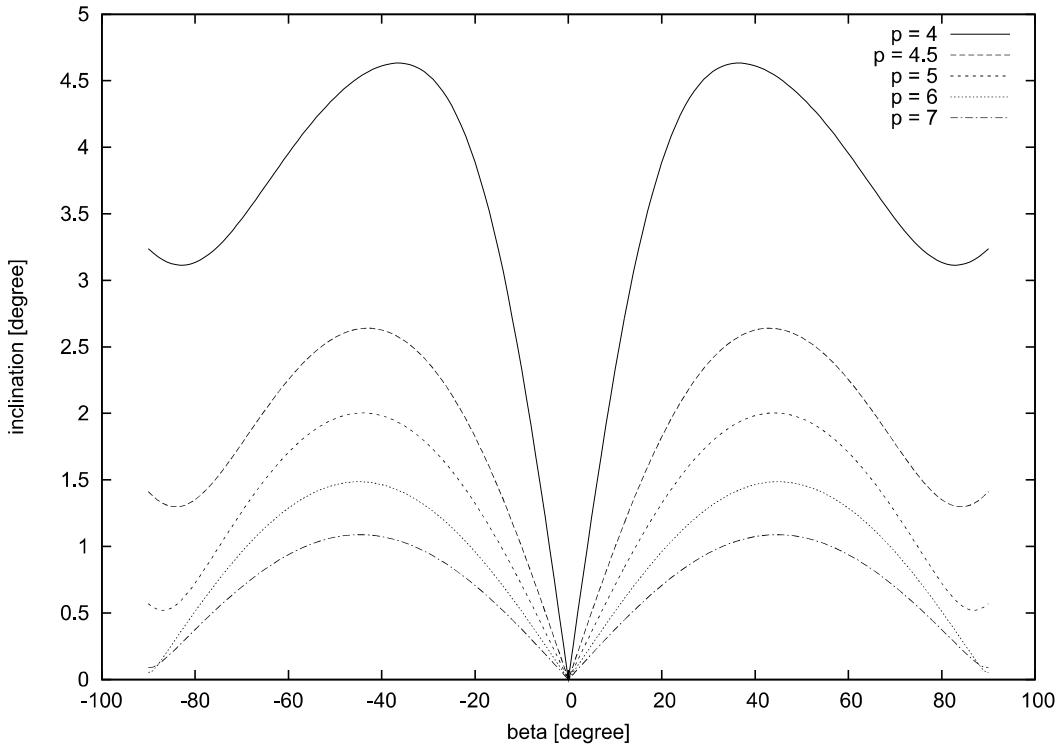

Figure 10. changing of i in β

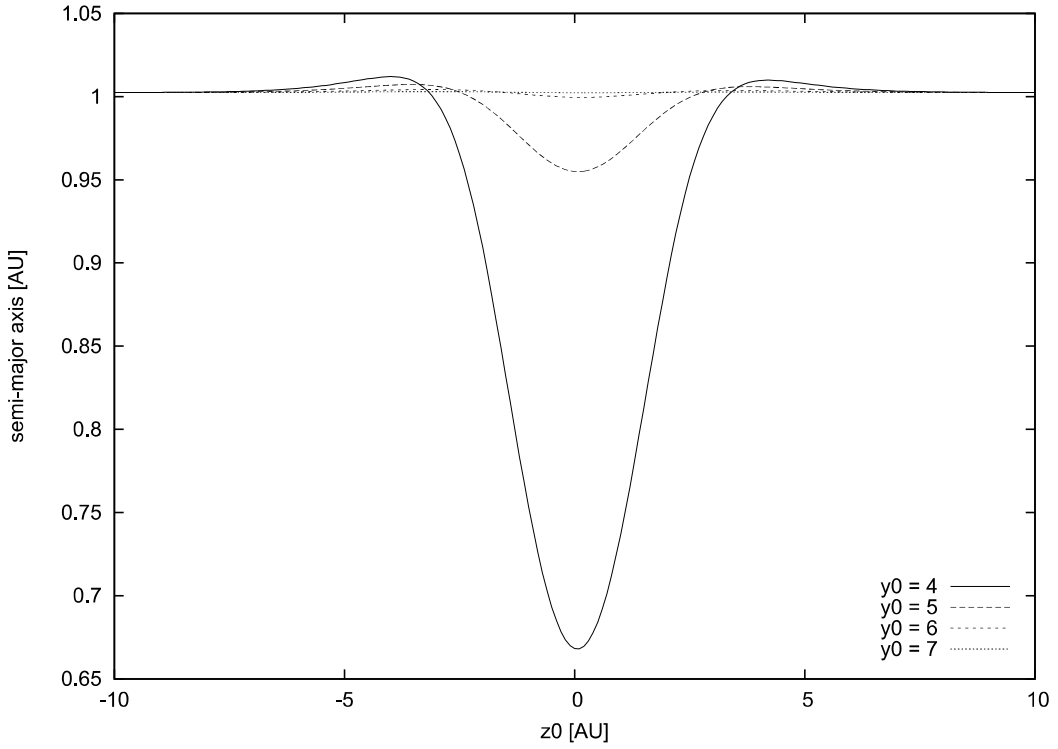

Figure 11. changing of a in parameter z_0

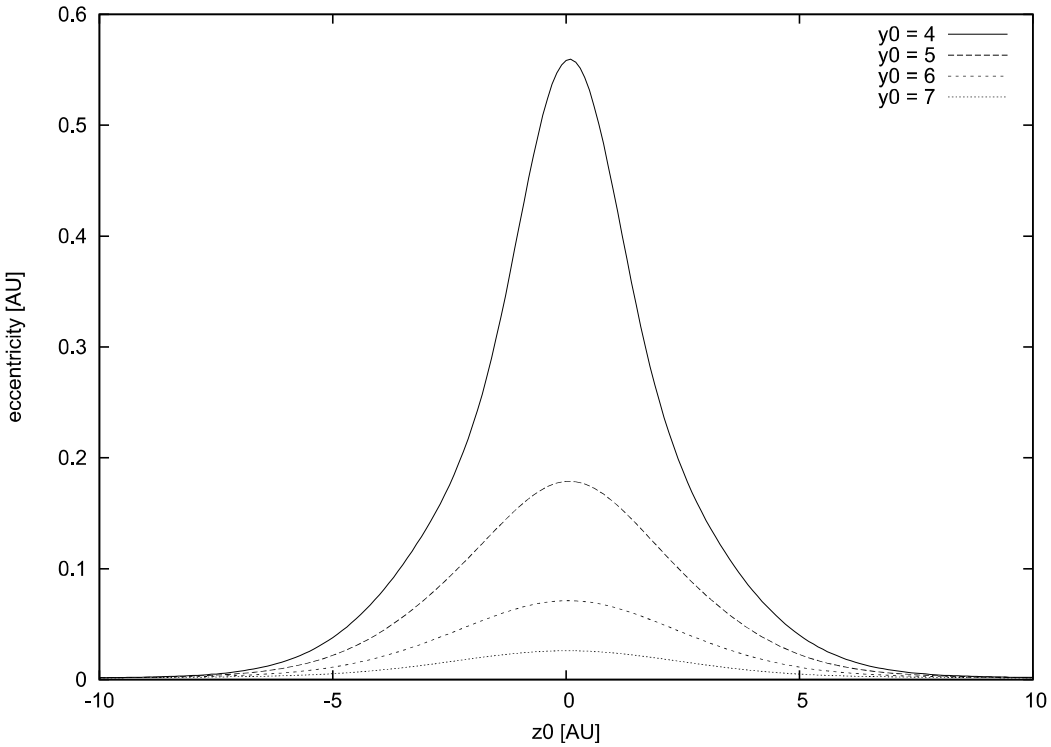

Figure 12. changing of e in parameter z_0

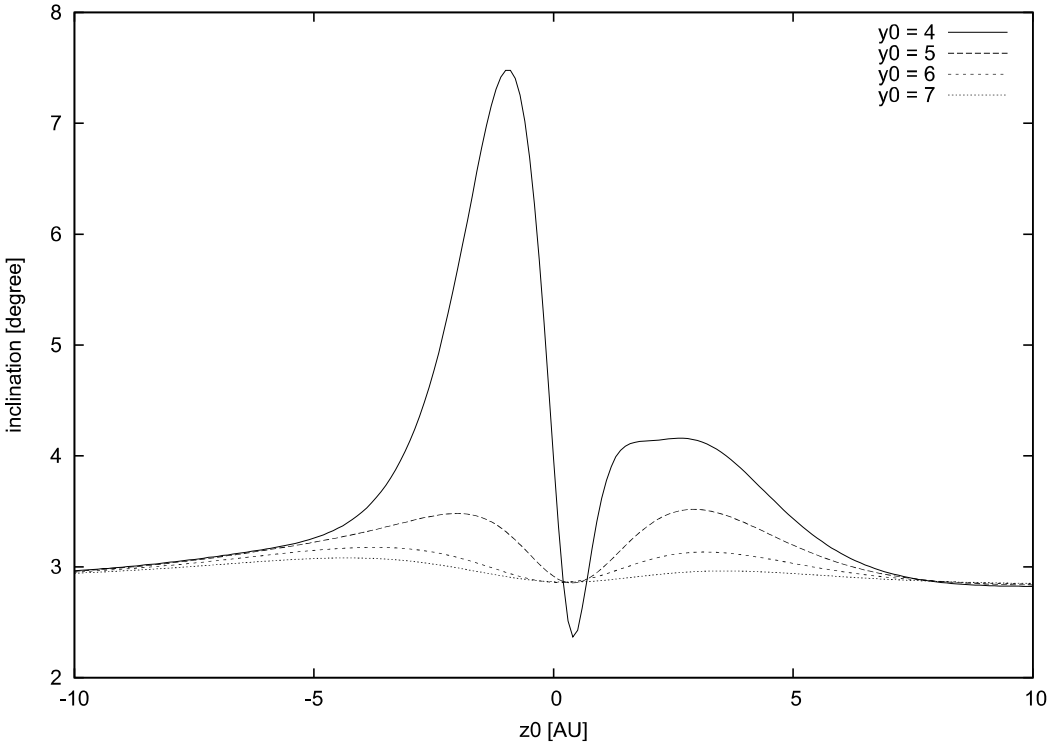

Figure 13. changing of i in parameter z_0

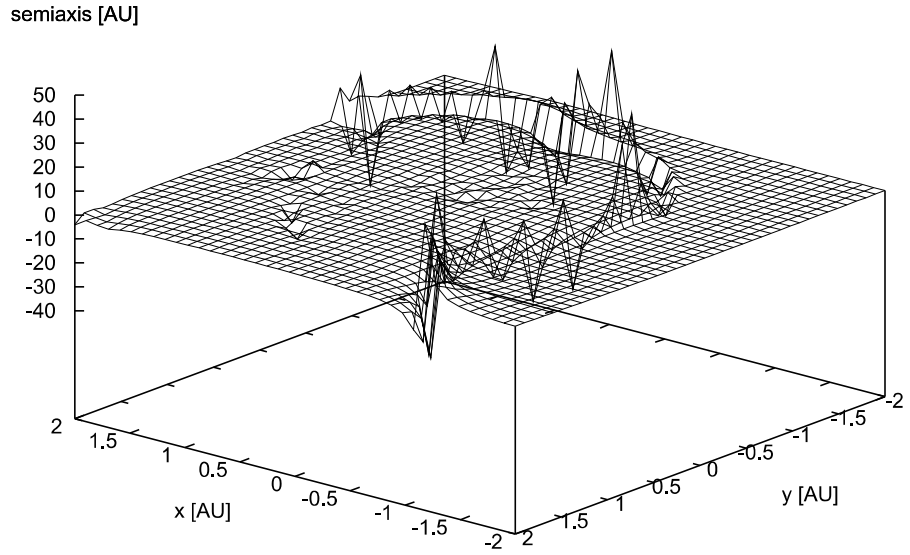

Figure 14. changing of a at close encounters

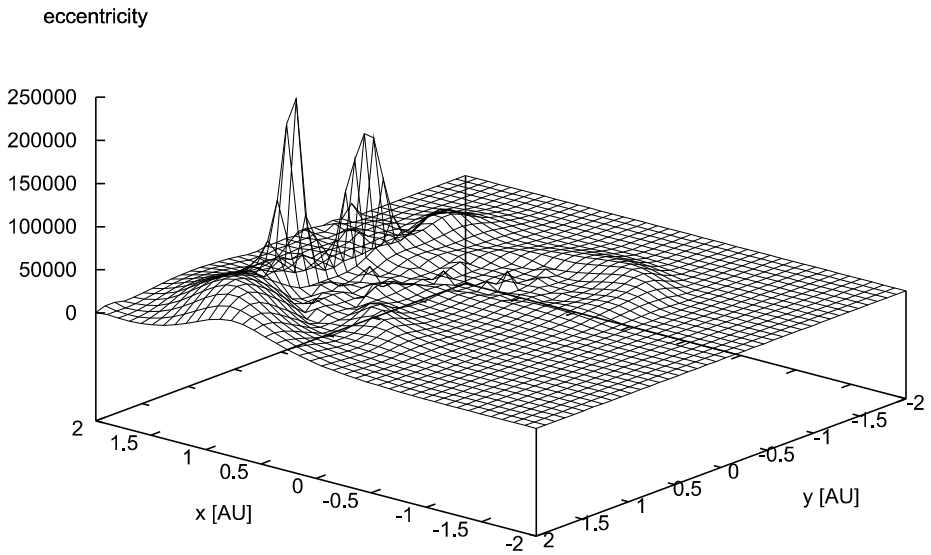

Figure 15. changing of e at close encounters

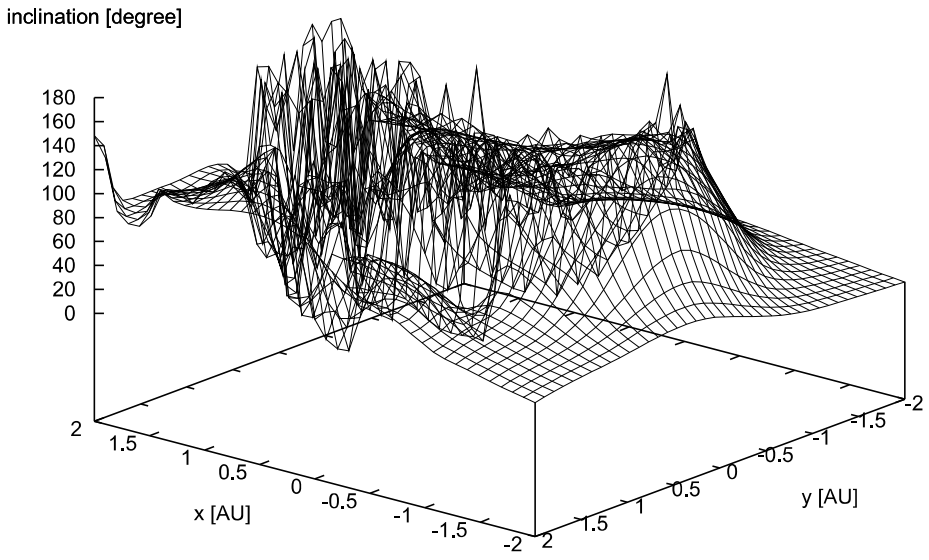

Figure 16. changing of i at close encounters

DYNAMICAL CONFINEMENT OF THE ECCENTRICITY OF EXOPLANETS FROM TRANSIT PHOTOMETRY

Zsolt Sándor
Department of Astronomy,
Loránd Eötvös University
Pázmány Péter sétány 1/A
H-1117 Budapest, Hungary
Zs.Sandor@astro.elte.hu

Abstract The probability of detection of Earth-like exoplanets may increase after the launch of the space missions using the transit photometry as observation method. By using this technique, however, only the semi-major axis of the detected planet can be determined, and there will be incomplete information regarding its orbital eccentricity. On the other hand, the orbital eccentricity of an Earth-like exoplanet is a very important parameter, since it gives information about its climate and habitability. In this paper a procedure is suggested for confining the eccentricity of an exoplanet discovered by transit photometry if beside the Earth-like planet, an already known giant planet also orbits in the system.

Keywords: exoplanets – planetary transit – restricted three-body problem – stability – chaos detection

1. Introduction

After the discovery of the first extrasolar planet around 51 Pegasi (Mayor & Quéloz, 1995), more than 190 exoplanets have been observed. The detection of exoplanets has a great importance, since they form planetary systems around their hosting stars, and by studying the main properties of these systems the characteristics, the formation and the evolution of the Solar System could be treated as a part of a more general phenomenon. The above picture is unfortunately rather ideal than complete yet, since the exoplanets observed by now are mainly Jupiter-like gas giants. This is the consequence of the fact that by using radial-velocity measurements, which is the most effective ground-based observing technique, there is no chance to detect Earth-like planets yet.

On the other hand, one of the most challenging questions of exoplanetary research is the discovery of the Earth-like planets. Beside their importance in testing and improving the formation theories of the planetary systems, another major question is their habitability. If an Earth-like planet revolves in the habitable zone of the hosting star, there may be chances of developing (a water based) life on its surface. The habitable zone is that region around the star, where liquid water can exist on the surface of a planet (Kasting et al 1993).

In order to find Earth-like planets, there are space missions in construction and planning phase. Such a mission is COROT (sponsored by CNES, ESA and other countries) to be launched in 2006, the Kepler Mission (NASA) with a launch in 2008, Darwin (ESO), and Terrestrial Planet Finder (TPF, NASA) with a launch in the next decade. The first two missions (COROT and Kepler) will use the transit photometry as detection technique, which is based on measuring the periodic dimming of the star's light intensity caused by an unseen transiting planet. Measurements performed by these instruments will provide the semi-major axis a of the transiting planet calculated from Kepler's third law

$$\frac{a^3}{T^2} = \frac{k^2}{4\pi^2}(m_* + m_p),$$

where T is the period of the transits, m_* is the mass of the hosting star, and m_p is the mass of the transiting planet, respectively (k is the Gaussian gravitational constant). In the case of Earth-like planets $m_p << m_*$, so neglecting m_p does not affect significantly the accuracy of a. An uncertainity in the semi-major axis a can appear since the stellar mass is known only with limited accuracy. If this is for example 3%, the inaccuracy in a will be 1%. (We note that the mass of the hosting star can be determined by spectroscopic observations and by stellar model calculations.) However, in this paper we do not investigate the error propagation due to these uncertainities in stellar mass and semi-major axis, we intend to perform these studies in a future research.

In this paper we present a procedure which helps in confining the orbital eccentricity and inclination of the transiting planet if (i) the duration of the transit is known, and (ii) there is another (giant) planet in the system. We derive such an equation, which connects the mass and the radius of the star, the semi-major axis, the eccentricity, the argument of the periastron, the inclination of the transiting planet, and the duration of the transit. In this equation there are three unknowns, namely e, ω, and i. By fixing i, the corresponding (ω, e) pairs can be visualized as curves on the $\omega - e$ parameter plane. Thus the problem is underdetermined and there is no way to confine the orbital eccentricity e of the transiting planet.

On the other hand, as suggested by planetary formation scenarios, we expect that next to the Earth-like planets Jupiter-like giant planets can also be found in the majority of the planetary systems. Having discovered an Earth-

like planet around a star, by using complementary techniques (as observations by Space Interferometry Mission and ground-based Doppler spectroscopy) additional more massive planets can be identified in the system, and their orbital parameters can be determined too.

The presence of a giant planet (beside the transiting one) results in that both ordered and chaotic regions can be found in the phase space of the system. If the trajectory of the Earth-like planet is in the ordered region of the phase space, the motion of the planet is stable for arbitrary long times. If the initial conditions of its orbit are in a chaotic region of the phase space, the motion of the planet can be unstable after a certain time. In this paper we exclude those orbital parameters of the transiting planet, which result in chaotic motion. We shall demonstrate that in some cases it is possible to determine an upper limit for the eccentricity and a lower limit for the inclination of the transiting planet. We stress again that the eccentricity is a very important orbital parameter not only from dynamical point of view but also in studying the habitability and climatic variations of the Earth-like planet.

The paper is organized as following: first we derive a connecting equation between the duration of the transit and some important parameters of the star and the transiting body, then we solve this equation numerically. After examining the solutions of this equation, we map the stability structure of the system assuming the presence of a known giant planet. Then we can determine lower limits for the inclination and an upper bounds for the eccentricity of the transiting planet depending on the eccentricity and the semi-major axis of the known giant planet.

2. A connecting equation between the orbital parameters of the transiting planet

In this section we shall derive an equation between the orbital parameters of the transiting planet, the star's mass, and the duration of the transit from the geometry of the transit.

Let us suppose that the star's disc is a circle with a radius R, and a planet is moving in a front of this disc with an average velocity $v_{\rm tr}$. If the duration of the transit is denoted by τ and the lenght of the path of the transiting planet is d (see Fig. 1), the following approximation holds:

$$v_{\rm tr} \approx \frac{d}{\tau}. \tag{1}$$

We note that according to Kepler's second law, the velocity of the planet is changing during the transit (except in the case of circular orbits), however this change is negligible, if the planet orbits far enough the star. Since the triangle

in Fig. 1 is a pythagorean one, it can be written

$$R^2 = m^2 + \left(\frac{d}{2}\right)^2 . \tag{2}$$

From Equation (2) the lenght of the transit's path d can be expressed as

$$d = 2\sqrt{R^2 - r^2 \cos^2 i}, \tag{3}$$

where, according to Fig. 2,

$$m = r \cos i, \tag{4}$$

where i is the inclination (e.g. the angle between the orbital plane and the tangent plane to the celestial sphere), and r is the distance between the center of the star and the planet.

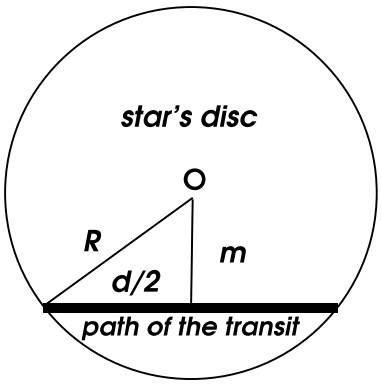

Figure 1. The transit of a planet in the front of the stellar disc. The straight sections denoted by R, m, and $d/2$ form a pythagorean triangle.

By using the well known formula for r:

$$r = \frac{a(1-e^2)}{1 + e\cos v} , \tag{5}$$

(where a is the semi-major axis, e is the eccentricity, and v is the true anomaly of the transiting planet), and Equations (1) and (3), the average orbital velocity of the transiting planet ($v_{\rm tr}$) can be written as

$$v_{\rm tr} = \frac{2}{\tau}\sqrt{R^2 - \left[\frac{a(1-e^2)}{1 + e\cos v}\right]^2 \cos^2 i} . \tag{6}$$

On the other hand, $v_{\rm tr}$ can also be approximated on the basis of the two-body problem. In the coordinate system (ξ, η), in which the axes of the orbital

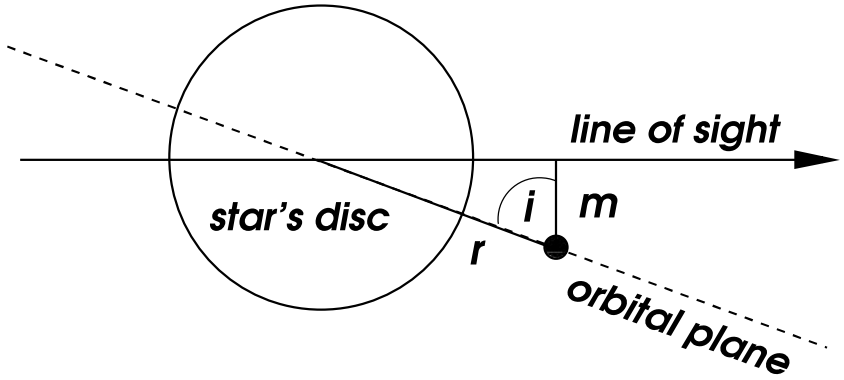

Figure 2. Side-view of the transit, where r is the distance of the planet from the star's center and i is the inclination of its orbital plane.

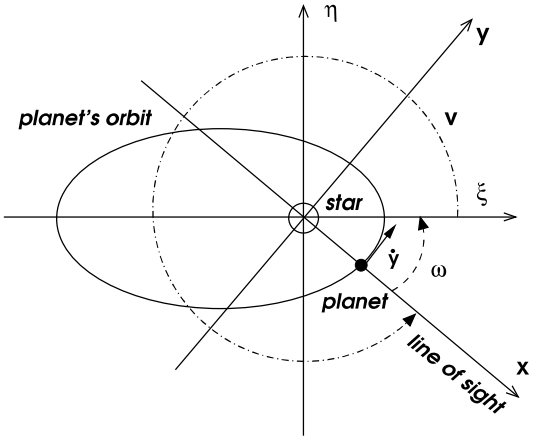

Figure 3. The transit as viewed from above. At the mid of the transit $v_{\rm tr}$ is nearly equal to $\dot{y}$. The coordinate system (ξ, η) is the rotation of the coordinate system (x, y) by ω.

ellipse are on the axes ξ and η, the components of an orbital velocity vector are (see Murray and Dermott, 1999):

$$\dot{\xi} = -\sqrt{\frac{\mu}{p}} \sin v \, , \tag{7}$$

$$\dot{\eta} = \sqrt{\frac{\mu}{p}} (e + \cos v) \, ,$$

where $p = a(1 - e^2)$ is the parameter of the ellipse and $\mu = k^2(m_* + m_p)$, m_* and m_p are the stellar and planetary masses, respectively. Let (x, y) denote a cartesian coordinate system where the x-axis is parallel to the line of sight (e.g. the line connecting the center of the star to the observer). From Figure 3 it can be seen that the system (ξ, η) is the rotation of the system (x, y) by

ω, which is the argument of the periastron of the transiting planet. Thus in the coordinate system (x, y) formulae (7) transform as

$$\dot{x} = \dot{\xi}\cos\omega - \dot{\eta}\sin\omega \,, \tag{8}$$

$$\dot{y} = \dot{\xi}\sin\omega + \dot{\eta}\cos\omega \,.$$

From Fig. 3 it is clearly visible that the average velocity of the transiting planet $v_{\rm tr}$ can be approximated with $\dot{y}$, which is the velociy of the planet at the mid of the transit. (We note that this approximation fails for large eccentricity of the transiting planet.) Then by using the above approximation and Equations (7) and (8) we find

$$v_{\rm tr} \approx \dot{y} = -\sqrt{\frac{\mu}{p}}\sin v \sin\omega + \sqrt{\frac{\mu}{p}}(e + \cos v)\cos\omega. \tag{9}$$

Studying again Figure 3, it is also true that at the mid of the transit

$$v + \omega = 360^\circ \,, \tag{10}$$

thus the average orbital velocity of the transiting planet is

$$v_{\rm tr} = \sqrt{\frac{\mu}{p}}(1 + e\cos\omega) \,. \tag{11}$$

Combining Equations (6), (10), and (11) we obtain the following equation:

$$\sqrt{\frac{\mu}{p}}(1 + e\cos\omega) - \frac{2}{\tau}\sqrt{R^2 - \left[\frac{a(1-e^2)}{1 + e\cos\omega}\right]^2 \cos^2 i} = 0 \,, \tag{12}$$

where the unknown quantities are the eccentricity e, the inclination i, and the argument of the periastron ω. The other quantities, such as the semi-major axis a, the mass parameter (μ), the radius of the star (R), and the duration of the transit (τ) are known with certain accuracies already discussed in the Introduction.

3. Solution and analysis of Equation (12)

According to the last paragraph of the previous section, the unknown quantities in Equation (12) are the inclination i, the argument of periastron ω, and the eccentricity e of the transiting planet. Thus by fixed values of i, Equation (12) can be solved numerically, and the (ω, e) pairs of the solutions can be represented as curves on the $\omega - e$ parameter plane.

In order to study the solutions of Equation (12), we give specific values for the parameters in Equation (12). Let us assume that the mass of the transiting

planet is 1 Earth-mass, and it revolves around a 1 Solar-mass star with radius $R = 6.96 \times 10^8$ m, in an elliptic orbit characterized by $a = 1$ AU, $e = 0.1$ being its inclination $i = 89.95°$. Then we suppose that the direction of the observation of the planetary transit is $\omega = 30°$. It can be calculated easily that in this case the duration of the transit ise $\tau = 0.488029$ day.

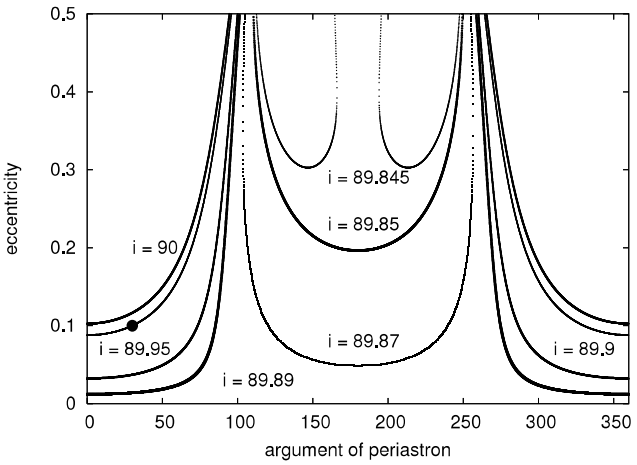

Figure 4. Solutions of Equation (12) for different inclinations when $\tau = 0.488029$ day. The original solution, which results in the above τ, is marked with a filled circle at $\omega = 30°$, $e = 0.1$, and $i = 89.95°$.

By observing transits caused by the above planet, we can measure their duration τ and period T, from which the semi-major axis a can be calculated. In our case $\tau = 0.488029$ day, and for different values of i the corresponding $\omega - e$ curves are plotted in Fig. 4. We show these curves only for $e < 0.5$ since we think that larger values of e are unrealistic for Earth-like planets. We also mark the real (ω, e) solution by a filled circle on the curve corresponding to $i = 89.95°$, but as we can see, there is no way to restrict efficiently the infinite set of solutions. The only restriction is that the solutions can not be chosen from the region above the $\omega - e$ curve corresponding to $i = 90°$.

Equation (12) has an infinite set of solutions formed by pairs of (ω, e) values. If only the duration of the transit is known, it is not possible to choose which (ω, e) pair represents the real parameters of the transiting planet.

4. A possible confinement of the eccentricity of the transiting planet

In this section we shall investigate the case when, beside the newly discovered planet, an already known giant planet orbits around the hosting star. The presence of such a planet makes the problem non-integrable and both ordered and chaotic regions can be found in the phase space of the system. We suppose that the most probable orbital solutions of the transiting planets are those, which emanate from the ordered regions of the phase space. The orbital pa-

rameters of the transiting planet, which would result in chaotic behaviour are unlikely, since in long terms the orbit of the planet could be unstable, therefore these solutions might be avoided. We expect that the presence of a second (giant) planet r epresents a dynamical constraint reducing the infinit set of solutions of Equation (12) by giving an upper limit for the maximum eccentricity of the transiting planet. We shall also demonstrate that by studying the solution-curves of Equation (12) together with the stability structure of the $\omega - e$ plane, a lower bound for the inclination can also be determined. In what follows we shall investigate the stability in the $(\omega - e)$ plane within the framework of the planar restricted three-body problem.

In order to map the stability properties of the $(\omega - e)$ plane we used the Relative Lyapunov Indicator (RLI) (Sándor et al. 2000, 2004). The initial ω and e values are chosen from the intervals $e \in [0, 0.5]$ and $\omega \in [0°, 360°]$ with $\Delta e = 0.025$ and $\Delta\omega = 2°$. The initial value of the semi-major axis of the transiting planet is always $a = 1$ AU, while its true anomaly is calculated from Equation (10) as $v = 360° - \omega$ (see also Figure 3).

For each pair of the initial (ω, e) values we assign the RLI of the corresponding orbit calculated for 500 periods of the transiting planet. If the RLI is small ($\sim 10^{-12} - 10^{-13}$), the corresponding orbit is ordered and stable. If the RLI $\sim 10^{-11} - 10^{-9}$ the orbit is weakly chaotic. In practical sense this orbit could be (Nekhoroshev) stable for very long terms as well, however, it can not be stable for arbitrary long time. Thus the regions characterized by these RLI values can already be the birth places of unstable orbits. Orbits having larger RLI $\sim 10^{-8} - 10^{-5}$, are strongly chaotic orbits, and they will be unstable after certain time. In our stability maps the ordered regions are denoted by light, the weakly chaotic regions by grey, and the strongly chaotic regions by dark shades.

In what follows we consider the cases where the parameters of the known giant planet having 1 Jupiter mass are the following: $a_1 = 2.0$ AU, $e_1 = 0.1$, 0.2, and 0.3 respectively. We fix the angular elements of the giant planet to $\lambda = \omega = 0°$. In Fig. 5, Fig. 6, and Fig. 7 we show the dynamical structure of the $\omega - e$ parameter planes for increasing values of the eccentricity of the giant planet. In these figures we also plot the solution curves of Equation (12) by using $\tau = 0.488029$ day.

From Fig. 5 it can be seen that there are two upper bounds for the eccentricity of the transiting planet depending on whether the transit occurs near the periastron, or near the apoastron. If the transit is near the periastron $\omega < 80°$, the upper limit of the eccentricity is $e < 0.3$, since the $\omega - e$ curves cross the chaotic region around this value. If the transit would happen at the apoastron $\omega \in [180°, 200°]$, the upper limit of the transiting planet's eccentricity is higher, $e < 0.4$. The real solution is marked (as a filled circle) on the curve corresponding to $i = 89.95°$.

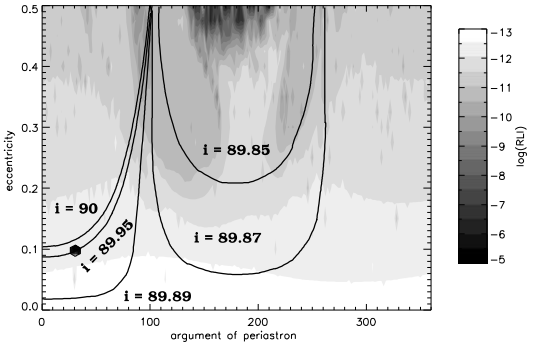

Figure 5. The stability map of the $\omega - e$ parameter plane, when $a_1 = 2.0$ AU and $e_1 = 0.1$. The $\omega - e$ curves for different i are also plotted when $\tau = 0.488029$ day.

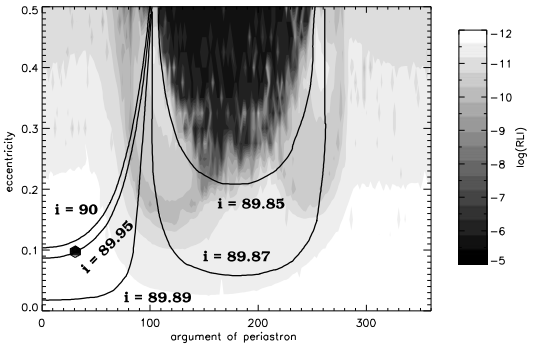

Figure 6. The stability map of the $\omega - e$ parameter plane, when $a_1 = 2.0$ AU and $e_1 = 0.2$. The $\omega - e$ curves for different i are also plotted when $\tau = 0.488029$ day.

In Fig. 6, corresponding to $e_1 = 0.2$, there are two upper limits of the eccentricity of the transiting planet as well. For $\omega < 80^\circ$ the eccentricity is $e < 0.27$, for $\omega \in [150^\circ, 220^\circ]$ the eccentricity is $e < 0.22$. In this case a lower limit can be given for the inclination too, $i > 89.^\circ 85$.

If the eccentricity of the giant planet is $e_1 = 0.3$, see Fig. 7 the maximum upper limit of the transiting planet's eccentricity is $e < 0.18$. However, in this case there exists a lower limit $e > 0.05$ as well. If the transit would take place around the periastron the corresponding ω and e values would result in weakly chaotic orbits. A lower bound of the inclination in this case is $i > 89.89^\circ$. Among the three possible values of the giant planet, this latter would represent the most effective dynamical constraint for the orbital parameters of the transiting planet, which are $a = 1.0$ AU, $e = 0.1$, $\omega = 30^\circ$, and $i = 89.95^\circ$.

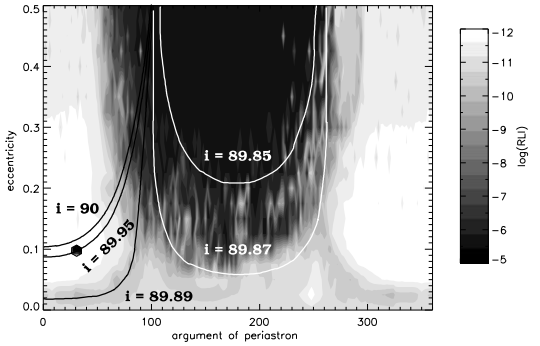

Figure 7. The stability map of the $\omega - e$ parameter plane, when $a_1 = 2.0$ AU and $e_1 = 0.3$. The $\omega - e$ curves for different i are also plotted when $\tau = 0.488029$ day.

We have also investigated the cases when the semi-major axis of the known giant planet were smaller and larger than 2 AU. If a_1 is smaller, a smaller e_1 is enough to result in an effective dynamical constraint. If a_1 is larger, the eccentricity of the giant planet should be larger as well for an efficient dynamical constraint.

5. Conclusions

The detection of Earth-like extrasolar planets by using ground based spectroscopic methods is beyond the present capabilities of observational astronomy. In the near future there will be launched space instruments such as COROT and KEPLER which are devoted to observe such planets by using transit photometry.

In this paper we addressed the question whether it is possible to determine the orbital elements of Earth-like planets discovered by transit photometry if, apart from the period, the duration of the transit can be measured too. We supposed that the mass and the radius of the hosting star is known. We derived an equation, which connects the stellar and planetary masses, the duration of the transit, the semi-major axis, the eccentricity, the argument of periastron and the inclination of the transiting planet. By fixing the inclination, this equation contains two unknown variables, the argument of periastron ω and eccentricity e of the transiting planet. Thus the solutions for different inclinations can be represented as curves on the $\omega - e$ parameter plane.

In the last section of the paper we assumed that beside the transiting Earth-like planet a giant planet orbits around the star as well. This assumption is quite reasonable if we accept the formation theories of planetary systems supporting the simultaneous presence of both rocky, Earth-like and gaseous, Jupiter-like

planets. Since the detection of giant planets is possible by measuring their radial velocity by Doppler-effect, we assumed their orbital parameters to be known. By using the framework of the restricted three-body problem, we investigated the influence of the known giant planet to the $\omega - e$ parameter plane of the transiting planet. We found that on the $\omega - e$ parameter plane there appeared chaotic regions as well, which in long terms may result in unstable motion for the transiting planet. Assuming that chaotic behaviour for the transiting planet are unlikely, we could determine an upper limit for the eccentricity, and a lower limit for the orbital inclination of the transiting planet.

In a future work we plan to extend our studies by investigating systematically the stability structure of the $(\omega - e)$ parameter plane for various values of the giant planet's semi-major axis and eccentricity. Since the mass of the hosting star is known only with a limited accuracy, we also plan to follow the propagation of this error throughout the method presented in this paper. In our future investigations we intend to consider the cases of more massive transiting planets as well.

Acknowledgments

This work has been supported by the Hungarian Scientific Research Fund (OTKA) under the grants D048424 and T043739. The support of the Austrian-Hungarian Scientific and Technology Cooperation, grant number A-12/04 is also acknowledged.

References

[1] Kasting, J. F., Whitmire, D. P., and Reynolds, R. T. (1993) "Habitable Zones around Main Sequence Stars" *Icarus* **101**, 108.

[2] Mayor, M., and Quéloz, D. (1995) "A Jupiter-Mass Companion to a Solar-Type Star" *Nature* **378**, 355

[3] Murray, C. D. and Dermott, S. (1999) *Solar System Dynamics*, CUP, Cambridge

[4] Sándor, Zs., Érdi, B., Efthymiopoulos, C. (2000) *Cel. Mech. & Dynam. Astron.* "The phase space structure around L_4 in the restricted three-body problem." **78**, 113-123.

[5] Sándor, Zs., Érdi, B., Széll, A., and Funk, B. (2004) "The Relative Lyapunov Indicator: An Efficient Tool of Chaos Detection."*Cel. Mech. & Dynam. Astron.* **90**, 127.

TERRESTRIAL TROJAN PLANETS IN EXTRASOLAR SYSTEMS

Richard Schwarz
Institute of Astronomy
University of Vienna
Türkenschanzstrasse 17
A-1180 Vienna, Austria
schwarz@astro.univie.ac.at

Abstract In this article we examine, that terrestrial planets in extrasolar planetary systems can have stable orbits in the 1:1 mean-motion-resonance (MMR) with a Jovian like planet. In our stability study of the so-called Trojan planets in the habitable zone, we used the restricted three-body problem with different mass ratios of the primary bodies. The application of the three-body problem showed that even very massive Trojan planets can be stable in the 1:1 MMR. From the approximately 145 extrasolar planetary systems with about 170 planets only 15 systems were found where a giant planet is in the habitable zone. In our numerical studies we examine the orbital behaviour and the size of the stable zone respectively of extrasolar systems where the initial orbit of the gas giant lies fully in the habitable zone. The investigation of either the initial mean anomaly (M) or the initial argument of perihel (ω), showed, that the variation of ω yield more stable orbits than the variation of M.

Keywords: trojan planets – exoplanets – habitable zone

1. Habitable planets

Today we have only observational evidence of extrasolar planets of 7 earth masses (Gliese 876 d) and larger. The size of such planets is to large for formation of life and only a few of these planets lie in the 'Habitable Zone' (=HZ[1]). That's the reason why a study of dynamical stability of possible additional terrestrial planets (planets with a size comparable to Earth) is a hypothetical one. But what we can do is to ask, which dynamical configurations are possible to host a habitable planet in the HZ of an extrasolar planetary system? From the dynamical point of view, there are four possible configurations for terrestrial like planets in the HZ (shown in Fig. 1).

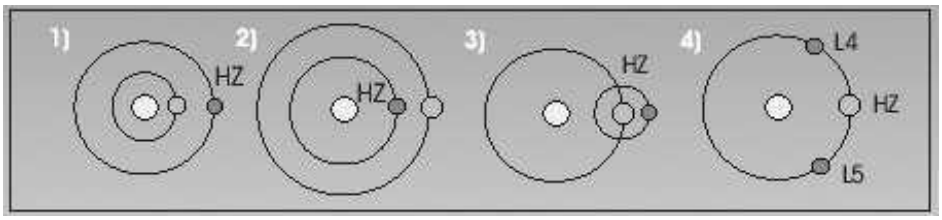

Figure 1. Four different classes of orbits where possible terrestrial planets may exist.

1 The HZ is outside the giant planet (=OHZ): Most of the discovered gas giant (=GG) planets are located very close to their star. From the dynamical point of view, there may exist terrestrial planets with stable orbits in the HZ and sufficiently small eccentricity over time scales long, enough to develop a biosphere.

2 The solar configuration (=SOL): When a Jupiter like planet moves far enough from its central star to allow additional planets moving on stable low eccentric orbits closer to the star inside the HZ.

3 The satellite configuration (=SAT): A terrestrial planet that orbits a GG in the HZ (as the ones orbiting Jupiter, e.g. Europa) could have the right conditions to develop a biosphere.

4 The Trojan configuration (=TROJ): When the GG moves in the habitable region a terrestrial Trojan planet may move in a stable orbit around the Lagrangian equilibrium points L_4 or L_5.

Menou and Tabachnik (2003) quantified the dynamical habitability of extrasolar planetary systems in general via simulations of their orbital dynamics in the presence of potentially habitable terrestrial plantes. The OHZ and the SOL configurations have been the subject of a number of investigations (e.g. Sándor(2006), Érdi and Pál (2003), Pál and Sándor (2003), Dvorak et al. (2003a, 2003b and 2004)). If the gravitational zone of a GG overlaps with that of a terrestrial planet in the HZ, gravitational perturbation can push the terrestrial planet out of the HZ. For this reason, we focus our work on the dynamical stability of the TROJ configuration, in which possible terrestrial planets have a 1:1 MMR with a GG. Nauenberg (2002) found a stable configuration for motions in the 1:1 MMR, where the more massive planet has an almost circular orbit, while the smaller body has a high eccentric orbit. Further investigations of the TROJ configuration focused on Trojan planets in the HZ (Érdi and Sándor (2005)). We are mainly interested in Trojan planets in 1:1 MMR with a GG that moves fully in the HZ. The main goal was to see how many orbits (of the Trojan planets) of the stable region are fully in the HZ after the calculation. These stable orbits are a main requirement for a possible formation of

life. Laughlin and Chambers (2002) considered the possibility of two planets in a 1:1 MMR as a result of an interaction with the protoplanetary accretion disc. We emphasize that the discussion of habitable regions around a host star is an interdisciplinary one: astrophysics is involved, because the spectral type and the age of the host star define the HZ (e.g., Lammer et. al. (2003)), atmospheric chemistriy is fundamental when we considering planetary habitability (e.g., Kasting et. al. (1993)), and astrodynamics is important with regard to the determination of the orbital stability.

2. Numerical setup

More than 170 extrasolar planetary systems were discovered (Extrasolar planets catalogue maintained by Jean Schneider[2]), 14 systems are binaries and 18 are multiplanetary systems. Only 10 single-star systems have a giant planet in the HZ and an initial eccentricity smaller than 0.3, which is important for the stability (see Schwarz, 2005 p.65). We selected in Table 1 six planetary systems, namely HD93083, HD17051, HD28185 , HD108874 and HD27442 (the bold written), for which the initial orbit lies fully in the HZ. We studied their size of the stability region by using direct numerical integrations of the equation of motion. The other systems which lies only partly in the HZ were also investigated, see Schwarz et al. (2005a) and Schwarz (2005b). The integration was carried out with the LIE-integration method – which uses an adaptive step size (Hanslmeier and Dvorak, 1984; Lichtenegger, 1984) – in the dynamical model of the elliptic restricted three-body problem consisting of the central star, the GG and a hypothetical (massless) terrestrial planet. The integration time was up to 10^5 years.

2.1 Initial conditions

We have taken the following initial conditions for the terrestrial planet: first, the semimajor axis of the massless planet (starting at the fixed semimajor axis of the GG) was computed for a grid with $\Delta a = 0.003 AU$. The argument of pericenter ω of the massless planet extends from 20° to 140° and has a grid-size of $\Delta\omega = 2^\circ$. The extension and the geometry of the stable region for the Trojan planet of several extrasolar systems varies. We change the number of the calculated orbits for each system to reduce the calculation-time (the larger the unstable region the more calculation-time were needed). During the integration time, the largest value of the eccentricity (=$e_{\max}$) of the hypothetical Trojan planet was determined. The so called maximum eccentrictiy method (=MEM) shows how much the orbit differs from the circular one. For larger eccentricities it becomes more probable that the asteroids have close encounters and collisions. The stability criterion for a Trojan was, that the eccentricity should not exceed e=0.5; this is good measure which were tested and compared

to other definitions like crossing the line of syzygy (alignment of Sun, Jupiter and the Trojan).

Table 1. List of all single GG moving in the HZ of their host stars, depending on the spectral type the host stars. Main parameters: *1st column:* Name, *2nd column:* spectral type, *3rd column:* mass of the star, *4th column:* the minimum mass of the giant planet [=M_{jup}], *5th column:* distance (semimajor axis a[AU]) from the central star, *6th column:* initial eccentricity of the extrasolar planet, *7th column:* extension of the HZ [AU], and *8th column:* partly inside the HZ at the beginning (initial conditions) in [%] .

Name	Spec.	mass [M_{sol}]	mass [M_{jup}]	a [AU]	e	HZ [AU]	partly in HZ [%]
HD93083	**K3V**	**0.70**	**0.37**	**0.48**	**0.14**	**0.40-1.30**	**100**
HD134987	G5V	1.05	1.58	0.78	0.24	0.75-1.40	58
HD17051	**G0V**	**1.03**	**1.94**	**0.91**	**0.24**	**0.70-1.30**	**100**
HD28185	**G5**	**0.99**	**5.7**	**1.03**	**0.07**	**0.70-1.30**	**100**
HD108874	**G5**	**1.00**	**1.65**	**1.07**	**0.20**	**0.70-1.30**	**100**
HD27442	**K2IVa**	**1.20**	**1.28**	**1.18**	**0.07**	**0.93-1.80**	**100**
HD188015	**G5IV**	**1.08**	**1.26**	**1.19**	**0.15**	**0.70-1.60**	**100**
HD114783	K0	0.92	0.99	1.20	0.10	0.65-1.25	50
HD20367	G0	1.05	1.07	1.25	0.23	0.75-1.40	76
HD23079	(F8)/G0V	1.10	2.61	1.65	0.10	0.85-1.60	35

3. Global results

The stability region around the Lagrangian points was studied in the model of the elliptic restricted three-body problem by many investigations (e.g. Rabe, 1967, Lohinger and Dvorak, 1993 etc.). Furthermore, a study by Marchal (1991) was undertaken in the framework of the general three-body problem (where $m_3 > 0$[3]). These results were used to show the positions – in the stable zone (see Fig. 2) – of all extrasolar systems where the gas giant is near the HZ. This is given in Table 1, where m_3 is equal to one earth mass. Therefore it is necessary to define the mass parameter μ through the equation

$$\mu = \frac{m_2 + m_3}{M} + m_2 \cdot m_3 + O\left(\frac{m_2^3 \cdot m_3}{m_1^4}\right) \qquad (1)$$

which is used instead of the mass ratio in the elliptic restricted three-body problem. The stability zone (Fig. 2 depending on the mass parameter μ and the eccentricity show that all selected extrasolar systems of Table 1 lie in the zone of stable motion. Only HD141937 (partly in the HZ) which has a planet with 9.7 Jupiter masses is close to the border (see Fig. 2) of unstable motion. Consequently all planetary systems with one planet in the HZ can have stable Lagrangian points (L_4 and L_5).

We conclude that orbits of hypothetical Trojan planets with a small initial μ and e are stable. The stability analysis does not give any information about the extension of the stable region around the equilibrium points. A more detailed answer can be given with the results of numerical simulations of each extrasolar systems under consideration shown in the next paragraph.

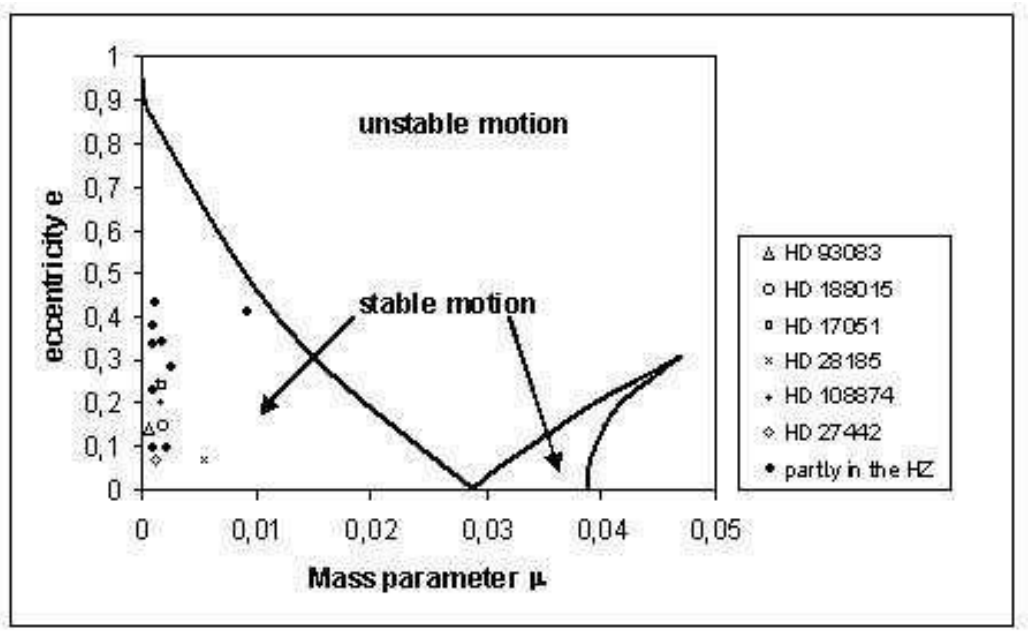

Figure 2. Stability zone depending on the mass parameter μ and the eccentricity e.

4. Results

Table 1 shows the parameters of all studied single[4] extrasolar systems. The six selected extrasolar planetary systems – printed in bold in Table 1 – have one GG lying at the starting positions fully in the HZ. Note that from the dynamical point of view there is no difference to the other systems.

4.1 HD17051

HD17051 is a G0V star with one solar mass (M_{sun}=1.03) which hosts a GG of 1.94 Jupiter masses (=M_{jup}) on an eccentric orbit (e=0.24) with a semimajor axis of a=0.91 AU. This system was calculated for 0.1 Myrs, to see how the stability region shrinks – this is shown by the number of stable orbits – (see Table 2). To get the number of stable orbits it was necessary to determine the value of $e_{\max}$ after 0.1 Myrs (this new $e_{\max}$ of the stable region ranges from 0.06 to 0.32), as it is shown in Table 2. New $e_{\max}$ means that we set the upper limit for the Trojans eccentricity so that they are still in the region of stable motion (more details about the MEM are shown in Sec. 2.1).

The results are shown in Fig. 3 and Fig. 4, where we can see a convex structure which extends from $\omega = 25°$ to $35°$. The convex structure is getting flatter, if the initial eccentricity is very small. After this convex region (well visible in Fig. 4) the value of e_{max} rises up to 0.32. Our calculations also revealed that the e_{max} of the stable region was twice as large as that of the e_{ini} (shown in Table 2), a result that illustrates how the size of the stable region and the value of e_{max} depends on e_{ini}. The numerical simulation shows that the stable region extends from $\omega = 20°$ to $65°$ and the semimajor axis from a=0.89 [AU] to 0.94 [AU]. We can conclude that 17% or 286 orbits of the 1680 calculated ones are stable.

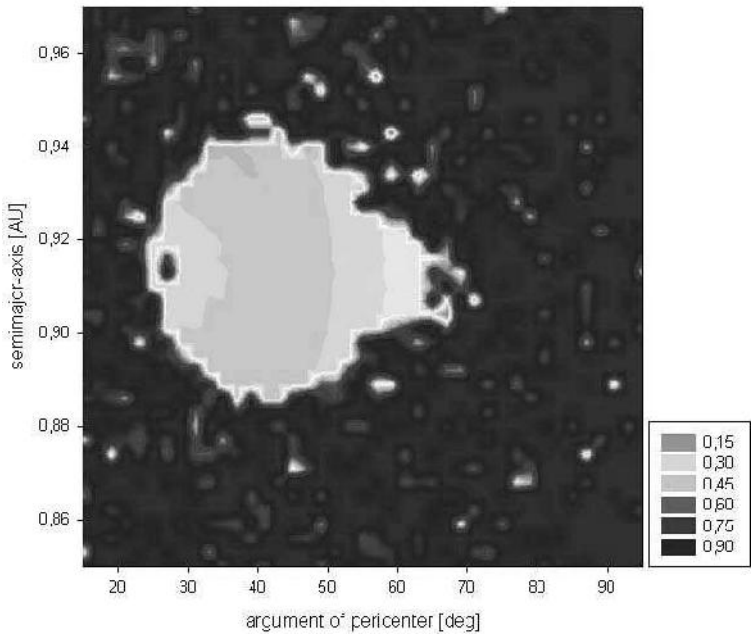

Figure 3. This figure shows system HD17051 for a computation time of 0.1 Myrs. The light region is the most stable whereas the dark region indicates chaotic motion.

4.2 Stability regions of HD93083 and HD27442

Both extrasolar systems have main sequence stars, but no sun like spectra. HD27442 has a large stable region, because the new e_{max} (shown in Table 2) of the Trojan planet is very small and lies fully in the HZ after 0.1 Myrs (see Fig. 6). The stable region of HD93083 which is smaller has an elongated shape (see Fig. 4). That's the reason, because the GG is very close to the star (a=0.48 AU) and has a relatively large initial eccentricity (e=0.14) shown in Table 1. The new e_{max} (see Table 2) of the stable region go up to 0.26, but nevertheless the orbits lie 96 percent in the HZ.

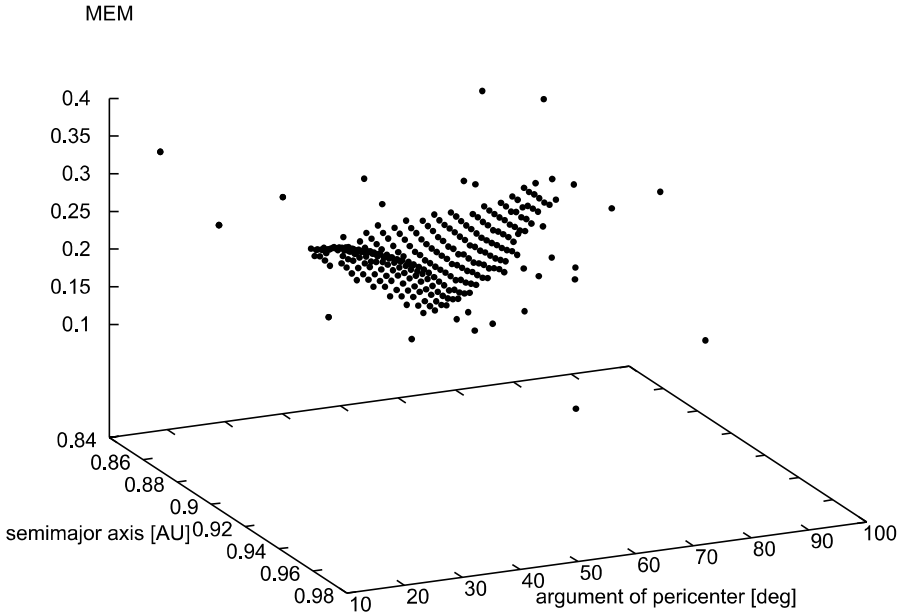

Figure 4. Shows a 3D depiction for the system HD17051. A large MEM indicates unstable motion.

Table 2. List of all results for four of the systems listed in Table 1, which illustrates the extension of the stable region of the Trojan planets after 0.1 Myrs. *1st column:* name of the investigated system, *2nd column:* inital eccentricity of the GG, *3rd column:* new e_{max} of the stable region, *4th column:* number of the stable orbits vs. the calculated one, *5th column:* minimum of the perihel with the new e_{max}, *6th column:* maximum of the aphel with the new e_{max}, *7th column:* partly in the HZ [%] after 0.1 Myrs. The number of the calculated orbits were changed, because of the different geometry of the stable regions.

System	e_{ini}	**new** e_{max}	**Number of stable orbits** /calc. orbits	**min. of the perihel** [AU]	**max. of the aphel** [AU]	**partly in the HZ** [%]
HD93083	0.14	0.00 - 0.26	318 / 2580	0.36	0.61	96
HD17051	0.24	0.06 - 0.32	286 / 1800	0.62	1.20	87
HD28185	0.07	0.02 - 0.19	555 / 1800	0.83	1.23	100
HD108874	0.20	0.11 - 0.30	421 / 2000	0.76	1.38	87
HD27442	0.07	0.00 - 0.19	360 / 2000	0.96	1.40	100
HD188015	0.15	0.00 - 0.25	684 / 2250	0.89	1.49	100

4.3 Stability regions of HD108874 and HD188015

From the examination of HD108874 and HD188015 - both are main sequence stars (G5) - followed that the Trojan planets of the GGs are mainly

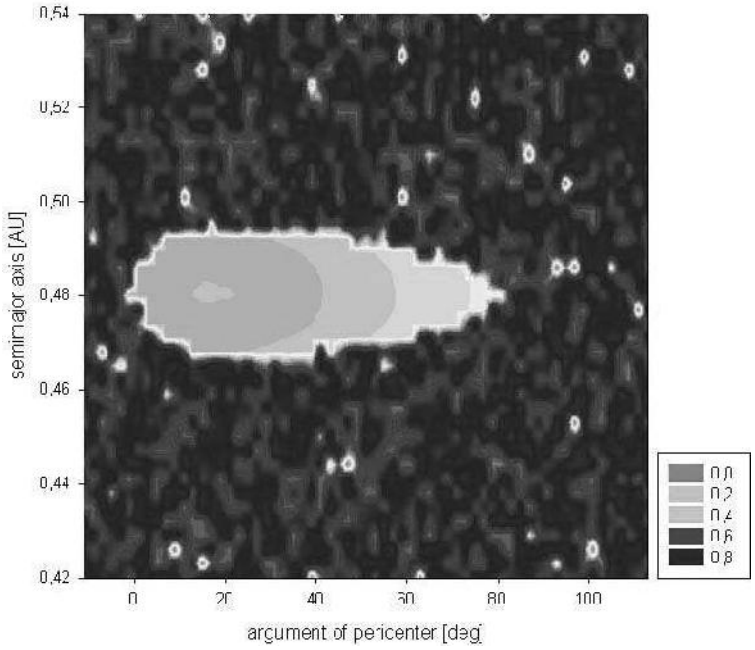

Figure 5. System HD93083 for a computation time of 0.1 Myrs. The light region is the most stable whereas the dark region inidcates chaotic motion.

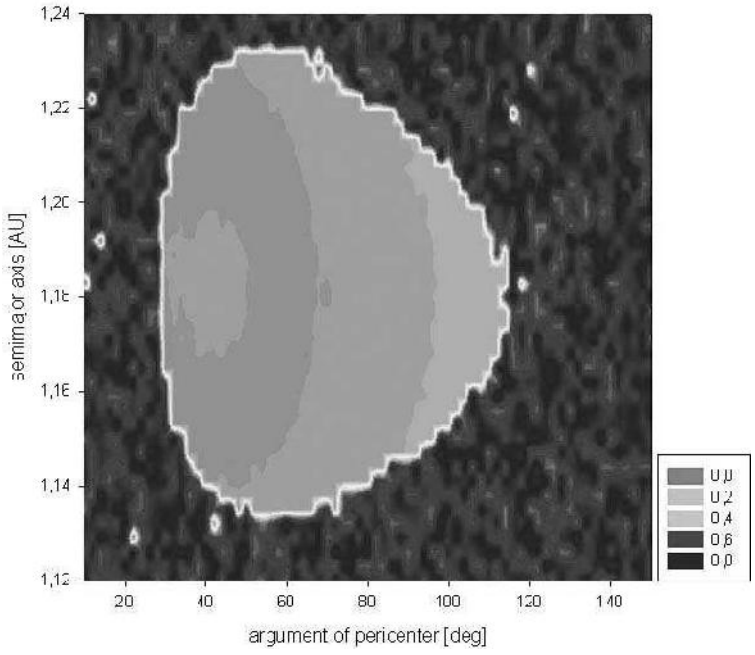

Figure 6. System HD27442 for a computation time of 0.1 Myrs. The light region is the most stable whereas the dark region indicates chaotic motion.

in the HZ with a new e_{max} (see Table 2) not higher than 0.29. The results are shown in Table 2 or Fig. 7 for HD108874 and Fig. 8 for HD188015. The results

show that the system HD108874 has a large stable region, but lies only partly in the HZ, because the new e_{max} is to large. Whereas HD188015 has a large stable region which lies fully in the HZ. We investigated Trojan like motion in 10 single planetary systems where the initial eccentrictiy is not larger than 0.3 and the gas giant lies partly or fully in the HZ. Than we selected 6 systems, where the gas giant lies also mainly in the HZ. Numerical simulations show, how much orbits of the Trojan planet lie in the HZ after an integration time of 0.1 Myrs. That happens if the new e_{max} continues (during the integration) very small so that the stable region in the HZ becomes very large. We found out that from the six selected extrasolar systems only three extrasolar systems are completely inside the HZ (see Table 2), but only two of them have Sun like spectra.

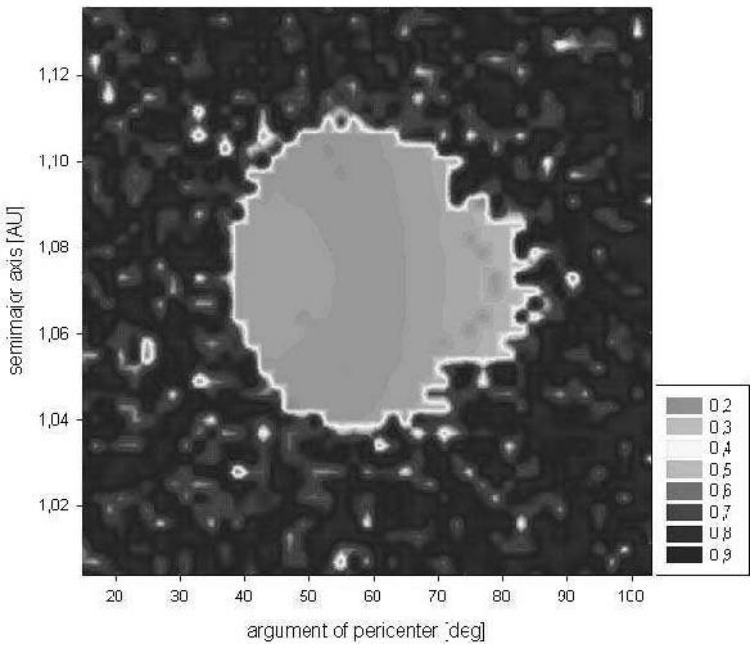

Figure 7. Stability region for the system HD108874 for a computation time of 0.1 Myrs. The light region is the most stable whereas the dark region indicates chaotic motion.

5. Influence of the orbital elements M and ω

In the last chapter the size and structure of the stable zones were investigated. This was done by the variation of ω, but former investigations (see Schwarz 2005a and Schwarz et al. 2005b) used the variation of M. Now we are able to compare the variation of this two parameters and show if there is any difference. A variation of of M changes the location of the Trojans whereas, if we use the orbital element ω we change the location of the Trojans ellipse. Table 3 shows the calculation of the four extrasolar systems. In this table we compare

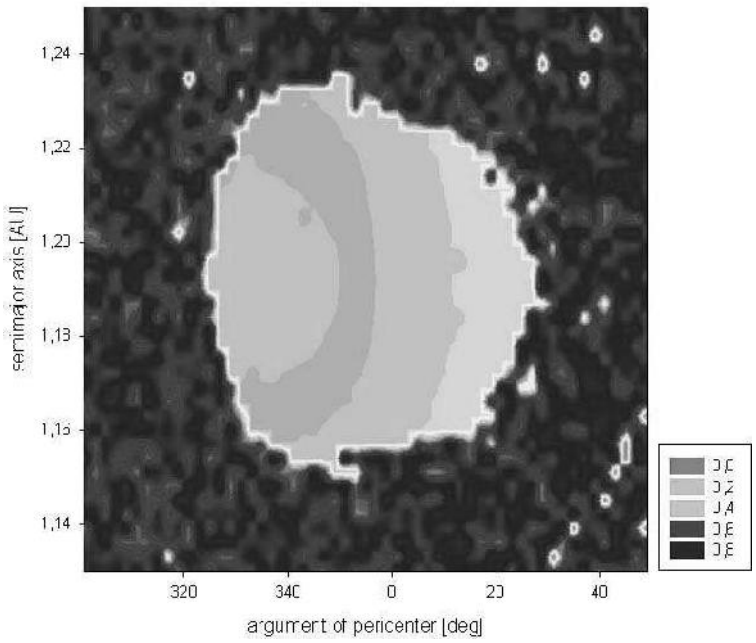

Figure 8. Stability region for the system HD188015 for a computation time of 0.1 Myrs. The light region is the most stable whereas the dark region indicates chaotic motion.

the number of stable orbits for M and ω. It is well visible, that the number of stable orbits is larger for ω than for M. This can also be seen in the new $e_{\max}$ of the stable region. New $e_{\max}$ has two values,because the eccentricity of the stable region is not homogeneous (Table 3 shows two values the upper and the lower limit of the new $e_{\max}$). Therefore we have an example HD17051, were the Fig. 3 and Fig. 4 shows how the new $e_{\max}$ is distributed.

Now I want to present the interaction of the initial M vs. the initial ω (shown in Fig. 8). The comparison of both orbital elements was done for the extrasolar system HD17051 for an integration time of 10^4 years (initial conditions see Table 1). The ω and M extends from $0°$ to $360°$ and have a gridsize of $\Delta\omega = 4°$ and $\Delta M = 4°$. The first thing to notice is that in Fig. 9 we have two stable diagonal regions. The left region (goes from $\omega = 275°$ to M=275°, the width of the stable region is approximately between +-25°) shows the L_5 region and the right one ($\omega = 50°$ to M=50° the width is also +-25°) that of L_4. There are also two small stable regions in the left lower corner and in the right uper corner, which belongs to the L_4 and L_5 regions. Another investigation of the extrasolar systems (HD 28185) shows that the stable region (of ω vs. M) depends on the mass of the gas giant (HD28185 has a very massive gas giant $M_{jup} = 5.7$) and the eccentricity of both (Trojan planet and gas giant). This investigation (shown in Fig. 10) was undertaken for a smaller gridsize of $\Delta\omega = 2°$ and M=2° and also for an integration time of 10^4 years. For higher eccentricities

the continous stable region will splitted in to two islands (see Fig. 10, lower panel). We can conclude that there exist for a mass of the gas giant of about $M_{jup} = 6$ and an initial eccentricity higher 0.15 no continous stable region. The fact that we have a linear continous stable region for the Lagrangian points give us the possibility to depict ω and M in a simple ratio. This could be used for future calculations to vary both orbital elements (ω and M) during the integrations.

Table 3. Results of four systems listed in Table 2, which illustrates the extension of the stable region of the Trojan planets after 0.1 Myrs for the variation of the mean anomaly and the argument of perihelion. *1st column:* name of the investigated system, *2nd column:* inital eccentricity of the GG, *3rd column:* new $e_{\max}$ of the stable region for the mean anomaly, *4th column:* new $e_{\max}$ of the stable region for the argument of the perihel, *5th column:* number of the calculated orbits, *6th column:* Nr. of stable orbits for M, *7th column:* Nr. of stable orbits for ω, The number of the calculated orbits were changed, because of the different geometry of the stable regions.

System	e_{ini}	**new** $e_{\max}$ **of** M	**new** $e_{\max}$ **of** ω	**Nr. of calc. orbits**	**Nr. of stable orbits for** M	**Nr. of stable orbits for** ω
HD17051	0.24	0.4 - 0.5	0.06 - 0.32	1800	73	286
HD28185	0.07	0.1 - 0.2	0.02 - 0.19	1800	161	591
HD108874	0.20	0.3 - 0.4	0.11 - 0.29	2000	159	421
HD27442	0.07	0.1 - 0.15	0.00 - 0.19	2000	926	1259

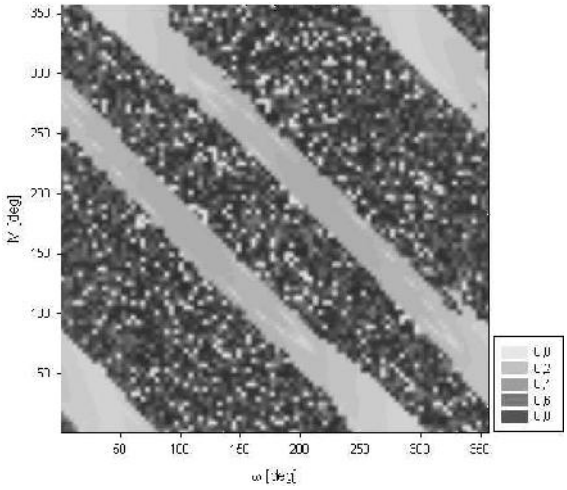

Figure 9. Stability region for the system HD17051 for a computation time of 10^4 yrs. The light region is the most stable whereas the dark region indicates chaotic motion.

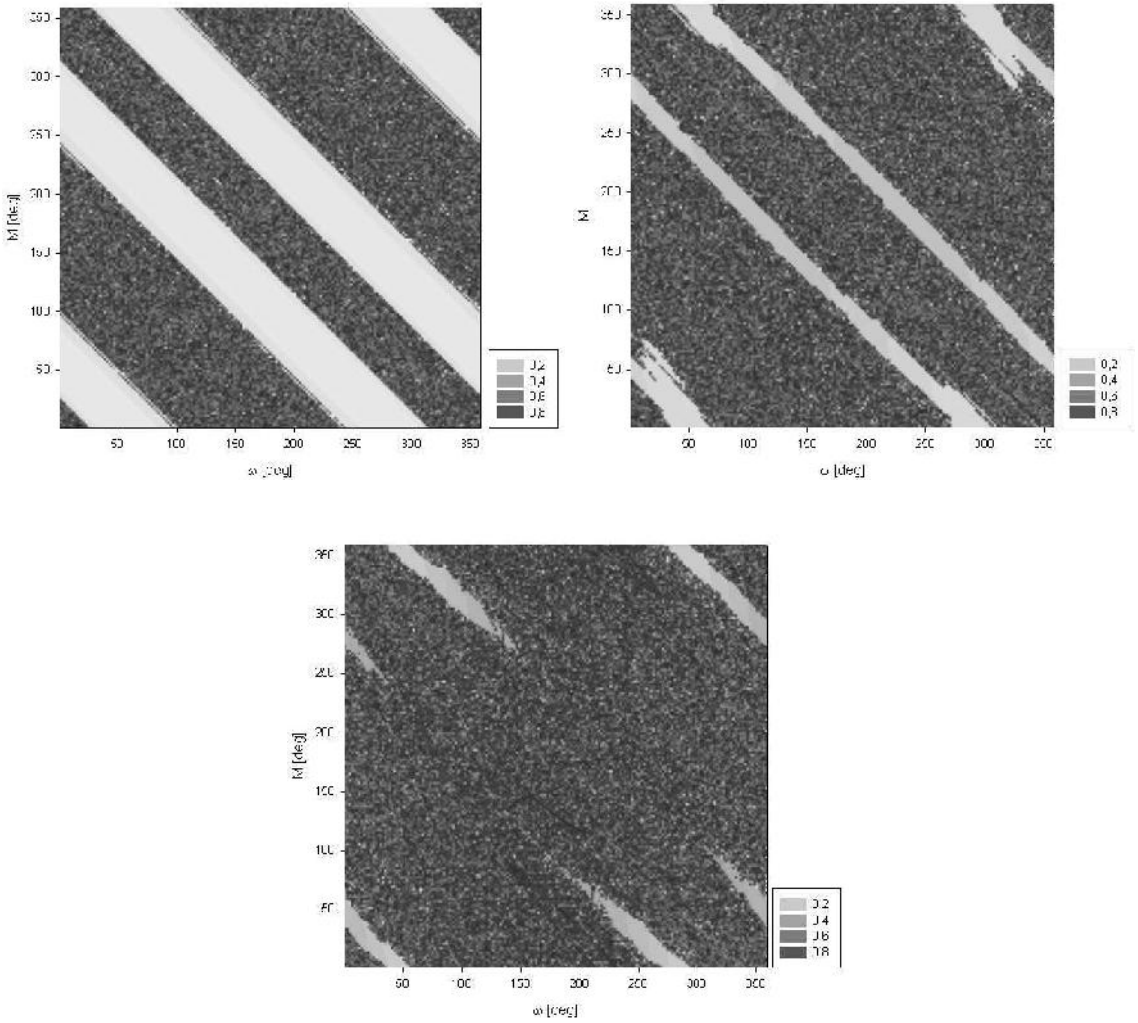

Figure 10. Stability region for the system HD28185 for a computation time of 10^4 yrs and different initial eccentricities: $e_{\rm ini} = 0$ (upper Figure), $e_{\rm ini} = 0.07$ (middle Figure) and $e_{\rm ini} = 0.15$ (lower Figure). The light region is the most stable whereas the dark region indicates chaotic motion.

6. Discussion

We investigated Trojan like motion in 10 extrasolar planetary systems by using the restricted three body problem. The GG of the selected systems are partly or fully in the HZ and the initial eccentricity dont exceed the value of 0.3. We checked the extrasolar sytems - by using the studies of Marchal - in the 1:1 MMR for the selected systems, where the gas giant moves near the HZ. We can conclude that only one of the investigated systems have no stable region (HD 141937) and that the stable region of the Trojan planets are getting smaller with larger values of μ and e (see Fig. 2).

Numerical simulation were done to investigate the dynamical stability of six extrasolar planetary systems, which lie fully in the HZ. The MEM were

used to detemine the stability of the Trojan orbits. We find out that three systems dynamical lie completely in the HZ after a calculation time of 0.1 Myrs (HD28185, HD108815 and HD27442), but only two of them have Sun like stars (HD28185 and HD108815). The other three systems could also be candidates for habitable Trojan planets, because the stable orbits lie 87 percent (HD17051 and HD108874) and 96 percent (HD93083) in the HZ. Another part of this work was to investigate the interaction, if we change the initial mean anomaly (M) or the initial argument of perihel (ω) during the calculation. The comparison of both orbital elements was done for the extrasolar system HD17051 and HD28185 for an integration time of 10^4 years. We could find out that, if we vary the ω there are much more stable orbits than for M. Because of that, future calculations should include both orbital elements, to become a more realistic simulation. Therefore further calculations should be done to analyse the stability region of ω and M for different masses, eccentricties and inclinations.

Acknowledgments

The support of the Austrian-Hungarian Scientific and Technology Cooperation, grant number A-12/04 is acknowledged.

Notes

1. i.e. the region where possible terrestrial plantes can have (a) liquid water on the surface and (b) a stable atmosphere shown in Fig. 1
2. The Extrasolar Planets Encyclopedia at http://www.obspm.fr/encycl/encycl.html
3. A thrid body, which always remains in the orbital plane of the primaries, feels their gravitaional attraction, but does not influence their motion, because the mass is very small
4. that means only one planet in these extrasolar systems is known.

References

[1] Dvorak, R., Pilat-Lohinger, E., Funk, B., and Freistetter, F. (2003a) Planets in habitable zones: A study of the binary Gamma Cephei. Astron. Astrophys. 398, L1-L4.

[2] Dvorak, R., Pilat-Lohinger, E., Funk, B., and Freistetter, F. (2003b) A study of the stable regions in the planetary system HD 74156can it host Earth like planets in habitable zones? Astron. Astrophys. 410, L13-L16.

[3] Dvorak, R., Pilat-Lohinger, E., Schwarz, R., and Freistetter, F. (2004) Extrasolar Trojan planets close to habitable zones. Astron. Astrophys. 426, L37-L40.

[4] Érdi, B. and Pál, A. (2003) Dynamics of resonant exoplanetary systems. In Proceedings of the 3rd Austrian- Hungarian Workshop on Trojans and Related Topics, edited by F. Freistetter, R. Dvorak, and B. Érdi, Eötvös University Press Budapest, Vienna, p. 3.

[5] Érdi, B. and Sándor, Zs. (2005) Stability of co-orbital motion in exoplanetary systems. CMDA., Vol. 92,Issue 1-3, p113-121.

[6] Hanslmeier, A. and Dvorak, R. (1984) Numerical integration with Lie series. Astron. Astrophys. 132, 203-207.

[7] Kasting, J.F., Whitmire, D.P., and Reynolds, R.T. (1993) Habitable zones around main sequence stars. Icarus 101, 108-128.

[8] Lammer, H., Dvorak, R., Pilat-Lohinger, E., Funk, B., Freistetter, F., Ribas, I., Selsis, F., Guinan, E.F., Weiss, W.W., and Bauer, S.J. (2003) Atmosphere and orbital stability of exosolar planets orbiting gamma Cephei. In EGS-AGU-EUG Joint Assembly, Abstracts, Abstractbook [abstract 12443], Nice, France.

[9] Laughlin, G. and Chambers, J.E. (2002) Extrasolar Trojans: The viability and detectability of planets in the 1:1 resonance. Astron. J. 124, 592-600.

[10] Lichtenegger, H. (1984) The dynamics of bodies with variable masses. CMDA. 34, 357-368.

[11] Lohinger, E. and Dvorak, R. (1993) Stability regions around L4 in the elliptic restricted problem. Astron. Astrophys. 280, 683-687.

[12] Nauenberg, M. (2002) Stability and eccentricity for two planets in a 1:1 resonance, and their possible occurrence in extrasolar planetary systems, Astron. J., 124,Issue 4, 2332-2338.

[13] Marchal, C. (1991) The three-body problem [book review]. Observatory 111, 192.

[14] Menou, K. and Tabachnik, S. (2003) Dynamical habitability of known extrasolar planetary systems. Astrophys. J. 583, 473-488.

[15] Pál, A. and Sándor, Zs. (2003) Dynamical stability of the habitable zone of exoplanetary systems. In Proceedings of the 3rd Austrian-Hungarian Workshop on Trojans and Related Topics, edited by F. Freistetter, R. Dvorak, and B. Érdi, EÄśtvÄśs University Press Budapest, Vienna, p. 25.

[16] Rabe, E. (1967) Third-order stability of the long-period Trojan librations. Astron. J. 72, 10.

[17] Sándor, Zs. and Érdi, B. (2003) Symplectic mapping for Trojan-type motion in the elliptic restricted three-body problem. CMDA. 86, 301-319.

[17] Sándor, Zs., Süli, Á., Érdi, B. (2006) Stability Maps of Hypothetical Terrestrial Planets in Extrasolar Planetary Systems, preprint

[18] Schwarz, R. (2005a), Global stability of L_4 and L_5 Trojans, PHD thesis, Universität Wien, also online under http://dissdb.bibvb.ac.at

[19] Schwarz, R., Pilat-Lohinger, E., Dvorak, R., Érdi, B., Sándor, Zs. (2005b) Trojans in Habitable Zones (Special Collection of Papers:Bioastronomy 2004), Astrobiology Journal Vol. 5, No. 5: 579-586

CHAOS IN SIMPLE DYNAMICAL SYSTEMS – THE SITNIKOV PROBLEM

Tamás Kovács
Department of Astronomy
Loránd Eötvös University
Pázmány Péter sétány 1/A
H-1117 Budapest, Hungary
t.kovacs@astro.elte.hu

Abstract It is well known that in low degrees of freedom dynamical systems chaotic behaviour appears. To examine this phenomenon the Sitnikov problem is a very good example which is a special case of the restricted three-body problem. In this paper we investigate the changing of the phase space structure due to the variation of the initial positions of the primaries in the configuration.

Keywords: dynamical systems – chaos – resonances

1. Introduction

The investigation of the dynamical systems in the past 50 years shows that chaotic behaviour appears not only in difficult, many degrees of freedom systems but in simple configurations as well. Therefore one of the most relevant tasks is to study these simple dynamical systems to understand the chaos, and on the other hand it is a good starting point to investigate the more difficult problems.

Out of the simplest and most interesting system in celestial mechanics is the Sitnikov problem. Essentially, it is a special case of the restricted three-body problem. Namely there are two equal masses m_1 and m_2 revolving in Keplerian orbits around each other, a the third massles body m_3 moves on an axis perpendicular to the plane of the primaries through its barycenter.

Mac Millan (1913) [6] showed that in the circular problem, when the primaries revolve on circular orbit, the problem is integrable and the solution is expressed by elliptic integrals. The motion of the masless body is more various when we allow the two primaries to move in eccentric orbits. In this case quasi-periodic and chaotic orbits appear beside the periodic ones. The solution of the problem was first given by Sitnikov in 1960 [9], after that many authors

examined the existence of periodic orbits in this configuration. The first mapping model was derived by Liu and Sun (1990) [5], who showed that for small eccentricities the phase space becomes very complex. Perdios and Markellos (1998) [8] studied the stability and the bifurcations in the Sitnikov problem. Dvorak (1993) [1] investigated numerically the problem by using Poincaré's surfaces of section. Martínez Alfaro an Chilart (1993) found that for certain eccentricities the fixed points $z = \dot{z} = 0$ in the center becomes unstable. Kallrath et al. (1997) [4] explored the phase space in detail laying emphasis on resonances. For small eccentricities Hagel (1992) [3] and Faruque (2003) [2] applied perturbation methods and gave an analitical approximation to the problem.

In this study we investigate the phase space structure for different initial conditions, eminently for different initial positions of the primaries. For the visualization of the results we use Poincaré's surfaces of section.

2. Equation of motion

As mentioned above, we investigate the motion of a massles body which moves along a line perpendiclar to the plane of the primaries through their baricenter (see Fig. 1). By introducing suitable units we can write the equation of motion. We choose the total mass of the primaries as mass unit, the rotating period equal to 2π, the semi-major axis of the orbit of the primaries as distance unit (m_1 and m_2), so the Gaussian constant becomes 1. Then the equation of motion of the massles body is

$$\ddot{z} = -\frac{1}{r^3} z, \tag{1}$$

where

$$r = \sqrt{R^2 + z^2}, \qquad R = 1 - e\cos E. \tag{2}$$

R is the distance between the primaries , z is the distance of the massles body from the plane of primaries, e is the eccentricity, and E is the eccentric anomaly, which depends on the time according to Kepler's equation:

$$t - \tau = E - e\sin E. \tag{3}$$

The $\tau = 0$ phase constant corresponds to the pericenter passage at $t = 0$. Since the problem is only one degree of freedom, we can introduce the true anomaly v as for independent variable instead of the time. (See [4].)

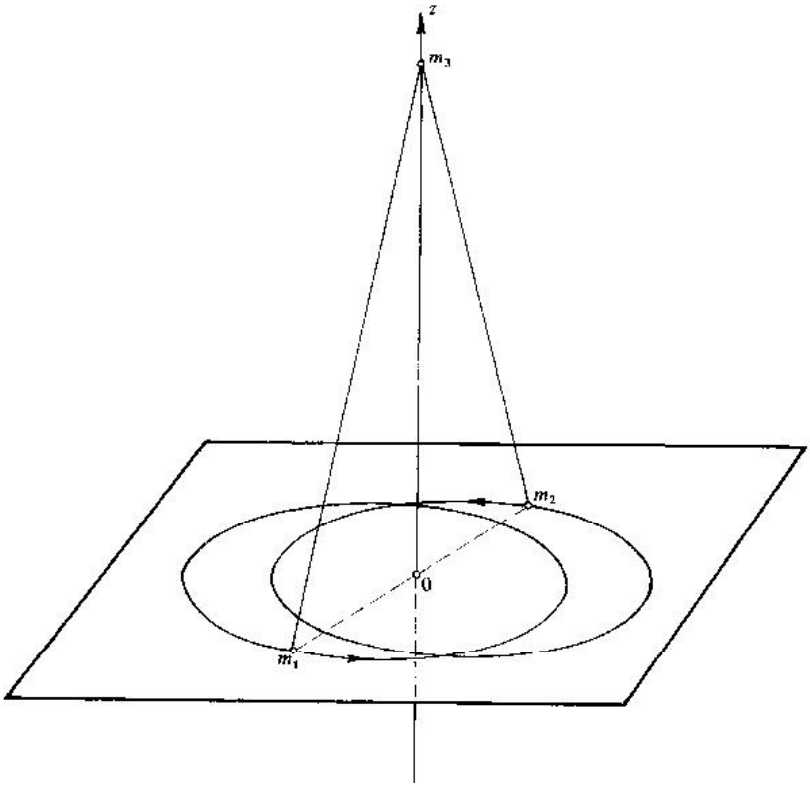

Figure 1. The Sitnikov problem.

3. Structure of the phase space

We studied the Sitnikov problem for different initial conditions. On the phase portraits we plotted many trajectories corresponding to different initial conditions. The set of initial conditions was $z_0 = 0.15 - 1.8$ with $\Delta z = 0.05$, and the initial velocities were $\dot{z} = 0$ in all cases. We choosed the integration time to be 10000 periods of the primaries.

The circular case is equivalent to the two center problem, which was solved already by Euler in 1764. In this case, when the third mass has bounded motion, the solutions are periodic or quasi-periodic depending on the initial conditions. The trajectories corresponding to these latter give close curves on a convenient surface of section in the phase space. Such curves are shown in Fig. 2.

In the eccentric case we have more various phenomena in the phase space. It is well known that increasing the parameter e the structure of the $z - \dot{z}$ space is also changing (Kallrath et al., 1997) [4]. For initial conditions close to the plane of the primaries the solutions are quasi-periodic motions by invariant cueves on the surface of section (see Fig. 3). However, small islands appear

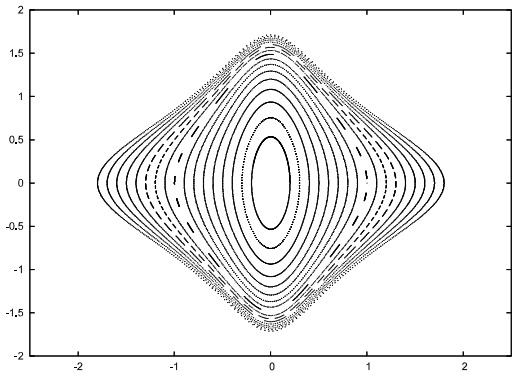

Figure 2. Invariant curves in the circular case of the Sitnikov problem. There are 17 initial conditions, $z_0 = 0.2 - -1.8,\ \Delta z = 0.1$.

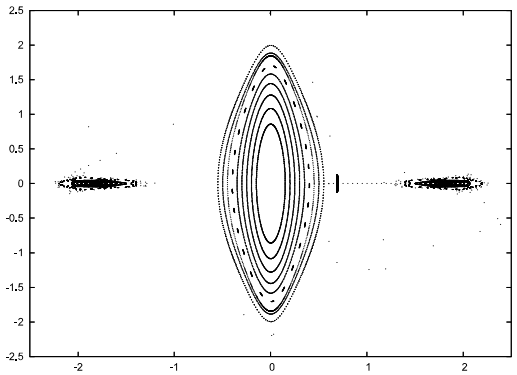

Figure 3. $e = 0.4$ and $v_0 = 0^\circ$ (pericenter passage). The islands outside the invariant curves correspond to the 1:1 and 2:1 mean motion resonances. Between the islands there are escaping trajectories.

for particular initial distances outsid these invariant curves. These formations correspond to reasonances with the primaries. The massles body escapes from the system in the region between the islands (see Fig. 3).

In this paper we investigated the changing of the phase portraits when the primaries are not in the pericenter at $t = 0$. We calculated the motions for four initial positions of the primaries $v_0 = 45^\circ$, 90°, 135° and 180°. Fig. 4 and Fig. 6 show the results.

The eccentricity of the binary was 0.4 (see Fig. 4). It can be seen that the 2:1 mean motion resonance (the two small islands in the Fig. 3) remains in all cases except $v_0 = 180^\circ$. For example in the case $v_0 = 45^\circ$ these islands dissolve to three smaller ones (see Fig. 4, top left panel). In addition, chaotic motion appears close to the separatrices. In Fig. 4 the bottom right panel shows a quite distinct picture. Except for initial conditions close to the baricenter, there are chaotic motions.

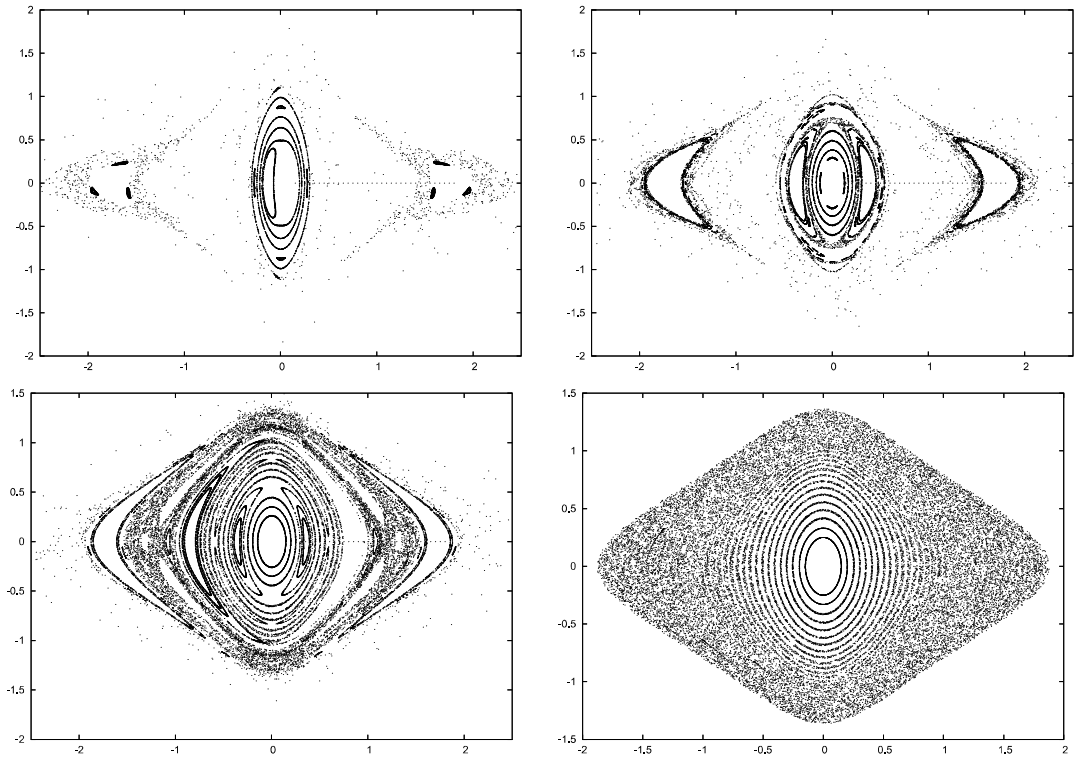

Figure 4. $e = 0.4$. Top left panel: $v_0 = 45^\circ$, the islands split up at the edge of the figure and the trajectories appear close to the separatrix. Top right panel: $v_0 = 90^\circ$, here it can be seen that a separatrix appears also between the invariant curves, and the 2:1 resonance is more unstable. Bottom left panel: $v_0 = 135^\circ$, the area of the chaotic region increases between the invariant curves and the 2:1 resonance. Bottom right panel: $v_0 = 180^\circ$, the total phase space is chaotic except some initial conditions close to the primaries' plane.

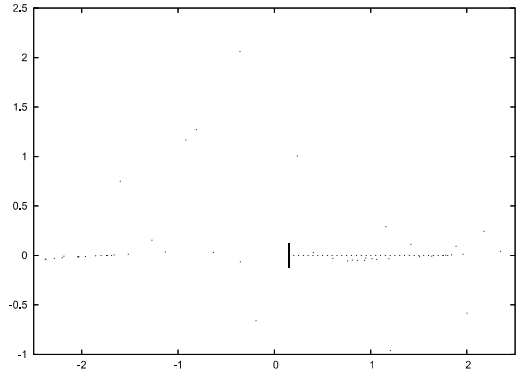

Figure 5. $e = 0.8$ and $v_0 = 0^\circ$. It is an interesting phase space portrait of the problem. Close to this value of the eccentricity (0.8) the fixed point in the middle becomes unstable. This was studied by Martínez Alfaro and Chiralt in 1993 [7]. In our case there is only one invariant curve for the initial distance $z_0 = 0.15$. In [7] the center is unstable for $e = 0.8558625$.

Fig. 5 shows the case where the eccentricity of the primaries was 0.8 and $v_0 = 0^\circ$. This is an interesting phase space portrait, because the parameter e

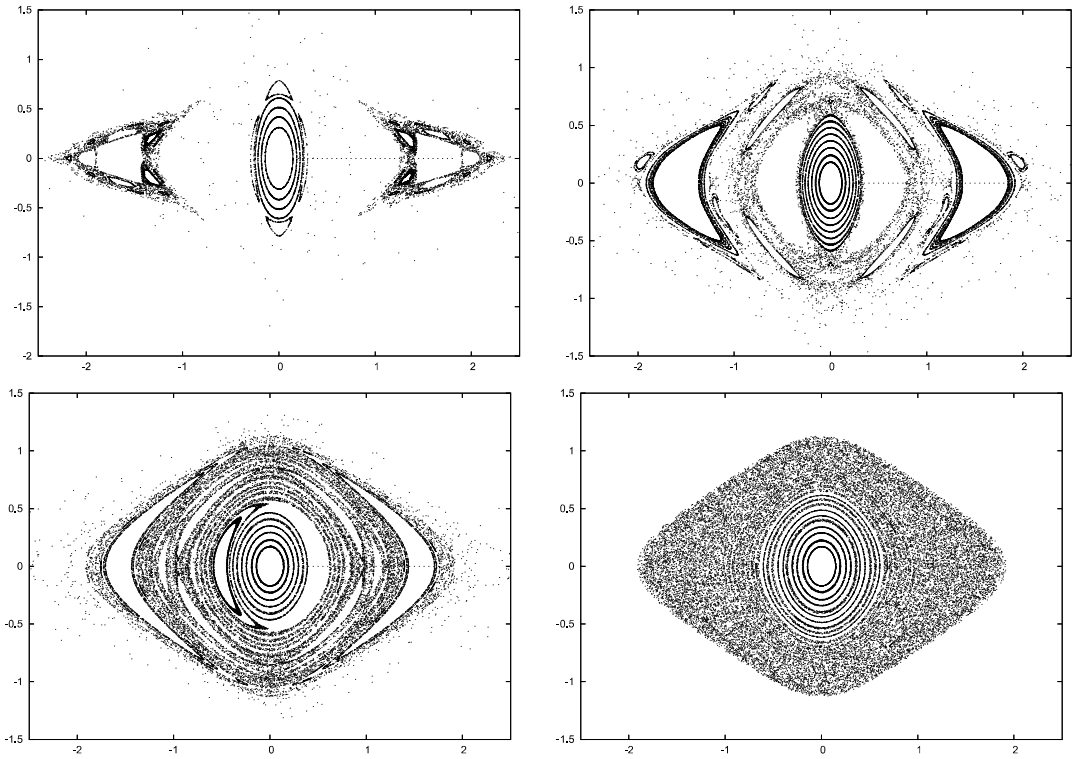

Figure 6. The eccentricity of the primaries is 0.8. Top left panel: $v_0 = 45^\circ$, the structure of the phase space is very similar to that of Fig. 4. However, in this panel the resonances are more complex. Top right panel: $v_0 = 90^\circ$, the chaotic domain grows between the islands. Bottom left panel: $v_0 = 135^\circ$, there are many islands in the chaotic sea. Bottom right panel: $v_0 = 180^\circ$, the phase space is mostly chaotic.

is very close to the value where the stable fixed point becomes unstable in the center of the $z - \dot{z}$ plane [7]. We can see only one island which corresponds to $z_0 = 0.15$ initial distance from the primaries orbital plane.

The four panels in Fig. 6 where $e = 0.8$ are similar to those of Fig. 4. There are resonances and for this larger the eccentricity there are stronger separatrices. The phase space is also very chaotic when the primaries are in the apocenter at $t = 0$.

4. Concluding remarks

We investigated the phase space of the Sitnikov problem for different initial conditions. Four initial positions of the primaries were studied beside the pericenter passage. There are closed curves on the surfaces of section corresponding to quasi-periodic orbits and small islands which means resonances. These small islands break up with varying the initial true anomaly, or higher order resonances appear. It is important to note that increasing the initial value

of v more and more chaotic motion occur close to the separatrices. Finally, if the initial true anomaly is $180°$ then almost the whole phase space is chaotic.

References

[1] Dvorak, R.: 1993, "Numerical results to the Sitnikov-problem."

[2] Faruque, S. B.: 2003, ”Solution of the Sitnikov problem.” *Celestial Mechanics and Dynamical Astronomy* **87**, 353-369.

[3] Hagel, J.: 1992, ”A new analytical approach to the Sitnikov problem.” *Celestial Mechanics and Dynamical Astronomy* **53**, 267-292.

[4] Kallrath J., Dvorak, R., Schödler, J.: 1997, "Periodic orbits in the Sitnikov problem", in The Dynamical Behaviour of our Planetary System (ed. R. Dvorak and J. Henrard) Kluwer Academic Publishers, The Netherlands, pp. 415-428.

[5] Liu, J., Sun Y.: 1990, ”On the Sitnikov problem.” *Celestial Mechanics and Dynamical Astronomy* **49**, 285-302.

[6] Mac Millan, W.D.: 1913, ”An integrable case in the restricted problem of tree-bodies.” *Astron. J.* **27**, 11.

[7] Martínez Alfaro, J., Chiralt C.: 1993, ”Invariant rotational curves in Sitnikov’s problem.” *Celestial Mechanics and Dynamical Astronomy* **55**, 351-367.

[8] Perdios, E., Markellos, V.V.: 1998, ”Stability and bifurcations of Sitnikov motions.” *Celestial Mechanics and Dynamical Astronomy* **42**, 187-200.

[9] Sitnikov, K.: 1960, ”Existence of oscillating motions for the three-body problem.” *Dokl. Akad. Nauk. USSR,* **133**, 303-306.

RECURSIVE FORMULAE FOR THE LIE-INTEGRATION OF LINEARIZED EQUATIONS

András Pál
Department of Astronomy
Loránd Eötvös University
Pázmány Péter sétány 1/A
H-1117 Budapest, Hungary
apal@szofi.elte.hu

Abstract Several methods used in celestial mechanics require to solve ordinary differential equations (ODEs) and also derived equations like linearized ones. Lie-integration is known to be one of the fastest ODE-integrators and it is widely applied in long-term investigations. However, an inconvenience of this method is that auxiliary recurrence relations must be deduced which is different for each problem.

We present a lemma which can be used to derive such recurrence relations almost automatically for the linearized equations *if* the relations for the original ODEs are known. This lemma is then applied to the equations of the classical 2-body problem. The knowledge of such relations may imply other chaos detection methods; some concerning (and preliminary) results are also presented.

Keywords: Numerical integration – Lie-integration – Linearized equations

1. Introduction

The integration method based on the Lie-series ([1]) is widely used in celestial mechanics (see [2] and articles refering to it). The basis of this method is to generate the coefficients of the Taylor expansion of the solution by using recurrence relations. Let us write the differential equation to be solved as

$$\dot{x}_i = f_i(\mathbf{x}), \tag{1}$$

where $\mathbf{x}$ is an $\mathbb{R} \to \mathbb{R}^N$ and $\mathbf{f} \equiv (f_1, \ldots, f_N)$ is an $\mathbb{R}^N \to \mathbb{R}^N$ function. Let us also introduce the differential operator

$$D_i := \frac{\partial}{\partial x_i}, \tag{2}$$

and the derivation

$$L_0 := \sum_{i=1}^{n} f_i \frac{\partial}{\partial x_i} \equiv f_i D_i. \tag{3}$$

The latter is known as the Lie-derivation which is also a differential operator: it is linear and Leibnitz's rule stands for it,

$$L_0(ab) = aL_0(b) + bL_0(a). \tag{4}$$

It can easily be proved that the solution of Equ. (1) at a given instance $t + \Delta t$ is formally

$$\mathbf{x}(t + \Delta) = \exp\left(\Delta t \cdot L_0\right) \mathbf{x}(t), \tag{5}$$

where

$$\exp\left(\Delta t \cdot L_0\right) = \sum_{k=0}^{\infty} \frac{\Delta t^k}{k!} L_0^k. \tag{6}$$

Hence, the Lie-integration is the finite approximation (up to the order of M) of the sum in the right-hand side of Equ. (6), namely

$$\mathbf{x}(t + \Delta t) \approx \left(\sum_{k=0}^{N} \frac{\Delta t^k}{k!} L_0^k \right) \mathbf{x}(t) = \sum_{k=0}^{N} \frac{\Delta t^k}{k!} \left(L_0^k \mathbf{x}(t) \right). \tag{7}$$

The proof of Equ. (5) and other related properties of the Lie-derivation can be found in [2].

2. Linearized equations

For numerous chaos detection methods the knowledge of the solution of linearized equations is required. Let us again write the differential equation as

$$\dot{x}_i = f_i(\mathbf{x}). \tag{8}$$

The linearized equations can be written as

$$\dot{\xi}_i = \sum_{m=1}^{n} \xi_m \frac{\partial f_i(\mathbf{x})}{\partial x_m}. \tag{9}$$

Using the above conventions (see Equ. (2)) it can be re-written as:

$$\dot{\xi}_i = \xi_m D_m f_i. \tag{10}$$

Let us introduce the differential operator

$$\partial_i := \frac{\partial}{\partial \xi_i}. \tag{11}$$

Thus the coupled system of equations (both the original and the linearized) is

$$\left.\begin{aligned} \dot{x}_i &= f_i, \\ \dot{\xi}_i &= \xi_m D_m f_i. \end{aligned}\right\} \tag{12}$$

Using the differential operators defined in Equ. (2) and Equ. (11), one can write the Lie operator of Equ. (12) as

$$L = L_0 + L_\ell = f_i D_i + \xi_m D_m f_i \partial_i. \tag{13}$$

Lemma. Using the same notations as above, the Lie-derivatives of ξ_k can be written as

$$L^n \xi_k = \xi_m D_m L^n x_k = \xi_m D_m L_0^n x_k. \tag{14}$$

Proof. Obviously, Equ. (14) is true for $n = 0$:

$$D_m L^0 x_k = D_m x_k = \delta_{mk}, \tag{15}$$

hence

$$\xi_m D_m L^0 x_k = \xi_m \delta_{mk} = \xi_k. \tag{16}$$

Let us suppose that it is true for all $0 \leq j \leq n$ and calculate the $(n+1)$th Lie derivative of ξ_k:

$$\begin{aligned} L^{n+1}\xi_k &= L\left(\xi_m D_m L^n x_k\right) = \\ &= \left(f_i D_i + \xi_j D_j f_i \partial_i\right)\left(\xi_m D_m L^n x_k\right) = \\ &= f_i D_i \xi_m D_m L^n x_k + \\ &\quad + \xi_j (D_j f_i)[\delta_{im} D_m L^n x_k + \xi_m D_m \partial_i L^n x_k]. \end{aligned} \tag{17}$$

Here the last term $(\xi_m D_m \partial_i L^n x_k)$ cancels, because x_k and $L^n x_k$ for all $0 \leq n$ do not depend on ξ. So:

$$\begin{aligned} L^{n+1}\xi_k &= f_i D_i \xi_m D_m L^n x_k + \xi_j (D_j f_i) D_i L^n x_k = \\ &= \xi_m f_i D_m D_i L^n x_k + \xi_m (D_m f_i)(D_i L^n x_k) = \\ &= \xi_m \left(f_i D_m + D_m f_i\right)\left(D_i L^n x_k\right) = \\ &= \xi_m D_m (f_i D_i)(L^n x_k) = \\ &= \xi_m D_m L(L^n x_k) = \xi_m D_m L^{n+1} x_k = \xi_m D_m L_0^{n+1} x_k. \end{aligned} \tag{18}$$

Here we have used the Young's theorem:

$$D_m D_i = D_i D_m, \tag{19}$$

and Leibnitz's rule,

$$D_m (f_i D_i) X = D_m f_i (D_i X) = f_i (D_m D_i X) + (D_m f_i)(D_i X), \tag{20}$$

where X can be any function of $\mathbf{x}$, in Equ. (18) $X \equiv L^n x_k$. Thus Equ. (18) is the same relation for $n+1$, as Equ. (14) for n. Continuing the scheme described above, the relation Equ. (14) can be proved for all positive integer values of n.

3. Equations for the two-body problem

The recurrence relations for the Lie-derivatives of the equations of motion of the N-body problem can be found in [2]. Here we present the equations for the two-body problem with almost the same notations. Let us detone the relative coordinates and velocities by $\mathbf{r} = (r_1, r_2, r_3)$ and $\mathbf{w} = (w_1, w_2, w_3)$, respectively and introduce the following variables:

$$\rho := |\mathbf{r}| = \sqrt{r_1^2 + r_2^2 + r_3^2}, \tag{21}$$

$$\phi := \rho^{-3}, \tag{22}$$

$$\Lambda := r_1 w_1 + r_2 w_2 + r_3 w_3 = r_i w_i. \tag{23}$$

The total mass of the system is $M + m$. Using these notations, the equations of motion are

$$\begin{aligned} \dot{r}_i &= w_i, \\ \dot{w}_i &= -G(M+m)\phi r_i. \end{aligned} \tag{24}$$

(Here $G \equiv k^2$, the gravitational constant.) The differential operators D_i and Δ_i are defined as

$$D_i := \frac{\partial}{\partial r_i}, \tag{25}$$

$$\Delta_i := \frac{\partial}{\partial w_i}, \tag{26}$$

and the Lie-operator of Equ. (24) can be written as

$$L_0 = w_i D_i - G(M+m)\phi r_i \Delta_i. \tag{27}$$

It can be proved easily (see [2]) that the recurrence relations are

$$L^{n+1} r_i = L^n w_i, \tag{28}$$

$$L^n \Lambda = \sum_{k=0}^{n} \binom{n}{k} L^k r_i L^{n-k} w_i, \tag{29}$$

$$L^{n+1} w_i = -G(M+m) \sum_{k=0}^{n} \binom{n}{k} L^k \phi L^{n-k} r_i, \tag{30}$$

$$L^{n+1} \phi = \rho^{-2} \sum_{k=0}^{n} F_{nk} L^{n-k} \phi L^k \Lambda, \tag{31}$$

where

$$F_{nk} = (-3)\binom{n}{k} + (-2)\binom{n}{k+1}. \tag{32}$$

Using the lemma Equ. (14) the recurrence relations for the linearized equations of Equ. (24) can be derived *without* knowing these equations explicitly. Let us denote the linearized variables by ξ_i and η_i (respecting to r_i and w_i) and introduce

$$\Xi_i := (\xi_i \quad \eta_i), \tag{33}$$

$$\mathcal{D}_i := \begin{pmatrix} D_i \\ \Delta_i \end{pmatrix}, \tag{34}$$

$$\Xi\mathcal{D} = \Xi_i\mathcal{D}_i = \xi_i D_i + \eta_i \Delta_i. \tag{35}$$

Since the right-hand sides of the equations Equ. (28) – Equ. (31) are only bilinear in the Lie-derivatives of r_i, Λ, w_i and ϕ, using Leibnitz's rule the recurrence relations for ξ_i, w_i and the auxiliary variables $\Xi\mathcal{D}\phi$ and $\Xi\mathcal{D}\Lambda$ can be calculated automatically:

$$L^{n+1}\xi_i = L^n\eta_i, \tag{36}$$

$$\Xi\mathcal{D}L^n\Lambda = \sum_{k=0}^{n}\binom{n}{k}(L^k\xi_i L^{n-k}w_i + L^k r_i L^{n-k}\eta_i),$$

$$L^{n+1}\eta_i = -G(M+m)\sum_{k=0}^{n}\binom{n}{k}\left[(\Xi\mathcal{D}L^k\phi)L^{n-k}r_i + L^k\phi L^{n-k}\xi_i\right],$$

$$\Xi\mathcal{D}L^{n+1}\phi = -2\rho^{-2}\xi_i r_i L^{n+1}\phi + \\ +\rho^{-2}\sum_{k=0}^{n}F_{nk}\left[(\Xi\mathcal{D}L^{n-k}\phi)L^k\Lambda + L^{n-k}\phi(\Xi\mathcal{D}L^k\Lambda)\right].$$

For the initialization of the recurrence method, the value of $\Xi\mathcal{D}L^0\phi = \Xi\mathcal{D}\phi$ has to be known:

$$\Xi\mathcal{D}\phi = -3\rho^{-5}\xi_i r_i. \tag{37}$$

References

[1] Gröbner, W., Knapp, H.: 1967, "Contributions to the Method of Lie-Series"

[2] Hansmeier, A., Dvorak, R.: 1984, "Numerical integration with Lie-series" *Astronomy and Astrophysics* **132**, pp. 203-207

SPEED AND EFFICIENCY OF CHAOS DETECTION METHODS

Áron Süli
Department of Astronomy
Loránd Eötvös University
Pázmány Péter sétány 1/A
1117 Budapest, Hungary
a.suli@astro.elte.hu

Abstract In this article four chaos indicators were compared using the framework of the 2D standard map. These methods, namely the LCE, FLI, RLI and SALI may provide a global picture of the evolution of the mapping. Until now a detailed comparison of these methods have not been performed. This imperfection should be supersede. This is the aim of the paper.

Keywords: Chaos detection methods – Standard map

1. Introduction

The problem to separate ordered and chaotic motion in dynamical systems, especially in one with many degrees of freedom, is a fundamental task in several area of modern research. In order to determine the type of an initial condition in the phase space one needs fast and reliable tools. These tools are extremely useful in those cases when the inspected dynamical system has more than two degrees of freedom and therefore it's phase space can't be explored in a direct way or the classical method of Poincaré surface of sections can not be applied.

The mathematical foundation of the theory of Lyapunov characteristic exponents (hereafter LCE) arose progressively in the literature. The use of such exponents dates back to Lyapunov [9], but was firstly applied by [11] to characterize trajectories. In his paper Oseledec provides a general and simple way to compute not only the largest, but all the LCEs. The first numerical characterization of stochasticity of a phase space trajectory in terms of divergence of nearby trajectories was introduced by the classical paper of [6]. They found that two orbits initially close diverge either linearly or exponentially depending

Table 1. Enumeration and classification of the methods.

analysis of the orbits	**analysis of the tangent vector**
1. Poincaré surface of section	1. Lyapunov characteristic exponents (LCE) [9]
2. Frequency analysis method (MFT) [8]	2. Generalized Lyapunov indicators (GLI) [3]
3. Low frequency power spectra [16]	3. Spectra of stretching numbers [14]
4. Sup-map method [8]	4. Spectra of helicity and twist angles [2]
5. Spectral analysis method (SAM) [10]	5. Fast Lyapunov indicators (FLI) [4]
	6. Spectral distance [15]
	7. Mean exponential growth of nearby orbits (MEGNO) [1]
	8. Relative Lyapunov indicator (RLI) [12]
	9. Smaller alignment index (SALI) [13]

on whether the initial points lie in an integrable or in a stochastic region of the phase space.

In the last three decades much work, both analytical and numerical have been performed to investigate the chaotic properties of classical dynamical systems. In addition to the elaborated theory of LCE several new methods have been developed in order to establish the true nature of an orbit in the shortest possible timespan. These methods are based on the analysis of the orbits, or on the time evolution of the tangent vector i.e. the solution of the linearized equations of motion. Accordingly the methods can be classified in two groups (see Table 1).

In this paper the LCE, the FLI, the RLI and the SALI methods will be investigated and compared in the framework of the 2D standard map, defined by the

$$\begin{aligned} x_{i+1} &= x_i + y_i, \\ y_{i+1} &= y_i - K\sin(x_i + y_i), \end{aligned} \qquad \texttt{mod } 2\pi \tag{1}$$

equations, where $K \geq 0$ is the non-linearity parameter. Throughout the paper the $K = 0.3$ case is considered. For this value of the non-linearity parameter the complete phase space of the system and the vicinity of the hyperbolic point (π,0) is depicted in Fig. 1.

In Section 2 the methods are shortly described. In Section 3 the speed of the methods are presented and compared, and also their dependence on the initial tangent vector ξ is discussed. In Section 4 the results are summarized.

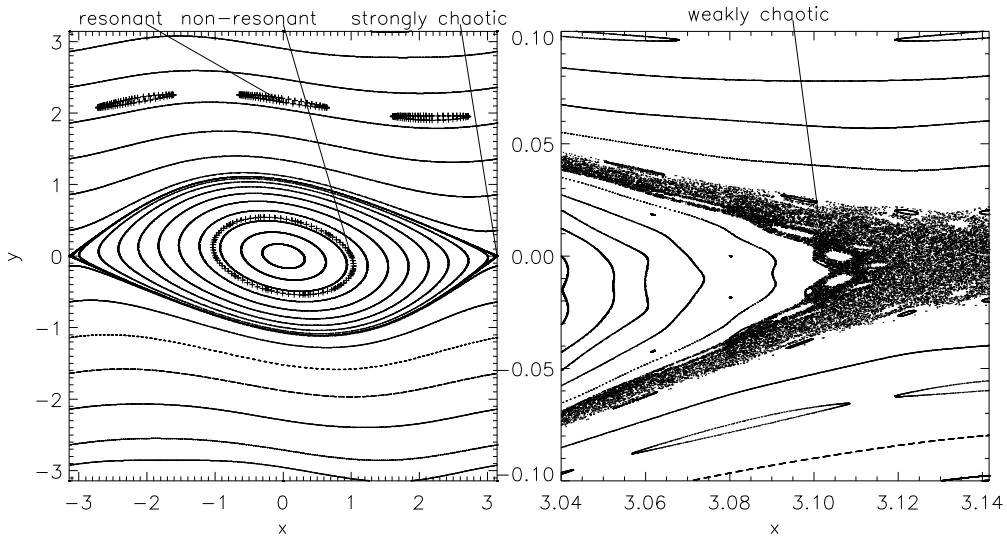

Figure 1. The phase space of the standard map for $K = 0.3$. The vicinity of the hyperbolic point is enlarged to visualize the initial condition of the weakly chaotic orbit.

2. Methods: LCE, FLI, RLI and SALI

Let us briefly review the definition of the different methods! The definition of the largest LCE for an initial value problem or mapping

$$\frac{\mathrm{d}\mathbf{y}(t)}{\mathrm{d}t} = \mathbf{f}(t,\mathbf{y}), \quad \mathbf{y}(0) = \mathbf{y}_0, \tag{2}$$

$$\mathbf{y}_{i+1} = \mathbf{M}(\mathbf{y_i}), \quad \mathbf{y}_{i=0} = \mathbf{y}_0, \tag{3}$$

is given by

$$\mathtt{LCE} = \lim_{t\to\infty} \frac{1}{t-t_0} \log \frac{||\xi(t)||}{||\xi(0)||} = \lim_{t\to\infty} \gamma(t,\mathbf{y}_0,\xi_0), \tag{4}$$

where $\xi(t)$ is the solution of the first order variational (i.e. linearized) equations and the function $\gamma(t,\mathbf{y}_0,\xi_0)$ measures the mean rate of divergence of the orbits. The linearized equations are:

$$\frac{\mathrm{d}\xi(t)}{\mathrm{d}t} = \frac{\partial \mathbf{f}(t,\mathbf{y})}{\partial \mathbf{y}}\xi, \quad \xi(0) = \xi_0, \tag{5}$$

$$\xi_{i+1} = \frac{\partial \mathbf{M}(\mathbf{y_i})}{\partial \mathbf{y}}\xi_\mathbf{i}, \quad \xi_{i=0} = \xi_0. \tag{6}$$

The value of LCE reveals the sensitivity of the given trajectory to the initial conditions. The problem of the LCE is that it is defined as a limit. Though the largest LCE can be calculated up to a (very) large time T but the limes as t tends to infinity cannot be evaluated numerically. Therefore the function $\gamma(t,\mathbf{y}_0,\xi_0)$ is called the Lyapunov characteristic indicator (hereafter LCI),

which is a finite estimate of the LCE. Thus the evolution of LCI(t, x_0, ξ) is followed up and we plot logLCI versus $\log t$. If the curve has a negative constant slope, the trajectory is ordered; if it exhibits an inflection of the slope, which comes close to 0 and the function converges to a certain value, the orbit is chaotic.

The FLI was introduced as the initial part (up to a stopping time t_s) of the LCE's computation:

$$\texttt{FLI}\left(\xi(0), \mathbf{y}_0, t_s\right) = \sup_{j=1,\ldots,n} ||\xi_j(t)||, \tag{7}$$

where n is the dimension of the phase space. To determine the FLI of a given orbit one has to follow the evolution of n tangent vectors, which initially span an orthogonal basis of the tangent space. The FLI tends to zero in both ordered and chaotic regions as the number of iterations (in the case of maps) or the time (in Hamiltonian systems) increases, but on completely different time scales which makes it possible to separate the phase space.

The RLI was introduced as the difference between the LCIs of two initially nearby orbits:

$$\texttt{RLI}(\xi(0), \mathbf{y}_0, t_s) = \frac{1}{t}|\mathrm{LCI}(\xi(0), \mathbf{y}_0, \mathrm{t_s}) - \mathrm{LCI}(\xi(0), \mathbf{y}_0 + \Delta \mathrm{y}, \mathrm{t_s})|, \tag{8}$$

where Δx is the distance in phase space between the two orbits.

The basic idea behind the SALI method is the intoduction of a simple quantity that indicates if a tangent vector is aligned with the direction of the eigenvector corresponding to the maximal LCE.

In order to check the directions of the vectors, the evolution of two tangent vectors are followed. The parallel and the antiparallel alignment indices are respectively defined as

$$d_- = ||\xi_1(t) - \xi_2(t)||, \quad d_+ = ||\xi_1(t) + \xi_2(t)||.$$

The SALI is defined as the minimum of the indices:

$$\mathrm{SALI}(t) = \min\left(d_+, d_-\right). \tag{9}$$

SALI tends to zero when to orbit is chaotic, and to a non-zero positive value when to orbit is regular. In the special case of 2D maps, SALI tends to zero for every initial conditions but follows completely different time rates for ordered and chaotic orbits.

3. Efficiency and dependence

Both the efficiency and the dependence was study in the case of four different kinds of orbits. The initial conditions are given in Table 2, the corresponding orbits are plotted on Fig. 1.

Table 2. Classification of the orbits and initial conditions.

Orbit			
Ordered		Chaotic	
non-resonant	resonant	strongly	weakly
(1;0)	(0;2.15)	(3.14;0)	(3.1024048;0)

First the number of iterations needed to establish with certainty the nature of an orbit was determined. An orbit can be classified as ordered (regular) or chaotic. An ordered orbit can be divided into two subclasses: non-resonant and resonant. An orbit is non-resonant, when there does not exist such linear combination of the frequencies of the motion which vanishes, otherwise the orbit is resonant. The chaotic orbits may be further classified, accordingly to the rate of divergence of nearby orbits. In this context, one can speak about strongly and weakly chaotic orbits. If two initially nearby trajectories diverge fast, the orbit is strongly chaotic, if the divergence is slow (comparing to the previous case), we speak about weakly chaotic or sticky orbit. The above classification is presented in Table 2, where also the initial conditions of the different orbits for the standard map are listed.

In Fig. 2 the time evolution of the four indicators are plotted for the above mentioned different kinds of orbits. The stopping time was set to 10^9 iterations. In the case of FLI, RLI and SALI an additional stopping criteria was used: whenever the FLI, RLI or SALI reached 10^{20}, 10^{-20} or 10^{-16}, respectively the computation was stopped.

Between 1 and some times 10 iterations none of the methods is capable to establish the type of the orbit: all four curves are overlapping each other inhibiting the classification. At the earliest at 100 iterations the strongly chaotic orbit can be separated from the ordered one, but with certainty the classification can be done at 1000 iterations.

In the case of LCI, FLI and SALI the indicator corresponding to the weakly chaotic orbit (dotted line) follows exactly the curve belonging to the strongly chaotic orbit (solid line) for the first 10 iterations. Afterwards the weakly chaotic curve essentially follows the curves corresponding to the ordered orbits for approximately 10^6 iterations. In the case of LCI the classification is only possible after approximately 10^6 iterations, when the curve has a turning point, and its slope becomes zero. It is worth noting, that after some 10^8 iterations the LCI suddenly jumps form 1.21×10^{-5} to 6.03×10^{-3}, than it climbs to 2.55×10^{-2} which is very close to the value belonging to the strongly chaotic orbit (3.45×10^{-2}). This is a numerical evidence, that both orbits originate in the chaotic domain. In the case of the FLI approximately 2×10^6, whereas in the case of the SALI about 9×10^5 iterations are needed for the assignment.

In the case of the RLI, the weakly chaotic curve does not follow any other, but it wildly oscillates around 10^{-12}. Between 100 and 1000 iterations it overlaps with the ordered curves, beyond 10^6 it goes close to the strongly chaotic curve. The classification is possible after 10^4 iterations.

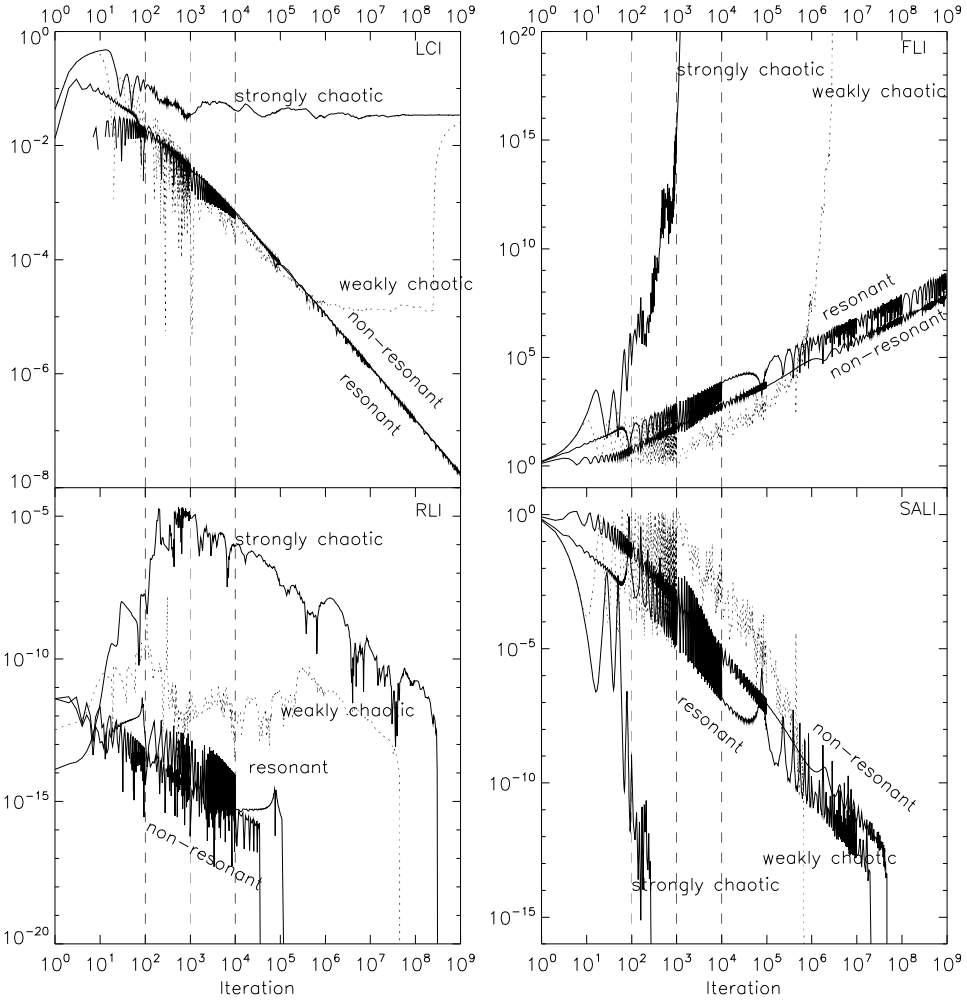

Figure 2. Variation of the CIs with the number of iterations for four kinds of orbits of the standard map. The dotted curves correspond to the weakly chaotic orbit.

A careful examination of the curves in Fig. 2 allows one to distinguish also between resonant and non-resonant motion. Although the curves corresponding to a non-resonant and a resonant motion are separated in the case of FLI, RLI and SALI, the oscillations prevent definite distinction between the two cases. Therefore, following the idea of [5], the definitions are replaced by their running average

$$\widehat{\mathrm{CI}}(t) = \frac{1}{2N} \sum_{k=i-N}^{i+N} \mathrm{CI}_k, \tag{10}$$

where CI denotes one of the methods and N is the width of the running window. In the following $N = 50$ was used.

In Fig. 3 the running average of the indicators are shown. In the case of LCI and SALI the two curves can not be distinguished from each other, whilst the FLI and RLI curves are well separated after 100 iterations. It appears clearly that using $\widehat{\mathrm{FLI}}(t)$ and $\widehat{\mathrm{RLI}}(t)$ resonant and non-resonant motion are clearly separated. We note that the corresponding lines appear to be parallel. This averaging technique does not influence the behaviour of the indicators in the case of chaos.

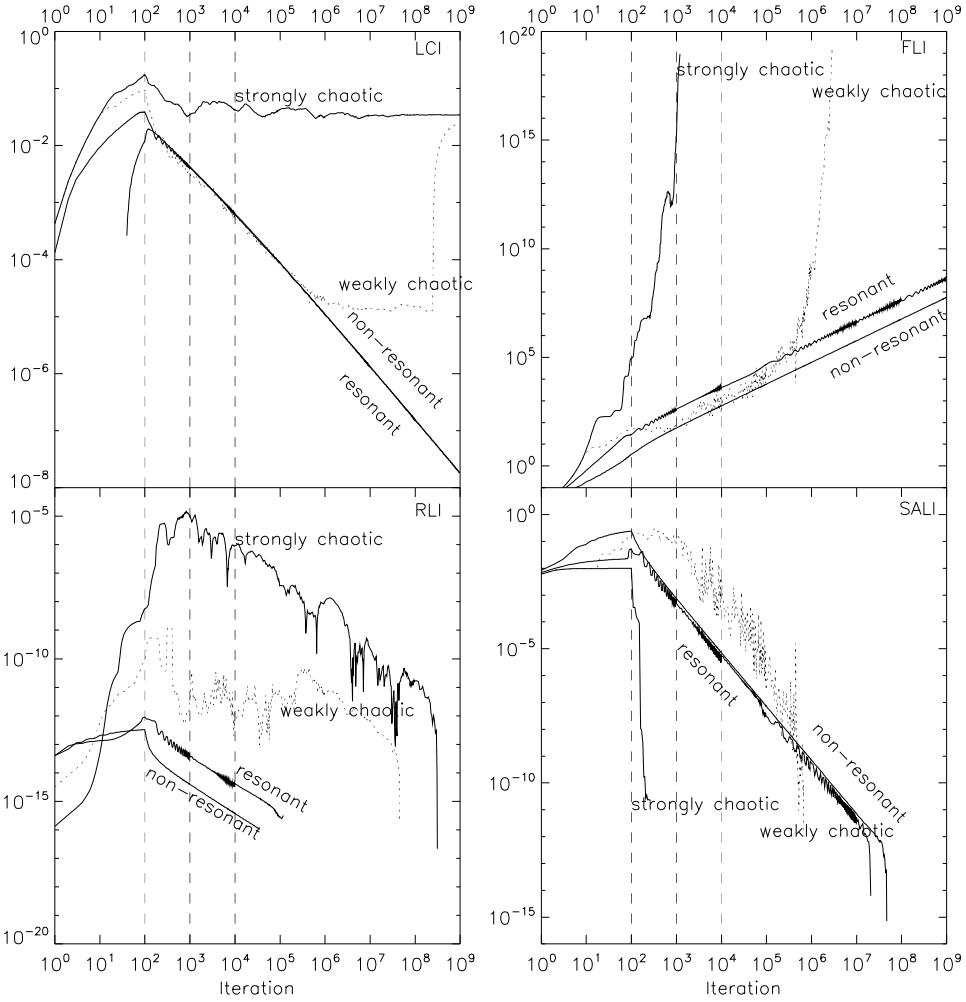

Figure 3. Variation of the $\widehat{\mathrm{CI}}(t)$s with the number of iterations for four kinds of orbit of the standard map.

It is obvious, that the methods are sensitive to the initial direction of the tangent vector $\xi(0)$. To quantify therefore the methods' dependence on the direction of $\xi(0)$, the tangent vector is rotated, and the indicator is calculated up to several stopping times. This dependence is confirmed in Fig. 4 in which the values of the CIs are plotted against the angle ϕ, for the resonant, non-

resonant and chaotic orbits for 1000 iterations. The ϕ is the angle between $\xi(0)$ and the (1,0) vector (x-axis). From Fig. 4 it is obvious that these values are far from being constant when varying the angle ϕ. In order to plot all four curves together, a normalization was performed, i.e. the CI values were divided by their maximum value (see Table 3).

The normalized curves have extremum at the same ϕ, which is a natural consequence of that, that all four methods are based on the evolution of the tangent vector. The LCI and RLI are periodic with π, since these methods are based on one $\xi(0)$, while the FLI and SALI are periodic with $\pi/2$, because they are based on two tangent vectors which are initially perpendicular to each other.

Table 3. Dependence and relative variation for the resonant orbit.

	LCI	**FLI**	**RLI**	**SALI**
max	0.00653987	692.198	5.77967e-15	0.00307465
min	-0.00075530	489.790	2.97609e-15	4.17417e-06
Δ_{CI}	1.937	1.15	1.288	3.867
ϕ_{max}	81°.5 (261°.5)	81°.5 (171°.5)	171°.5 (351°.5)	81°.5 (171°.5)
ϕ_{min}	171°.5 (351°.5)	36°.5 (126°.5)	171°.0 (351°.0)	36°.5 (126°.5)
$\Delta\phi$	180°	90°	180°	90°

In Table 3 the maximum and minimum values for the resonant orbit are listed. Introducing the quantity

$$\Delta_{\mathrm{CI}} = 1 - \log_{10}\left(\frac{\min(CI)}{\max(CI)}\right), \tag{11}$$

also the measure of dependence was determinded. According to the third line of Table 3, we see that the SALI has the largest, and the FLI has the smallest value which could already be observed in Fig. 4.

4. Summary

In this article a possible classification of the chaos detection techniques was given, and four methods, namely the LCI, the FLI, the RLI and the SALI were briefly described in Section 2. These methods were compared using the 2D standard map. The efficiency of these techniques was tested via applying them to four different types of orbits. It was shown that all the four methods are capable to distinguish between strongly chaotic and ordered motion after approximately 100 iterations. To reveal the true nature of a weakly chaotic orbit, it turned out that the new methods are not superior to the classical method of LCI: in short time interval they failed to properly classify the orbit. This is because the weakly chaotic orbit pretends regular behaviour for a priori un-

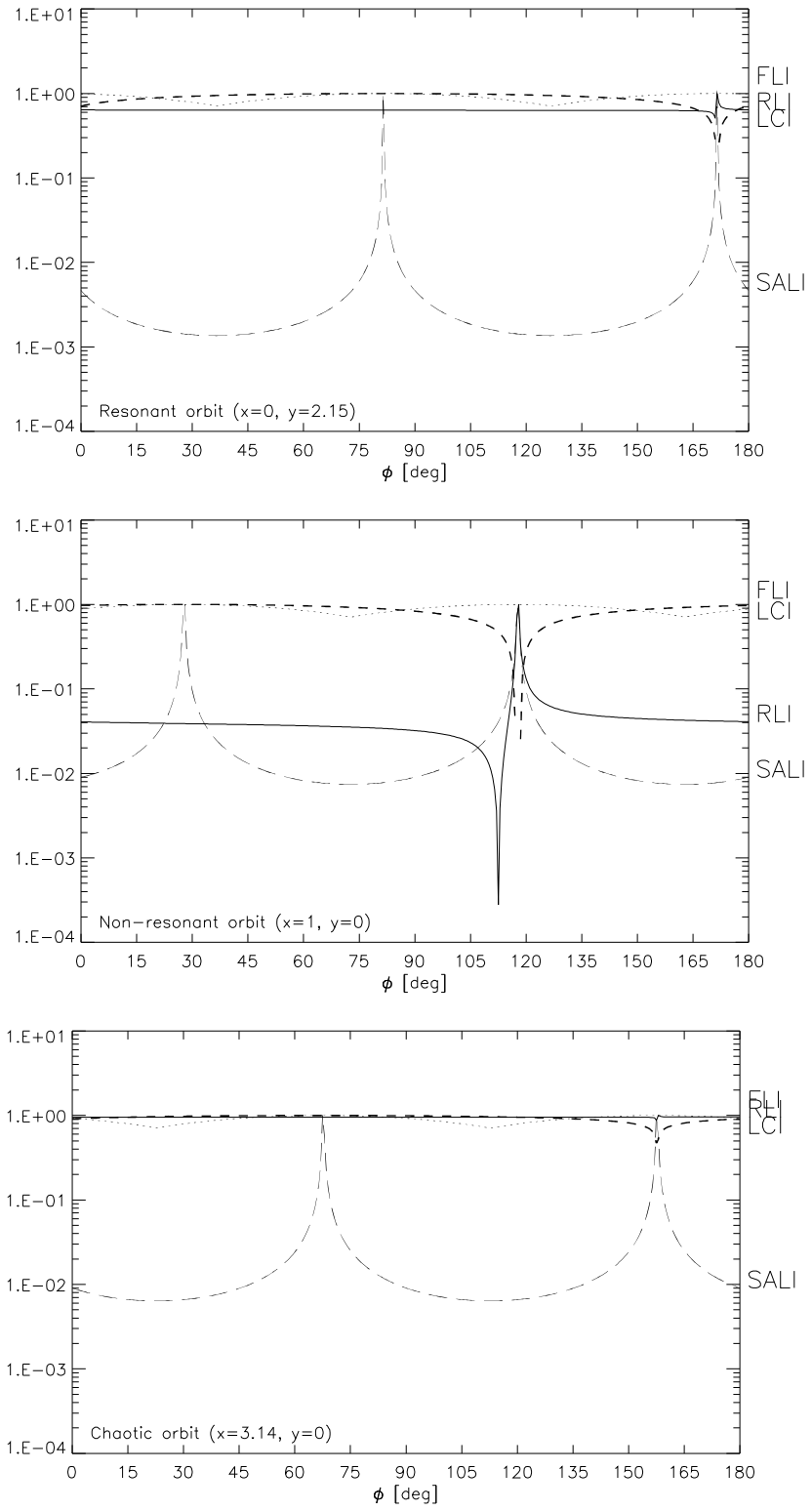

Figure 4. Variation of the CIs as a function of the initial direction of the tangent vector(s) for the resonant (top), non-resonant (middle) and chaotic (bottom) orbit.

known time interval. The length of this time interval may be considered as the measure of chaos: the longer the interval the weaker the chaos is.

Introducing the running average technique, the $\widehat{\mathrm{FLI}}$ and the $\widehat{\mathrm{RLI}}$ can separate between resonant and non-resonant orbits. This technique does not improve the capabilities of LCI and SALI.

The sensitivity of the methods to the initial direction of the tangent vector $\xi(0)$ was demonstrated and compared. It was shown for three types of orbits that the CIs have extremum at the same ϕ, which is the angle between $\xi(0)$ and the x-axis. The LCI and RLI are periodic with π, while the FLI and SALI are periodic with $\pi/2$. With the definition of Δ_{CI} the dependence of the methods were quantitatively described. The least sensitive is the FLI, the most one is the SALI.

In the future it is necessary to calculate these methods on a large portion of the phase space, and also to extend these calculations for Hamiltonian dynamical systems.

Acknowledgments

The support of the Austrian-Hungarian Scientific and Technology Cooperation, grant number A-12/04 is acknowledged.

References

[1] Cincotta, P.M. and Simo C.: 2000 "Simple tools to study global dynamics in non-axisymmetric galactic potentials - I", *Astron. Astrophys. Suppl. Ser.* **147**, 205.

[2] Contopoulos, G., Voglis, N.: 1996 "Spectra of Stretching Numbers and Helicity Angles in Dynamical Systems" *Celest. Mech. & Dyn. Astron.* **64**, 1.

[3] Froeschlé, C., Froeschlé, Ch., Lohinger, E.: 1993, "Generalized Lyapunov characteristic indicators and corresponding Kolmogorov like entrophy of the standard mapping", *Celest. Mech. & Dyn. Astron.* **56**, 307.

[4] Froeschlé, C., Lega, E., Gonczi, R.: 1997 "Fast Lyapunov Indicators. Application to Asteroidal Motion" *Celest. Mech. & Dyn. Astron.* **67**, 41.

[5] Froeschlé, Claude; Lega, Elena: On the Structure of Symplectic Mappings. The Fast Lyapunov Indicator: a Very Sensitive Tool Celestial Mechanics and Dynamical Astronomy, v. 78, Issue 1/4, p. 167-195 (2000)

[6] Henon, M., Heiles, C.: The applicability of the third integral of motion: Some numerical experiments Astronomical Journal, Vol. 69, p. 73, 1964

[8] Laskar, J.: 1990, "The chaotic motion of the Solar System: A numerical estimate of the size of the chaotic zones", *Icarus* **88**, 266-291.

[8] Laskar, J.: 1994, "Large-scale chaos in the solar system", *Astr. Astrophys.* **287**, L9-L12.

[9] Lyapunov A. M.: (1907) Ann. Math. Studies 17, Princeton, 1947

[10] Michtchenko, T. A., Ferraz-Mello, S.: 1995 "Comparative study of the asteroidal motion in the 3:2 and 2:1 resonances with Jupiter. I. Planar model", *Astronomy and Astrophysics*, **303**, 945.

[11] Oseledec V. I.: Trans. Moscow Math. Soc. 19, 197, 1968

[12] Sándor, Zs., Érdi, B., Efthymiopoulos, C.: 2000 "The Phase Space Structure Around L4 in the Restricted Three-Body Problem", *Cel. Mech. & Dyn. Astron* **78**, 113.

[13] Skokos, Ch.: 2001 "Alignment indices: a new, simple method for determining the ordered or chaotic nature of orbits" *Journal of Physics A*, **34**, 10029.

[14] Voglis, N., Contopoulos, G. J.: 1994 "Invariant spectra of orbits in dynamical systems" *Journal of Physics A* **27**, 4899.

[15] Voglis, N., Contopoulos, G., Efthymiopoulos, C.: 1999 "Detection of Ordered and Chaotic Motion Using the Dynamical Spectra", *Cel. Mech. & Dyn. Astron* **73**, 211.

[16] Voyatzis G. and Ichtiaroglou S.: 1992 "On the spectral analysis of trajectories in near-integrable Hamiltonian systems", *J. Phys. A* **25**, 5931